DOCTOR OF PHILOSOPHY

Face milling of nickel-based superalloys with coated and uncoated carbide tools

Köksal, Sakip

Award date:
2000

Awarding institution:
Coventry University

FACE MILLING OF NICKEL-BASED SUPERALLOYS WITH COATED AND UNCOATED CARBIDE TOOLS

SAKIP KÖKSAL
BSc. (Gazi, Turkey), MSc. (Coventry, UK)

A thesis submitted in partial fulfilment of the University's requirements for the award of the Degree of Doctor of Philosophy

October 2000

School of Engineering
Coventry University
Coventry, England

SYNOPSIS

Face milling machinability investigation of two difficult-to-machine nickel-based superalloys, namely Inconel 718 and Waspaloy, has been carried out with four different types of tungsten carbide tools under various cutting conditions. The tools comprised of one double-layer CVD-TiCN+Al_2O_3 coated (KC994M), two PVD-TiN coated (KC720 and KC730) and one uncoated (KMF) tungsten carbide tools. The objectives of the study include investigation of tool performance, failure modes and wear mechanisms under the cutting conditions employed. In addition, surface integrity of the machined surfaces, with regard to surface finish, subsurface microhardness and metallographic examination of the subsurface microstructure, was investigated.

CVD-coated KC994M gave the best overall performance in terms of tool life at low and high cutting conditions on both workpieces. The second best-performing tool was the uncoated KMF grade which gave as high tool lives as KC994M at lower cutting speeds. However at higher cutting speeds, KMF was generally outperformed by PVD-TiN coated tools. Short tool lives were obtained at higher cutting speeds of 75 and 100 m/min due to premature failure by chipping.

Tool wear at low cutting speed range was due to a combination of progressive microchipping and plucking through a fracture/attrition related wear mechanism associated with cyclic workpiece adhesion and detachment and abrasion/diffusion-related flank wear. Plucking and microchipping were the dominant wear mechanisms. Coating layers on the rake face of both CVD and PVD coated tools were almost completely removed within the first few seconds of cutting at all cutting speeds tested, thus becoming ineffective. On the flank face, however, they remained intact for a longer period and hence increasing tools performance at the medium cutting speed range.

Analysis of the subsurface microstructures and microhardness measurements showed that plastic deformation was the predominant effect induced onto the machined surface, the degree of which influenced by the cutting speed, tool wear and prolonged machining. In addition surface irregularities in the form of tearing and embedded hard particles were found to occur which was mainly associated with the chipping dominated wear mode.

DECLARATION

The research work presented in this thesis represents the original work of the author except where otherwise acknowledged by references. The project was carried out in the School of Engineering, Coventry University, England, under the supervision of Professor Ashraf Jawaid. The work has not been submitted to any other institution for another degree or award.

ACKNOWLEDGEMENT

The author wishes to express his endless gratitude to the Almighty Creator (Allah) for His mercies and kindness in granting the means for achieving the goals of this work. The author is sincerely grateful to the people of his homeland for being the real source of financial assistance and particularly to those who initiated, prepared and managed such kind of projects at Sakarya University of Turkey and other involving institutions. My sincere thanks go to the Vice-chancellor of Sakarya University Professor Ismail Calli, former Rector Professor Ramazan Evren, former Dean of The School of Engineering Professor Fevzi Yilmaz and all other involving academic and admin staff for their support and excellent management.

Special thanks to Professor Ashraf Jawaid (Jaguar Professor of Manufacturing and Associate Dean of the School of Engineering) for his supervision, valuable advice and continuous encouragement during the course of this project. His patience, understanding, openness and readiness to help, particularly at times of difficulty, are deeply appreciated. The author is also grateful to the former Dean of the School of Engineering, Emeritus Professor Stan Harvey and head of Manufacturing Subject Group Dr. Stuart Spraggett for their valuable help, advice, encouragement and departmental assistance for this study. Thanks to the collaborating institutions; Rolls-Royce, Kennametal (UK) and Inco Alloy International (UK) for providing all the necessary consumable and aids in assisting this work.

Personal thanks to the technical staff of Coventry University, in particular Mr. D Pheasy, Mr. R. Johnson, Mrs. C. Lovering and ex-member of staff Mr. H. Woodgate for sharing their expertise and willingness to assist in carrying out the experimental works. The author wishes to express his sincere thanks to his colleagues of the machining research team Dr. Che Haron, Dr. K. A. Olajire and Dr. S. Sharif for their excellent collaboration and help in both material and immaterial terms. Sincere appreciation to all Turkish friends studying in the UK for their moral and personal support and encouragement.

The author would like to acknowledge his wholehearted appreciation and special gratitude to his beloved mother Leyla and father Ahmet and parent-in-law Hanim and Cemalettin and all the family members for their patience and numerous personal contributions. Last but not least, the author wishes to express his sincere gratitude to his beloved wife Menekse for her resolute support, encouragement, patience and concern throughout this study and to his precious son Burak and daughter Beyza for being a pleasant source of heavenly joy and happiness when it was needed most.

LIST OF TABLES

LIST OF FIGURES

NOTATION

α_{ew} : Wiper edge clearance angle
α_f : Face clearance angle
κ: Approach angle
γ_a : Axial rake angle
γ_c : Insert edge clearance angle
γ_e : Effective rake angle
λ_i : Inclination angle
γ_r : Radial rake angle
γ': Precipitates
a_p: Axial depth of cut
APB: Anti phase boundary
a_r : Radial depth of cut (workpiece width)
b : Cutter centre offset from the workpiece central line
BCC/bcc: Body centred cubic
BUE: Built up edge
CAD: Computer aided design
CAM: Computer aided manufacture
CAPP: Computer aided process planning
CBN: Cubic boron nitride
CNC: Computer numerical control
CVD: Chemical vapour deposition
D: Nominal cutter diameter (mm)
D_c : Nominal cutter diameter
DOC: Depth of cut
DOCN: Depth of cut notch wear
EDM: Electro discharge machining
EDAX: Energy dispersive x-ray analysis
EDS: Energy dispersive spectroscopy
EPMA: Electron micro probe analysis
F: Friction force, cutting force
FCC/ fcc: Face centred cubic
F_r: Radial force
F_S : Partial area of engagement
f_z: Feed per tooth (mm/tooth)
h: Peak-to-valley height
HCP/hcp: Hexagonal close packed
HIP: Hot isostatic pressing
HSM: High speed machining
HSS: High speed steel
HV: Vickers hardness
i_n : Angle of index line
LAM: Laser assisted machining

l_e : Insert edge length
MC: Matrix carbide
N: Rotational speed of the spindle (rpm)
ODS: Oxide dispersion strengthening
PCBN: Polycrystalline cubic boron nitride
PCD: Polycrystalline diamond
PEM: Plasma enhanced machining
P_f : Assumed working plane
PM: Powder metallurgy
P_p : Tool back plane
P_r : Tool reference plane
P_s : Tool cutting edge plane
PVD: Physical vapour deposition
Q: Volume of removed material
R_a: Average surface roughness
r_c : Insert corner radius
r_e : Insert edge radius
r_{ef}: Effective radial runout
r_m: Measured radial runout
R_w : Radius of the pre-machined curve
s_e : Insert thickness
SEM: Scanning electron microscope
T: Tool life (min)
t_i : Instant apparent chip thickens during engagement
TRS: Transverse rupture strength
t_ω : Instantaneous actual chip thickness
V: Cutting speed (m/min)
VB: Flank wear
V_f: Feed rate (mm/min)
w_e : Insert wiper length
Z_i : Number of insert on the cutter
ε_n : Angle of cutter engagement
ε_x : Angle of cutter exit
κ_i : Angle of transient surface
θ: Cutting edge lead angle
ω : Instantaneous angular cutter position

TABLE OF CONTENTS

CHAPTER 3: CUTTING TOOL MATERIALS

CHAPTER 4: TOOL WEAR MECHANISMS AND FAILURE MODES

CHAPTER 5: NICKEL-BASED ALLOYS AND THEIR MACHINABILITY

CHAPTER 6: EXPERIMENTAL TECHNIQUES

CHAPTER 7: EXPERIMENTAL RESULTS

CHAPTER 8: DISCUSSION

CHAPTER 1

INTRODUCTION

1.1 Introduction

The unprecedented global trend of competition within the manufacturing sector requires increasing product quality, productivity and efficiency while maintaining or decreasing the costs of products. Driven by this reality, improving machinability of materials and the machining performance of cutting tools through new inventions and/or optimisation has been the ultimate goal of many research programmes associated with the manufacturing industry.

Machining is a metal removing process in which thin layers of workpiece material are removed in the form of swarf or small chips by the action of a wedge shaped cutting tool utilised within a machine tool system [1]. It is an indispensable and widely-used manufacturing process to give final shapes to the majority of industrial components required by a wide range of manufacturing sectors, including aerospace, automotive and defence. Metal cutting is a relatively complex and broad subject and a full appreciation involves considering some aspects of various scientific disciplines such as solid-state physics, physical metallurgy, engineering mechanics, thermodynamics, tribology and their interaction during the cutting process.

The invention of the steam engine is considered to be the starting point and the impetus for today's development in machine tools and cutting tool industry [2]. As new materials and alloys with enhanced properties that are different from the easy-to-machine grey cast iron and wrought iron were developed, the need for higher productivity and reduced machining costs drew the attention of researchers to the problem of *machinability* which then became one of the important areas of interest. Thus attempts were made to understand the wear behaviour of cutting tools in action with respect to the material being cut and to the type of the machining process. F. W. Taylor pioneered the first scientific and rational research in this field to establish the interaction between the

tool life and cutting speed for the turning operation, whereby predetermined flank wear was taken to be the life limiting factor [3]. Today research activities carried out in the field of metal cutting include generating machinability data, investigation of tool wear mechanisms and failure modes and integrity of the machined surface for a particular tool-work-process combination when a new material or tool is introduced, and detailed theoretical study, modelling or simulation of the cutting processes.

Although, the term machinability can simply be described as the degree of ease or difficulty with which a particular material is machined [1], it has, in fact, three main aspects; (a) tool life, (b) surface integrity and (c) power requirement. Therefore machinability characteristics of a particular material can include one or more of these aspects [4].

Understanding the interaction between the tool and the material at the area of contact and the behaviour of the tool from a mechanistic and materials point of views is the focal point to make improvements in the elements of machining that involve reducing the cost of machining, increasing the rate of metal removal, improving the properties of the cutting tool and to achieve better surface finish, integrity and precision. Therefore, the information and the data obtained directly or indirectly from the tool-work contact zone is of great significance in determining the performance of tools, machinability of workpiece material and the quality of the machined surface [1].

Nickel-based superalloys are a unique generation of materials with high thermal resistance and the ability to retain much of their mechanical strength properties and resistance to hot corrosion and erosion at elevated temperatures over 600 °C which make them desirable for demanding applications. They are extensively used in the aircraft industry and the growing interest and application span of these alloys has widened to include nuclear power systems, chemical and petrochemical industries and heat treatment plants etc. [5]. These superalloys, being primarily used for aerospace jet engine construction, account for approximately 60% by weight of typical aerospace engine components, some of which are able to withstand working temperatures as high as 1100 ^{0}C [6].

From the machinability point of view, they are regarded as difficult-to-machine materials due to their complex metallurgical composition with various hard intermetalic phases and high shear strength and creep resistance at elevated temperatures generated

during machining. Besides their work hardening and galling tendency, the presence of metal matrix carbides exerts particular difficulties during cutting [5, 7]. The improvements in machinability of these alloys has been inferior when compared to commonly used steels and other materials. Poor machinability of these high temperature strength materials has been forcing researchers to explore new alternatives of improving machining quality and productivity.

Surface integrity aspect of these materials is also as important as improving metal removal rate. During machining, the surface finish generated and the condition of the surface layer to a certain depth, i.e. the sub-surface, are affected by the type of cutting process, tools and by the cutting conditions. While surface finish is concerned with the topography (geometrical aspect) of the machined surface, the term 'surface integrity' is used to refer to the condition of the material itself, within the surface region, from metallurgical and mechanical aspects that can be quite different from the interior section of the material. [8].

Machining components of high strength materials used in severe applications that involve high service temperatures, high alternating stresses and corrosive atmospheres, requires that the condition of the surface integrity is well within the expected quality limits. The importance of surface integrity becomes more pronounced, if the failure of such components during service can inflict damage to individuals and property. It has been found that altered surface integrity can seriously diminish the fatigue strength and other mechanical properties, such as hardness, ductility, of a component when exposed to hostile environments, as in the case of jet engines.

Both conventional and non-conventional machining operations can produce components with impaired surface integrity under abusive cutting conditions. The principle causes of poor surface integrity are (a) high temperatures developed during cutting, (b) plastic deformation and plastically deformed debris, (c) chemical reaction of the surface with tool material, coolant and/or surrounding atmosphere. The reflection of these effects on the surface integrity can be in various forms, namely residual stresses, micro-cracks, re-crystallisation or phase transformations.

Successful applications of various ceramic and CBN cutting tools to aerospace nickel based material in turning operations have been reported in the published literature [9, 10], whereas the performance of ceramic tools in interrupted cutting has been reported to

be poor due to their low mechanical and thermal shock resistance [11]. The failure of ceramic and CBN tools, during face milling high strength materials was due to premature fracture at low cutting speeds and yielding very low tool life at high cutting speeds, where failure was due to flank and notch wear [11, 12].

Tungsten carbide tools are still in dominant use for milling high strength aerospace materials due to their superior toughness, thermal and mechanical shock resistance than that of ceramic tools. [13].

The performance and cutting capability of carbide tools have been dramatically increased over the last few decades. Major breakthroughs in the continuous development cycle of the carbide tools have been achieved by the addition of cubic carbides, sub-micron fine grained structure, hot isostatic pressing, CVD coating with harder carbides, oxides or nitrides, PVD coating process, multilayer CVD and PVD coatings, low temperature CVD coating process and improved cutting edge geometry. The continuous improvement of cutting tools has resulted in increased efficiency and productivity in the metal cutting industry, with subsequent cost reductions.

Carbides tools with finer grain and better balanced structures performed better, particularly in milling applications, allowing the cutting edge to be worn by flank wear instead of being chipped or plastically deformed [14].

Introduction of CVD coated carbide tools to the manufacturing industry in the late 1960's created a big impact by providing up to 50 % increase in cutting speeds or correspondingly longer tool lives over the uncoated equivalent of the same grades under identical cutting conditions in turning carbon steels and cast-irons [14]. By the 1980's, a machining time of less than one minute was achieved with multilayer coated carbide tools, for a certain component, that took 100 minutes to machine with hardened carbon steel tools in the 1900's. In today's metal cutting industry, various types of coated carbide tools are being used for more than 75 % of turning and 40 % of milling operations [14]. The importance of coated carbides lies in their possession of hard single or multiple layers of various pure nitrides, carbonitrides and/or oxides on the surface while maintaining a substrate with relatively high toughness which makes them suitable for interrupted cutting processes.

Most of the machinability data on nickel based superalloys has been based on orthogonal and/or semi-orthogonal turning operations where a continuous engagement of

tool/work material exists. Due to the relative complexity of the milling process as well as high costs of such exotic materials as superalloys, very little work has been carried out on the milling of these superalloys [13, 15]. Data obtained from turning process cannot be generally applicable to the milling process where interrupted cutting takes place [16]. Tools tend to perform differently in the milling process whereby the effects of cyclic thermal and mechanical stresses/impacts play significant roles in controlling the tool life, failure modes and wear mechanisms. These cyclic stresses are responsible for cracking, chipping and sometimes catastrophic failure of the cutting edges [17, 18].

In addition, the relative geometrical condition between the tool and workpiece during the moment of cutter engagement and exit within a complete rotational cycle, can influence the performance of the tool to a large extent. This influence would be negative under unfavourable geometrical conditions whereby premature tool failure by chipping or fracture occurs. In this respect, the phenomena of 'point of initial contact', 'impact factor' [19], 'partial area of engagement' [20], 'foot formation' and 'negative shearing' [21] were developed through the detailed studies of the interaction between the tool and workpiece. Each of these phenomena, none of them present in continuous turning process, influences the cutting performance of the tool in a particular manner during the milling operation. Therefore, to increase productivity in the milling process, more precise data regarding failure modes, wear mechanisms and tool-workpiece interactions should be generated through detailed experimental work.

1.2 The objectives of this research:

The aim of this project is to study machinability of nickel based superalloys; Inconel 718 and Waspaloy, with respect to the face milling process when cutting with different grades of coated and uncoated tungsten carbide tools. The specific objectives are as follows;

- To study the wear behaviour and cutting performance of two different coating systems deposited by CVD ($TiCN+AL_2O_3$) and PVD (TiN) techniques on identical grade tungsten carbide tools.
- To study the wear behaviour and cutting performance of two different grades of tungsten carbide tools with an identical PVD (TiN) deposited coating system.

- Compare the performance of coated tools with that of an uncoated tungsten carbide tool.
- Study the effect of cutting conditions and tools on surface integrity of Inconel 718 and Waspaloy.

Aerospace alloys are very expensive and in short supply. Mostly, short machinability trials are conducted and results are extrapolated. For the equipment, workpiece materials and cutting tools used in this study were supplied by the collaborating companies and hence detailed tests were carried out.

CHAPTER 2

MILLING PROCESS

2.1 Milling process

2.1.1 Introduction

Milling is a machining process in which metal is removed by the relative motion between a workpiece and a rotating cutter with multiple edges. In this process, the cutting action is inherently interrupted and chip thickness constantly changes in a periodic manner due to the cutter-workpiece relative motion.

More frequently the workpiece, fixed onto the machine table, is fed at a constant feed rate toward a rotating milling cutter. There are however applications whereby the workpiece is held stationary while a rotating cutter is advanced at a given feed rate along the main axes. The relative movement of the cutter and workpiece can be independent of or in combination with each other depending on the type of the milling machine, cutting tool and workpiece configuration. A wide variety of operations that include production of flat, contoured and free-form surfaces, slots, holes, threads etc. can be performed on different types of milling machines with conventional or CNC control. The accuracy and efficiency of the milling machines and operations have been increased to a great extent through CNC control and integrating with industrial CAD/CAM and CAPP systems [22].

2.1.2 Milling methods

There are two principal milling methods namely face milling and peripheral (slab) milling as schematically shown in Figure 2.1. The other types of milling processes such as end milling, gear milling, are considered to be derivatives of one or combination of these two basic methods with respect to the cutter-workpiece relative motion [8, 23].

In peripheral milling, the machined surface is generated by the teeth located on the periphery of the cutter, the axis of which holds parallel to the surface. The peripheral profile of the cutter is therefore reflected onto the machined surface.

In face milling, cutting is performed simultaneously by two edges of a tool located on the periphery and face of the cutter as illustrated in Figure 2.2. The cutter or spindle axis is normal to the machined surface which is always flat regardless of the cutter type.

In the subsequent sections, the technical details will be given in regard to the face milling process which has been used in this project to study machinability of nickel-based alloys, Inconel 718 and Waspaloy.

2.1.3 Terminology used in milling operation

2.1.3.1 Cutting speed

Cutting speed in face milling is the peripheral speed of the cutter with respect to the nominal diameter. It is related to the spindle revolution and cutter diameter through the following formula.

$$V = \frac{\pi D N}{1000} \quad \text{(m/min)} \qquad \text{Eq. 2. 1}$$

Where,

V: Cutting speed (m/min)

D: Nominal cutter diameter (mm)

N: Rotational speed of the spindle (rpm)

2.1.3.2 Feed rate:

Feed rate in milling is the travelling speed of the workpiece which is usually expressed in millimetres per minute. It is a function of feed per tooth, the number of teeth and the rotational speed of the spindle. The relationship is given by the following formula.

$$V_f = f_z \, Z_i \, N \qquad \text{Eq. 2. 2}$$

Where,

V_f: Feed rate (mm/min)

F_z: Feed per tooth (mm/tooth)

Z_t: Number of teeth on the cutter

N: Spindle revolution (rpm)

2.1.3.3 Axial depth of cut

Axial depth of cut (a_p) is the depth of the cutter engagement into the workpiece along the axis of spindle rotation as shown in Figure 2.2. Axial depth of cut is one of the two elements which determine the chip cross section area.

2.1.3.4 Radial depth of cut

Radial depth of cut (a_r), also known as the width of cut, is the width of radial projection of the cutter into the workpiece as shown in Figure 2.5-c. In face milling, radial depth of cut is usually smaller than the cutter diameter and can never be greater than this.

2.1.4 Milling cutter geometry

Based on the relevant ISO standard (3002/1-1982) [24] the geometric properties of a face milling cutter with indexable inserts are described in Figure 2.3. Some of the important geometrical properties of an insert are also depicted in 3-D view in Figure 2.4.

2.1.5 The working (operational) angles of the cutting edge in face milling

In metal cutting, many of the machining variables, such as chip formation, cutting forces, surface finish and tool life, are affected by the geometry of the tool. The angles of the cutting edge of a face milling cutter are referred to as 'working angles' [24]. Definitions of the most effective standard working angles (Figure 2.4-b) are given as follows.

2.1.5.1 Axial rake angle (γ_a)

Axial rake angle is the angle between 'tool reference plane', P_r, and the tool rake face in a plane parallel to the cutter axis and perpendicular to the machined surface (Figure 2.4-b).

2.1.5.2 Radial rake angle (γ_r)

Radial rake angle is the angle between the tool reference plane, P_r, and the tool rake face in a plane perpendicular to the cutter axis and parallel to the machined surface (Figure 2.4-b).

2.1.5.3 Tool approach angle (κ)

Tool approach angle (also called 'tool cutting edge' angle or lead angle) is the angle between the machined surface and a plane in tangential location on the periphery of the cutter and parallel to the major cutting edge measured in the tool reference plane, P_r (Figure 2.4-b).

2.1.5.4 True (effective) rake angle (γ_e)

True rake angle is the angle between a tangent to the tooth face at a given point on the major cutting edge and a radial line to this point measured in a plane perpendicular to the cutting edge (Figure 2.3). It is the resultant product of radial, axial and approach angles.

2.1.5.5 Angle of engagement (ε_n)

Angle of engagement, which can also be called 'entry angle', is the angle between the line passing through both the cutting edge and cutter centre and the plane of engagement, measured in a plane parallel to the machined surface (Figure 2.6).

2.1.5.6 Angle of disengagement (ε_x)

Angle of disengagement, which can also be called 'exit angle', is the angle between the line passing through both the cutting edge and cutter centre and the plane of disengagement, measured in a plane parallel to the machined surface (Figure 2.6).

2.1.6 Modes of face milling

Face milling process can be classified into two distinct categories as 'up' and 'down' milling, on the basis of both the cutter-workpiece relative position and motion, (Figure 2.5.a and b). They are also known as conventional and climb milling modes. A combination of both cases is obtained in neutral and mixed cutting modes depending on

the entry and exit angles between cutter and workpiece (Figure 2.5-c) [6]. In both of these modes, the chip thickness varies along a trochoidal path which was assumed circular until Martellotti [25] established the kinematics of the process on the basis of trochoidal cutter path. Up and down milling have their own specific advantages and disadvantages and the decision is made depending on many factors such as machine tool, cutter type, workpiece configuration and setup etc.

The extreme conditions of up and down milling with respect to the cutter offset b, which is depicted in Figure 2.5-c, are represented by the following relationship.

$$b = \pm\frac{1}{2}(D_c + a_r) \qquad \text{Eq. 2. 3}$$

Where

b : Cutter centre offset from the workpiece central line

D_c : The cutter diameter

a_r : The width of the workpiece

When b equals to zero (b = 0), the milling mode is neutral, i.e. balanced combination of up and down milling modes.

2.1.6.1 Up milling

In up milling the undeformed chip thickness constantly increases as the cutting tooth rotates from the initial engagement point (A) toward exit point C as shown in Figure 2.5-a. Chip thickness is minimum at point A and increases to a maximum at the point of exit. The maximum chip thickness becomes equal to the feed per tooth along the horizontal axis of the cutter. The cutter axis does not intersect the workpiece under a total up milling condition.

Up milling should be preferred when the machine feeding system has no backlash eliminator as the cutting forces in this mode oppose the feed force and prevent detrimental sudden workpiece withdrawal into the cutter. When milling components with irregular or scaly outer surface, up milling is preferred to avoid unexpected tool failures. On the other hand, the following disadvantages in up milling make down milling more favourable.

a) Cutting forces are higher than that of down milling since tangential force of rotating cutter acts against table feed force.

b) As the chip thickness is theoretically zero at the point of engagement, the tool tends to rub and the material may workharden in this area. A work-hardened layer could cause premature tool failure or excessive tool wear.

c) It is very possible for strongly adhered chips onto the cutting edges to wedge between tool and workpiece and cause breakage during up milling. [26, 27].

2.1.6.2 Down milling

As depicted in Figure 2.5-b, the cutter axis does not intersect the workpiece and the rotation of the cutter is such that the undeformed chip thickness constantly decreases towards point (A) where cutter exits. It is recommended that down milling should be the first choice due to its advantages mentioned in the preceding paragraphs, if the machine has backlash eliminator.

2.1.7 The influence of entry and exit conditions on milling cutter life

2.1.7.1 Entry conditions

The influence of entry conditions on tool life when face milling was first investigated by Kronenberg [19] and later by Opitz and Beckhaus [20].

As shown in Figure 2.5-c, when face milling a blank of width a_r with a cutter of diameter D_c, b is the offset of the cutter centre line with respect to the centre line of the blank. It is clear that, a change in b, which is the primary variable investigated, results in changes in the shape of the chip, the equivalent feed rate, the cutting and non-cutting periods and the entry and exit conditions. If the secondary variables of chip shape and entry-exit conditions have no influence on the process, it is evident that a plot of tool life versus distance offset, b, should be symmetrical about the line where b is zero (Figure 2.6).

In many cases, however, when milling high strength and extremely work-hardening materials, the relationship between tool life and cutter offset is not symmetrical about the line where b equals to zero. This relationship becomes non-uniform and takes the form as shown in Figure 2.7. Kroneneberg [19] studied the condition of initial cutter engagement

and defined the engagement area as shown in Figure 2.8, and established the mathematical model for the geometric interactions between cutting tooth and workpiece. The area of initial contact in the shape of a parallelogram and its projection on the tool rake face was represented by **S-T-U-V** letters (Figure 2.8). He experimentally showed all the possible contact conditions in relation to cutter geometry and cutter-workpiece relative position. These conditions include point contacts at S, T, U, V, line contacts along ST, SV, TU and UV and cross sectional area of STUV. Among these conditions, S point contact, which is the corner of cutting edge and the weakest spot resulted in the lowest tool life when cutting steel (SAE 1112) with a tungsten carbide insert. He introduced the associated concepts of 'penetration time' and 'impact factor', and defined another variable, the 'index line' (Figure 2.9). In a later paper, Opitz and Beckhaus [20] found that the concepts of penetration time or impact factor were not sufficient to explain the effect of initial contact on tool life and went on to define the phenomenon of 'partial area of engagement' (F_s) as new criteria. The partial area of engagement is defined as the area which is crossed by the index line before the point S is reached (Figure 2.9). They found that the functional curve of the partial area of engagement, when plotted against the angle of engagement, gave a better agreement with the tool life results of Kroneneberg. The higher the partial area of engagement the higher the resulting tool life.

Gilbert et al. [28] studied the influence of transient vibrations, generated during initial contact, on tool life. They attributed increased tool wear in interrupted cutting to the transient vibrations which they reported to be 8 times higher than in continuous cutting.

Phillips [29] who also investigated the effect of entry conditions on tool life of various grades of tungsten carbide inserts when milling hardened steels, attributed the premature tool fracture to a number factors namely, initial impact stresses, cyclical temperature fluctuations at the tool chip interface and severe mechanical loading of the cutting edge.

Some other investigators believed that radial runout [30] which causes variation in chip load between consecutive teeth, and bulging of the tool flank [31] due to plastic deformation were responsible for premature failure. Asai et al [32] reported that presence

of welded chip to the cutting edge from previous cutting cycle reduced the efficiency of the tooth during initial engagement by trapping between the tool and workpiece.

2.1.7.2 Exit conditions

Okushima and Hoshi et al [33] observed that the presence of chip material adhering to the cutting edge during exit influenced its performance through stress amplification generated at the moment of next entry. The tool failure under the presence of a sticking chip was of a chipping nature that occurred generally regardless of the cutting conditions employed. Thus it was suggested that the exit angle should be increased to remove the stock with a gradually decreasing chip thickness to minimise chip sticking. Yellowley [34] suggested that chip adhesion was more pronounced when cutting work-hardening materials and attributed tool failure by fracture to the tensile stresses on the rake face induced due to changes in the shear pattern at the moment of exit. Loladze [35] attempted to describe the stress conditions on the cutting edge at the moment of cutter entry and exit. By means of high speed photography and photoelastic techniques, it was found that the magnitude of tensile stresses increased considerably and shifted towards cutting edge during the exit. It was also reported that the stress condition was not dangerous when the uncut chip thickness was sufficiently small at exit.

Lat and Ber [36] studied the effect of entry and exit conditions on wear behaviour of a P25 carbide insert when face milling steel AISI-1067 within a range of cutting speeds. They showed experimentally that the tool wear was lower at favourable exit conditions than at favourable entry conditions.

Probably the most detailed study of the effect of exit conditions on tool life was performed by Pekelharing and his co-workers [21, 37, 38]. They identified the 'safe' regions of cutter exit in relation to the relative position of the tool and workpiece and rendered entry shocks much less harmless.

They observed that the formation of 'negative shearing', as shown in Figure 2.10, was responsible for premature tool fracture during face milling with carbide tools. When negative shearing occurs, a peculiar chip type with foot-like extension at its lower end is also produced indicating the presence of this phenomenon (Figure 2.10). The tool life was found to be shorter in a range of exit angles approximately between - 30° and 20°, narrowing with the decrease in uncut chip thickness. They simulated the loading

condition of the cutting edge at exit by means of finite element analysis and observed that the location of the maximum tensile stresses shifted towards cutting edge and caused fracture. They reported that the results of their analysis was in good agreement with that of Loladze [35] who experimentally studied the stress conditions.

Shaw [39] on the other hand, argued that because of the strain energy stored in the tool material during cutting period, a compressive stress reverts to a tensile stress upon sudden unloading at exit. When the rate of unloading is sufficiently high, the magnitude of the tensile stress is equal to the compressive stress and can cause edge fracture.

2.1.8 Cutting forces in face milling

The intermittent nature of the face milling process together with variable undeformed chip thickness makes the analysis of the mechanisms of cutting more complicated than orthogonal cutting.

Martelloti's [25, 40] analytical analysis of the milling process laid down the foundation for the face milling cutting force modelling efforts. This was followed by others proposing various other methods of cutting force analysis and prediction models [41, 42].

Cutting force prediction models are generally based on estimating forces acting on a single tooth cutter. Forces of a multitooth cutter can then be predicted depending on the number of teeth (Z_i) cutting simultaneously and their instantaneous radial locations (ω). Both the direction and amplitude of the forces change in a periodic manner during the engagement period of each tooth. The magnitudes of the forces reach to a maximum at an instant where the chip thickness is also maximum.

2.1.8.1 Cutting force components

In face milling, two reference systems can be adopted to determine the components of the cutting forces as shown in Figure 2.11.

1- Cutter reference system of cutting forces

2- Table reference system of cutting forces

2.1.8.2 Cutter reference system

Cutter reference system consists of the following three force components that act on the cutting edge (Figure 2.11-a).

Tangential force (F_t): It acts tangentially to the effective radius of the cutter and represents the resistance to the cutter rotation. In a normal operation, the magnitude of tangential force is the highest of all other force components and accounts for 99 % of the total power required by the operation.

Radial force (F_r): It acts perpendicular to the cutter axis along the radius of the cutter. It is usually about 50 % of the tangential force, but it accounts for only about 1 % of total power consumption. This is because the radial velocity (the velocity of feed) is generally very small in relation to the cutting velocity.

Axial force (F_a): It acts parallel to the spindle axis and contributes to the thrust force if the cutter has an approach or lead angle. Axial force is usually the smallest of the three force components and is about 50 % of the radial force. Because there is usually no velocity in the axial direction in face milling, its effect on power requirements is generally neglected.

Resultant force (F_R): It is the vectoral sum of these three force components and can be determined by the following formula:

$$F_R = \sqrt{F_t^2 + F_r^2 + F_a^2} \qquad \text{Eq. 2. 4}$$

2.1.8.3 Table reference system

In this force reference system, the resultant force can be divided into three individual force components along X, Y, Z axes as shown in Figure 2.11-b. These force components can be measured by means of a cutting force dynamometer.

Feed (longitudinal) force (P_x): It is the force component parallel to the machined surface and the feed direction

Normal (traverse) force (P_y): It is the force component parallel to the machined surface and perpendicular to the feed direction.

Vertical force (P_z) : It is the force component parallel to the cutter axis and perpendicular to the feed direction.

2.2 Surface integrity

Surface integrity can be defined as the inherent or enhanced condition of a surface produced in a machining process. It encompasses many aspects of a machined surface pertaining to the surface topography, metallurgical, mechanical and physical conditions generated as a result of a given machining process [43].

The nature of the surface layer generated by machining is of dramatic importance besides dimensional accuracy, when the safety of individuals and property is of prime concern. Investigations of the characteristics of surface layers of the components which are subjected to such demanding service conditions as high temperature and alternating stresses, must be carried out in order to prevent possible failures and accidents which would harm individuals and property [8].

Almost all cutting processes somehow produce a surface layer with different characteristics from inner sections of a given component. A cutting process, thus generates a new surface with new topography and metallurgical features. The alterations generated on the surface layer may have considerable effects on the fatigue strength of dynamically-stressed aerospace components and some other mechanical properties under extreme environments [8, 44, 45]. Therefore, when machining high temperature alloys, the amount of tool wear should not be as high as those generally considered in cutting steel. Because using excessively worn tools can cause sub-surface deformation of the machined components [4].

2.2.1 The types and main causes of metallurgical surface alterations

The following are the principle causes of surface alterations in a given machining process. Depending on the type of machining process, work and tool materials and process parameters, one or more of these causes can be present and have various influences.

a) The high working temperature or high temperatures generated during machining,

b) Plastic deformation on the surface and plastically deformed debris

c) Chemical reactions between tool and workpiece. Chemical reactions can also occur within workpiece and tool materials involving constituents elements. [8] [43]

The types of surface alterations associated with various conventional and unconventional machining can be summarised as follows [8]:

- Formation of heat affected zone
- Poor surface finish
- Plastic deformation and plastically deformed debris
- Laps and tears and crevice-like defects
- Microcracks
- Intergranular attack
- Untempered martensite
- Overtempered martensite
- Overaging
- Austenite reversion
- Recast, respattered metal or vapour deposited metal

Possible surface alterations which would happen to nickel-based alloys during abusive conventional machining conditions include the followings:

2.2.1.1 Plastic deformation

Due to the pressure applied to the cut surface by the cutting tool, a plastically affected zone may be formed on the surface of the workpiece. The extent of plastic deformation depends on the process parameters and geometry of the tool. This manifests itself by an elongated grain structure or numerous arc-like slip of atomic layers along the top edge of the individual grains. An increase in hardness is also observed in the plastically deformed regions to a certain depth. The extent of deformation and hardness variation depends on the severity of thermal and mechanical effects in the surface region[45]. It becomes more obvious and serious when the cutting tool is dull and a built-up edge is present. [8].

2.2.1.2 Phase transformation

The high temperatures generated during abusive cutting conditions can cause metallurgical phase transformations in certain materials. Phase changes do occur in the heat affected zones and work in two ways depending on the material type being cut.

Surface hardness can either be reduced due to the effect of high cutting temperatures on the aged-sections or increased because of the formation of martensitic structure. In steels, formation of 'untempered martensite (white layer)' or 'overtempered martensite' are the most common examples to phase changes, the former being harder and the latter being softer than the inner sections of the bulk material. A component with such an inconsistent structure is highly susceptible to fatigue failure [8]. Phase changes do not occur in materials which do not undergo crystallographic transformations as in the case of nickel based alloys.

2.2.1.3 Cracks

Cracking can occur in the form of micro-cracks or macrocracks when machining brittle materials and materials with brittle inclusions. Cracks are usually detrimental to fatigue and stress corrosion properties of components and should be prevented [8]. Warburton observed asymmetrical cracks and tears in the machined surfaces of nickel based alloys, when rough machining with heavy cuts. This was attributed to the combination of a number of thermal and mechanical effects being present under such severe conditions [46]. Fatigue related cracking process in nickel-based alloys can be associated with previously cracked carbides within the matrix caused by the machining process [5].

2.2.1.4 Residual stresses

Machining processes generally induce residual stresses into the surface layer. The stresses may be tensile or compressive or combination of both. The magnitude of residual stresses and the depth of affected surface layer has been found to be proportional to the thermal and mechanical distortion (stresses) induced by the machining processes. [43].

2.2.2 Surface Finish

Surface finish is a term that describes the general quality of a machined surface. Surface finish consists of four key elements that describe the geometrical and visual properties of a machined surface. These elements are surface roughness, waviness, lay and flaws as shown in Figure 2.12 [8].

Flaws are random irregularities such as scratches, cracks, depressions, holes and inclusions etc. In practice, flaws are very rare and generally not specified. Lay is the direction of predominant surface pattern (cutting edge marks) generated by the machining method used. Waviness is recurrent deviations from the ideal surface that have larger spacing than roughness sampling length.

Among these elements, surface roughness is the most commonly used feature to specify the quality of a surface. Surface roughness is generally defined by the arithmetic average, R_a, of the finest measurable geometric irregularities in a machined surface texture [47, 48]. R_a is defined as the arithmetic average of the absolute value of the heights of geometric irregularities from the mean line measured within a standard number of sampling lengths. The sum of the sampling lengths is referred to as 'evaluation length' over which one R_a reading is obtained. The size and the number of a sampling length, also called 'cut-off length', has been standardised based on the range of R_a values required [49].

The final surface finish produced in a machining process is the sum of deterministic and non-deterministic factors. Deterministic factors are the tool geometry and feed rate which are the two main elements used in calculations to predict surface roughness. Non-deterministic factors include the presence of built-up edge, chatter, deflection of cutter or workpiece during cutting, setup errors, inconsistent material etc.

2.2.3 Surface roughness in face milling

Surface finish in milling is less uniform than that in turning where the surface is formed by a single cutting edge at relatively stable conditions. In face milling surface finish can be worsened by the following factors that are not present in turning. The cutter used in face milling consists of multiple cutting edges that usually have variations (runout) in axial and radial directions due to setup and production errors or tolerances. This subsequently causes each cutting edge to cut at slightly different feed rates and depth of cuts. The inherently interrupted nature of the process creates vibration that changes the stability of workpiece and fixture.

When face milling with radiused inserts, the surface roughness can approximately be calculated by using the following formula [8]:

$$R_a = \frac{r - \sqrt{r^2 - \left(\frac{f_z}{2}\right)^2}}{2} \times 10^3 \qquad \text{Eq. 2. 5}$$

Where,

R_a: Arithmetic average surface roughness (micron)

r : nose radius (mm)

f_z : feed per insert (mm)

If the insert used has straight edges without corner radius, as in Figure 2.13, the surface roughness, R_a, is calculated as follows:

$$R_a = h \times 3.18 \times 10^2 \qquad \text{Eq. 2. 6}$$

Where, h is peak-to-valley height and can be found by using the following formula:

$$h = \frac{f_z}{\tan\theta + \cot\alpha_f} \qquad \text{Eq. 2. 7}$$

Where:

fz : feed per insert

α_f : face clearance angle

θ : Cutting edge lead angle

2.3 Chip formation

Chip formation in metal cutting involves localised shear deformation of the work material by the cutting edge of a tool. The relative motion between the cutting tool and the workpiece compresses the material and induces a shear deformation along the primary shear plane that consequently forms the chip. The chip flows over the rake face of the tool and is subjected to a secondary deformation because of the shearing and sliding against the tool. All the phenomena involved in this process of chip formation, such as shear stresses, shear plane, shear angle, cutting forces and velocity, chip thickness, chip velocity etc., are studied and interrelated by metal cutting theories that are usually based on the mechanics of the process. To use orthogonal cutting models has been the general practice in order to develop metal cutting theories. This is due to the

relative simplicity of the orthogonal cutting in comparison with the oblique cutting that involves a three-dimensional geometry [4, 50].

Earlier attempts to explain chip formation process were made by Time and Tresca as reported in reference [51], the former concluding that chip was formed by shear while the latter wrongly attributed it to the compression of the metal being cut. In 1900, Reuleaux, as reported in reference [2], caused a misconception by claiming that the chip was formed by a splitting action due to a crack initiated within material ahead of the tool. This long lasting theory was later disproved in favour of the shear plane theory.

2.3.1 Shear plane models

It has been reported in reference [4] that Piispanen, in 1937, proposed a descriptive model of the chip formation process, known as the 'card model' that contained the basic concept of concentrated shear within a perfect plane (Figure 2.14). According to Shaw [4] this model depicted the basic chip forming process and was used by some other researchers to develop dimensional analysis of the chip formation process and the force relations at the tool point, despite its limitations. However, machining models developed on the basis of simple shear plane theory did not provide good agreement with a wide range of experimental conditions tested [4].

2.3.2 Shear zone models

In fact chip formation occurs within a zone of finite width, rather than in a single plane, which is referred to as the 'primary deformation zone' or 'shear zone' (Figure 2.15) [1, 4]. The analysis of Lee and Shaffer [52] using shear zone based model was followed by many other workers to develop more realistic machining theories on the basis of various assumptions and for different cutting conditions. Oxley [53] presented a model in which strain hardening and variation of shear stress on the tool face were taken into account as opposed to the earlier assumption of ideal plasticity in which the work material was assumed to be non-strain-hardened. Shaw argues that all of the proposed machining theories emphasise one or at most two of important elements at a time and offer good solutions over a limited range of operating conditions. According to him, a perfect machinability theory should concurrently take into account all the important aspects of a chip-forming machining process.

2.3.3 The tool-chip interface

The condition at the tool-chip interface has been one of the important areas of study in metal cutting receiving particular attention. The manner in which the chip flows over the rake face and workpiece moves across the faces and around the cutting edge of a tool strongly influences the performance of a metal cutting process. The presence of built-up edge and of seizure at the tool-chip interface indicates that the chip-flow over the tool rake face is not simple frictional engineering sliding.

2.3.3.1 Friction at the tool-chip interface

The classical friction concept does not apply to the tool-chip interface in most of the metal cutting conditions. According to the Amonton-Coulomb's friction law, the friction force, F, required to initiate sliding, is independent of (a) the apparent area of contact, (b) the speed of sliding and (c) proportional to the normal force, N, acting on the interface where sliding occurs [1].

$F = \mu N$ Eq. 2. 8

Where μ is coefficient of friction

Surfaces of components in engineering applications are never completely flat on microscopic scale and made of small 'peaks' and 'valleys'. Therefore when two surfaces are in contact, under loading conditions in engineering sliding, the 'real area of contact' (Ar) is often less than 1 % of the 'apparent area of contact' (A) [1]. An increase in normal force will cause a corresponding proportional increase in the real area of contact through plastic deformation of the peaks, thus the mean stress on the surface remains constant.

When the normal force is increased to such an extent that it is no longer possible for the real area (Ar) to increase proportionately to the applied load and it becomes independent of the normal force. In this case, for the movement to occur, frictional force is needed to shear the weaker material over the whole area of contact. Three distinctive regimes in solid friction were graphically depicted by Shaw et al [4] as shown in Figure 2.16.

In metal cutting, the condition at the tool-chip interface is mostly one of this third regime, due to typical high value of normal stresses (up to 3.5 GN/m2 when machining

steel [48] over the large portion of the tool-chip contact zone. Therefore the above formula for the classical engineering friction cases does not apply to the case of tool-chip interface.

Zorev [54] presented a model of stress distribution on the rake face of the tool assuming that it consisted of two regions namely 'sticking' and 'sliding' where regime-III and I hold respectively (Figure 2.17). The tangential force acting on the tool rake face therefore equals to the sum of tangential force components in sticking and sliding regions.

2.3.3.2 Seizure conditions at tool-chip interface

The behaviour and wear characteristics of a cutting tool and the characteristic of chip formation for a given process-tool-workpiece combination can only be thoroughly understood by investigating tool-chip interface. Trent [1], having presented the results of the metallurgical analysis of various used tools, chips and quick-stop sections, concluded that the contact between tool and chip is so complete that sliding is not possible over a large part of the interface under most machining conditions. This phenomenon is referred to as 'condition of seizure' as depicted in Figure 2.18. When the condition of seizure exists, the surfaces of tool and chip are mechanically interlocked or bonded over the corresponding area, and chip movement takes place by shearing action. Therefore, a zone of extremely intense shear is generated within the chip close to the interface. This zone is known as 'flow zone' or 'secondary shear zone' an example of which is seen in Figure 2.19. In the flow zone a steep velocity gradient exists and the chip is sheared under extremely high rates of strain, temperatures and compressive stresses [55, 56]. The presence of these three factors at the contamination-free tool-chip interface encourages the formation of seizure [57].

Most commonly, seizure and sliding coexist at the tool-chip interface, the latter being in the peripheral regions (Figure 2.18) [58]. At low cutting speed and feed rates where temperature is below the recrystallisation level of the work material, the presence of seizure causes extreme strain hardening in the flow zone. Stacking of elongated layers due to strain hardening results in the formation of built-up edge at the interface. Alternatively, the presence of seizure at higher cutting conditions where temperature is

high enough to cause recrystallisation in the work material, strain hardening ceases and yield stress is reduced by dynamic recovery that occurs as temperature increases [59].

Wright [60] performed machining tests on commercially pure lead, aluminium, copper, iron and nickel using high speed steel, tungsten carbide and sapphire cutting tools. He observed that sliding occurred for a short period when cutting soft metals with sapphire tools at low cutting conditions. This was attributed to the presence of contaminants on the tool surface that prevented seizure. The size of the seized area is influenced by such factors as material purity, tool material and geometry, cutting time, cutting speed and feed, lubrication and the stability of the machine [61].

2.3.3.3 Built-up edge (BUE) in machining

At certain machining conditions, generally when cutting alloys at relatively low speeds and feeds, a built-up edge is formed on the rake face within the vicinity of cutting edge (Figure 2.20). It is of a dynamic nature and constructed by successive thin layers of strain hardened material in the flow zone where seizure also takes place. As built-up edge grows, the flow zone shifts from the tool face to the top of the BUE. It can act as an extension of cutting edge and hinders surface finish and cutting edge geometry. After reaching a certain height, BUE becomes unstable and carried away by the flowing chip or workpiece when it cannot resist the shearing forces induced by chip flow. [1]

Four typical forms of BUE (Figure 2.21) were observed associated with the changes in cutting speed and hence with the consequent rise in cutting temperature [62]. These are (1) positive wedge, (2) rectangular wedge, (3) negative wedge and (4) flow layer wedge, in order of formation with increasing cutting speed. The growth and the type of BUE are affected also by the amount of fracture, micro cracks in the highly strained and plastically deformed layers [62].

Oishi [63] has reported that increasing workpiece hardness helps to eliminate BUE in machining steels. The effect of increasing feed rate and rake angle of the tool was shown to have similar effect.

The nucleation and bonding mechanisms of built-up edge were attributed to the presence of one or more of the following physical-chemical interactions on atomic or molecular scale; a) metallic bonding, b) diffusion at the interface, c) metallic compound or alloy production at the interface [1, 4, 62].

2.4 Heat in metal cutting

In metal cutting, almost 99 % of the work done is converted into heat due to large amount of plastic strain in the deformed chip [1]. When cutting high strength and high temperature resistant materials such as nickel-based and titanium alloys, the performance of the cutting tools is limited due primarily to the high temperatures and stresses generated. Taylor [3] realised the effect of heat on tool wear and developed a system to apply coolant during cutting to improve tool life.

There are three regions where heat is generated in metal cutting, as shown in Figure 2.22 [4, 64]:

a) Primary shear zone,

b) Secondary shear zone on the rake

c) Contact area on the clearance (flank) face

Under normal cutting conditions, about 80 % of the energy is consumed in the primary and secondary shear zones, 18 % at the rake face and about 2 % at the flank face [65]. Most of the heat generated remains in the body of the chip, but a variable proportion is conducted into the workpiece. Boothroyd [48] has shown that this proportion is approximately 10-15 % for high metal removal rates at high cutting speeds and can be as much as 50 % at very low cutting speeds. The temperature generated in the chip body depends on the properties of the material being cut and on the cutting conditions. At comparable cutting conditions, the chip body temperature is between 200 °C to 350 °C, for low or medium carbon steel, while it can be as high as 650 °C to 850 °C when cutting hardened steel, nickel based and titanium alloys. This range of temperature is high enough to cause changes in hardness and the structure of steel and tungsten carbide tool materials [1, 66, 67].

With the presence of seizure or built-up edge, secondary shear or flow zone becomes the main heat source to raise the tool temperature, as the strain and strain rates in this zone are many times greater than in the body of the chip, being of the order of 100 and 10^4 s^{-1} respectively for multi-phase alloys. The heat conducted into the chip from the flow zone is very limited due to very short contact time (fraction of a second) and relatively large volume of the chip body. However as the tool is almost in constant contact with the flow zone, it acts as a heat sink that has the same temperature as the flow

zone at the interface. This process results in a stable temperature gradient (Figure 2.23) within the tool which is an important factor limiting the tool life and metal removal rates when cutting high strength materials [1].

2.4.1 Temperatures in face milling

In interrupted cutting operations, tool temperatures vary periodically due to cyclic engagement and disengagement of the tool with the workpiece. Cyclic variations in tool temperatures can lead to tool failure due to thermal fatigue that causes crack initiation within tool material as suggested previously by some workers [21, 68]. The rate of crack growth increases with the peak temperatures during cutting cycle and with the increase in the difference between peak and low temperature levels [69].

As shown in Figure 2.24, peak temperatures in intermittent cutting are lower than that of continuous cutting at identical cutting conditions. This, together with the fact that peak temperatures are reached for short periods only, leads to a reduction in diffusion or chemical wear [70]. Figure 2.24 suggests that peak temperatures depend more on the duration of cutting cycle than on that of non-cutting cycle.

During the cutting cycle, induced thermal stress in the tool is compressive and of a maximum value. However, it gradually diminishes with depth, X, from the tool surface and becomes tensile beyond certain distance as shown in predicted model by Chakraverti et al.[71] in Figure 2.25. This is due to the fact that interior sections of the tool is much cooler than its surface. During non-cutting cycle, the stress in the tool surface is tensile and gradually diminishes to zero at certain depth. It has been reported by several researchers [68, 72] that thermally induced cyclic stresses are responsible for the formation of 'comb cracks' initiation during milling operations.

CHAPTER 3

CUTTING TOOL MATERIALS

3.1 Introduction

The cutting tool is an important element of the machining system and is frequently one of the most critical elements affecting the productivity in metal cutting operations. The need to increase (a) productivity, (b) the quality of machined components and (c) to machine harder or difficult-to-cut materials have been the driving force for the development of various cutting tool materials, following the advancement in metallurgical and materials science and technology [74]. Figure 3.1 shows the introduction of various cutting tools materials and a comparison of their relative performance in terms of cutting speed. At present, the variety of cutting tool materials is very large when considering the number of different grades that each generic group has.

3.2 Requirements of tool materials

Cutting tool materials are required to have following properties, ideally to the maximum degree possible, in order to perform satisfactorily in machining operations [75, 76]:

a) High hardness and hot hardness

b) High fracture toughness

c) High tensile and compressive strength at elevated cutting temperatures

d) Good thermal and mechanical shock resistance

e) High chemical stability

f) High abrasion resistance

General trends of the above properties for some selected tool material groups are presented in Figure 3.2.

In practice, machining conditions and the expected outcome from a given machining operation can vary to a great extent. No single tool material can meet the whole range of requirements expected from a specific operation such as high rates of

metal removal, surface finish, dimensional accuracy, long tool life and reduced costs etc. Therefore a proper selection of tool material for a specific application is of great importance and provides substantial advantages. This means that the best tool material is usually the one which meets the objectives with maximum efficiency at the lowest total cost per component in a specific application. Tool cost alone can never be a reliable indication of the overall performance [4].

3.3 Major classes of tool materials

A wide range of cutting tool materials of different properties and performance is available today for very diverse machining applications. Among these, coated and uncoated cemented carbides and high speed steel tool materials are the most widely used cutting tool materials. Ceramic tool materials with improved toughness and thermal shock resistance are increasing their share in metal cutting industry. They are the best suited tool materials for high speed machining applications [77].

Tool materials can be classified into following major families:

1) High speed steels (HSS)
2) Cemented carbides
3) Cermets
4) Ceramics
5) Ultra-hard tool materials

3.3.1 High speed steels (HSS)

Taylor and White [3] developed a new heat treatment technique and applied it to a modified Mushet alloy tool steel by increasing the amount of tungsten and chromium to 8 % and 3.8 % respectively [4]. This heat treatment involved heating the alloy to just below the solidus temperature (1250-1290 °C) and cooling first to 620 °C in molten lead and then to room temperature. Following this process, the tool was tempered at temperatures about 600 °C. This tempering process resulted in the formation of finely dispersed tungsten, molybdenum and vanadium carbides (secondary phase) within a main martensitic structure. Presence of these carbides increased the hot hardness of HSS tools up to 600-650 °C [1]. With the HSS tools, cutting speed and metal removal rates were increased by 4-6 times that of traditionally heat treated carbon or low alloy tool steels [1].

HSS tools are broadly classified as 'T type' and 'M type' with respect to the prime alloying elements, being tungsten (up to 22 %) and molybdenum (up to 9.5 %) respectively. The other alloying elements are carbon (0.7 -1.5 %), chromium (4-4.5 %) vanadium (1-5 %) and cobalt (up to 9.5 %) [78]

High speed steels are produced by three different techniques; cast, wrought and powder metallurgy (PM). Among these, the PM technique produces a more uniform microstructure which ensures consistent and increased performance of the tools [74]. Further coating and surface treatment processes such as nitriding, oxidation and ion implantation [79] and physical vapour deposition (PVD) of various nitrides [80] are applied in order to improve specific properties of HSS tools. HSS is principally used to make cutting tools such as drills, taps, dies, end mills, broaches, reamers etc. The use of HSS tools is restricted to relatively low cutting speeds compared with cemented carbides.

3.3.2 Cemented carbides

Cemented carbides were first introduced in Germany in 1923 and used for making drawing die components [81]. Currently cemented carbide cutting tools are probably the most common high production tool materials employed in industry. They have superior hardness (~ 1400 to 1700 HV), hot hardness and chemical stability than HSS.

They are fabricated by powder metallurgy technology in which fine particles of tungsten carbide, WC, (varying from ~ 0.5 to 5 μm) are mixed with a metal binder, usually cobalt, and pressed into compacts. The proportion of cobalt binder varies from 4 to 12 % by weight in grades for metal cutting applications. These compacts are then sintered at the temperature of around 1350 °C whereby cobalt melts and wets carbide particles [79]. Using low pressure 'HIP-vacuum sintering' furnace, carbides with enhanced microstructure completely free from pits, flaw and porosity have been produced [82].

Various combination of toughness and hardness properties can be achieved by controlling the amount of cobalt content, grain size of WC particles and proportion of one or more of the cubic carbides (TiC, TaC, NbC).

Cemented carbides can be classified into three main categories as follows:

1.Straight tungsten carbides (WC/Co alloys)

2.Mixed cemented carbides (WC/TiC/TaC/NbC/Co)

3.Coated cemented carbides

3.3.2.1 Straight tungsten carbides (WC/Co alloys)

Straight WC/Co grades are regarded as the simplest and basic cemented carbides. As a result of carefully controlled processing, only two phases, WC and Co, should be present in the microstructure, without porosity, free carbon or eta phase. Too high a carbon content results in free carbon while too low a carbon content leads to the formation of eta phase (Co_3W_3C) [83]. Presence of porosity and these phases in the microstructure degrade the properties of cemented carbide tools.

Sometimes cubic carbides, up to 3 wt %, (carbides of tantalum, titanium, vanadium or niobium) are added to ensure grain refinement and maintain a consistently fine microstructure.

The properties of hardness and toughness of the straight tungsten carbides are dependent on two factors [84]

1. Cobalt content

2. The grain size of WC particles.

Increasing cobalt content increases the toughness while reducing the hardness and compressive strength of the tool. This means better shock resistance but poor wear resistance and hot hardness. The finer the grain size the harder and more brittle the tool becomes for a given composition of WC/Co alloy.

Straight tungsten carbides grades are primarily used for machining cast iron, non-ferrous and non-metallic materials. They are not effective in machining steels, as WC/Co atoms diffuses into the steel chip over the contact zone which causes severe crater wear on the rake face of the tool.

3.3.2.2 Mixed cemented carbides (WC/TiC/TaC/NbC/Co)

Mixed cemented carbides contain relatively small amounts of titanium carbide (TiC), tantalum carbide (TaC) and niobium carbide (NbC). These carbides are also referred to as 'cubic carbides' due to their cubic crystal structure and are of higher hardness than WC [79]. Tungsten carbide, WC, has the largest proportion in the matrix that constitutes usually about 20 wt % cubic carbides [85]. Addition of TiC carbide

increases the hot hardness and diffusion wear resistance (chemical stability) of the tool particularly when cutting steels and ductile cast iron at high cutting speeds due mainly to their lower free energy of formation (Table 3.1). Tantalum and niobium carbides also increase crater wear resistance and improves thermal shock resistance of the tool which is very useful in interrupted cutting. In most cases matrix carbide of tantalum and niobium (TaNb)C is added as separation requires expensive processes because of their chemical similarity. However addition of cubic carbides increases brittleness which is not desired in interrupted cutting, despite giving good diffusion and abrasion wear resistance [75].

3.3.3 Classification of cemented carbides

International Standard Organisation (ISO) has classified carbide tools in respect of their broad application areas, hardness (wear resistance) and toughness properties [86]. The ISO standard uses an alpha-numeric system accompanied with particular colour codes for the classification tungsten carbide tools (Table 3.2).

It is manufacturers' responsibility to decide in which category their product falls. It helps tool users to choose right product for their applications and tool manufacturers to classify their products.

In the ISO classification system there are three main groups of tool materials; P, M and K series that are also accompanied by colour codes of blue, yellow and red respectively for easy recognition. P, M and K series are subdivided into 6, 4 and 5 categories respectively that are designated with numbers of increments of 10. For example P series are numbered as P01, P10, P50 in order of increasing toughness (Table 3.2).

P grades are highly alloyed mixed carbide grades (WC/TiC/(Ta/Nb)C/Co) mainly used for machining wrought, cast and hardened steels which produce long, continuous chips. M grades are low-alloy mixed carbides used for machining ferrous and non-ferrous materials with long and short chips including high temperature resistant materials such as nickel-based and titanium alloys. K grades are straight cemented carbides used for machining cast irons, ferrous, non-ferrous and non-metallic materials that produce short, discontinuous chips.

In the United States, an application-oriented classification system, known as C-grade system, is used to assists in the selection of proper tools. C-grade classification system is simpler than ISO system, and does not reflect the properties of tool materials but classifies the work materials in a very broad term. C-grade system has two main groups for metal cutting applications. Each group contains 4 grades designated as such from C1 to C4 and from C5 to C8. First group is for machining cast iron, non-ferrous alloys and non-metallic materials and the second group for carbon and alloy steels [79, 87].

3.4 Coated Cemented Carbides

Although toughness, hardness, especially hot hardness, and chemical stability are the prime requisites from a cutting tool, these properties become highly important when cutting difficult-to-cut materials under unstable cutting conditions such as interrupted cutting and milling where severe cyclic mechanical impacts and temperature fluctuations are present.

But with uncoated carbide tools, tool makers have to balance these properties at a certain ratio as increasing one of them may mean decreasing the others whereas all are requested to be of as high value as possible. However to take one step forward was virtually impossible when there are only a few parameters to change, namely cobalt content, cubic carbides, grain size and the geometric design until the introduction of coatings [88].

Since late 1960s, coating cemented carbide inserts with refractory compounds using first CVD and subsequently PVD techniques has opened a new era in the cutting tools history of development. An average of three to four times increase in tool life when milling steel and cast iron has become possible. It has been reported that more than 60 % of the inserts sold in the USA are coated, a large proportion of which (~ 80 %) is employed in turning operations. [80, 85].

This development trend of coated tools is still continuing in mainly two areas. The first broad area of research is to develop new refractory compounds for coating applications. Examples include PVD coating with TiCN, TiAlN, TiZrN and CrN compounds [85] and CVD synthetic polycrystalline-diamond (PCD) coating of ceramic and carbide cutting tools [89]. The second area of interest is to improve coating process through new methods and application techniques. It has been reported that with a new

multi layer CVD coating method, deposition of 60 alternating layers of TiN and TiCN at nanometer level (~ 50 nm) improved tool life by 300 % when face milling a steel casting component [90]. Functionally graded interface between substrate and coating would be another promising development to increase bonding strength as reported by Kohno [91].

3.4.1 Chemical vapour deposited coating (CVD)

CVD process involves the depositing of refractory coatings at temperatures from 900 °C to 1100 °C through chemical reaction in a sealed reactor (Figure 3.3). Single layer TiC of ~ 5 μm thickness was the first compound deposited by this technique. Later refractory compounds of TiN, TiCN, Al_2O_3 and occasionally HfN were deposited in multilayer form to combine such properties as diffusion wear resistance, abrasion resistance, better lubrication and hot hardness (Table 3.1). Multilayer coatings involves alternating deposition of more than one coating material to make use of their outstanding properties in combination (Figure 3.4) [82].

When the tool was first TiC coated by CVD technique, a 25 % loss in transverse rupture strength (TRS) was found largely due to the formation of brittle eta-phase, (surface decarburization in the form of Co_3W_3C or Co_6W_6C) in the substrate just below the coating (Figure 3.5) [82, 88]. Deficiency in carbon content results in the formation of eta-phase. Therefore it is important to produce stoichiometric tungsten carbide with 6.13 wt. % carbon content to attain structural stability [79, 83]. This reduction in TRS is also attributed to tensile residual stresses formed in the coated layers [82, 92].

Although this hard phase of carbide has contributed to tool's resistance to abrasion it is very detrimental, when its thickness is considerably high and uncontrollable, to the tool's performance causing premature failure in milling operations[85]. This is why coated milling tools were initially not accepted by the industry until improvements in coating process were achieved.

While high temperatures employed in the CVD process provides strong bonding at the interface [85], thermal expansion mismatches between the substrate and the coating materials cause tensile residual stresses and adversely effect the coating adhesion. These stresses tend to concentrate more at sharp corners of the tool and often produce cracks in the coating [85]. Formation of thermally induced cracks within the coating

layer intensifies edge chipping in milling applications [80, 82]. Therefore sharp corners have to be eliminated by honing to minimise eta phase formation and increase strength prior to the coating process [85].

By using much tougher grades as substrate than normally used grades in milling, successful applications of the coated tools started to appear, including milling high temperature titanium and nickel-based alloys. The development of cobalt-enriched tungsten carbide substrates (Figure 3.4) and medium-temperature (700 - 900 °C) CVD TiCN coating increased the application of coated tools in milling and interrupted processes. Lower process temperatures and faster deposition rates in the medium-temperature CVD coating process hindered the formation of eta phase at the interface and thermally induced tensile cracks within layers [79].

Particularly for interrupted cutting applications, engineered substrates with cobalt-enriched peripheral zone up to 10 to 40 μm depth, which contains about three times the cobalt level of normal matrix, were developed to combine good deformation resistance and fracture toughness in one tool. The inner sections of these substrates were strengthened by adding higher levels of cubic carbides [93].

3.4.2 Physical vapour deposited coating (PVD)

The application of PVD coating techniques to the cutting tools became available in the 1980s. In PVD coating process, metal atoms (Ti, Hf, Zr, etc.) of the coating compounds are evaporated, ionised and accelerated toward the tool surface by applying a high voltage in the presence of reactive gases that contain nitrogen or carbon atoms such as N_2, CH_4, NH_3. The process is performed in vacuum chamber at temperatures in the range of 200 to 500 °C (Figure 3.6).

In many application PVD coated tools were found to perform better than CVD coated tools [94]. According to Edwards [76], in finish milling of steels, the performance of CVD multi-layer coated carbide is relatively less than PVD TiN coated tool when compared in terms of the surface finish produced. The poor performance of CVD coated tools is attributed to its requirement of edge honing (rounding) prior to coating without which the tool edge becomes too sensitive to mechanical impacts after coating [93]. Hard coatings, particularly TiN, improve chip flow by reducing the frictional forces and associated temperatures at the tool-chip

interface (Table 3.1) [93]. In a face milling experiment on 1020 steel [85] a PVD-TiN coated insert outperformed an uncoated tool with an increase in metal removal rate and tool life by 40 % and 42 % respectively. It is stated that PVD TiN inserts would perform well on high-temperature alloys and in low speed applications due to the lubrication effect of fine grain TiN coating.

3.4.3 General advantages and disadvantages of PVD coating relative to the CVD

1. Eta phase formation is eliminated in the PVD coating process due to lower temperatures (< 500 °C) than in CVD process. [80, 82].
2. PVD coating results in negligible loss in edge strength
3. With PVD coating little or no honing of substrate is necessary [95].
4. PVD coating can be applied to a wider range of substrate materials including HSS
5. PVD coating allows more precision in dimensional accuracy of the tools.
6. PVD coating tends to reduce built-up edge formation and offers better chip evacuation when milling titanium and a wide range of carbon and alloyed steels [80].
7. PVD coating performs better at lower cutting speed range where CVD coated tools fails due to chipping or breakage known as 'lower speed breakage' of carbides. This was attributed to the better chip adhesion/abrasion resistance of PVD/TiN coating acting as a solid lubricant at the tool/chip interface, hence diminishing or eliminating BUE formation [80].
8. PVD coating is better applied to sharp tools required for finish cuts [82, 85].
9. PVD process produces crack-free coating with finer grain sizes. [85].
10. In some cases compressive residual stress can be induced to the PVD coatings which results in as high transverse rupture strength as that of uncoated tools [80, 85].
11. The adherence strength of PVD coating layer is relatively less than that of CVD coating.

3.5 Cermet cutting tools

The term 'cermet' is derived from the words *ceramic* and *metal* and refers to the cutting tools composed mainly of titanium carbide and titanium carbonitride based ceramics particles with a metallic binder phase (nickel, cobalt and molybdenum). As

with cemented carbides, cermets are manufactured through liquid phase sintering process. The distinguishing feature of cermets is that the hard particles of cermets have their typical two-phase core-rim microstructure resulting from spinodal decomposition. As schematically represented in (Figure 3.7), the core is rich in titanium and nitrogen while the rim is rich in molybdenum and carbon which promotes wetting with binder phase [79]. Good adhesion results in higher toughness by forcing crack propagation through the ductile binder. Cermets of molybdenum carbide and tantalum-niobium carbide grades are capable of enduring thermo-mechanical cyclic impacts associated with the milling process [79]. Representative values of some of properties of cermets are shown in Table 3.3.

3.6 Ceramic tool materials

Ceramic tools are broadly classified as aluminium oxide (Al_2O_3) and silicon nitride (Si_3N_4) based [96]. They posses higher hot hardness, wear resistance, plastic deformation resistance, chemical stability and compressive strength properties over cemented carbide cutting tools [97]. However, ceramic tools have inferior thermal shock resistance and fracture toughness compared to cemented carbides. Although the use of ceramic tools in overall mass production lines reaches nearly 15 % of the whole consumption of indexable inserts, in some specific applications, however, for example machining cast iron automotive components, this ratio is more than 50 % [98]. Significant improvements in processing, sintering aid refinements and addition of various toughening and alloying compounds led to the development of ceramic tools with better overall strength, thermal shock resistance and fracture toughness. As a result, the application area of the ceramics tools widened including alloy steels, nickel based aerospace materials [99].

3.6.1 Alumina-based ceramic tools

Monophase alumina (Al_2O_3) ceramic tool was the first developed and successfully used ceramic tool for machining cast iron and steels at high speeds and feed rates due to good hot hardness and chemical stability [100]. Their poor fracture toughness and low thermal conductivity make them very susceptible to mechanical and thermal shocks respectively. To improve thermo-mechanical properties 25-40 vol. % TiC dispersed powder were added to improve thermal conductivity and thermal shock resistance

[101]. The presence of TiC second phase also increased the hardness and hot hardness properties of the alumina-titanium carbide composite but fracture toughness was still poor.

The fracture toughness of the alumina was increased by alloying with either zirconia (ZrO_2) or silicon carbide (SiC) whiskers. Zirconia-toughened alumina ((Al_2O_3- ZrO_2) consists of partially stabilised tetragonal zirconia particles (5-30 vol. %) [79] dispersed in alumna matrix [102]. Fracture toughness of zirconia-toughened alumina can reach twice as much as that of pure alumina with a reduction in hardness. Increase in fracture toughness results from the energy-absorbing ability of metastable ZrO_2 during transformation into a stable monoclinic crystal structure under thermal stress [103].

Adding SiC whiskers (20-40 vol. %) into alumina matrix with subsequent hot pressing results in a twofold increase in toughness [104]. Whiskers are small fibres of single crystal SiC having a diameter of 0.5 to 1 μm and a length of 10 to 125 μm.. Fracture toughness is enhanced by the resistance of whiskers to displacements. SiC whiskers have also a higher thermal conductivity and a lower thermal expansion coefficient than Al_2O_3 both of which improve the thermal shock resistance of the matrix [104]. SiC whisker-reinforced Al_2O_3 tools are successfully employed in some machining applications on nickel based superalloys [105].

3.6.2 Silicon nitride (Si_3N_4) based ceramics tools

Silicon nitride (Si_3N_4) based ceramic tools posses higher hot hardness, thermal shock resistance and fracture toughness than traditional Al_2O_3 based tools. However, the high chemical reactivity of Si_3N_4 renders these tools unsuitable for machining steels where high rates of flank and crater wear limit the tool life [106, 107]. There are three families of silicon nitride (Si_3N_4) based cutting tools:

1.Pure silicon nitride with binding phase

2.Sialons

3.Silicon nitride based composites

Densification of Si_3N_4 particles during sintering is achieved by addition of various oxides such as Y_2O_3, MgO and Al_2O_3, that react with SiO_2 and form a glassy liquid-

phase during sintering. Thus pure silicon nitride ceramics consists of two phases; Si_3N_4 crystals and an intergranular glassy binding phase.

Sialon tools are produced by reacting Si_3N_4 with Al_2O_3 and AlN at high temperatures and pressure. The new compound is called β'-Sialon in which some of the silicon atoms are replaced with Al and some of the nitrogen with oxygen atoms. Densification is achieved by adding yttria (Y_2O_3) that form the glassy binding phase. Successful application of Sialon tools in turning nickel-based aerospace alloy (Incoloy 901) at a speed range of 125 to 185 m/min has been reported by Jawaid [9].

Si_3N_4 based composites tools are produced by adding refractory materials such as TiC, TiN, HfC, etc. as dispersed second phase into the matrix. The presence of dispersed phases increases the tool hardness and fracture toughness [108].

3.7 Ultra hard tool materials

There are three kinds of ultra hard tool materials viz. diamond, polycrystalline diamond (PCD) and Cubic Boron Nitride (CBN).

3.7.1 Single-Crystal Diamond

Single crystal diamond is the hardest material known with a hardness ranging between 6500 and 12000 HV depending on the measured crystallographic directions due to its anisotropic character [109]. Diamond has a crystal lattice consisting of two interpenetrating face-centred cubic structure in which each carbon atom is attracted to four neighbouring atoms by covalent bonds [110].

The following properties make them attractive tool materials for particular applications (Table 3.3) [112]:

1.Extreme hardness.

2.Outstanding wear resistance.

3.Low coefficient of friction.

4.Low thermal expansion and high thermal conductivity which give good thermal shock resistance.

5.Sharp cutting edge.

However natural diamond is very brittle and reacts extensively with ferrous materials [111]. Reaction involves transformation of diamond to a graphitic form or

interaction with iron and/or surrounding atmosphere (oxygen) at high cutting temperatures over 730 °C [1]. The main application areas includes machining of non-ferrous metals (such as aluminium alloys, copper, brass, etc.) and abrasive non-metallic materials such as fibre reinforced plastics, fibreglass, graphite etc. [112].

3.7.2 Polycrystalline Diamond (PCD)

PCD tools become available after synthetic diamond was produced by heating graphitic carbon at high pressures and temperatures over 8 GPa and 1500 °C. PCD tools consist of randomly oriented diamond particles (2 to 25 μm) sintered together with a metallic or ceramic bonding material to maximum densification [113].

Unlike single crystal diamond, PCD tools behave as isotropic materials and possess higher toughness while maintaining still exceptional wear resistance. As with natural diamonds, PCD tools are mainly used for machining non-ferrous and non-metallic materials [114, 115].

3.7.3 Cubic Boron Nitride (CBN)

By utilising the same technology used for synthetic diamond, synthesis of CBN from hexagonal boron nitride was achieved in the late 1960s. CBN has an identical crystal structure to that of diamond, consisting of boron and nitrogen atoms. Its hardness is in the range of 3500 to 4500 HV which is second to that of diamond [116]. At 1000 °C temperature, the hardness is around 1800-2000 HV which is similar to that of tungsten carbide at room temperature [116]. The other properties include superior abrasion resistance and thermal conductivity, lower friction and thermal expansion coefficient (Table 3.3)

Polycrystalline cubic boron nitride (PCBN) tools are produced following a sintering process as in the case of PCD. Properties of PCBN tools vary depending on the grain size, the type and proportion of second-phase material [116].

CBN tools can be used for machining iron, cobalt and nickel based materials because the reactivity of CBN with these materials is much less than that of diamond at high cutting temperatures. However, CBN easily reacts with nitride and boride-forming metals such as titanium, aluminium, zirconium etc. [117]. CBN has oxidation resistance up to 1400 °C and conversion resistance back into hexagonal (graphitic) structure up to 1700 °C indicating that CBN is chemically more stable than diamond [118].

3.8 Selection of tool materials

As complete an economic analysis as possible should always be carried out in order to chose the best suited cutting tool material for a given workpiece and process. It is feasible to consider the entire economic frame of any machining operation in order to justify ultrahard and very expensive cutting tool materials such as PCD and PCBN. Followings should be taken into account for such an analysis:

1.The capability and constraints of the machine tool (available speeds, power etc.)

2.The quality requirements of the product (surface finish, tolerances etc.)

3.Production schedules (minimum costs per piece, maximum productivity, etc.)

When the tool-change time is long and the tool life is relatively short, selecting a tool material on the basis of longer tool life would be an appropriate choice so as to minimise non-productive down time. However, if tool-change time is very short or has no influence on machine's up time, a tool which will increase productivity should be selected [119].

CHAPTER 4

TOOL WEAR MECHANISMS AND FAILURE MODES

4.1 Introduction

In almost all conventional metal removal applications where single or multi-tooth cutters with solid tips are used, after a certain period of time the cutting tool ceases to cut efficiently or fails entirely due to deformation of various types in its original geometry which is called wear. The wear rate of a given tool depends very much on the type of wear process and/or contributing mechanisms. Therefore realistic tool life predictions and selection of a suitable tool material for a particular operation require correct diagnosis of the controlling wear mechanisms and an understanding of the ways in which cutting tools fail [1, 123].

Tool wear is caused by mechanical and/or chemical interaction between cutting tool and workpiece during metal cutting processes. In some cases it is not possible to see these changes on the tool without using microscopes but as soon as they become significant, the indications of severe wear can be detected by looking at the presence of one or more of the following conditions:

a) Unexpected increase in power consumption
b) Rapid increase in cutting temperature
c) Excessive chatter or vibration
d) Operation becomes very noisy
e) Dimensional instability
f) Deteriorated surface finish

Wear resistance of cutting tools cannot be determined by one simple laboratory test or related to only one of its properties such as hardness. The wear in metal cutting applications differs, in a number of ways, from the wear types encountered in other mechanical systems. In metal cutting, the factors that influence the wear mechanisms and failure modes include

the tool material, workpiece material, tool geometry, the type of machining process, and the cutting conditions employed.

Commonly observed tool failure modes and primary contributing mechanisms will now be discussed.

4.2 Tool failure modes

According to the ISO 8688-1 standard for tool life testing in face milling [124], there are three major classes of tool deterioration:

a) Failure by progressive tool wear

b) Brittle fracture, chipping and cracking

c) Plastic deformation

4.2.1 Progressive tool wear

Flank and crater wear are the most common wear modes resulting from the progressive loss of tool material during machining. Tool failure by progressive types of wear is always favoured due to its high level of predictability and reliability from the aspects of production and quality control in manufacturing [125].

4.2.1.1 Flank wear

The wear land that develops along the flank (clearance) faces of major and minor cutting edges of the tool, is known as 'flank wear'. It is usually caused by abrasive wear mechanisms, however attrition wear mechanism at low cutting speeds and temperature-depended diffusion wear mechanism at high cutting speeds can be major contributing factors [1, 4]. Flank wear is widely used as a tool rejection criterion due to its progressive nature and higher levels of predictability than other failure modes [126].

The rate of flank wear changes with cutting time and cutting speed as shown in Figure 4.1. The wear rate is rapid during initial cutting after which it increases at a steady rate until a critical wear land width is reached. Beyond this point, wear rate increases rapidly.

In practice, different types of flank wear can occur during machining. ISO 8688-1 [124] describes the following three common types of flank wear:

a) Uniform flank wear (VB1): As shown in Figure 4.2, uniform wear land is normally of constant width and extents over those portions of the tool flanks adjoining the entire length of the active cutting edge.

b) Non-uniform flank wear (VB2): Non-uniform flank wear has an irregular width along the lower border of the worn area as shown in Figure 4.3.

c) Localised flank wear (VB3): Exaggerated forms of flank wear can develop at localised points of tool flank as illustrated in Figure 4.4. Notch wear or notching is one special form of this type of wear which can develop on the part of the major flank adjacent to the depth-of-cut line, while groove wear, similar to notching but usually smaller, develops at the free section of the minor edge. The factors that cause notching include the presence of (a) abrasive inclusions or work-hardened layers, (b) stress concentration, formation of thermal cracks and mechanical fatigue due to force fluctuations at the free surface, (c) chemical reaction between tool and/or workpiece surfaces and atmospheric oxygen at the interface between the tool and atmosphere [1, 4, 127].

4.2.1.2 Rake face wear

Progressive tool wear on the rake face of the tool occurs in two distinctive fashions, namely crater wear and stair-formed face wear (Figure 4.5) depending on tool-workpiece combination and cutting conditions. Crater wear forms parallel to and some distance away from the main cutting edge whereby the highest temperatures are generated on the rake face when cutting steels and cast iron. However, the hottest point on the tool is very close to the cutting edge when machining some materials, such as pure nickel and nickel-based alloys [66], hence stair-formed wear can develop as shown in Figure 4.5-b.

Rake face wear is usually controlled by temperature-dependant diffusion wear mechanisms [1] with, in some cases, an attendant superficial and discrete plastic deformation [128]. In the low speed regime however, mechanically activated abrasion and/or attrition wear occurs caused by loose tool particles due to flow-induced microfracture, grain boundary separation and thermal and mechanical fatigue [129].

4.2.2 Brittle fracture

Brittle fracture of the tool material in the form of chipping, flaking or catastrophic breakage (Figure 4.6) occurs as a direct consequence of sudden unfavourable mechanical loading or following a crack formation due to mechanical and thermal fatigue during milling or interrupted cutting, where the tool is cyclically subjected to loading and unloading [130]. Thermo-mechanical fatigue during interrupted cutting can cause subsurface crack nucleation leading to chipping and plucking of cutting tools. Therefore tools having subsurface defects or porosity are highly susceptible to fatigue related failure [131]. Concerning the chipping at the cutting edge of carbide tools, two types have been reported as 'mechanical type' and 'adhesion type' when face milling hardened steel and stainless steel. Mechanical type has been attributed to the plastic deformation of the binder phase due to cyclic stress while adhesion type chipping is caused by repeated adhesion and breaking off chip from tool surface or presence of BUE at the interface [132]. Speaking of the mechanical type chipping that occurs prematurely particularly at low cutting speeds, Al-Tornachi [133] reported that there were no observable early cracks prior to chipping, suggesting their abrupt character. Using a honed cutting edge was reported to have almost completely eliminated this type of chipping when cutting hardened steel.

Fracture that occurs as a result of initial plastic deformation and associated cracking is not considered brittle [1]. It is, therefore, important to correctly diagnose the mechanisms involved in order to prevent this kind of failure.

With coated tools, coating may also serve as a region of easy crack initiation, increasing the tendency towards fracture due to stress intensification caused by thermal expansion mismatch and tensile residual stress induced by the CVD process. The reduction, by ~50 %, in fracture toughness and transverse rupture strength of CVD coated tools is another factor encouraging brittle fracture by chipping [134, 135].

The geometry of the tool is of major importance in tool fracture. Cutting edge chipping is also very common when using tools with very sharp edges and high positive rake angles with smaller included angle during interrupted cutting. Therefore tools with honed or chamfered cutting edges are more fracture resistant. Vibration and lack of rigidity in the tool

or workpiece setup also promote brittle fracture. Improper selection of cutting parameters, i.e., cutting speed, feed rate or depth of cut, is another source of brittle fracture.

Failure by fracture is not desired because of its unpredictable nature and the high risk of damage to the workpiece, cutter and machine tool. Brittle fracture can be minimised or prevented by (a) modifying cutting parameters, (b) increasing the rigidity of the cutting system, (c) selecting a tool with higher fracture toughness, thermal shock resistance and/or stronger geometry [1, 126].

4.2.3 Plastic deformation

Plastic deformation appears in the form of distortion of the cutting edge from its original shape without initial loss of tool material. Typical plastic deformation of the cutting edge occurs in the form that the rake face is depressed while the flank or nose bulges out or vice versa, as shown in Figure 4.7.

It occurs when the cutting edge softens and loses its strength due to high cutting temperatures and compressive stress induced during machining of steels and high strength materials, particularly at high cutting speeds and feed rates. With cemented carbide tools, softening of the cobalt binder phase leads to the plastic deformation of the cutting edge. Cemented tungsten carbide-cobalt tools melt at WC-Co eutectic temperatures 1325 °C and the strength of he composite rapidly falls above 1100 °C [136].

Deformation characteristics of coated cemented carbides or coated HSS tools are dependent on the high temperature properties of the substrates. Coating with wear resistant refractory materials requires a substrate of increased hot strength and does not relax this requirement [136, 137].

Plastic deformation results in accelerated wear on tool flank and rake faces and can initiate cracks that could lead to loosening of relatively large tool fragments and sudden failure of the cutting edge.

In the case of carbides, grades with low cobalt content and smaller grains or tools with higher hot hardness such as ceramics can be used because of increased resistance to deformation. Using a coolant where applicable dissipates heat and prevent softening of tools

to some extent. Plastic deformation can also be eliminated by reducing cutting speed and feed rate [126, 138].

4.3 Tool wear mechanisms

The failure modes of the tools with high fracture strength will be such that a progressive wear pattern develops as a function of cutting time and normally appears on the tool/chip contact zones of the inserts and determines the useful tool life. Tool wear in metal cutting is a relatively complex phenomenon and results from mechanical and chemical interaction between the cutting tool and workpiece [129, 139].

Tool wear involves gradual loss of tool material from the surfaces that are in contact with chip or workpiece during cutting and by some distinct mechanisms. The most common wear mechanisms include abrasion, attrition and diffusion processes of various kinds. Depending on the cutting conditions, cutting process, tool material and workpiece, one or more of these wear mechanisms can be present [1, 140]. These mechanisms are now briefly discussed.

4.3.1 Abrasive wear

Abrasive wear is a kind of physical (mechanical) damage occurring on the surfaces of the tool in contact with flowing chip and workpiece. The characteristic of a surface subjected to abrasive wear is such that in the surface topography there are longitudinal scratches or grooves running parallel to the direction of motion, being largely responsible for flank and rake wear on the tool at medium cutting speed range. Depending on the severity of the abrasive wear process, the extent of the damage may vary from simple scratching to gouging [1].

The hard abrasive particles can be introduced from various sources into the contact zones. Such hard inclusions in workpiece materials as carbides, oxides and nitrides of certain elements are responsible for this type of wear under sliding or intermittent contact cutting conditions. For example, carbide inclusions in nickel based alloys [9, 141] and free silicon particles in aluminium-silicon alloys are reported to be responsible for poor machinability of these types of alloys [123]. The same type of elements in the structure of

the cutting tools in the form of worn particles or dislodged grains from tool surfaces can also contribute to abrasive wear [138].

In some cases, wear debris in the contact zone can undergo chemical reaction, such as oxidation, and they may change their characteristics and become highly abrasive particles. These particles can either be the ones produced at the interface as wear debris during cutting or introduced from the environment as a contaminant such as sand particles from cast components [4].

There is not strong evidence indicating abrasion wear to have an important effect on the areas where seizure occurs. However, sliding and seizure may occur simultaneously, with sliding usually confined to the peripheral regions of the contact areas. The wear in these regions results primarily from reaction with the atmosphere and to lesser extent from abrasion mechanisms [58].

When using tungsten carbide tools, abrasion can be minimised employing grades with lower cobalt content and finer grain size. Tools with higher hot hardness, better surface finish and are compatible with workpiece materials, to give lower coefficient of friction, should be chosen [1, 4].

4.3.2 Attrition Wear

Attrition wear, also known as adhesive wear, occurs when there is a strong adhesion or welding between surfaces of the tool and workpiece material over the area of intimate contact [140]. When this type of bond becomes stronger than the local strength of the tool material, small fractured microscopic particles or dislodged grains from the tool surface are carried away by flowing chip and/or newly generated transient surface of the workpiece. Particles formed in this manner, subsequently can damage the underlying surface by tearing or ploughing or as a free-moving wear debris increasing the wear rate [4].

Attrition wear is generally encountered when cutting at low cutting speed ranges. The cutting action at low cutting speeds tends to produce a less laminar chip and intermittent chip flow which causes instability due to the presence of built-up edge and variation in contact zone. In addition chatter, lack of rigidity and interrupted cutting favour attrition type of wear [1].

The worn surface of the tool by attrition mechanisms has a rougher texture, when compared with abrasion, as the tool particles pulled away are bigger and have a tendency to fracture along the grain boundaries. In such an uneven surface, localised tensile stresses induced by flowing chip play an important role. In case of cemented carbides, the rate of attrition wear is directly related to the grain size, fine-grained tools being more attrition resistant than coarse-grained. The effect of cobalt ratio is of minor influence on attrition wear rate [138].

When cutting with coated tools, the type of adhesion between the coating and chip can induce localised or discrete detachment of coatings at regions where it becomes stronger than the bonding at the substrate-coating interface. Kramer and Hartung [142] observed that when machining Inconel 718 and Inconel X with TiC and HfC coated cemented carbides tools, some of the coating from the rake was detached by the chip welded to the coating.

Refractory carbide cutting tools are more sensitive to attrition wear than HSS tools under the same cutting conditions due to their composite microstructure. Therefore HSS tools having higher tensile strength than cemented carbides perform better at low cutting speeds.

4.3.3 Diffusion wear

Diffusion wear of cutting tools is a process activated at high cutting temperatures over 700 °C where the atoms of some of the constituting elements chemically react with or diffuse into the chip and workpiece material passing or seized over the rake face of the tool [1, 127]

Diffusion does not only take place from tool material to chip but it may also be from work material to the tool whereby the property of its surface region can be altered. Rate of diffusion determined from static diffusion studies cannot represent tool wear by diffusion nor be used to predict tool wear rate because of the complexity of interaction at tool-chip interface during cutting. However this can be useful in screening the solubility of different pairs of tool/workpiece materials [4]

Within the temperature region where plastic deformation of the tool does not occur, diffusion, along with abrasion and attrition, is one of the most effective wear mechanisms responsible for cratering and flank wear [127, 143]. Formation of a crater with smooth

surface texture on the rake face is a very strong indication of diffusion dominated wear [144, 145].

Diffusion wear depends on the following factors:

a) Tool/chip and tool/work interface temperature.

The rate of diffusion wear increases exponentially with the increase in tool-chip interface temperature.

b) Chemical affinity between the atoms of the tool material and workpiece.

Another factor influencing the diffusion rate is the solubility of different phases of tool material within the work material. Therefore diffusion wear is most likely the life limiting factor for those tool/work material combination having strong affinity for each other, for example cutting steel with diamond (due to the affinity between Fe and C atoms). The hardness of the tool material has no effect on the rate of diffusion wear. The proportion of diffusive elements in the tool is of significance as too high a quantity can give rise to diffusion wear [4].

c) The presence and thickness of stagnant material at the interface.

d) Rate of flow of chip or work material at the interface.

Increase in chip flow rate also promotes diffusion rate as it helps more quickly carrying away the tool atoms diffused into chip, accelerating the diffusion process [1, 4].

It has been reported that when cutting steel, diffusion resistance of WC-Co cemented tools has increased considerably by adding carbides of Ti, Ta and Nb at various percentages that have lower solubility in steel [128, 138]. Using coated tungsten carbide with TiN, TiC and Al_2O_3, when machining steel, markedly reduces diffusion related cratering and flank wear, provided that the coating remains intact during the process [127]. Diffusion wear can control the tool life when machining nickel based alloys with carbides and ceramics at high cutting speeds. It has been reported by Ezugwu et. al.[13] and [142] that diffusion wear was observed when machining a nickel-based superalloy (Inconel 718) with cemented carbides tools. A similar observation was reported by Bhattacharyya and Jawaid [145] when cutting another nickel-based alloy, Incoloy 901, with Sialon ceramic tools, resulting in smoothly worn surfaces on tools which is characteristic of diffusion wear.

The rate of diffusion wear is influenced by the presence of stagnant workpiece material at the interface, either due to BUE formation or seizure. Kramer [129] reports the effect of such mechanisms when studying the crater wear behaviour of a CBN tool tested in turning heat treated Inconel 718. The tool behaved such that there was a decrease in the crater wear rate with increasing cutting speed up to 1.5 m/sec, beyond which the crater wear rate risen exponentially. He attributed this to the fact that at a certain range of cutting speed, a layer of work material adheres to the contact zone at the rake face due to seizure. This layer then becomes saturated with the diffused tool constituents and serves as a diffusion barrier preventing further transaction of the elements from tool material, hence resulting in a reduction in the wear rate at that particular speed range. Increasing the speed beyond that certain limit will generate much higher temperatures whereby diffusivity is accelerated and the wear rate starts to increase rapidly.

4.4 Tool life criteria

Up to the present time, tool life phenomenon, which is considered to give an indication of tool replacement or resharpening, has been defined by using a number of different approaches, as outlined below [146].

a) Actual cutting time to failure (for continuous engagement)
b) Total cutting time to failure (for interrupted engagement)
c) Number of component produced to failure
d) Volume of material removed to failure
e) Length of cut surface to failure
f) Cutting speed for a given time to failure.

Depending on the nature of the process and production requirements, one of these approaches can be utilised. Behind all these approaches, there are certain predetermined tool failure criteria such as the size of flank wear, crater depth and/or chipping developing under progressive wear conditions. In some cases, the criterion could be the acceptable level of surface finish or limits of dimensional tolerances of the workpiece [147].

According to Sabberwall and Fleischer [148], tool wear tests under laboratory conditions often yields confusing and unreliable results. Therefore, test under the actual cutting and working conditions should be preferred to study machinability of materials and

cutting performance of the tools. Shaw [4] highlights the importance of actual cutting tests. He is of the opinion that it is not possible to use non-cutting tests to evaluate the performance of cutting tools and machinability of materials due to complexity of the cutting process in which cutting temperatures and forces play a significant and complex role.

Trent [1] also emphasises that wear resistance of cutting tools cannot be determined by one simple laboratory test or correlated with one single property such as hardness. Correct diagnosis of the factors controlling wear mechanism and tool life for a particular operation is of major importance in selecting the optimum tool material, tool design and cutting conditions and in developing new tool materials, tool geometry and lubricants.

International Standard Organisation (ISO) has documented detailed procedures for tool life testing in turning [54], face milling [124] and end milling [149] operations. They are intended to unify procedures in order to increase reliability and comparability of the test results relative to the cutting tools, workpiece materials, cutting parameters or cutting fluids.

The ISO standard for face milling test [124] outlines recommended procedures for tool life testing with cemented carbide tools in face milling steel and cast iron workpieces. However it also recommends that these procedures are applicable to face milling test on other workpiece materials or with different types of tools.

In machinability studies, standard cutting tests involve the following stages:

1. In the first stage, the machining operation is conducted under controlled cutting conditions of feed rate, cutting speed and depth of cut within a predetermined range. Consistency and compliance in all other initial conditions pertaining to the workpiece size and microstructure, tool-workpiece relative positions, cutting fluid, fixing methods are important for the validity and reliability of the tests.

2. Second stage involves measurement of tool life and tool wear according to the identified tool failure criteria (e.g. flank wear, crater depth, notch size surface finish etc.).

3. In the third stage, tool failure modes and wear mechanisms are investigated by using advanced microscopy and analysis techniques such as scanning electron microscope (SEM) and energy dispersive spectroscopy (EDS).

Flank wear is the most extensively used tool life criterion by researchers in the field of machining. ISO standard [124] on face milling test recommends a uniform flank wear of 0..5

mm and non-uniform flank wear of 1.5 mm as the tool rejection criteria when machining steel and cast iron. These values are considered to be too high when machining high temperature resistant nickel-based and titanium alloys. Shaw suggests [4] that a flank wear of 0.25-0.38 mm width should be adopted when cutting high temperature alloys as excessive wear can lead catastrophic tool failure and poor surface integrity of the machined surface.

During milling operation, brittle wear modes of chipping and/or flaking usually coexists with flank wear and can sometimes control the tool life. Ezugwu and Machado [13] rejected the inserts when a maximum flank wear of 0.76 mm was reached on any of the inserts of face milling cutter or when chipping or severe flaking occurred during face milling two nickel-based alloys Nimonic 75 and Inconel 718 with carbide tools.

El-Bestawi et. al. [16] used an average flank wear of 0.3 mm as well as a notch wear of 1 mm, 100 % flaking and total edge fracture when face milling Inconel 718 with ceramic inserts.

Alauddin et. al. [15] pointed out that uniform flank wear during interrupted cutting hardly occurred when machining (end milling) Inconel 718 with indexable cemented carbides. They adopted a maximum flank wear of 0.75 mm as the tool failure criteria. and suggested that in situations where it is not clear to distinguish the uniform flank from non-uniform flank.

In this study, in accordance with ISO standard [124] on tool life testing in face milling, tool life is defined as the total cutting time of the tool to failure based on the specified tool life criteria. The detail of the tool life criteria adopted in this study is given in the chapter on experimental techniques.

CHAPTER 5

NICKEL-BASED ALLOYS AND THEIR MACHINABILITY

5.1 Introduction

The term 'superalloy' refers to a group of sophisticated alloys with remarkable high strength and corrosion resistance properties at elevated temperatures. They are divided into three main categories according to the base alloying element and called nickel-based, cobalt-based or iron-based superalloys. The first practical nickel-based superalloy was Nimonic 80A of which various parts were produced for turbo super-charger in the 1940's. It was developed from 80Ni-20Cr base by the addition of titanium that provided precipitation hardening to some degree. Today various wrought and cast superalloys comprise over 50 % by weight of a modern jet engine structure [156].

Although superalloys are mainly used in the aerospace industry and nuclear power stations, where high strength and structural stability at elevated working temperatures is prime concern, it is found that they have been utilised in a wide range of industrial areas mainly for their corrosion resistance, high-temperature strength, low thermal expansion, electrical resistance, contamination resistance and thermal shock resistance properties. In aerospace engines wrought superalloys, are used primarily in making components such as compressors and turbine blades, vanes, discs, shafts, flame tubes, ducting, exhaust systems, afterburners, thrust reversers etc. [150]

Increased knowledge of structure and property relationships led to the development of various superalloys and there are over 80 different types at present, for a wide range of industrial applications, including power generation, chemical and petrochemical processing, marine engineering, thermal processing and aerospace engineering etc. [150].

Developed in 1962 for gas turbine engineering applications, the age-hardenable nickel-based superalloy Inconel 718 is recognised as the 'workhorse' alloy for this type service [151].

5.2 Properties of nickel and nickel-based alloys

The properties of superalloys can be modified by controlling the amount of alloying elements, adopted method of production, and by heat treatment. These alloys consist of various formulations of nickel, chromium, cobalt and iron as well as lesser amounts of tungsten, molybdenum, tantalum, niobium, titanium, aluminium, carbon, hafnium, boron and zirconium.

These alloys have a density range of about 7.8 to 8.9 gr./cm^3. The extent of variation is influenced by the alloying elements. Density is increased by the addition of such alloying elements as tungsten, molybdenum and tantalum having higher atomic weight than nickel, whereas addition of higher contents of lighter elements such as aluminium and titanium reduces it. The chemical composition of Inconel 718 and Waspaloy and the effects of alloying elements on the microstructure and properties of the alloys are shown in Table 5.1.

Nickel-based alloys have a stable austenitic, face-centred-cubic (FCC), crystal structure that does not undergo allotropic transformations up to the melting temperature. However, incipient melting temperatures and dissolution of strengthening phases determine the maximum temperature at which they can operate. The base matrix is a solid solution known as gamma phase (γ) and primarily strengthened by gamma prime (γ'), $Ni_3(Al,Ti)$ and gamma double prime (γ''), Ni_3Nb secondary phases.

Some of the important mechanical and physical properties of the nickel-based alloys used in this study are given in Table 6.4 [152].

5.3 Physical metallurgy of nickel-based alloys

There are four basic mechanisms utilised to strengthen wrought nickel-based superalloys in addition to various grain size and grain boundary modifications. These are

(a) solid solution hardening, (b) precipitation hardening, (c) carbide precipitation and (d) oxide dispersion strengthening.

5.3.1 Solid solution hardening

Atoms of some of the alloying elements, effectively tungsten, tantalum and molybdenum, substitute for nickel atoms within the crystal lattice upon heating at a temperature range over 800 °C. When the alloy is cooled, the solute atoms are blocked in the nickel's FCC crystal lattice which then causes the lattice to expand due to the differences in atomic diameters of the substituting elements. Thus the resultant distortion in the crystal structure increases the strength of the alloy system.

5.3.2 Precipitation Hardening of superalloys

Precipitation hardening is one of the main methods for strengthening some of the nickel-based alloys including Inconel 718 and Waspaloy. The mechanism of precipitation hardening which was first discovered by Paul D. Merica as a result of adding aluminium and titanium to a nickel alloyed steel.

This process involves ageing of solid solution heat-treated alloys for a particular period of time at temperatures of about 75-85 % of the solution heat treatment temperature. The precipitation of γ' intermetallic phase consisting of $Ni_3(Al, Ti)$ from the supersaturated solid solution main matrix, γ, is the mechanism giving the principle high strength property to the alloy. This phenomenon is described in Figure 5.1, showing the formation of precipitates as a function of time and temperature [153].

The γ' precipitates can strengthen the alloys in two ways. First coherency strains between γ and γ' phases make it difficult for the dislocation to penetrate the precipitates and second, the need for creating anti phase boundary (APB) energy to penetrate precipitates due to the ordered γ' structure [154, 156]

Increasing both the volume fraction of γ' phase and its solid solution temperature is the dominant theme to the development of high-temperature strength superalloys that results in high creep strength at elevated temperatures. Two important properties of the γ' intermetallic phase, which are its FCC crystal structure, the same as that of the main

matrix, and lattice parameters almost identical (with max. 1% mismatch) to that of the γ matrix, provide low surface energy and long term stability of the structure. The size and the volume fraction of the precipitated γ' particles control the level of strengthening of the alloy. The higher the volume fraction the stronger the alloy becomes. The shape of the γ' precipitates is spheroidal in lower volume fraction and tends to become cuboidal in higher volume fraction of over 35 % [5].

Overaging of the alloy will cause γ' particles to coarsen and to become less in numbers in a given volume which results in softening of the structure. To diminish coarsening and keep the strength at elevated temperatures, niobium and tantalum, which have high-partitioning and slow-diffusing properties, are added to form the required precipitate.

Some other secondary intermetallic phases can form if the alloy is supersaturated in titanium, niobium or tantalum. For example, γ' phase with excess titanium can transform to eta (η) phase (Ni_3Ti), a hexagonal close-packed phase, upon prolonged exposure to temperatures between 700 and 900 °C. The η phase precipitates reduce rupture strength but not ductility. On the other hand, excess niobium, over 4 %, will result in formation of γ'' phase (Ni_3Nb), which has body-centred tetragonal crystal structure, as being primary strengthening intermetallic phase in Inconel 718. Niobium and nickel can also form another intermetallic phase called delta (δ), Ni_3Nb, with orthorhombic crystal structure which is observed in overaged Inconel 718. This phase is detrimental to the alloys microstructure, if present in large amounts. [153].

In addition to the phases already discussed, μ, σ, and Laves phases can also form in superalloys. They are classified as topologically close packed and have platelike structures. They are generally deleterious and are believed to promote crack formation [156].

5.3.3 Carbide strengthening

Although nickel is not a carbide-forming element, formation of various types of carbides are possible within the microstructure of superalloys depending on the alloying elements and processing.

Some of the essential carbides found in superalloys are MC, M_6C, $M_{23}C_6$ and M_7C_6 where M represents one or more metallic carbide-forming elements. The carbides $M_{23}C_6$ and M_7C_6 are formed by chromium, MC by titanium, tantalum, hafnium and niobium and M_6C by molybdenum and tungsten. Figure 5.2 shows a representative nickel-based alloy microstructure with dominant phases.

Depending upon their morphology, properties, amount and location in the matrix structure, they can either be desired to form or not as they can alter the mechanical properties of the alloys. The presence of carbides at the grain boundaries as segregated globular precipitates is required to develop optimum stress-rupture and ductility properties and for grain size control in some wrought alloys. They provide sufficient ductility in the surrounding grains due to stress relaxation effect without premature failure. In contrast, strength properties can severely be degraded if the carbides form as a continuous grain boundary film [5].

Formation of MC is generally not desired due to their uneven distribution and large blocky shape. M_6C carbides, also blocky in shape, are used to control grain size since they generally occur as a grain boundary precipitate.. If dispersed throughout the grains, they can reduce ductility and rupture strength. M_7C_6 carbides form intergranularly in the matrix. They can improve the strength when precipitated as discrete particles throughout the grains. Their aggregation, however , along the grain boundary can increase brittlement.

$M_{23}C_6$ carbides tend to precipitate intergranular areas resulting in enhanced rupture properties by inhibiting grain boundary sliding. Figure 5.2 shows some of the carbides in the microstructure of a nickel-base alloy. The alloy chemistry and applied heat treatment process are the two important and sensitive means in obtaining suitable carbide structures and morphologies.

5.3.4 Oxide dispersion strengthening

Oxide dispersion strengthening (ODS) is another technique that utilises the presence of dispersed oxide particles, such as yttrium oxide and thorium dioxide, in the alloy structure through powder metallurgy and mechanical alloying processes. The dispersed

oxide phase within the structure is of thermal stability up to the melting point and maintains excellent tensile and creep rupture strength at temperatures where γ', γ'' and carbide phases either dissolve or coarsen [155]. This is due to the reduction of grain boundary sliding both through the grain shape and by the dispersed oxide at the grain boundaries. Even distribution of very fine oxide particles within the grains is the prime reason for their strength at elevated temperatures.

5.3.5 Effect of grain size

The grain size, grain boundary chemistry and grain boundary morphology are all important elements affecting each alloy's fatigue and creep rupture properties. It is recognised that majority of high temperature creep and low cycle fatigue failures are initiated in the grain boundaries.

Creep resistance of an alloy is generally reduced by small grains while large grains, particularly with respect to the section size, can cause sliding and lead to premature failure. It should be balanced, depending upon the priority of required properties. Grain size is controlled by the presence of carbide and gamma prime phases in the microstructure.

The composition of grain boundary differs from the nominal composition of the alloy and is rich in elements such as boron, zirconium, hafnium and magnesium. Small addition of these elements improves mechanical properties to some degree. They may modify the initial grain boundary carbides or tie up deleterious elements such as sulphur and lead. Grain boundary diffusion rates could be reduced by suppressing carbide agglomeration and creep cracking [5, 156].

5.4 Processing techniques of wrought nickel based alloys

Wrought nickel-based alloys are generally produced through double vacuum induction melting followed by vacuum-arc or electroslag re-melting processes. Vacuum-induction melting lowers the content of hydrogen, nitrogen and oxygen gases and evaporates trace elements such as lead, bismuth, cadmium, arsenic etc. whose presence can degrade mechanical properties and workability of ingots and adversely affect service

life. Alloys are further refined by secondary re-melting using vacuum-arc and electroslag processes to eliminate gases, metallic and non-metallic impurities and inclusions. High sulphur levels, in particular are detrimental to the workability and properties of many wrought nickel-based alloys. Removal of sulphur is very effective by electroslag re-melting which is done by arc melting under a protective cover of slag. Thus ingots of uniform composition and dense homogeneous structure are obtained [156].

Powder metallurgy (PM) is another technique by which some of the nickel-based superalloys are processed. PM permits, through hot isostatic pressing (HIP) and mechanical alloying, the production of near-net-shape components with segregation-free, homogeneous structure that require little machining [5, 156].

5.5 Machinability of Nickel-based Alloys

5.5.1 Introduction

The importance of machining in manufacturing superalloy components of the aerospace industry, becomes apparent as conventional metal removal processes accounts for 75-80 % of the total machining applications [44] and 90 % of the cost of some parts of an aircraft engine [157]. The high rate of employing conventional machining methods is due to the fact that conventional metal removal processes provide much higher metal removal rates than unconventional processes [44].

Research works in machining of nickel-based alloys were initiated in the early 1950's by the United States Air Force (USAF) due to an increasing demand for these alloys and the difficulties faced when machining [44]. The USAF, recognising the need for guidance from industry in machining of high-strength thermal-resistant alloys, has sponsored many programmes to determine machining properties of these materials and generate machinability data [44]. Results of some of the studies on aerospace materials, with respect to various machining methods such as turning, milling, drilling and tapping, were published [44]. Since then studies on the machinability of nickel-based alloys using various types of tool materials have been undertaken extensively by many researchers.

In general, the machinability of nickel-based alloys vary quite significantly. Theoretically, the machinability decreases with increased hardness, strength and alloy content. Nickel-based alloys are classified into groups with respect to machining characteristics. The full detail of this classification can be found in references [81, 158]. In brief, Group A consists of nickel alloys with moderate mechanical strength and high degree of toughness. They contain over 97 % nickel with not more than two other alloying elements. Group B includes mainly nickel-copper alloys that have higher strength and slightly lower toughness than those in Group A. Group C consists largely of the nickel-chromium and nickel-iron-chromium alloys. The materials of these three groups can only be hardened by cold work. They are best machined in cold-drawn or cold-drawn and stress-relieved conditions as they are quite gummy in the annealed and hot-worked conditions [158].

Group D consists primarily of the age-hardenable alloys characterised by high temperature yield and shear strength. The nickel-based alloys in this group are regarded as the most difficult-to-machine due to unfavourable mechanical and physical properties from the machinability standpoint. Rough machining of these alloys is usually performed in the non-aged condition due to their relative low strength. However, alloys in the fully-aged condition are machined to obtain components with fine finishes, close tolerances and free from possible distortions which can otherwise be caused by the heat treatment after the final machining process [81, 158].

It has been reported by many researchers that usually the same characteristics that make superalloys capable of resisting high stresses at elevated service temperatures are also responsible for their poor machinability [7, 9, 44, 46, 144, 157, 159, 160, 161, 162, 163].

The principal problems associated with the inherent characteristics of these materials are discussed next.

5.6 The principal problems in machining nickel-based alloys

5.6.1 Strength at high cutting temperatures

Nickel-based alloys retain their strength at high cutting temperatures where HSS tools and binding phase of WC-Co tools begin to soften [157, 164]. Kramer and Hartung [142] observed that carbide tools failed because of thermal softening of the cobalt binder

phase leading to plastic deformation of the cutting edge when machining Inconel 718 above 30 m/min. Trent [165] has pointed out that when machining age hardenable nickel-based alloys, the cutting tool wears rapidly due to their high creep-rupture and shear strength in the flow zone on the surface of the tool. He gives an example of machining Nimonic 80, a nickel-based alloy with 200 HB hardness and steels of 300 HB that the former was cut at a maximum cutting speed of 100 ft/min (30 m/min) while the latter at 400 ft/min (121 m/min) for an equal tool life. Howard [164] also reports that with highly-alloyed nickel-based materials, the high temperature creep resistance is such that cutting under the conditions where workpiece yields thermally to appreciably assists in machinability, takes the temperatures at the tool-work interface to a degree at which the tool edge softens and/or diffusion is encouraged. Giving an example of Nimonic 90 alloy which has a tensile strength of 80 and 55 tons per sq. inch at 20 and 750 °C respectively, Howard concludes that it is necessary to reach temperatures in excess of 1000 °C to obtain a beneficial reduction in stress similar to that of conventional steels. However this involves a tool-work interface temperature considerably above this value whereby a rapid tool deterioration would occur. This example clearly shows the effect of creep-rupture strength of nickel alloys on their machinability being greater than the room temperature properties and hardness alone.

A correlation between tool life and creep-rupture strength of nickel-based alloys was also depicted by Warburton [46] as shown in Figure 5.3. This figure shows the increasing difficulty of machining nickel-based alloys with different levels of creep-rupture strength. High temperature strength of the nickel-based alloys is largely due to the most common hardening phase, γ' (Ni_3Al/Ti), the hardness of which raises with increasing temperature as shown in Figure 5.4 [157].

Trent [1] reports that a temperature of 800 °C is generated during cutting one of the least creep resistant nickel-based alloys containing 19.5 % chromium and 0.4 % titanium at a cutting speed of 21 m/min. He suggests that the temperatures in the flow zone at the tool-chip interface may well be over 1000 °C when cutting highly creep resistant nickel alloys at a speed range high enough to prevent BUE. The result, however, would be the destruction of the cutting tool under the action of shear and compressive stresses at high temperatures generated, leading to short tool life.

As the conventional cutting involves material shearing, the higher the material strength the more difficult it is to cut and the more power is required. Strength of most of the materials is expected to lessen due to large amount of heat generated during cutting. But this is not the case when cutting superalloys, since the reduction in tensile strength can not be considered as significant at elevated cutting temperatures in excess of 760 °C as shown in Figure 5.5. Hence it does not improve the machinability to a great extent [162].

5.6.2 Rapid work-hardening tendency

Nickel alloys have rapid work-hardening tendency which is also referred to as strain-hardening. This has been attributed to their austenitic matrix structure [4, 158, 166]. The effect of cold reduction on the hardness of selected nickel alloys, including Inconel 718, and some other materials (mild steel, copper, aluminium) is a clear indication of the high work-hardening tendency of nickel-based alloys as shown in Figure 5.6. Cutting forces and specific power requirements are also greater for a given material with significantly high work-hardening tendency [50] that accelerates the wear rate of the cutting tool [13]. Therefore high pressures developed during cutting produce a stressed and deformed layer on the surface of the workpiece which retards further machining due to hardening effect.

The problems of BUE formation, workpiece material welding or galling and disturbed subsurface layer of the workpiece are closely associated with this work-hardening tendency. Conaway [162] reports that Galling of workpiece material occurring on tool/chip and tool/workpiece interface zones is among the important causes of poor surface finish and tool performance. Ezugwu and Machado [13] report that the chip adhering onto the tool edge causes chipping and significant distortion of the insert during re-engagement when face milling Nimonic 75 and Inconel 718. Makarov et al. in reference [7], observed workpiece adhesion over the 75-85 % of the worn areas of a carbide cutting tool when turning a creep-resistant nickel alloy at 30-45 m/min, where the mean tool/work interface temperature was measured as in the range of 850-950 °C. While the mean hardness of the bulk material was 400-430 HV, that of the pressure-welded-layer was recorded to be in the range of 715-1020 HV. This evidence clearly

shows the intense plastic deformation and work-hardening tendency in this kind of materials.

When successive cuts are taken, depth of cut and feed rate should be greater than the thickness of the work-hardened layer to prevent further work-hardening, workpiece burnishing and rubbing. To minimise work-hardening, sharp tools with positive rake angles which cut metals rather than pushing are required. Further, tools should not be allowed to rub against the workpiece, either because of too small a clearance or by being allowed to dwell in the cut due to excessive feed rates [4, 44, 67, 81, 158, 162, 166].

5.6.3 Presence of highly abrasive refractory phases

The presence of hard phases in nickel alloys, such as carbides, nitrides, carbonitrides, oxides and intermetallic γ' (Ni_3Al/Ti) type strengthening phases has abrasive effect during cutting, hence causes rapid tool wear. Focke et al [150] report that generally increasing the volume of γ' phase, by increasing the amount of titanium and aluminium in alloy composition, accelerates the rate of tool wear. The classes of carbides commonly present in age-hardenable nickel alloys include MC, $M_{23}C_6$, Cr_7C_3 and M_6C types of which the MC type carbides (such as TiC, NbC and TaC) are the hardest and most abrasive [158, 162]. They are precipitated along with γ' (Ni_3Al/Ti) during age hardening. The refractory nature of these carbides, along with their strengthening effect, causes age-hardened nickel alloys to become less machinable, despite improved chip action. The abrasive effect of the carbide phases on tool wear has been reported by many researchers during machining with carbide cutting tools [15, 141, 162, 163, 166, 167].

5.6.4 Diffusion between tool and workpiece

Diffusion between tool and the workpiece material begins when the tool-work interface temperature of around 750 °C is reached approximately at a cutting speed of 20 m/min. In the case of carbide tools, the diffusion mechanisms involves migration of tungsten atoms from the tool into the chip with cobalt and nickel diffusing from the chip into the tool. Diffusion of titanium from the workpiece into the tool material was also

detected with increased temperature when cutting at 45 m/min [7]. It has also been reported that the chemical affinity between the tool and workpiece material promotes workpiece galling and adhesion [167]. High rates of diffusion alter the composition of the tool materials and degrade its mechanical properties [7, 44, 163].

Addhoum and Broussaud [168] pointed out that no chemical wear was observed in the case of alumina-based ceramics owing to its substantially low free energy of formation. Moreover, they have detected a liquid phase on the rake face of a Sialon tool (Kyon 2000), which is enriched mostly with nickel and silicon, when turning Inconel 718 and Waspaloy at a cutting speed of 180 m/min. A similar liquid phase was also detected during their diffusion test at 1200 °C. They have observed no such liquid phase on the zirconia toughened alumina tool confirming its chemical stability for Inconel 718 during diffusion tests. Bhattacharyya et al.[169] have found the presence of a diffusion band at the flank face of a Sialon tool when turning Incoloy 901 at 185 m/min and 0.16 mm/rev. They detected the formation of titanium nitride and chromium nitride in that zone where titanium and chromium from Incoloy 901 reacted with nitrogen from the β'-Sialon crystal causing it to decompose. Following this reaction, the elements of β' crystal, namely silicon and aluminium, dissolved in the glassy binding phase. Aucote and Foster [107] have shown that the flank wear resistance of β'-Sialon is increased by introducing α-Sialon phase which is more resistant to dissolution wear than the former due to its higher aluminium and oxygen contents, when turning Incoloy 901.

5.6.5 Adverse distribution of tool temperature

The temperature distribution in cutting tools when machining commercially pure nickel and nickel alloys has been studied and compared with the tools used to cut steels [66, 160, 170]. When machining nickel alloys, the outstanding feature of temperature distribution is that the tip of the cutting edge is frequently the region of the highest temperature whereas in machining steel, this is always on the rake face some distance away from the cutting edge as shown in Figure 5.7. The results of the tests on an age-hardened Inconel 718 by Focke et al., (Figure 5.7), show that there is no plateau of unworn tool material on the rake face. Furthermore, the deepest point of the crater,

where the highest temperatures are developed, moves closer to the cutting edge with increasing cutting speed, leading to quick deformation of the cutting edge either due to softening or chemical reaction with the workpiece [169].

In addition, the temperatures developed on the tool when machining nickel alloys are much higher than in the case of conventional steels [7, 171]. The experiment by Smart and Trent [66] on cast iron and Nimonic 75 nickel alloy at a cutting speed of 10 m/min showed maximum rake face temperatures of 320 and 800 °C respectively.

Therefore tools used for machining nickel alloys tend to be deformed along the main cutting edge which is subjected to high compressive stresses and temperatures even at relatively low cutting speeds [1, 166]. This is also supported by Wrigth and Chow [160] who observed that the normal stresses on the tool are roughly twice as high for machining nickel alloys as for machining steel at the same cutting condition.

5.6.6 Low thermal conductivity

Thermal conductivity of nickel-based superalloys is about 10 to 30 % of that of pure nickel, iron and cobalt because of the effect of extensive alloying [236]. Thermal conductivity of Inconel 718, for instance, is 11.4 W/m °C, whereas that of 99.9 % pure nickel is 86 W/m °C [172]. It would be desirable to have high thermal conductivity in the workpiece materials, from the machinability point of view, to rapidly dissipate heat and minimise temperature gradients at the tool-work contact zone [4, 14].

Many researchers have reported the adverse effect of the coexistence of low thermal conductivity together with high cutting temperatures in machining nickel-based superalloys hindering its machinability [9, 119, 141, 163, 167]

5.7 Tool Materials for Machining Nickel-based Alloys

Literature reveals that cutting tool materials used for machining nickel-based alloys include HSS, cemented carbides, ceramics and PCBN with the widespread use of HSS and cemented carbides at present [173, 174]. HSS and carbide tools are often used in applications where positive rake angle is required. Negative rake is preferred with ceramics and CBN tools in order to add strength to the cutting edge against fracture [173]. Many cutting operations such as drilling, tapping, reaming, broaching and some

milling and interrupted cutting require high speed steel tools owing to its supreme toughness and reliability at low cutting speeds. Where applicable, cemented tungsten carbides of medium to fine grain size are more efficient than HSS tools, and mainly used for continuous cutting (turning, boring, facing) and for some milling operations in particular face and end milling. According to Trent [1] and Howard [164] alloyed grades of tungsten carbides which include TiC, TaC have been found to give shorter tool life than straight WC-Co grades. Trent also states that carbide tools are rarely employed over the cutting speed of 60 m/min.

5.7.1 Coated carbides in machining nickel alloys

Early studies with coated cemented carbides tested on superalloys generally suggest that they were not found to offer any advantages over uncoated carbides [1, 4, 14, 175]. Gorsler [175] attributed the poor performance of coated carbides to inability of WC-Co substrates to resist deformation at substantially high temperatures, regardless of the coating materials while Edwards [88] ascribed to the loss of edge strength (toughness) of about 25 % due to eta-phase formation (Co_3W_3C) in the early application of CVD coating process on carbide tools. On the other hand, Kramer and Hartung [142], as well as agreeing with Gorsler, pointed out the problem with coated tool as being poor coating adhesion onto the substrate and differences in mechanical properties between the two. They also reported removal of coating layer as large portions due to chip welding and transition between sliding and sticking of the chip on the rake face when turning Inconel 718 and Inconel X.

Recent advances in coating technology, over the last decade in particular, have led to the introduction a wide range of coated cemented carbide tools which tend to increase achievable cutting speed over 50 m/min in continuous turning and offer longer tool life [174]. Hanasaki et al. [176], performed dry turning experiment on a high nickel alloy with an uncoated and four different coated P10 grade carbides at a cutting speed of 100 m/min, DOC of 0.5 mm and feed rate of 0.1 mm/min. The tools were coated with TiC, TiN, TiC/TiN and TiC/Al_2O_3 layers. The results showed that all the coated tools outperformed the uncoated grade by giving 2 to 3 times longer tool lives based on the

depth of cut notch wear as the tool life limiting factor. They associated the better performance of coated tools with their favourable physical and mechanical properties.

The work of Ezugwu and Jawaid [141] on turning age hardened Inconel 718 with an uncoated and two different coated tungsten carbide tools with TiC/Al_2O_3 /TiC and TiC/ TiC-N/TiN coating systems, showed that the geometry of the tool had a considerable effect on the performance of the coated tools. With rhomboid shaped tools, the uncoated grade lasted significantly longer than the latter coated tool at cutting speeds of 47, 55 and 70 m/min and than the former at 47 m/min. The former coated tool however gave much better tool life than that of uncoated at cutting speed of 47 and 70 m/min. They concluded that better performance of square shaped tools was due to its grater strength compared with that of the rhomboid shape. The poor performance of the second coated tool was attributed mainly to the plucking of minute or large tool particles from the worn regions which was related to insufficient substrate strength to withstand tensile forces developed.

Investigation of Quigley and Monaghan [177] with three CVD coated (TiC/Al_2O_3, TiC/Al_2O_3 /TiN and Al-O-N) and two uncoated carbide tools when turning aged Inconel 718 shows varying performances in relation to the cutting speeds employed. Their test showed that coated tools demonstrated no benefits over the uncoated ones at a cutting speed of 20 m/min while considerable improvement was noted with coated tools at 40 m/min based on flank wear resistance. The degrading effect of the CVD coating process on the tool toughness was proposed as the main cause for the poor performance of coated tools at low cutting speed of 20 m/min.

Comparing PVD versus CVD coated carbide tools when turning solution treated Inconel 718 Rahman et al [179] and Ezugwu and Wang [178] presented consistent results in terms of the failure mode, namely notching, by which CVD coated tools failed, despite having different coating systems. In the case of Rahman et al, CVD multi layer Al_2O_3 coated tool was outperformed by PVD-TiN coated tool for which no specific reason was put forward. Whereas in the second case the CVD- TiC/Al_2O_3 /TiN coated tool outperformed the single layer PVD-TiN. This was attributed to the good wear resistance of TiC and high hot hardness, excellent chemical stability and low thermal conductivity at elevated temperatures of Al_2O_3 coating.

Choudhury and El-Baradie [181] carried out turning experiment on solution treated and aged Inconel 718 with an uncoated and a CVD-TiC/Al_2O_3 coated carbide insert whereby investigating the effect of major cutting parameters of cutting speed, feed rate and depth of cut. The uncoated grade performed better than or as equally as coated grade at all conditions with the exception that over the depth of cut of 1 mm, coated tool gave slightly longer (10 -25 %) tool life. The greatest difference between the tools in terms of tool life was at the lowest cutting speed of 20 m/min. The reason given for this was the loss of substrate toughness due to the CVD coating process.

5.7.2 Machining with ceramics

Pure aluminium oxide (Al_2O_3) tools, despite having greater chemical stability, hot hardness and wear resistance than WC-Co tools [182], have not been effective in machining nickel-based alloys due to their poor thermal shock resistance and inadequate fracture toughness [7, 183].

Aluminium oxide (Al_2O_3) ceramics were then alloyed with one or more of the compounds of ZrO_2, TiC or TiN, in order to improve thermal shock resistance and fracture toughness properties [101]. The application of Al_2O_3-TiC ceramic tools in machining superalloys provided a substantial increase in cutting speeds ranging between 120-240 m/min [183]. Baker [184] tested Al_2O_3-TiC ceramic tools in turning Incoloy 901 and showed its cost effective use at the cutting speed of 230 m/min, feed rate of 0.2 mm/rev and DOC of 2 mm. Another alumina-based mixed ceramic tool, (Al_2O_3-ZrO_2-W), has been used for turning Inconel 718 in a production environment at 244 m/min [8]. In comparison with this tool, Al_2O_3-TiC ceramic tool failed by severe notching and chipping when machining at 137 m/min.

Excessive notching at the depth of cut has been the major problem with alumina ceramics which was attributed to the mechanical wear via welding and plucking action due to relatively low fracture toughness [184, 185].

Favourable properties of silicon nitride-based ceramics (Si_3N_4), with even greater hot hardness, thermal shock resistance and improved fracture toughness than mixed alumina tools, enabled them to machine nickel-based alloys at higher speeds and feed rates [186]. Baker [186] observed a significant reduction of 70 % in the rate of notch

formation with silicon nitride based ceramic tools compared with mixed alumina ceramics, after 2 minutes turning of Incoloy 901 at 230 m/min. Bhattacharyya et al [187] achieved 4 min tool life when turning Incoloy 901 with 'Syalon' ceramic at 310 m/min and 0.18 mm/rev while alumina tools lasted 3 minutes at a cutting speed of 250 m/min where failure occurred due to severe notching.

In another study by Bhattacharyya et al [169], the failure modes for Syalon tools were reported to vary depending on the cutting speed. They observed that notching was the dominant failure mode at 125 m/min whereas at 185 m/min notching and flank wear were responsible for the tool failure. Combination of diffusion and attrition wear mechanisms was shown to be operative. At the speed of 310 m/min, however, flank wear controlled the tool life which was caused by plastic deformation and cracking. The findings of Aucote and Foster [107] as regard to the wear mechanisms causing flank and notch wear in machining Incoloy 901 with Sialon tools slightly differs from that of Bhattacharyya et al [169]. They claimed that diffusion and/or dissolution wear were major contributory factors to flank wear while principle wear mechanism for DOC-notching was the intermittent removal of microscopic fragments of tool material i.e. attrition wear. Baldoni and Buljan [188] attributed the mechanism of DOC-notching in ceramic tools to the very irregular chip-workpiece separation process in the primary shear zone that produced interrupted seizure and pullout effect with irregular saw-tooth-edged chip morphology. Besides, combined action of work-hardened surface and its hard constituents created abrasive effect which were related more to the mechanical properties and thermal shock resistance than chemical interactions between the tool and workpiece at the DOC-notch region. This conclusion on DOC-notching was supported by Brandt et al. [189] who investigated the wear mechanisms of Sialon and silicon carbide whisker-reinforced alumina when turning Inconel 718 of 370 HB hardness at 150 and 450 m/min.

Silicon carbide whisker reinforced alumina ceramic tools (Al_2O_3-SiC_w) were primarily introduced for machining nickel-based super alloys [183] extending the cutting speed ranging from 200 to 750 m/min with corresponding feed rates of 0.18 to 0.375 mm/rev [7, 190].

Vigneau et al. [191] investigated the performance of Al_2O_3-SiC_w tools when turning solution treated and aged Inconel 718 and recorded longer tool life by 30-100 % than with Sialon and Al_2O_3-TiC counterparts under identical conditions within a cutting speed range of 120 to 210 m/min. Better performance has been ascribed to toughening effect of the SiC whiskers that reduce the wear resulting from microfracture and particle removal mechanisms i.e. the attrition [192].

Mehrotra and Beeghly [193] comparatively studied the performance of Al_2O_3-TiC, Al_2O_3-SiC_w and Sialon tools when machining Inconel 718 and Waspaloy. Their findings showed that performance ranking of the tools was very much dependent upon the cutting condition and heat treatment given to the workpiece material. Sialon tool was reported to have the highest fracture and DOC-notch resistance. Sialon tool was followed by Al_2O_3-SiC_w with better fracture resistance relative to Al_2O_3-TiC tool. This has been correlated with the higher fracture toughness and thermal shock resistance of Sialon tool. On the other hand Al_2O_3-TiC tool resulted in minimum flank wear outperforming Al_2O_3-SiC_w and Sialon at a cutting speed of 305 m/min, DOC of 1.52 mm and feed rate of 0.25 mm/rev in the case of tempered Inconel 718 of 26 HRC. The high flank wear resistance of Al_2O_3-TiC tool was associated with its better chemical stability owing to the lowest free energy of formation as compared to the other two [194]. The investigation of Narutaki et al. [17] demonstrated results which were in agreement with that of Mehrotra and Beeghly [193] as to the superior flank wear resistance of Al_2O_3-TiC tool in comparison with Sialon and Al_2O_3-SiC_w grades, over the cutting speed of 400 m/min when turning Inconel 718 of 420 HB.

5.7.3 Machining with PCBN Tools

According to Richards and Aspinwall [7] tested CBN tools with 30-95 % CBN contents on Inconel 718 and found that notching decreased with increasing CBN content whereas flank wear showed little variation being minimum at about 55 % CBN content. They have also noted the presence of pressure-welded workpiece material on the tool surface, the degree of which was found to increase with the decrease of CBN content whereby promoting notch wear. Superior performance of high CBN content tools in

turning Inconel 718 was also reported. This was associated with higher hardness of CBN increasing almost linearly with the CBN content.

A recent investigation of Richards et al. [195] have demonstrated that PCBN tool (3 90-95 % PCBN of 3 micron grain size and 5-10 % Ni/Co binder phase) gives shorter tool life than the other four types of Al_2O_3-SiC_w grades tested within a cutting speed range of 160-260 m/min when turning Inconel 718 of 386 HV employing a DOC of 2 mm and feed rate of 0.3 mm/rev.

It has been reported however that finish turning of a number of different nickel-based alloys with PCBN tool (GE's BZN6000) demonstrated 40 to 250 times better tool efficiency compared with C-2 carbide at a depth of cut from 0.05 to 0.38 mm and feed rates between 0.05 and 0.25 mm/rev [196]. The cutting speed for the PCBN tools was between 91 to 365 m/min while being 30 to 90 m/min for C-2 carbide grade.

Kato et al [197] showed successful application of PCBN tools which consists of 55 % CBN particles and TiN based ceramic binder phase, in finish end milling of aged Inconel 718 of 450 HV hardness. The test was performed at a cutting speed of 150 m/min, DOC of 0.1 mm and feed rate of 0.05 mm/tooth with high pressure coolant supply through the spindle. They found that tool life was substantially increased by the application of high pressure coolant (at 5 MPa) thereby preventing workpiece adhesion on the rake face of the tool. They also increased chipping resistance of the tool by 0.03 mm edge honing which resulted in smooth wear after cutting a length of 600 m.

5.8 Milling of nickel-based superalloys

Cutting tools are subjected to different cutting conditions and wear modes depending upon the machining operations or methods being adopted. This heavily influences the choice of optimum cutting tool material for a given machining methods and set of conditions [193]. Most of the published machinability work on nickel-based superalloys are related to the turning process which involves continuous cutting. On the other hand, there are very few studies available in the open literature dealing with the milling machinability, in particular face milling, of these alloys [11, 13, 16, 194]. This lacking of literature has been associated with relative high costs encountered when working with exotic aerospace materials [13, 194].

5.8.1 Milling with HSS, Uncoated and Coated Carbide Tools

Field studied [44] the performance of carbide cutting tools on various high strength materials with respect to different machining processes including face milling. He suggested C-2 carbide tools to be used to turn aged nickel-based alloys such as Inco 700, Rene 41 and Udimet 500, whereas for face milling of the same alloys HSS tools were recommend from the economical machining point of view at a cutting speed range of ~ 6 to 12 m/min (18-37 sfm).

It has been stated in one of the earliest machinability report [166] on heat resistant alloys that, when using HSS tools, wear was confined largely to the flank face whereas crater wear being negligible at low cutting speeds. Rapid failure of the cutting edge was observed when higher cutting speeds were attempted with HSS tools.

The report also states that in milling nickel-based heat resistant alloys, carbide tools were found to be unpredictable mainly due to failure by chipping or breakage. The relatively inferior toughness of carbide tools has been the main reason for not recommending them for interrupted cutting applications on nickel alloys [198]. However, according to the same report, using modified carbide tips and cutters to minimise chipping, longer tool lives were achieved in milling. Face milling of Inconel X-750 with C-5 carbide with 45°x0.18 mm edge chamfer and using a negative/negative (-8° to -15°) cutter, at a speed of 18 m/min (60 sfm) and feed rate 0.22 mm/tooth (0.009 ipt) resulted in 25 % increase of tool life under the climb milling mode and presence of soluble oil.

Takeyama et al [171] investigated the mechanism of adhesion on the tungsten carbide tool when interrupted turning of Inconel 718 on account of the fact that metal adhesion is one of the prime causes of brittle tool fracture and chipping. They observed that structural deterioration of the tool face is more pronounced and some WC grains are pulled out because of the adhesion between workpiece material and both WC grains and cobalt binder phase even after cutting 3 mm at 5 m/min. Surface cracking was found to initiate in the rake face after 15 min of cutting for which intensified local tensile stresses at the periphery of adhered areas was proposed to be the reason.

Chandrasekaran and Nordgren [199] have machined Inconel 718 with an end mill of 25 mm diameter. It was a four-tooth cutter operating at 19 m/min and inserts being straight carbide grade with 6% cobalt. They performed a stress analysis which showed calculated effective stress to reach the compressive flow stress of the carbide tool at about 600 °C. They correlated this with the plastic deformation of the cutting edge which was proposed as the predominant wear mechanism.

Ezugwu and Machado [13] have tested K20, K40 and P25 WC/Co grades in face milling of Nimonic 75 (235 HV) and Inconel 718 (364 HV) at cutting speeds of 27 and 23 m/min respectively, with the presence of a water-based coolant. They found that K20 outperformed K40 and P25 and resulted in the highest metal removal at a feed rate of ~0.08 mm/tooth when milling both materials. Tool rejection was due to severe chipping believed to be enhanced by attrition and thermal cracking. Severe parallel and perpendicular cracks to the cutting edge of P25 grade were observed at the high feed rate of ~0.15 mm/tooth. Better resistance of K20 to plucking and fracture was attributed to its higher hardness and finer grain size relative to K40 and P25 grades. Higher thermal expansion coefficient and lower thermal conductivity of P25 and K40 made them more susceptible to fracture and cracking than K20 under the influence of thermal shocks.

In another study, Ezugwu and Phasby [167] investigated the performance of three different grades of carbide tools in face milling annealed nickel-based Nimonic 75 with a mean hardness of 235 HV. The inserts used were P40, K20 and K40 carbide grades. P40 grade inserts were mounted to a high positive, 100 mm diameter cutter with 70° approach angle. K20 and K40 grades were used with a negatively raked cutter of 45° approach angle.

Unlike expectations, P40 showed a remarkable performance at a cutting speed of 36 m/min lasting 86.8 min and the failure was due to progressive flank wear. With this grade, power consumption was much lower than with the other tools that caused reduction in cutting temperatures and provided good surface finish. The best overall cutting performance for the K20 grade was obtained under the following conditions of a cutting speed of 27 m/min, feed rate of 57 mm/min and depth of cut of 2.5 mm resulting in a tool life of 32.2 min. The superior performance of K20 grade over K40 was attributed to its higher hardness and thermal conductivity and lower thermal expansion

coefficient as well as having a higher compressive strength than K40. Chipping and/or fracture of the cutting edge were the dominant failure mode under most of the conditions tested. The combination of high temperatures, high thermo-mechanical stresses and workpiece adhesion was indicated as the reason for this type of failure.

Ohtani and Fujise [200] investigated the performance of three different types of round and square K10 grade cemented carbides when face milling of aged Inconel 718 of 415 HB hardness. A depth of cut of 0.2 mm, feed rate of 0.1 mm/tooth and cutting speeds ranging from 29 to 98 m/min were used.

They report that longer tool life was recorded with the round insert when the cutter was in neutral position. Under the same conditions a smaller surface roughness was obtained with the presence of oil-type coolant than that obtained from the other conditions tested. Up to the speed of 50 m/min, the rate of increase in flank wear was considerably low. However beyond this speed, the wear increased exponentially leaving the cutting edge chipped.

Investigating the effect of different sets of entry-exit conditions, Ohtani and Fujise observed that the tool life increased with the decrease in entry angle and with the increase in exit angle. In order to find out which angle has more influence on the tool life, they kept one of the angles at 90° constant position while changing the other. The effect of changing exit angle on tool life was greater than that of entry. Chipping at the cutting edge was observed at low range of exit angles. Flank wear (VB) was reduced at different rates with increase in entry or exit angles.

A TiN-Steel composite 4-flute end milling cutter of 12 mm diameter was tested on Nimonic 75 (235 HV) and Inconel 718 (364 HV) [141]. The tool was coated with a layer of PVD-TiN. It has been reported that when machining Nimonic 75, a 69 % and 100 % increase in the cutting speed and table feed respectively was achieved over the carbide counterpart. This performance was related to the good oxidation resistance of TiN within the matrix at high temperature range between 1100 and 1400 °C that ensures lower chemical reaction and diffusion between the tool and workpiece during high speed machining. WC-Co tools, however, exhibits good oxidation resistance at a temperature range of 50 to 800 °C. The results of milling Inconel 718 however, were not satisfactory due to rapid wear and/or chipping of the individual cutter flutes. The poor wear

resistance of the tool was primarily related to higher hardness and toughness of Inconel 718.

Alauddin et al. [15] reported the effects of varying cutting parameters and of different immersion ratios on tool life and wear behaviour of K20 grade carbide inserts when end milling Inconel 718. The cutter was of 25 mm diameter and accommodated 2 inserts. They observed that the edges of the inserts were micro-chipped at an axial depth of cut of 2 mm and cutting speeds of 11.7 and 16.1 m/min with the chip loads of 0.15 and 0.11 mm/tooth respectively at a constant feed rates of 45 mm/min. However this was not observed at higher cutting speed of 24.3 m/min where the chip load is 0.09 mm/tooth whereby a combination of adhesion, abrasion, diffusion and fatigue wear mechanisms was found to be acting on the tool.As for the effect of cutter immersion, full immersion milling gave the longest tool life of 9.5 min for which no satisfactory explanation was proposed. Comparing the other two modes of cutting, half immersion down-cut resulted in a tool life 5 times longer than that obtained in half immersion up-cut. They concluded that the rubbing action of the tool flank in up-cutting against newly generated transient surface by which the tool is guided, gave rise to the tool deterioration. This rubbing action occurring just before the tool starts removing chip, also causes a work-hardened layer to form changing material behaviour where the tool is subjected to high radial forces due to the increased elastic stress level in the work-hardened layer. High radial forces may become the most influential deterioration factor when cutting workpieces with high tendency to work-hardening. Moreover in the up-milling, chips are most likely be trapped between cutting edge and workpiece which can influence chip formation and surface finish. The contribution of the chip welding on the rake face to tool wear was also found to be very significant. Chip welding is very likely to occur due to the high temperature at the end of the cutting cycle where the chip thickness and consequently the pressures on the rake are at their maximum level.

Despite widespread use of TiN and Al_2O_3 as coating compounds, research into the development of alternative coating mediums are being carried out [201]. Coll et al. [202] has reported that (Ti,Al)N coated HSS end mill performed better than TiN and Ti(C,N) coated tool by 60 % and 23 % respectively during end milling of Inconel 718. They attributed better performance of (Ti,Al)N to the formation of a thin Al_2O_3 layer on the

contacting areas of the cutter at temperatures in excess of 500 °C. This layer acts as a thermal shield due to its low thermal conductivity and provides better chemical stability. In addition, (Ti,Al)N coating possesses higher ductility index, hardness and adhesion strength (1.5, 2400 HV and 65 N respectively) than the other two coatings.

5.8.2 Milling Superalloys With Ceramic Tools

Shook [11] tested face milling performance of Greenleaf's WG300 50 % silicon carbide whisker reinforced ceramic insert (Al_2O_3-SiC_w) on age-hardened Inconel 718 to 47 RC. The machining tests were performed at cutting speeds of 1000 (3300), 1212 (4000) and 1515 (5000) m/min (sfpm), feed rates of 63, 79, 90 in/min. and a DOC of 1.27 mm (0.05") and 1.9 mm (0.075") were employed.

He reports that the insert is very sensitive to DOC notch wear being the primary failure mode. A tool life of maximum 3 min. was obtained at the best cutting condition where the speed was 1000 m/min. Increasing speed shortened the tool life despite the more stable surface finish recorded up to the point where life limiting criterion was reached. In face milling operations, a round insert with negative rake geometry was proved to be the most effective in comparison to the other two geometries namely round-positive and square inserts. He did not observe any evidence showing the contribution of coolant to thermally induced cracks. Using flood coolant prevented small particles of the chip from being embedded into the workpiece surface.

Noaker [6], however, has reported the applicability of whisker-reinforced aluminium oxide ceramic tools in face milling Waspaloy. According to Noaker, whisker-reinforced aluminium oxide ceramic (WG-300) inserts were used to perform rough and finish face milling on a Waspaloy forging. It yielded a reduction in cycle time by a factor of 80 when compared with carbide inserts. A four-insert cutter of 76 mm diameter was used at a cutting speed of 958 m/min, a feed rate of 0.1 mm/tooth and depth of cuts of 1.27 and 0.64 mm for roughing and finishing respectively. The lack of detail as to the test condition in this case does not permit to make any comment about the reasons for different performances between the two cases.

El-Bestawi and his co-workers [16.] studied the wear behaviour of round and square whisker-reinforced alumina ceramic inserts in face milling Inconel 718. Fly cutting test

was employed under the conditions of a range of cutting speeds, from 200 to 700 m/min and at various feeds, depth of cuts and immersion ratios. They stated that formation of DOC-notch wear at full-immersion cutting was activated by a mechanism favoured by the serrated edge of the chip This type of chip was produced by uneven tearing from the workpiece and forced to rub against the cutting edge at the depth of cut line. As a consequence, the depth of cut area was thermally softened and hence became sensitive to seizure and pull out of tool materials [16]. They observed that at high cutting speeds and feed rates, trailing edge wear was the dominant failure mode. The reason proposed for trailing edge wear was the stress concentration at the free boundary of the tool causing localised wear. Moreover cyclic nature of the stresses on the rake face was correlated with crack initiation and subsequent grain removals leading to severe trailing edge failure.

As with the round insert, the best cutting condition where the tool wear was minimum, was obtained at the speed of 700 m/min whereas cutting speed of 500 m/min gave similar results for square ceramics. They reported that the difference in thermal expansion coefficients of alumina and workpiece material could cause cracking on the rake face of the tool during the cooling cycle because of the presence of adhered workpiece material. Increasing the feed rate up to 0.125 mm/tooth resulted in reduced flank and DOC-notch wear. This was due to reduced sliding contact length at the tool-work interface as a function of increased feed rate.

Mehrotra and Beeghly [193] have reported that round sailon inserts provided a tool life increase of 60 % when tested against Al_2O_3-SiC_w tool during end milling of Inconel 718 at 424 m/min (1400 sfm) and DOC of 2.5 mm whereby a cutter of 1.5" diameter having 3 inserts was employed under dry condition. Better performance of Sialon was attributed to its superior thermal shock resistance to that of Al_2O_3-SiC_w.

5.9 Unconventional techniques in conventional machining of nickel alloys

The difficulty in machining nickel-based alloys has been forcing the researchers to explore new techniques to assist conventional machining of these alloys. In this section, a brief account of promising techniques associated with various aspects of machining superalloys to improve productivity has been given.

5.9.1 Thermally-assisted machining

Laser-assisted machining (LAM) of nickel-based materials has been reported to enhance machinability as the modern laser application technologies permit precise control of the temperatures and the heat-affected zone [203]. Komanduri et al have reported that LAM provided 40 % less tool wear and 18 % less cutting force at a metal removal rate 33 % greater than in conventional turning of Inconel 718 with ceramic tools.

It has been reported that by adopting plasma-enhanced (PEM) machining it is possible to reduce tool wear and cutting forces by 40 % and 13-25 % respectively when turning cobalt-based alloys [203]. Novak et al [204] investigated the feasibility of PEM when turning Inconel 718 with Greenleaf's WG-300 (Al_2O_3-$SiC_{(w)}$) ceramic tool at a cutting speed of 5.45 m/sec, DOC of 0.82 mm and feed rate of 0.12 mm/rev. With plasma heating, they recorded an approximate 20 % reduction in all three force components and significant reduction in tool DOC-notch wear.

5.9.2 Rotary Tool

Using rotary tool in milling and turning of nickel and titanium based alloys has been reported to increase tool life and productivity when compared to stationary tool [205, 206]. Rotary tools are reported to provide better cooling and lubrication action of the cutting edge and lower wear rates [4]. Komanduri et al. obtained a tool life improvement on the order of 20 times when turning Inconel 718. Face milling of Inconel 718 with rotary tool using C-5 carbide inserts resulted in productivity increases in the range of 200-300 % and a cost reduction by approximately 50 %.

5.9.3 Taper turning

Longer tool lives have been obtained by adopting taper turning technique (also called 'ramping') by which DOC-notch wear is significantly reduced or avoided to become a tool life deciding factor. Using this technique, Ezugwu and Jawaid [144] reported that the notch formation was suppressed when machining Inconel 718 with coated and uncoated cemented carbides. Jun and Smith [183] reported that the ramping technique is the most significant method of extending tool life by eliminating notch formation in machining nickel alloys with silicon carbide whisker reinforced alumina

composite ceramic tools (Al_2O_3-$SiC_{(w)}$). They also mentioned the benefit of pre-chamfering of the workpiece edges which ensures progressive entry and exit of the tool from the workpiece to conserve the cutting edge from shock loading. The beneficial effect of this phenomenon in face milling steel with carbide tools was also shown by Lat and Ber [36]. Bhattacharyya et al [207] reported that the transition from notch wear to flank wear as the dominant cause of tool rejection was achieved by applying taper turning when machining Inconel 718 and Incoloy 901 with Sialon and Al_2O_3-$SiC_{(w)}$ ceramic tools.

5.9.4 Tools with unconventional geometry

Inserts with radically different geometry have been developed as a partial solution to the tool life problem in machining aerospace materials. Such a tool which is called 'ledge tool', has been used in face milling of a forged titanium alloy at a cutting speed approximately five times higher (213 m/min) than that for a conventional insert (53 m/min) [205] whereby providing a 2/3 reduction in machining costs. The unique design of the cutting edge enabled a progressive development of the combination of flank wear and micro-chipping, though at a faster rate in milling than in turning.

Hanasaki et al. [176], comparatively tested two P20 grade carbide inserts one with unique convex rake face and the other with conventional rake face when turning a high nickel alloy. They observed significant reduction in the rate of DOC-notch wear. Similar effect has also been observed by Narutaki et al. [17] when turning Inconel 718 with geometrically modified Al_2O_3-TiC ceramic tool (named as 'button with nick') at a cutting speed of 300 m/min, feed rate of 0.19 mm/rev and DOC of 0.5 mm whereby a 150 % reduction in trailing edge notch formation was obtained with attended improvement in surface finish.

Vigneau and Boulanger [208] have reported that they obtained a tool life increase by a factor of four with the geometric modification given to the standard cermet and Sialon tips when turning tempered and aged Inconel 718. The modification, which resulted in significant reduction in cutting and feed forces, was made depending on the wear modes produced by the standard geometry and involved altering the nose part of the tool.

5.9.5 Machining with variable feed

Variable-feed machining concept has been investigated during face milling and turning processes. It has been reported that varying the feed rate, when cutting is in progress, increases tool-chip contact area, reduces crater and flank wear and hence improves cutting tool life substantially [209]. A tool life improvement between 30-130 % has been reported when variable-feed face milling of Inconel 600 with M40 carbide tools at 22.6 m/min [210].

5.10 Surface Integrity of Machined Nickel-based Alloys

It has been pointed out by many researchers that the surface integrity of the machined components which includes surface roughness, strain-hardening (plastic deformation) and residual stress, has a significant effect on the fatigue and stress corrosion properties of many engineering components, in particular of those used under dynamically-stressed working conditions. Therefore, functional behaviour of machined surfaces depends particularly on the machining processes and the conditions under which they are carried out. It has also been reported that assessment of surface integrity is reliably accomplished by means of a number of techniques, usually in combination, that include micro hardness measurement, metallographic analysis and residual stress measurements [43, 45, 211, 212].

Nickel-based components used in aerospace industry generally function under severe conditions of high temperature and are subjected to high dynamic loads. Analysis of used and/or failed components during service shows that the vast majority of fatigue-related failures are initiated on or near the surface of the components [211, 213].

When conventional machining of nickel-based alloys, mechanically induced alterations such as plastic deformation, laps, tears and cracks are the most prevalent. Phase transformations do not generally occur with nickel-based alloys due to inherent metallurgical characteristics, i.e. it does not undergo phase alteration when subjected to high temperatures. Plastic deformation and subsequent strain-hardening in the affected areas were detected when milling, turning and drilling aged nickel-based alloys to a depth of approximately 0.05 mm (0.002") [45, 211, 214]. The extent of the affected layer is dependent on cutting parameters, tool geometry and tool wear and has been found to

increase from gentle to abusive cutting conditions and determined by means of micro-hardness measurements [45, 167, 211].

In nickel-based alloys, plastic deformation in the surface zone is associated with a change in the grain shape where numerous arcuate slip lines occur due to slipping of atomic layers along certain crystallographic planes. Depending on the cutting conditions, the hardness of plastically deformed layer can increase by 100-200 Vickers unit [45].

Field and Koster [215] have observed no metallurgical alteration in the surface zone when gentle face milling of aged Waspaloy (45 RC) with T-15 HSS tool under the conditions of a cutting speed of 7.5 m/min, DOC of 0.5 mm and feed rate of 0.12 mm/tooth. Abusive conditions however, produced plastic deformation characterised by slight twinning to a depth of 0.025 mm and a total work-hardened layer of 0.05 to 0.076 mm deep.

It has been reported that the surface integrity, in terms of low surface roughness and small surface hardening has substantial effect on the high-cycle and low-cycle fatigue life of GH33A nickel-based superalloy. Machining parameters of feed rate, rake angle, engagement angle and depth of cut have been found to be the most effective factors on surface integrity of carbide-turned GH33A and strict control of these parameters is emphasised [213].

Ezugwu and Tang [167] examined the surface integrity of Inconel 718 turned with pure and mixed alumina ceramic tools at a cutting speed of 150 m/min, feed rate of 0.125 mm/rev and DOC of 2 mm. They obtained better surface finish on Inconel 718 when machining with round inserts than with rhomboid inserts. Prolonged machining resulted in an increase in the hardness of the surface layer by 80-120 HV units. This has been associated with the workpiece's high work-hardening tendency and increased compressive stresses due to tool wear. Excessive tearing and plastic deformation were observed with prolonged cutting which may have a degrading effect on the surface integrity and hence fatigue strength.

Klocke et al. [45] report that Inconel 718 and Waspaloy components machined with ceramics and PCBN attain a better surface finish by approximately 3 times than carbide-machined counterparts. Moreover, the high machining conditions when using ceramics and PCBN tools showed no significant negative effect on the surface zone structure and

on dynamic stress properties of Waspaloy turbine disk as compared to machining with carbide tools.

5.11 Conclusion

It is clear from the results outlined above that no one single tool works best on all nickel-based superalloys. Even in a specific work material one particular tool grade may be more advantageous for one machining application while a different grade may be the best choice for another. It is obvious that over the cutting speed of 100 m/min, the cutting tool to machine nickel-based alloys should be from the class of either ceramic or PCBN. However, choosing the right grade is very much dependent on other cutting conditions as well as the state of workpiece material. DOC-notching is the most common failure mode in continuous turning whereas chipping and cutting edge fracture are more pronounced in milling. It is highly desirable to have a progressive wear type on the cutting tool because of the importance of predictability, consistency and reliability in machining exotic aerospace materials.

CHAPTER 6

EXPERIMENTAL TECHNIQUES

6.1 Introduction

The objective of this research is firstly to investigate the wear behaviour of PVD-TiN single layer and CVD-TiCN+Al_2O_3 double layer coated carbide insets when face milling two nickel based superalloys namely Inconel 718 and Waspaloy. An uncoated carbide grade was also tested in order to compare the results. Secondly the effects of the cutting conditions and tools on the surface integrity of the machined workpiece were investigated by measuring surface roughness and an analysis of subsurface microstructure. The progress of wear was routinely monitored and measured using a microscope at certain intervals of time during the tests. In addition, a detailed SEM analysis on the cutting edge was performed after cutting for 5 seconds and at the end of the tool life.

6.2 Cutting conditions

6.2.1 Machining parameters

The cutting conditions were chosen on the basis that the wear behaviour and performance of the cutting tools could be best understood at both demanding and industrially used cutting conditions. Cutting parameters were determined by considering the recommendation of the tool manufacturer [218] as well as previously published literature [13, 167, 200]. The cutting parameters for the coated and uncoated inserts are shown in Table 6.1.

Depth of cut (DOC) was kept constant throughout the cutting tests because of the limited availability of material as well as being the least effective parameter on tool life [206, 219, 220].

The range of cutting speeds for the uncoated carbide tool was different from that of the coated carbide tools. The main reason for choosing higher cutting speeds in the case of coated tools was to investigate the behaviour of the coatings at those conditions.

6.2.2 Cutting fluid

All the cutting tests were performed under wet conditions using an emulsion with 6 % general purpose Hocat-808 water soluble mineral oil. The rate of coolant supply to the cutting zone was 21 litre/min. Two flare nozzles were used to direct the coolant to the peripheral cutting zone in order to provide uniform distribution and effective cooling as shown in Figure 6.1. The concentration and the pH value of the coolant were regularly monitored by using refractometer and pH-meter to ensure consistency during the tests. The average pH value of the coolant was 8.5.

6.2.3 The relative position of the cutter and workpiece

The centre of the face milling cutter has been nominally positioned at the centre line of the workpiece in accordance with the ISO 8688-1 standard [124]. However, a 0.5 mm offset was given to the cutter axis towards the entry side of the workpiece in order to ensure a stable cutting with uniform vibration pattern. Otherwise the possibility of small alignment errors in the workpiece setup would cause alteration in the direction and magnitude of the resultant force hence leading to a non-uniform vibration pattern and cutting mode. Therefore maintaining the position of the cutter axis on one particular side of the workpiece centre will ensure a uniform cutting mode along the whole length of the test bar.

The length, height and width of the workpiece were 400 x 125 x 40 mm respectively. The ratio between the width of the workpiece and the cutter diameter was 0.63 which is within the limit of 60 ± 5 % as recommended by the ISO 8688-1 standard.

The starting end of the workpiece was pre-machined to create a radius with respect to the cutter diameter in order to provide a steady cutting condition with constant entry and exit angles. For the same reason, the finishing-end of the workpiece was not completely machined as shown in Figure 6.2.

6.2.4 The geometric detail of cutter-workpiece initial engagement

Earlier detailed studies of cutter engagement by Kronenberg [19] and Opitz and Beckhaus [20] show that the condition of cutter-workpiece engagement which is associated with the phenomena of 'penetration time' and 'partial area of engagement', has a significant effect on tool life. Because of its importance, the geometric detail of the initial engagement is given in Figures 6.3. As shown in this figure, the contact area of the tool face when fully engaged, was customarily identified with STUV letters. Point S refers to the sharp lower corner of the tool being the weakest spot. Point T is the outward corner of the area whereby depth of cut line intersects with the main cutting edge. Points V and U are located at a distance away from point S and T respectively. The distance is approximately equal to the feed per tooth.

The face milling cutter used in this study is a V contact cutter and provided a V-S-U-T contact pattern, as shown in Figure 6.3. The contact pattern was found by using the following calculations and assumptions.

According to Kronenberg,

if, $\gamma_r < \varepsilon_n$ and $\kappa > i_n$ then the first point to contact of the cutter will be V.

Where

γ_r : Radial rake angle,

ε_n : Angle of cutter engagement

κ: Approach angle

i_n : Index angle

Depending on the magnitude of index and approach angles, the order of subsequent points of contact are found. Using the following equation 'i_n' was found to be - 20°. When index line is located as shown in Figure 6.4 the order of contact points is found to be as V-S-U-T .

$$\tan i_n = \frac{\tan \gamma_a}{\tan \gamma_r - \tan \varepsilon_n} \qquad \text{Eq. 6. 1}$$

where

γ_a : Axial rake angle

γ_r : Radial rake angle

ε_n : Angle of cutter engagement

6.2.5 Workpiece holding method

The workpiece was fixed directly to the machine table to provide maximum rigidity, hence reducing vibration to its lowest level possible. To achieve this a special fixture was designed which consisted mainly of two supporting blocks and 3 'pivoting side clamps' as illustrated in Figure 6.5.

6.2.6 Checking cutter runout

Runout is measured for each insert at the beginning of each test according to ISO 8688-1 [124]. Axial and radial cutter runout were measured at the cutting edges while the cutter was mounted into the machine spindle and recorded in the test data sheets. The tolerances permitted by the ISO standard for axial and radial runout are 50 and 100 μm respectively.

A dial gage with 2 μm resolution was used to measure the runout. Figure 6.6 shows the way the checking is performed. With this technique axial runout was directly measured whereas effective radial runout is worked out by a simple calculation after measuring as described in the same figure.

$$r_{ef} = r_m \cdot \cos \kappa \qquad \text{Eq. 6. 2}$$

where, r_m: measured radial runout

r_{ef}: effective radial runout

κ: approach angle

6.3 Machine tool

The cutting tests were carried out on a CNC controlled Cincinnati Milacron Sabre 750 vertical machining centre (Figure 6.7). It has infinitely variable spindle speed ranging from 60 to 8000 rpm and, a variable table feed control from 3 to 15000 mm/min and an Acramatic 850SX controller. The machine is equipped with an AC drive motor of 9 kW. Unidirectional positioning and repeatability accuracy along the linear axes are ±0.008 and ±0.0015 mm. respectively. The spindle accommodates an ISO 1264003 type tool holder (adaptor) with No 40 taper.

6.4 Workpiece materials

Two types of nickel based alloys, namely Inconel 718 and Waspaloy were used for the machining tests. Both of the alloys were heat treated by a 3-step process comprising in turn solution-treating, stabilising and age-hardening (precipitation hardening). They have excellent high temperature strength and resistance to corrosion and oxidation at elevated temperatures above 870 °C making them favourite for aerospace applications. The nominal chemical compositions and physical properties of the alloys are given in Tables 6.2, 6.3 and 6.4. Figures 6.8 and 6.9 show the microstructures of the alloys with equiaxed grains and visible complex carbides dispersed at the grain boundaries and through the grains in the base gamma matrix.

The final dimensions of the workpiece blocks were 400 x 125 x 40 mm being the length, height and width respectively. All the surfaces of the blocks were pre-machined to the above dimensions by removing a layer of approximately 3 mm depth prior to actual machining tests

6.5 Cutting inserts

Two different PVD-TiN coated carbide inserts, KC720 and KC730 (Figure 6.10) grades, a CVD-TiCN+Al_2O_3 (Figure 6.11) double-layer coated insert of KC994M grade and an uncoated carbide insert of KMF (Figure 6.12) grade were used in this study. Microstructures of all the tools are shown in Figures 6.13 to 6.16 respectively. All the cutting tools posses the same standard geometry with ISO designations SEKN1204AFN and SEKN1203AFN for the coated and uncoated inserts respectively. They were manufactured and supplied by Kennametal-Hertel UK. In the case of CVD coated inserts, the cutting edge was honed to a radius of ~ 0.025 mm prior to coating process. All the inserts were checked, prior to machining, for any physical deficiency by means of a microscope at a magnification of x8. Figure 6.17 shows the geometric properties of the inserts. Some of the important physical and mechanical properties of inserts are given in Tables 6.5 and 6.6.

6.6 Face milling cutter

A face milling cutter with 63 mm effective diameter and 45° approach angle was used for all the tests. The ISO designation number for the cutter is 63A06R-F45SE12F04. Figure 6.18 shows the geometric detail of the cutter.

6.7 Tool life criteria and tool wear measurement

The tool life was determined on the basis of the following tool wear criteria. Tools were rejected when either of them was reached.

(a) When the average wear on the main cutting edge and/or nose flank reached 0.3 mm.

(b) If a maximum flank wear of 0.7 mm is reached on any of the inserts

(b) When chipping or flaking bigger than 0.4 mm width occurred.

(c) Surface roughness, Ra $\geq$ 5.0 μm was recorded.

Tool wear was measured at predetermined intervals of cutting time, as follows; 5th second, 20th second, 1st minute and then at every 2 or 4 minutes of interval, depending on the expected tool life, until the tool failure. When, however, approaching the end of tool life, tool wear was monitored and measured, at much shorter intervals to prevent catastrophic failure. The regular tool wear measurements were performed by using an optical tool makers microscope at a magnification of x25 (Figure 6.19). The wear at the main cutting edge, nose, flank and the rake face of the insert were measured and checked by placing the face milling cutter into a jig with 5 axes of freedom (Figure 6.20).

The tools were examined under Scanning Electron Microscope (SEM) and where necessary Energy Dispersive X-ray Analysis (EDAX) was performed on the worn and contact areas of the insert after first 5 seconds of cut and at the end of tool life. The purpose of the initial SEM analysis was to reveal the initial wear modes and mechanisms that could affect the subsequent performance of the tool. A Philips-505 SEM microscope (Figure 6.21) coupled with a PV-9100 energy dispersive x-ray spectroscopy (Figure 6.22) was used for the analysis.

6.8 Preparation and examination of samples

6.8.1 Tool samples

Tool samples representing both low and high cutting conditions, where cutting speeds are generally 25 and 75 m/min for the coated tools and 25 and 50 mm/min for the uncoated tool respectively, were selected for microscopic surface and subsurface wear analysis. Samples of worn tools and initial cut (i.e. after 5 seconds of cutting) were analysed systematically. Some of the worn tool samples were sectioned perpendicular to the cutting edge to reveal any subsurface microstructural changes. For sectioning the tool samples, a

low speed slitting machine equipped with a diamond cutting wheel of 102 mm diameter and 0.3 mm width was used while applying a force of 250 grams and using water as coolant in order to prevent any process-induced effect on the samples. Sectioned tool samples were then mounted in a conductive bakelite resin prior to polishing. They were finally examined on the SEM and/or EDAX after being polished, cleaned and/or etched by following systematic procedures explained in this section.

Worn tool samples used for surface wear pattern analysis were cleaned with acetone to remove oil stains and dirt sticking on the surface before taking them to the SEM and EDAX machines. Under the SEM, important areas of the tools such as rake face, flank face, nose and the cutting edge were thoroughly examined at various magnifications and from various angles.

6.8.2 Workpiece samples

Workpiece samples for subsurface microstructural examinations and micro hardness measurements were taken systematically from various cutting conditions whereby low and high cutting speeds of 25 and 50 or 75 m/min were employed. In the case of uncoated tool however, the highest cutting speed was 50 m/min. Workpiece samples were taken from the sections of the bar machined towards the end of tool life. For comparison purposes samples from initially-cut areas were also prepared.

Workpiece samples were cut from the machined bar by using an EDM machine (electro-discharge machine). This was necessary due to difficulty in hand cutting such workpiece materials. The EDM-machined surfaces were then gently ground to remove any process affected layer prior to polishing.

As with tool samples, workpiece samples were mounted in a bakelite resin for polishing and further analysis. Etched workpiece samples were examined under an optical microscope with an attached camera and display unit (Figure 6.23).

6.8.3 Chip samples

Samples of chip were also prepared and examined in order to identify their effect on the wear mechanism of the tools. Some of the samples were taken directly to SEM and EDAX examination after being cleaned with acetone while others were mounted in a bakelite resin then polished and/or etched prior to microscopic examinations.

The mounting, polishing and etching procedure were identical in the case of chip and workpiece samples.

6.8.4 Polishing methods

Samples were polished on an automatic polishing machine (Figure 6.24) following a standard procedure as explained below.

The mounted specimens of tools and workpiece were ground using a series of silicon carbide papers of 200, 400, 600 and 1200 grit sizes in that order, for 3 minutes each, with the presence of water as lubricant. The samples were then polished to 6 and 1 micron finish on flat disks covered with Textmat cloth impregnated with diamond paste using normal polishing oil for 3 minutes each. The final polishing was carried out on a Mastertex cloth impregnated with 0.6 micron diamond paste for 6 minutes using Collodial Silica solution. A vertical force of 5 lb was applied to each sample during the polishing processes. Polished samples were rinsed with water and alcohol then dried with hot air to prevent any corrosion.

6.8.5 Etching the samples

Tool and workpiece samples were etched in order to reveal original microstructures and to observe any process-induced microstructural change after cutting. Essential information on wear behaviour and mechanisms can be obtained from etched tool samples. The reliability of the components used in critical aerospace applications depends not only on the quality of external surface and dimensional features but also the quality of microstructure. Etching is an effective technique to reveal the physical condition of the microstructure.

Murakami's reagent [79] was used to etch some of the sectioned tungsten carbide tool samples for 5 to 60 seconds. The composition of Murakami's reagent includes 10 g of potassium ferriccyanide ($K_3Fe(CN)_6$), 10 g of sodium hydroxide (NaOH) and 100 ml of distilled water (H_2O). Cobalt binder is usually unetched by the reagents while etching of the mixed carbides is given by dark border surrounding irregularly rounded shapes. Ferric chloride ($FeCl_3$) was used to etch the cobalt binder phase for about 10 seconds as no other constituents were attacked by this etchant.

The polished workpiece samples of Inconel 718 and Waspaloy were etched for 5 to 30 seconds with Rolls-Royce's mixed acid which consists of 80 g of cubricchloride ($CuCl_2$), 60

g of ferricchloride ($FeCl_36H_2O$), 850 ml of hydrochloric acid (HCl), 150 ml of nitric acid (HNO_3) and 1 litre distilled water (H_2O) [221].

Each sample, after etching, was rinsed in water and alcohol in that order. The rinsed sample was then dried with hot air to prevent corrosion.

6.9 Measurement of surface roughness

The surface roughness (Ra) measurement was taken at three different positions after each cutting interval and the average of these readings was used to plot the graph. A portable stylus type instrument, Taylor-Hobson/Surtronic-3, (Figure 6.25) that gives the opportunity to measure the surface roughness without the need to remove the test bar from the machine was used. The instrument was calibrated for each set of experiments for consistency and accuracy.

6.10 Measurement of subsurface microhardness

Microhardness measurement was performed on the sections beneath the machined surface of the workpiece samples to detect possible variations that may be an evidence for work hardening as a result of plastic deformation and metallurgical phase alteration. A Mitutoyo MVK-H1 model microhardness tester (Figure 6.26) was used with a Vikers indenter by applying a load of 100 g. Measurements were taken at different intervals up to 0.5 mm depth, starting from a point 20 micron beneath the surface. The average of three microhardness readings taken at three different positions for the same depth was plotted to observe the pattern of subsurface microhardness values.

CHAPTER 7

EXPERIMENTAL RESULTS

7.1 Introduction

In this chapter, experimental results for the machining of Inconel 718 and Waspaloy are presented independently in two separate sections of identical format. The results include tool life data, tool failure modes, tool wear modes at initial and final cutting stages, wear development versus cutting time, effect of cutting speeds and feed rate on tool life, a comparison of tools performances in terms of tool life, volume of material removed and surface finish, surface roughness versus cutting time, subsurface microhardness measurement and finally subsurface microstructural conditions of the machined surfaces.

While most of the results are presented in full (such as tool life data and wear development), some results, for example tool wear, subsurface microstructures and microhardness, are represented only for high and low cutting conditions.

7.2 Face milling of Inconel 718

7.2.1 Tool Life, Tool Wear and Tool Failure Modes when Face Milling Inconel 718 with KC994M Tools

The tool life data, failure modes and predominant wear modes when face milling Inconel 718 with KC994M inserts are presented in Table 7.1. The highest tool life of 54 minutes was obtained at the lowest cutting speed of 25 m/min and a feed rate of 0.08 mm/tooth. When the feed rate was increased to 0.14 mm/tooth, a maximum tool life of 22 minutes was achieved at the same cutting speed.

The effect of increasing cutting speed and feed rate is shown in Figure 7.1a. This figure suggests that increasing both the cutting speed and feed rate has significantly reduced the tool life, especially within the range of 25 and 75 m/min. It also suggests that

the effect of increasing cutting speed, particularly up to 75 m/min, is much more pronounced than that of feed rate. The data shows that increasing cutting speed from 25 to 50 m/min resulted in 75 and 77 % reduction in tool life, at the feed rates of 0.08 and 0.14 mm/tooth respectively. In terms of the effect of increasing feed rate from 0.08 to 0.14 mm/tooth, a tool life reduction of approximately 60 % was observed for both the cutting speeds of 25 and 50 m/min. At the speed of 100 m/min, the tool life values were very short, dropping under 1 minute, and the difference between tool lives at low and high feed rates of 0.08 and 0.14 mm/tooth was not significant. 100 m/min was therefore considered as the maximum speed at which the tools would generate a life of one minute. Rest of the tests were carried out below this speed.

Tools were rejected due to average nose wear at all cutting speeds and feed rates tested. The dominant wear modes at tool failure were chipping and material adhesion in the form of galling and/or sticking of relatively large particles. Figures 7.2, 7.3 and 7.4 show failed KC994M tools with wear modes of galling, chipping and flaking under various cutting conditions. Premature failure of the cutting edge, usually within 1 minute of cutting time, due to severe chipping, breakage and/or flaking was observed at higher cutting speeds of 75 and 100 m/min for both high and low feed rate conditions (Figure 7.2 and 7.3). However, at the lowest cutting speed of 25 m/min, a combination of progressive wear by plucking, pitting, microchipping and workpiece galling were the dominant causes of tool failure, as shown in Figure 7.4.

Figures 7.5 and 7.6 show the development of flank wear at feed rates of 0.14 and 0.08 mm/tooth respectively. Progressive development of flank wear, at a relatively constant rate, can only be observed at lower cutting speeds of 25 and 50 m/min, with an acceleration towards the tool life limit. Both figures show that, at higher cutting speed of 75 and 100 m/min, flank wear rate was significantly high, due to abrupt failure of the cutting tool caused by premature chipping or flaking.

Examination of the cutting tools at an initial stage, after cutting for 5 seconds, reveals important information on the wear behaviour of double-layer coating and of the cutting edge. Figures 7.7a to 7.13 show that workpiece galling and coating delamination occurred at all cutting speeds and feed rates investigated. At high cutting speeds of 75 and 100 m/min, in addition to galling and coating delamination, microchipping and adhesion of

relatively large workpiece material were found as shown in Figure 7.11a, 7.12a and 7.13. The presence of such phenomena was confirmed by performing EDAX analysis on the associated areas of the tools, the analysis is presented in Figures 7.7b to 7.12b.

7.2.2 Tool Life, Tool Wear and Tool Failure Modes when Face Milling Inconel 718 with KC720 Tools

Tool life values and failure modes for KC720 inserts when face milling Inconel 718 are summarised in Table 7.2. Maximum tool lives of 13 and 14 minutes were achieved at the feed rates of 0.08 and 0.14 mm/tooth respectively when machining at a cutting speed of 25 m/min. Figure 7.14 and 7.15 suggest that at the cutting speed of 25 m/min, the difference in wear rates at low and high feed rates of 0.08 and 0.14 mm/tooth was insignificant, up to the point of tool life criterion, with a wear progression of a relatively linear type. However, at the cutting speed of 50 m/min, increasing the feed rate to 0.14 mm/tooth resulted in a tool life reduction by 57 %, representing the largest reduction in tool life for KC720 inserts within the cutting speed range investigated, as shown in Figure 7.1b. This figure also shows the effect of increasing cutting speed on tool life. It suggests that increasing the cutting speed from 25 to 50 m/min resulted in tool life reductions by 55 and 79 % for the feed rates of 0.08 and 0.14 mm/tooth respectively. Figures 7.14 and 7.15 demonstrate that, at higher cutting speed of 75 and 100 m/min, tool life was less than 1 minute, due to premature failure of the cutting tool caused by severe chipping or breakage of the cutting edge (Figure 7.16 and 7.17).

Tool failure at the lowest cutting speed of 25 m/min was due to average flank wear which was caused by a combination of progressive chipping, galling, galling-related plucking and coating delamination as shown in Figures 7.18 and 7.19. At all other cutting speeds and feed rates, tool rejection was due to average nose wear dominated by severe chipping or breakage (Figure 7.16 and 7.17).

Figures 7.20 to 7.26 show the condition of the cutting edge after the initial cutting period of 5 seconds at the cutting speeds of 25 and 75 m/min and feed rates of 0.08 and 0.14 mm/tooth. It can be seen from these figures that, the prevailing failure and wear modes are severe galling, coating delamination, discrete plucking, microchipping and adhesion of relatively large chip particles at the cutting edge. EDAX analysis in Figures

7.21b, 7.25b and 7.26b were performed to confirm the presence of these failure and wear modes. The presence of microchipping and adhesion of chip particles was more pronounced at the initial cutting stage, when the cutting speed and feed rate were higher. Figure 7.24 shows a KC720 insert cutting for 18 seconds at the lowest speed of 25 m/min and feed rate of 0.08 mm/tooth with no visible microchipping and chip adhesion.

7.2.3 Tool Life, Tool Wear and Tool Failure Modes when Face Milling Inconel 718 with KC730 Tools

The tool life values and failure modes, when face milling Inconel 718 with KC730, are presented in Table 7.3. Tool failure was due to flank wear at almost all cutting conditions. Maximum tool lives of 23 and 14 minutes were achieved at the lowest cutting speed of 25 m/min and feed rates of 0.08 and 0.14 mm/tooth respectively. Figure 7.1c shows that the effect of increasing feed rate and cutting speed on tool life of KC730 inserts cutting Inconel 718. Increasing feed rate from 0.08 to 0.14 mm/tooth reduced the tool life by 40 and 60 % at the cutting speeds of 25 and 50 m/min respectively. Increasing the cutting speed from 25 to 50 m/min resulted in tool life reductions of 55 and 72 % for the feed rates of 0.08 and 0.14 mm/tooth respectively.

Figures 7.27 and 7.28 show that progressive wear development was observed when machining up to the cutting speed of 50 m/min for both the feed rate conditions. Short tool lives were recorded at the cutting speeds of 75 and 100 m/min. At the cutting speed of 75 and low feed rate of 0.08 mm/tooth, a tool life of 2.3 min was recorded which is the highest tool life value of all coated tools used on Inconel 718 at this particular cutting speed. Short tool life at higher cutting speeds was due to premature tool failure caused by chipping, breakage and/or flaking as shown in Figures 7.29 and 7.30. However, as shown in Figure 7.31, at low cutting speeds, a combination of progressive chipping, plucking and workpiece galling was the dominant wear modes at tool failure.

SEM micrographs in Figures 7.32 to 7.35 show the initial wear modes after cutting for 5 seconds at various cutting conditions. Coating delamination, workpiece galling and associated discrete substrate pitting were present at all cutting conditions. This was also confirmed by EDAX analysis shown in Figures 7.33b and 7.35b. However, discrete microchipping was found to occur at low cutting speeds (Figure 7.33a) whereas chipping

of almost entire cutting edge along with adhered workpiece was observed at high cutting speeds (Figure 7.34).

7.2.4 Tool Life, Tool Wear and Tool Failure Modes when Face Milling Inconel 718 with KMF Tools

Tool life values, failure modes and dominant wear modes for KMF inserts at tool failure are shown in Table 7.4. A maximum tool life of 32 minutes was recorded at the lowest cutting speed of 25 m/min and feed rate of 0.08. Increasing the feed rate to 0.14 mm/tooth at this cutting speed yielded a tool life of 22 minutes. The tool life values at the highest cutting speed of 50 m/min were 3 and 2.6 minutes for the feed rates of 0.08 and 0.14 mm/tooth respectively.

The effect of increasing cutting speed and feed rate on tool life is illustrated in Figure 7.1d. It was found that increasing the feed rate from 0.08 to 0.14 mm/tooth at the cutting speeds of 25 and 50 m/min reduced the tool life by 30 and 14 % respectively. Moreover, almost the same degree of tool life reduction, being 90 and 88 %, was recorded with increasing the cutting speed from 25 to 50 m/min for both feed rates of 0.08 and 0.14 mm/tooth. Figures 7.36 and 7.37 show the effect of cutting speed on flank wear. A notable acceleration in wear rate was observed when the cutting speed was raised from 32 to 40 m/min for both low and high feed rate conditions.

KMF tools were rejected on reaching the average nose wear limit at low cutting speeds of 25 and 32 m/min for high and low feed rate conditions. At higher cutting speeds of 40 and 50 m/min, average flank wear was the dominant cause of tool rejection. Figures 7.38 and 7.39 show that tool failure at the lowest cutting speed of 25 m/min, was due to a combination of wear modes of workpiece galling, plucking and chipping. Figure 7.40 shows that at the cutting speed of 50 m/min, combination of severe chipping, breakage, workpiece adhesion and associated plastic deformation was the prominent wear mode responsible for tool failure.

SEM micrographs of initial wear modes are shown in Figures 7.41 to 7.47. These figures suggest that workpiece galling and related pitting on the rake face were dominant at all cutting conditions. They also show the presence of adhered workpiece particles at

the cutting edge which are more prevalent at higher cutting speeds and most likely on the microchipped areas (Figure 7.46 and 7.47).

7.2.5 Comparative performance analysis of the cutting tools tested on Inconel 718

In order to evaluate the overall performance of cutting tools used on Inconel 718, a relative comparison and assessment have been made on the basis of tool life and volume of material removed by each tool.

7.2.5.1 Tool life

Tool life results of four different types of tools used for face milling Inconel 718 at various cutting speeds and feed rates are compared in Figures 7.48 and 7.49. All the coated tools showed a common trend of short tool life particularly at higher cutting speeds of 75 and 100 m/min. The uncoated tool KMF also exhibited similar behaviour of short tool life at a cutting speed of 50 m/min. This effect was more pronounced when face milling at a higher feed rate of 0.14 mm/tooth (Figure 7.49).

At lower cutting speeds of 25 and 50 m/min and lower feed rate of 0.08 mm/tooth, much longer tool lives were obtained. At the cutting speed of 50 m/min, all coated tools showed much better performance than the uncoated KMF grade. However, at the cutting speed of 25 m/min, the uncoated KMF tool significantly outperformed the PVD coated tools KC720 and KC730. The CVD-coated KC994M tool showed better performance, particularly at the lowest cutting speed of 25 m/min, than the PVD-coated and uncoated tools. Comparing the PVD-coated KC720 and KC730 tools, the latter gave longer tool lives at lower cutting speeds and feed rate conditions.

Figure 7.49 also shows that, at a higher feed rate of 0.14 mm/tooth and the lowest cutting speed of 25 m/min, CVD-coated KC994M tool gave better performance than the PVD-coated tools. The performance of uncoated KMF tool was observed to be similar to that of CVD-coated KC994M tool, both giving a tool life of 22 minutes. At this feed rate, PVD-coated KC720 and KC730 tools showed an equal performance by yielding a tool life of 14 minutes at the lowest cutting speed of 25 m/min. At the cutting speed of 50 m/min, the difference between the tool lives of KC720 and KMF tools was negligible, while KC730 and KC994M showed almost an equal performance by giving 4 and 5 minutes tool lives respectively, which was better than those of KMF and KC720 tools.

Based on tool life assessment, as shown in Figures 7.48 and 7.49, the CVD-coated KC994M inserts yielded the best overall performance when compared with all the other cutting tools in face milling Inconel 718.

7.2.5.2 Volume of material removed

The volume of material removed when face milling Inconel 718 under all cutting conditions with four types of cutting tools is presented in Figures 7.50 and 7.51. The volume of removed material has been calculated using the following formula;

$$Q = a_p a_r T V_f / 1000$$

Where

Q: Volume removed (cm^3), a_p: Axial depth of cut (mm), a_r: Radial depth of cut (mm), T : Tool life (min) and V_f: Feed rate (mm/min).

It can be seen from Figures 7.50 and 7.51, that the volume of material removed, before the tool reached its failure criteria, has generally decreased with increasing cutting speed, in particular at higher cutting speeds of 75 and 100 m/min due to corresponding short tool lives. All the cutting tools produced higher volumes of metal removal at high feed rate of 0.14 mm/tooth and cutting speed of 25 m/min, except for KC994M which removed more metal at the low feed rate of 0.08 mm/tooth due to exceptionally long tool life of 54 minutes.

The highest volume of metal removed was 65.3 cm^3 achieved by KC994M tool at the lowest cutting speed of 25 m/min and feed rate of 0.08 mm/tooth. At this cutting speed and at both feed rates of 0.08 and 0.14 mm/tooth, the CVD-coated KC994M and uncoated KMF tools produced significantly higher volume of metal than those of PVD-coated KC720 and KC730 tools. An equal amount of metal removed (~ 46 cm^3) was achieved with the CVD-coated KC994M and uncoated KMF tools at the lowest cutting speed of 25 m/min and feed rate of 0.14 mm/tooth. Figures 7.50 and 7.51 suggest that of the two PVD coated grades, KC730 gave better performance than KC720 under all cutting conditions. The differences in the volume of material removed was more pronounced when cutting at low feed rate of 0.08 mm/tooth.

On the basis of the volume of metal removed, CVD-coated KC994M gave the best overall performance particularly at lower cutting speeds of 25 and 50 m/min for both feed rates of 0.08 and 0.14 mm/tooth. The results suggest that, higher feed rate of 0.14 mm/tooth should be employed for efficient high volume of metal removal, despite relative reduction in tool lives, since this provided an approximate twofold increase in the metal removal rate at lower cutting speeds of 25 and 50 m/min.

7.2.6 Surface Integrity

The surface integrity aspect of machined aerospace components is highly critical as it affects the reliability of such products under severe service conditions. Metal cutting does impose surface alteration, the extent and nature of which must be investigated to ensure required high surface standards on machined nickel-based superalloys. Three important aspects of surface integrity which include surface roughness, subsurface microhardness tests and metallurgical analysis in relation to the machined surface were investigated and an evaluation of the results presented in this section.

7.2.6.1 Surface Roughness

The surface roughness values (R_a) of the machined surfaces with all four types of cutting tools used for machining Inconel 718 at various cutting conditions are presented in Figures 7.52 to 7.59. These figures generally suggest that at both feed rates of 0.08 and 0.14 mm/tooth, a similar trend of surface roughness pattern was produced, particularly at lower cutting speeds of 25 and 50 m/min.

The results show that surface roughness values were relatively high at the initial cutting stage, gradually dropping with the passage of cutting time, mostly in a fluctuating fashion. The high surface roughness values at the start of cut was due to the sharp cutting edge which is relatively more sensitive to interrupted cutting and associated vibration. The fluctuating nature of surface roughness values with the progress of machining can be associated with periodic workpiece adherence to and detachment from the cutting edge. The second cause for this fluctuation can be the wear pattern of the cutting tools which involved progressive chipping at various degrees of severity depending on the cutting speed and feed rate employed. These figures also indicates that, in most cases, slightly lower surface finish values were obtained with increasing cutting speed. This can be seen

clearly when the surface roughness plots in each individual figure are compared (Figures 7.52 to 7.59). Another notable common characteristics suggested by these Figures is that the difference in surface roughness values become marginal with prolonged machining regardless of the cutting speeds and feed rates employed.

The results also indicate that the effect of feed rate on surface roughness was marginal. This is most likely due to the geometric configuration of the cutting edge which features a flat wiper edge of 2.4 mm length (minor cutting edge) as depicted in Figure 6.17. Such an edge theoretically eliminates the geometric effect of changing the feed rate on surface roughness.

In order to compare the effect of each carbide tool tested on Inconel 718, the surface roughness values obtained at a cutting speed of 25 m/min and feed rates of 0.08 and 0.14 mm/tooth were plotted in Figures 7.60 and 7.61. These figures show that CVD-coated KC994M tool produced the highest average surface roughness at high and low feed rates of 0.08 and 0.14 mm/tooth. The uncoated KMF tool produced the second highest average surface roughness at higher feed rate of 0.14 mm/tooth. In comparison with these two cutting tools, PVD-coated KC720 and KC730 produced lower surface roughness at both the feed rates. The lowest average surface roughness at high feed rate of 0.14 mm/tooth was produced by KC730, whereas at low feed rate of 0.08 mm/tooth by KC720. It was noted that at low and high feed rate conditions, the differences in surface roughness were more pronounced at the initial period of machining which gradually reduced and became insignificant with prolonged cutting time. Moreover, the average surface roughness values obtained by PVD-coated KC720, KC730 and uncoated KMF tools were found to be very close to each other, being 0.44, 0.52 and 0.47 μm respectively, at the low feed rate of 0.08 mm/tooth.

The highest surface roughness reading recorded when face milling Inconel 718 was 1.45 μm with CVD-coated KC994M produced at a cutting speed of 75 m/min and feed rate of 0.08 mm/tooth (Figure 7.53). Hence, all the surface roughness values produced during the cutting tests were well below the rejection criterion of 5.0 μm.

7.2.6.2 Microhardness Tests

The results of subsurface microhardness measurements of the machined surface when machining Inconel 718 using all four types of cutting tools are presented in Figures 7.62 to 7.65. The measurements were performed on the samples produced at two cutting speeds of 25 and 75 m/min and feed rate of 0.08 and 0.14 mm/tooth, chosen to represent the low and high cutting conditions. For the uncoated KMF tools, surface samples were taken from the conditions where cutting speeds of 25 and 50 m/min were employed, the latter being the maximum speed used with this type of tool. The sample surfaces on which the microhardness tests performed were taken immediately after the tools had failed. To be able to compare the effect of worn tool with that of sharp, microhardness readings on the samples produced after 5 seconds of machining at the cutting speed of 25 m/min are also presented in Figures 7.62 to 7.65. The fluctuating nature of the plots is because of the microstructure of Inconel 718 which contains dispersed metal carbides (MC) being much harder than the main nickel-based solid solution matrix (γ phase). A relatively light weight was used during the microhardness testing and this may have also encouraged the above phenomenon.

In case of CVD and PVD coated tools, as shown in Figures 7.62 to 7.64, a similar trend of hardness pattern was observed on the machined surface samples. The results show that the hardness of the top surface layer was always higher than that of the inner section of the material and the hardness was reducing towards the nominal value of 515 HV with increasing depth below the surface.

At a depth of 0.020 mm below the surface, which was the closest measurable point to the surface, an increase in the hardness by 39 to 92 HV units (an increase between 7 to 17 %) was recorded with coated tools. The results suggest that the maximum increase in surface hardness was produced by CVD-coated KC994M tools, measuring 607 HV at the closest point to the surface. A minimum reading of 554 HV was recorded with PVD-coated KC730 tools at the same point. It can be seen from the results that between the depths of 0.1 and 0.2 mm, the measured hardness values generally dropped to the level of nominal hardness value of the workpiece.

Another common characteristic of the surfaces produced by coated tools is that the recorded readings up to the depth of 0.2 mm, produced at a cutting speed of 75 m/min

were notably higher than that of the other cutting conditions. This suggests that the degree of hardening of the machined surface increases with increasing cutting speed.

The plots in Figures 7.62 to 7.65, representing the effect of sharp tools on subsurface microhardness of the samples produced after 5 seconds of cutting at a cutting speed of 25 m/min and feed rates of 0.08 and 0.14 mm/tooth, suggest that there was no significant deviation from the nominal hardness value at early stage of machining. This indicates clearly that there exists a strong correlation between the tool wear and the extent of surface hardening as a result of prolonged machining. However, the micrographs showing the microstructures of the surface region, in section 7.2.6.3 indicate that plastic deformation occurred at this early stage of cutting within a narrow zone just beneath the surface where microhardness measurement was not possible to take.

7.2.6.3 Metallurgical Alterations

The subsurface microstructure of the machined surfaces was examined to determine the extent of metallurgical alterations. Samples, obtained from early machining period (after cutting 5 seconds) and at the end of tool life, were comparatively analysed for this purpose. Optical micrographs produced at 500X and 1220X magnification, showing the microstructure of the machined surfaces, were presented and evaluated. Microstructure of the samples produced at the cutting speeds of 25 and 75 m/min were analysed to represent low and high cutting conditions for Inconel 718 workpiece. Parallel and perpendicular sections of the samples to the feed direction were produced in order to observe possible microstructural alterations.

In the analyses of the subsurface microstructures, both workpiece materials (Inconel 718 and Waspaloy) showed similar microstructural alterations and surface damage pattern. This included, curved slip lines, in the direction of cutter rotation and/or the feed direction and disturbed microstructure within the surface regions which indicate plastic deformation during the face milling process. It has also been found that physical damage in the form of surface tearing and embedded or dislodged hard particles (WC) to occur which caused discontinuity and irregularity in the surface layer. These alterations are refereed to as 'plastic deformation' and 'surface tearing' or 'surface irregularity' in the text to avoid unnecessary repetition and lengthy descriptions. However, where necessary,

detailed descriptions have been given in the title of each figures. Moreover, the micrographs presented in this section suggest that plastic deformation, and associated strain hardening occurred at the beginning of machining (within 5 seconds) within a surface region of approximately 10 to 15 μm depth in which microhardness measurements was not possible to perform. Therefore the plots in Figures 7.62 to 7.65, representing the initial cutting conditions, show no microhardness increase in case of face milling Inconel 718. Micrographs showing the effect of initial cutting indicate that the extent of plastic deformation was generally more when machining at the high feed rate of 0.14 mm/tooth than that of low feed rate of 0.08 mm/tooth for Inconel 718 and Waspaloy workpieces. The results also suggest that whenever the tool is subjected to severe chipping, this has led to surface tearing or irregularities on the machined surface regardless of machining stage. This effect however was more evident as the cutting speed and feed rate were increased.

Figures 7.66 to 7.72 show that plastic deformation and surface tearing has occurred at the start of machining and at the end of tool life when face milling Inconel 718 with CVD-coated KC994M tools at the cutting speeds of 25 and 75 m/min and feed rates of 0.08 and 0.14 mm/tooth. The surface layer was generally smooth and less plastic deformation was evident in the surfaces produced at the beginning of machining. Comparing Figures 7.66 and 7.67 with 7.69 and 7.70 suggest that the extent of plastic deformation at earlier stage was less in case of low feed rate of 0.08 mm/tooth than that of high feed rate of 0.14 mm/tooth. Figure 7.68 and 7.71 show surface tearing, most probably caused by chipped and trapped tool particles towards the end of tool life at high cutting speed of 75 m/min. At this cutting speed, similar damage was also observed at the start of machining as shown in Figure 7.72.

Figures 7.73 to 7.77 show surface microstructure of Inconel 718 machined by PVD-coated KC720 inserts at various cutting conditions. At cutting speed of 25 m/min and feed rate of 0.14 mm/tooth, slight plastic deformation and occasional surface damage were detected at the end of tool life, as shown in Figure 7.74. At this feed rate, surface tearing occurred at start of machining when milling at cutting speeds of 25 and 75 m/min as shown in Figures 7.73 and 7.75. Given that the chipping is one of the dominant wear modes of early cutting period, particularly at high cutting speeds, it is very likely that

chipped and trapped tool particles (predominantly WC) are the causes for such kind of surface damage. Figure 7.76 and 7.77 show the presence of plastic deformation in the surface region, at the start and the end of tool life when machining at the lowest cutting condition of 25 m/min and feed rate of 0.08 m/min. Figure 7.77 indicates that the degree of plastic deformation at the start of the cut is less than that produced at the end of tool life. Examination of the entire surface region of the samples did not reveal any significant surface damage at both conditions compared to the samples generated at high feed rate which are shown in Figures 7.73 and 7.75. This is most probably due to rare microchipping both at start of the cut and during the process until the tool reached its failure criteria.

Figures 7.78 to 7.84 show subsurface microstructures when machining Inconel 718 with KC730 tools. These figures show that plastic deformation has taken place at the start and the end of machining when face milling at the cutting speed of 25 m/min and feed rate of 0.14 mm/tooth. In addition to this, occasional surface damage was observed at both stages as shown in Figures 7.79 and 7.80. Plastic deformation of similar extent was observed at the end of tool life when machining at a feed rate of 0.08 mm/tooth and cutting speeds of 25 and 75 m/min as shown in Figures 7.81 and 7.83 respectively. No significant alteration was detected in the microstructure of the surfaces generated at the start of cut, at low feed rate of 0.08 mm/tooth as shown in Figure 7.82. Rare surface damage was detected at both cutting speeds, an example of which is shown in Figure 7.84.

Comparing the samples taken at the end of tool life (Figures 7.85 and 7.86) suggests that more plastic deformation was induced at the high feed rate of 0.14 mm/tooth and cutting speed of 25 m/min when face milling with KMF tools. This was also the case at the cutting speed of 50 m/min. Samples taken from the initial cuts also suggest that the extent of plastic deformation was more in case of high feed rate of 0.14 mm/tooth as shown in Figures 7.87 and 7.88. Although no surface damage was detected on the samples, the fact that the tool failure was due to extensive chipping particularly at higher cutting speeds, suggests that rare surface damage similar to that encountered with other tools may well be present.

7.3 Face milling of Waspaloy

In this section the results obtained from face milling of Waspaloy alloy are presented in a format similar to the first section (7.2).

7.3.1 Tool Life, Tool Wear and Tool Failure Modes when Face Milling Waspaloy with KC994M Tools

The tool life data, failure modes and predominant wear modes when face milling Waspaloy with KC994M inserts are presented in Table 7.5. Maximum tool lives of 18 and 9 minutes were recorded at the lowest cutting speed of 25 m/min at feed rates of 0.08 and 0.14 mm/tooth respectively.

The effect of increasing cutting speed and feed rate is shown in Figure 7.89a, which suggests that increasing both the cutting speed and feed rate significantly reduces the tool life, especially within the range of 25 and 50 m/min. It also shows that the effect of increasing cutting speed to 50 m/min caused a steep reduction in tool life by 95 %, for both feed rates of 0.08 and 0.14 mm/tooth. As for the effect of increasing the feed rate from 0.08 to 0.14 mm/tooth, a tool life reduction of 50 % was recorded for the cutting speeds of 25 and 50 m/min. At the cutting speeds of 75 and 100 m/min, the tool life was under 1 minute for both the feed rates of 0.08 and 0.14 mm/tooth.

Tools were rejected due to average nose wear at all cutting speeds and feed rates tested. The dominant wear modes at tool failure were chipping and material adhesion in the form of galling and adherence of relatively large particles particularly at the cutting speed of 50 m/min and over. Figures 7.90, 7.91 and 7.92 show failed KC994M tools with predominant wear modes of galling, chipping and workpiece adhesion. Tools were also observed to have suffered from plastic deformation and mechanical cracking under various cutting conditions as shown in Figures 7.93, 7.94 and 7.95. Premature failure of the cutting edge due to macro chipping or breakage was observed at higher cutting speeds of 50 to 100 m/min for both feed rate conditions (Figure 7.90 and 7.92). However, at low cutting speed of 25 m/min, a combination of progressive wear by plucking, pitting, microchipping and workpiece galling was the dominant cause of tool failure, as shown in Figure 7.91.

Figures 7.96 and 7.97 show the development of flank wear at feed rates of 0.14 and 0.08 mm/tooth respectively. Progressive development of flank wear, at a relatively constant rate, can only be observed at the lowest cutting speeds of 25 m/min, with an accelerated phase towards the tool life limit. Figures 7.96 and 7.97 show that, for the cutting speeds of 50, 75 and 100 m/min, flank wear rate was significantly high, due to abrupt failure of the cutting tool caused by premature chipping or breakage.

Examination of the cutting tools after cutting for 5 seconds, reveals important information on the wear behaviour of coating and substrate. SEM micrographs in Figures 7.98 to 7.103 show that workpiece galling, coating delamination and substrate pitting occurred at all cutting speeds and feed rates investigated. At high cutting speeds of 75 and 100 m/min, in addition to galling and coating delamination, microchipping and adhesion of relatively large workpiece material were found as shown in Figure 7.101, 7.102a and 7.103a. The presence of these wear mechanisms were confirmed by EDAX analysis on the used tools and are presented in Figures 7.98b to 7.103b.

7.3.2 Tool Life, Tool Wear and Tool Failure Modes when Face Milling Waspaloy with KC720 Tools

Tool life values and failure modes for KC720 inserts when face milling Waspaloy are summarised in Table 7.6. Maximum tool lives of 5 and 3 minutes were achieved at feed rates of 0.08 and 0.14 mm/tooth respectively when the cutting speed was 25 m/min.

The effect of increasing cutting speed and feed rate is shown in Figure 7.89b which suggests that increasing both the cutting speed and feed rate significantly reduces the tool life, especially within the range of 25 and 50 m/min. It also shows that increasing cutting speed to 50 m/min causes a steep reduction in tool life. Tool life reductions, by approximately 75 and 85 % for the feed rates of 0.08 and 0.14 mm/tooth respectively, were recorded at the cutting speed of 50 m/min. As for the effect of increasing feed rate from 0.08 to 0.14 mm/tooth, tool life reductions were 40 and 65 % for the cutting speeds of 25 and 50 m/min respectively. Very short tool life values were obtained due to premature failure at the cutting speed of 50 m/min and above and the difference between tool lives at low and high feed rates of 0.08 and 0.14 mm/tooth was of no significance.

In most cases, tools were rejected due to the average flank wear at the cutting speeds of 25 and 50 m/min for both feed rates of 0.08 and 0.14 mm/tooth. Tool rejection was due to nose wear at the higher cutting speeds of 75 and 100 m/min. The dominant wear modes at tool failure were chipping and material adhesion particularly at the cutting speed of 50 m/min and over. Figures 7.104, 7.105 and 7.106 show failed KC720 tools with predominant wear modes of galling, chipping and workpiece adhesion. In addition, plastic deformation and associated cracking occurred under various cutting conditions as shown in Figures 7.107 to 7.110. Premature tool failure due to chipping or breakage was observed at higher cutting speeds of 50 to 100 m/min for both feed rate conditions (Figure 7.106 and 7.109). However, at low cutting speed of 25 m/min, a combination of progressive wear by plucking, pitting, microchipping and workpiece galling was the dominant cause of tool failure, as shown in Figure 7.104 and 7.105.

Figures 7.111 and 7.112 show the development of flank wear at feed rates of 0.14 and 0.08 mm/tooth respectively. Progressive flank wear development was observed only at the lowest cutting speeds of 25 m/min, with an accelerated phase towards the end of tool life. These figures indicate that, for the cutting speeds of 50, 75 and 100 m/min, flank wear rates were significantly high, due to premature tool failure caused by chipping or breakage.

Examination of the cutting tools, at an early stage of cutting for 5 seconds, reveals important information on the wear behaviour of coating and cutting edge. SEM micrographs in Figures 7.113 to 7.118 show that workpiece galling, coating delamination and substrate pitting occurred at all cutting speeds and feed rates used. At the cutting speeds of 50 to 100 m/min, severe chipping was observed in addition to galling and coating delamination, as shown in Figure 7.118. EDAX analysis, presented in Figures 7.116b and 7.117b, confirm the presence of galling, coating delamination and microchipping.

7.3.3 Tool Life, Tool Wear and Tool Failure Modes when Face Milling Waspaloy with KC730 Tools

Tool life values and failure modes for KC730 inserts when face milling Waspaloy are presented in Table 7.7. Maximum tool lives of 10 and 1.8 minutes were achieved at the

lowest cutting speed of 25 m/min for the feed rates of 0.08 and 0.14 mm/tooth respectively.

The effect of increasing cutting speed and feed rate on tool life is shown in Figure 7.89c. This figure suggests that increasing both the cutting speed and feed rate has significantly reduced the tool life, especially within the range of 25 and 50 m/min. Increasing cutting speed from 25 to 50 m/min reduced the tool life by approximately 90 %, for both feed rates of 0.08 and 0.14 mm/tooth. When the feed rate was increased from 0.08 to 0.14 mm/tooth, tool life reductions by 82 and 80 % were recorded at the cutting speeds of 25 and 50 m/min respectively. At the cutting speed of 50 m/min and above, the tool life was either 1 minute or under.

At all the cutting conditions investigated, tool rejection was due to average flank wear, except for the cutting speeds of 25 and 50 m/min and feed rate of 0.08 mm/tooth whereby the toll rejection was due to nose wear.

The dominant wear modes at tool failure were chipping and material adhesion. These failure wear modes became more pronounced at the cutting speed of 50 m/min and over. Figures 7.119 to 7.121 show failed KC730 tools with predominant wear modes of chipping and workpiece adhesion. It was also observed that plastic deformation and associated cracking occurred under various cutting conditions as shown in Figures 7.122 and 7.123. At low cutting speed of 25 m/min, a progressive tool wear, caused by combination of plucking, pitting, microchipping and workpiece galling was responsible for tool failure, as shown in Figure 7.119.

Figures 7.124 and 7.125 show the development of flank wear at feed rates of 0.14 and 0.08 mm/tooth respectively for various cutting speeds investigated. A notable acceleration in the wear rate was observed with increasing cutting speed. The lowest wear rate was observed when machining at the low feed rate of 0.08 mm/tooth and cutting speed of 25 m/min. Wear rate was very high at and over the cutting speed of 50 m/min for both feed rates of 0.08 and 0.14 mm/tooth. This was due to premature tool failure caused by chipping, breakage and/or flaking as shown in Figures 7.121 and 7.126a.

Examination of the cutting tools, at an early stage of cutting for 5 seconds, reveals important information on the wear behaviour of coating and substrate. SEM micrographs in Figures 7.126 to 7.131 show that workpiece galling, coating delamination and substrate

plucking occurred at all cutting speeds and feed rates investigated. At the cutting speeds of 50 to 100 m/min, the tool suffered from severe chipping, in addition to galling and coating delamination as shown in Figure 7.126a. The extent of chipping was also significant at the lowest cutting speed of 25 m/min when the feed rate was increased to 0.14 mm/tooth as shown in Figure 7.128. On the other hand, discrete microchipping was observed at the same cutting speed for the low feed rate of 0.08 mm/tooth (Figure 7.130). EDAX analysis presented in Figures 7.126b and 7.129b confirm the presence of galling, coating delamination and plucking phenomenon observed at this early stage of machining.

7.3.4 Tool Life, Tool Wear and Tool Failure Modes when Face Milling Waspaloy with KMF Tools

Tool life values, failure and wear modes for KMF inserts are presented in Table 7.8. A maximum tool life of 18 minutes was obtained at the lowest cutting speed of 25 m/min and feed rate of 0.08. Increasing feed rate to 0.14 mm/tooth at this cutting speed resulted in a tool life of 2 minutes.

Figure 7.89d shows the effect of increasing cutting speed and feed rate on the tool life when face milling Waspaloy with the uncoated KMF inserts. This figure suggests that increasing cutting speed from 25 m/min to 50 m/min yielded a reduction in tool life by approximately 82 and 90 %, for the feed rates of 0.08 and 0.14 mm/tooth respectively. As for the effect of increasing feed rate from 0.08 to 0.14 mm/tooth, tool life reductions by 89 and 94 % were recorded at the cutting speeds of 25 and 50 m/min respectively. At the cutting speed of 50 m/min and feed rate of 0.08 mm/tooth, a tool life of 3.2 minutes was recorded which is the highest value of all the tools tested on Waspaloy at this particular cutting condition.

Under all the cutting conditions investigated, tool rejection was due to average flank wear. SEM micrographs of failed KMF tools reveal that the dominant tool wear modes were chipping and material adhesion as shown in Figures 7.132 to 7.135. Severe chipping and material adhesion become more pronounced at the cutting speed of 50 m/min for both the feed rates. Cracking, predominantly of mechanical nature, was found to occur at cutting speeds of 25 and 50 m/min for both feed rates as shown in Figures 7.136 to 7.140. At low cutting speed of 25 m/min, a progressive tool wear due to combination of

plucking, microchipping and workpiece galling was the dominant cause of tool failure as shown in Figure 7.132.

Figures 7.141 and 7.142 show the development of flank wear at feed rates of 0.14 and 0.08 mm/tooth and different cutting speeds. These figures suggest that the wear rate gradually increases with increasing cutting speed whereby the biggest increment occurring between the cutting speeds of 32 and 40 m/min for the high feed rate of 0.14 mm/tooth, and between 25 and 32 m/min for the low feed rate of 0.08 mm/tooth.

SEM observations performed at an early stage of cutting for 5 seconds revealed important information on the wear behaviour of uncoated KMF tools.

Figures 7.143 to 7.148 show the presence of workpiece galling and substrate pitting and chipping at various cutting conditions. At the lowest cutting speed of 25 m/min, workpiece adhesion at tool-chip contact zones and associated rake face pitting were dominant for high and low feed rates as shown in Figures 7.143 to 7.145. Figures 7.147 and 7.148 suggest that microchipping and severe workpiece adhesion, mainly on the chipped areas, were prominent at the highest cutting speed of 50 m/min and feed rate of 0.08 mm/tooth. Increasing feed rate to 0.14 mm/tooth at the same cutting speed led to severe chipping and breakage, with attendant cracking of the entire cutting edge as shown in Figures 7.140 and 7.146.

7.3.5 Comparative performance analysis when machining Waspaloy alloy

In this section, the overall performances of the cutting tools tested on Waspaloy have been compared and assessed in terms of tool life values and volume of material removed.

7.3.5.1 Tool life

Tool life results of four different types of tools used for face milling Waspaloy at various cutting speeds and feed rates are compared in Figures 7.149 and 7.150. All the coated tools showed a common trend with short tool lives particularly at cutting speeds of 50 to 100 m/min. The uncoated KMF tool also exhibited similar behaviour of short tool life at the cutting speed of 50 m/min. This effect was more pronounced for all the tools tested and manifested by more reductions in tool life values when face milling at high feed rate of 0.14 mm/tooth as shown in Figure 7.150.

At the lowest cutting speed of 25 m/min each tool gave its own best performance and yielded much longer tool lives at low feed rate of 0.08 mm/tooth than that at high feed rate of 0.14 mm/tooth. At this cutting speed and feed rate of 0.08 mm/tooth, uncoated KMF grade and CVD coated KC994M inserts performed equally well, both producing a tool life of 18 minutes which is the highest value of all the tools tested on Waspaloy workpiece. The performance of these grades was better than the PVD coated tools KC720 and KC730 which produced tool lives of 5 and 10 minutes respectively, at the cutting speed of 25 m/min. When the cutting speed was increased to 50 m/min at the feed rate of 0.08 mm/tooth, the uncoated KMF grade gave the longest tool life of 3.2 minutes and thereby outperforming all the other coated tools giving tool lives of between 1 and 1.2 minutes.

Figure 7.150 shows that, at high feed rate of 0.14 mm/tooth CVD coated KC994M produced longer tool lives than all the other tools at all cutting speeds investigated. It produced a maximum tool life of 9 minutes at the lowest cutting speed of 25 m/min, which is 3 times higher than that of the second best performing tool KC720 which lasted for 3 minutes. The uncoated KMF and PVD coated KC730 performed almost equally by giving 2 and 1.8 minutes tool lives respectively. At the cutting speed of 50 m/min and over, the tool lives for all the tools were 30 seconds or less. The differences between tool lives become insignificant with increasing cutting speed.

Figures 7.149 and 7.150 indicate that the CVD-coated KC994M inserts showed the best overall performance of all the cutting tools based on tool life assessment when face milling Waspaloy material.

7.3.5.2 Volume of material removed

The volume of material removed when face milling Waspaloy under various cutting conditions is presented in Figures 7.151 and 7.152.

These figures suggest that the volume of material removed decreased with increasing cutting speed, particularly at 50 m/min and above owing to the corresponding short tool lives. All the cutting tools produced higher volume of metal removal when face milling at the low feed rate of 0.08 mm/tooth. The only exception was KC720 which removed

almost an equal amount of volume at the cutting speed of 25 m/min for both feed rate conditions as shown in Figures 7.151 and 7.152.

The CVD-coated KC994M and uncoated KMF tools gave similar performance and produced 21.7 cm^3 metal removal, which is the highest amount achieved when face milling Waspaloy, at a cutting speed of 25 m/min and feed rate of 0.08 mm/tooth. At this condition, PVD coated KC730 outperformed KC720 by producing 12 cm^3 metal removal which is twice as much as that produced by the latter. At the cutting speed of 50 m/min however, KMF yielded a much better performance than the other tools by removing 7.8 cm^3 metal which is 2 to 3 times that of coated tools. There was no significant difference in the results produced by all the coated tools at this cutting speed and feed rate.

When the feed rate was increased to 0.14 mm/tooth, CVD-coated KC994M outperformed all the other tools at all the cutting speeds tested and removed a volume of 19 cm^3 metal at the lowest cutting speed of 25 m/min. The second best performing tool at this cutting speed was PVD-coated KC720 with a metal removal volume of 6.3 cm^3. KC730 tool gave the poorest performance by removing a volume of 3.5 cm^3 material. The tools performance was similar at cutting speed of 50 m/min, however the amount of metal removed was very low and hence no comparison was made.

On the basis of the volume of metal removed, CVD-coated KC994M showed the best overall performance particularly at lowest cutting speed of 25 m/min for both the feed rates of 0.08 and 0.14 mm/tooth. The results suggest that, higher feed rate of 0.14 mm/tooth should be used for efficient high volume of material removal with KC994M despite relative reduction in tool life. Although there was a 50 % reduction in tool life at high feed rate for the cutting speed of 25 m/min, the difference in volume of martial removed was only 12 % and the rate of removal was almost twofold. At the lower feed rate of 0.08 mm/tooth and cutting speeds of 25 and 50 m/min, KMF gave the best performance, generating a volume of 7.8 cm^3 material before reaching the end of its tool life.

7.3.6 Surface Integrity

Metal cutting processes impose surface alteration, the extent and nature of which must be investigated to ensure that the components are produced to the required

standards. Three important aspects of surface integrity which include surface roughness, subsurface microhardness tests and metallurgical analysis in relation to the machined surface were investigated and an evaluation of the results are presented in the following section.

7.3.6.1 Surface Roughness

The surface roughness values (R_a) of the machined surfaces with all four types of cutting tools tested on Waspaloy at various cutting conditions are presented in Figures 7.153 to 7.160. These figures suggest that large variations in Ra values were recorded within approximately the first 2 minutes of cutting. After this period, the trend appears to become stable either by following a reduction pattern or fluctuating within narrow limits.

Figures 7.155 to 7.158 indicate that, in most cases when using KC720, KC730 and KMF, slightly higher surface finish values were obtained with increasing cutting speeds. Such a trend was not observed with the CVD-coated KC994M tools. The highest individual reading of 1.4 μm was recorded when cutting with KC994M at the cutting speed of 25 m/min and feed rate of 0.14 mm/tooth as shown in Figure 7.153.

Another notable common characteristic suggested by these figures is that the difference in surface roughness values become marginal with prolonged machining regardless of the cutting speeds and feed rates employed. The results also indicate that the effect of feed rate on surface roughness was also marginal.

In order to compare the effect of each type of tool tested on Waspaloy, the surface roughness values obtained at the feed rates of 0.08 and 0.14 mm/tooth for the cutting speed of 25 m/min were plotted in Figures 7.159 and 7.160. It was evident that at low and high feed rate conditions, the differences in surface roughness were more pronounced at initial period of machining which gradually reduced and became insignificant with prolonged machining, regardless of the type of cutting tools. However, as shown in Figure 7.160, the variations in surface roughness values were much smaller in the case of low feed rate of 0.08 mm/tooth whereby only 0.13 μm difference was found between the highest (0.67 μm) and the lowest (0.54 μm) average surface roughness values produced by KMF and KC720 inserts respectively. The initial high variations of Ra values in the

case of high feed rate can be related to the initial wear patterns of the minor cutting edge which shapes the surface.

Figures 7.159 and 7.160 show that the average surface roughness values obtained by PVD-coated KC720 and KC730 and CVD-coated KC994M were almost identical, being 0.54, 0.56 and 0.55 μm respectively, at the lower feed rate of 0.08 mm/tooth and cutting speed of 25 m/min where longest tool lives were recorded. The average surface roughness values were well below the rejection criterion of 5 μm, hence none of the tools was rejected on the basis of poor surface finish.

7.3.6.2 Microhardness Tests

The results of subsurface microhardness measurements when machining Waspaloy using all four types of cutting tools are presented in Figures 7.161 to 7.164. The measurements were performed generally on the samples produced at two cutting speeds of 25 and 50 m/min and feed rate of 0.08 and 0.14 mm/tooth, chosen to represent the low and high cutting conditions. The sample surfaces used for microhardness measurements were taken immediately after the tools had failed. To be able to compare the effect of worn tools with the sharp ones, microhardness readings on the samples produced after 5 seconds of machining at the cutting speed of 25 m/min were also presented in Figures 7.161 to 7.164.

Under the cutting conditions presented in Figures 7.161 to 7.163, a similar trend of hardness pattern was observed on the machined surfaces generated by the CVD and PVD-coated tools. The results show that the hardness of the top surface layer was always higher than that of the inner section of the material and the hardness was reducing towards the nominal value of 460 HV with increasing depth below the surface. Figure 7.161 suggests that the maximum increase in surface hardness was produced by CVD-coated KC994M tools while uncoated KMF tools caused the minimum increase in hardness at the end of their useful life (Figure 7.164). As for the PVD-coated tools, the effect of machining with KC720 inserts on the subsurface microhardness was more than that with KC730 inserts. Figures 7.161 to 7.164 also indicate that feed rate did not have any significant effect on subsurface microhardness. However, the effect of cutting speed was found to vary with regard to the type of cutting tools used. There was almost no variation in the

microhardness patterns generated at the cutting speeds of 25 and 50 m/min by KC720 and KC994M inserts. On the other hand the increase in microhardness was relatively less at the cutting speed of 50 m/min than at 25 m/min, when machining with KC730 and KMF tools.

At a depth of 0.020 mm below the surface, which was the closest measurable point to the surface, an increase in the hardness by 27 to 126 HV units (by 6 to 28 % increase) was recorded. The results suggest that the maximum increase in surface hardness was produced by CVD-coated KC994M tools, measuring 586 HV at the closest point to the surface. A minimum reading of 487 HV was recorded on the surfaces produced by uncoated KMF tools at the same point. Figures 7.161 to 7.164 suggest that subsurface hardness values dropped to the level of nominal hardness, approximately at a depth of 0.2 mm when the tools failed.

The plots in Figures 7.161 to 7.164, representing the effect of sharp tools on subsurface micro hardness produced after 5 seconds of cutting at a cutting speed of 25 m/min and feed rates of 0.08 and 0.14 mm/tooth, suggest that all the coated tools caused a surface hardness between 520 and 530 HV (13 to 16 % increase) at the closest point of 0.02 mm depth. Uncoated KMF tools resulted in the smallest variation by producing a hardness of 487 HV at the same point which represents an increase of 6 %.

The depth of affected layer at this initial stage of cutting was found to vary between 0.03 and 0.06 mm with regard to the cutting conditions and tool type. Figure 7.161 suggests that the depth of affected surface layer was the highest on the samples produced by KC994M tool.

7.3.6.3 Metallurgical Alterations

In this section, optical micrographs produced at 500X and 1220X magnification, showing the microstructures of the machined surfaces, are presented and evaluated. Samples, obtained from early machining period (after cutting for 5 seconds) and at the end of tool life, were comparatively analysed in order to determine microstructural alterations. Microstructure of the samples produced at cutting speeds of 25 and 50 m/min were analysed to represent low and high cutting conditions for Waspaloy workpiece. Parallel and perpendicular sections of the samples to the feeding direction were produced

in order to observe possible microstructural alterations. The common characteristics of the machined surfaces have been presented in the introductory paragraphs of the section 7.2.6.3.

Figures 7.165 to 7.168 show plastically deformed surface regions at the start and end of machining when face milling Waspaloy with CVD-coated KC994M tools at a cutting speed of 25 m/min and feed rates of 0.08 and 0.14 mm/tooth. The surface layer was generally smooth and less plastic deformation is evident in the surfaces produced at the early stage of machining (Figure 7.167 and 7.168). Comparing Figure 7.167 with 7.168 indicates that the extent of plastic deformation at the early stage is less in the case of low feed rate of 0.08 mm/tooth than that of high feed rate of 0.14 mm/tooth. Figure 7.169 shows that surface tearing occurs on the machined surface towards the end of tool life when cutting at a speed of 75 m/min and feed rate of 0.08 mm/tooth. This was most probably caused by chipped and trapped tool particles, towards the end of tool life at high cutting speed of 75 m/min.

Figures 7.170 to 7.174 show subsurface microstructure of Waspaloy workpiece machined with PVD-coated KC720 inserts at various cutting conditions. Comparing Figures 7.170 and 7.171 to Figures 7.172 and 7.173 suggests that surface tearing is more distinct on the samples produced at high feed rate of 0.014 mm/tooth than at low feed rate, when milling at a cutting speed of 25 m/min. Although some surface irregularities are noticeable on the initial surface samples of low feed rate as shown in Figure 7.171, the difference between the two cases is markedly evident. This can be attributed to the difference in the scale of the chipping observed at both conditions. Figure 7.174 shows the microstructure of the subsurface generated at the end of the tool life when machining at a cutting speed of 50 m/min and feed rate of 0.08 mm/tooth. As with other conditions, plastic deformation occurred with an embedded tool particle within the surface layer.

Figures 7.175 to 7.179 show microstructure of the surface layers produced at various cutting conditions when face milling with KC730 inserts. The main feature observed in all the micrographs is the presence of very distinguishing plastic deformation within the surface layer, the extent of which varies depending on the cutting condition employed. Comparison of the surfaces, generated at the start (Figures 7.176 and 7.177) and end of the machining stages (Figures 7.178 and 7.179), suggests that the depth of plastically

disturbed layer was greater at a cutting speed of 50 m/min than at 25 m/min for both stages. However, micrographs in Figures 7.175 and 7.176 indicate that changing the feed rate at the cutting speed of 25 m/min did not have any noticeable effect on the depth of plastically disturbed layer. As the mode of tool failure for KC730 inserts is similar to that of KC720, there may well be some surface irregularities in the form as shown in Figure 7.173, despite absence of such defects in the micrographs presented in Figures 7.175 to 7.179.

The microstructures of surfaces, produced by using uncoated KMF inserts at various cutting conditions, are shown in Figures 7.180 to 7.184. These figures indicate that plastic deformation is evidently the common feature of all the surfaces generated at the early (Figures 7.180 to 7.182) and final stages (Figures 7.183 and 7.184) of machining. Figures 7.183 and 7.184 suggest that the degree of plastic deformation increased with prolonged cutting time and with increasing feed rate. Examination of the entire surface line of the sectioned samples did not reveal any noticeable surface damage or irregularity. However it is highly possible that some rare localised surface damage, particularly at high cutting speeds and feed rate conditions, were caused by severe chipping of the tool.

CHAPTER 8

DISCUSSION

8.1 Introduction

In this chapter, a discussion on the results has been presented in line with the general objective of this research to establish a fundamental understanding of the wear behaviour of coated and uncoated tungsten carbide tools when face milling Inconel 718 and Waspaloy superalloys. Because of the similarities in the wear behaviour of the cutting tools when face milling both workpiece materials, the discussion of the machinability aspect has been presented together. However, attention has been drawn to any significant difference in the results obtained with regard to each material.

The discussion has been concentrated on the following aspects of machinability in line with the main objectives of this research:

a) Investigation of tool failure modes and associated wear mechanisms.

b) Evaluation of the effect of cutting variables, namely cutting speed, feed rate and tool geometry, on tool failure modes, wear mechanisms and performance.

c) The effect of workpiece materials on tool wear and performance.

d) Assessment of the surface integrity of the machined surfaces which includes surface finish and variations in subsurface microhardness and microstructure.

8.2 Tool failure modes and wear mechanisms

Examinations of the used tools show that all four types of cutting tools failed due to a combination of wear modes of chipping, workpiece adhesion, plucking, flaking, cracking, and plastic deformation of various degree. The most prominent wear modes

with regard to each cutting tool and workpiece materials are indicated in Tables 7.1 to 7.8 and respective SEM micrographs presented in sections 7.2 and 7.3.

However, optical and SEM analysis of the inserts at an early cutting stage (after cutting for 5 seconds) revealed that some of these failure modes were progressive in nature, encouraging other mechanisms to take place at later stages of machining. In order to better understand the wear mechanisms, detailed studies were carried out to identify the factors causing initial wear at the early stage of machining.

8.2.1 Initial wear modes and mechanisms

When face milling Inconel 718 and Waspaloy, the wear modes occurring at early stages of machining were galling and adhesion of the workpiece material, coating delamination and associated substrate pitting or plucking. In addition, discrete micro-chipping of the cutting edge along the entire contact line comprising major and minor cutting edges and tool nose. These were the dominant wear modes over the course of milling with discrete micro-chipping evolving into severe chipping, which led to the breakage of the cutting edge. This was the case for both PVD and CVD-coated tools. As for the uncoated KMF grade, all the above mechanisms, apart from coating delamination, were found to be present, despite slight variations in characteristics which will be highlighted in the following sections.

8.2.1.1 Workpiece galling and coating delamination at early stages of milling

Adherence and galling of workpiece material was found to occur on the rake and flank faces where chip/tool contact takes place. The presence of workpiece galling and coating delamination is clearly shown in Figures 7.7a, 7.9, 7.10a, 7.11a, 7.20, and 7.32 for Inconel 718 and in Figures 7.98a, 7.102a, 7.114, 7.116a, 7.127 and 7.129a for Waspaloy when face milling with CVD/TiCN+Al_2O_3 coated KC994M and PVD/TiN coated KC720 and KC730. Further when face milling with the uncoated KMF tools, the presence of workpiece galling is shown in Figures 7.41, 7.47 and 7.143, 7.144 for Inconel 718 and Waspaloy workpiece materials respectively. Workpiece adhesion and

associated early coating delamination took place regardless of the cutting speeds and feed rates employed.

These figures show that work material has adhered onto the tool surface in two distinguished manners, namely in the form of galling and adhesion of relatively large lumps of workpiece materials. Galling starts as soon as cutting takes place, the rake face gets almost completely adhered by layers of smeared workpiece material. These layers can clearly be seen in Figure 8.1. This is a characteristic nature of nickel-based alloys due to their austenitic matrix which provides high rate of strain hardening [4, 158, 166]. These very thin layers of smeared workpiece material (Figure 8.1) situated on top of each other, are strong indication of the fact that the chip undergoes a secondary shear process across the rake face and that a complete seizure has taken place at the interface.

As for the condition of the flank face of CVD and PVD-coated tools at the initial cutting stage, workpiece galling and discrete coating delamination were found to occur over the tool-workpiece interface along a region of ~0.03 to 0.05 mm width, as shown in Figures 7.22, 7.100a, 7.131, 8.2 and 8.3. Virtually no plucking of the substrate material was observed on the flank as it was on the rake face of the tool. This demonstrates that intermittent chip contact and its adhesion strength were the two important factors causing coating delamination and substrate plucking. Of these two factors, the former is not operative on the flank as there is no chip flow on it, whereas the latter is effective to a much lesser degree due probably to the radial force component acting on the flank. The magnitude of the radial force component is approximately 50 % of that of tangential force, being the major principal force component acting on the rake face [23].

Another evidence indicating the presence of firm workpiece adhesion and hence seizure, is that the underside of the root of the chip produced has a very rough surface texture where no sliding marks are present. This was detected when collected chip samples, just after few seconds of cutting, from the exit and the entry side of the work piece, were inspected under optical and SEM microscope. Patches of coating materials, namely TiN, TiCN and Al_2O_3, and substrate material (WC) from respective tools were found to have been attached to the lower ends of the chips when face milling both

Inconel 718 and Waspaloy by PVD and CVD-coated tools at various cutting conditions as shown in SEM micrographs presented in Figures 8.4a to 8.13a. The presence of tool materials were also proved by performing EDAX analysis, the results of which are presented together with the corresponding SEM micrographs in Figures 8.4b to 8.13b.

These micrographs indicate that a strong bond was established over a large portion of the tool-chip contact zone whereby detachment was encouraged by means of a momentary tensile force induced due to sudden release of the compressive forces and self-evacuation tendency of the chip itself with the help of its weight [14, 224]. If chip remained attached to the cutting edge after the exit, it was removed during re-entry by a pushing/lifting effect of the newly formed chip, most probably imposing a transient tensile stress to the tool-chip interface and/or to the tool tip [32, 132, 225]. This process resulted in rake face pitting and/or plucking, cutting edge micro chipping and could have contributed to early coating delamination as shown in Figures 7.21a, 7.22, 7.45, 7.99a and 8.14. The plucked areas were more intense along the vicinity of the cutting edge suggesting that the strength of the workpiece adhesion was greater in this area. This can be attributed to the fact that the workpiece adhesion was stronger towards the cutting edge due to intensified cutting force component acting normal to the rake face and to the intensity of the secondary shear in the flow zone. The rough texture of the plucked or pitted areas suggests that an attrition wear mechanism is taking place, in which individual grains or their small aggregates are pulled out of the substrate [1, 226]

It has also been found that the detachment of coating and substrate material by the underside of the chip occurred not only at the root of the chip during cutter exit or entry, but also when the chip was flowing over the rake face during the cutting cycle. SEM micrographs and accompanied EDAX analysis in Figures 8.5a and 8.12a show that detached bulk of coating and substrate material of the cutting tools were removed through attaching to the underside of the chip and carried away by the chip flow.

In some cases, the original grinding marks on the substrates of PVD and CVD-coated tools were clearly visible indicating that the coating was pealed off rather than being worn as shown in SEM micrographs in Figures 7.9, 7.32 and 7.129a. The SEM images in Figures 7.8a, 7.11a and 7.98a suggest that in the case of cutting with CVD

double-layer-coated KC994M tools, the top coating layer of Al_2O_3 was first separated, in a relatively clear fashion, from the second layer of TiCN, mostly in a pealed or fractured manner by the flow or detachment of the chip. This strongly suggests that the bonding strength between these two layers was less than that between the substrate and the bottom layer of TiCN. When delaminated areas on PVD and CVD-coated tools were compared, the exposed substrate was much rougher and uneven in the case of CVD-coated tools. This phenomenon demonstrates that the bonding strength between the substrate of CVD-coated tool and its adjacent coating layer of TiCN was greater than that of PVD-coated tools, a phenomenon which was also reported by other workers [127, 227, 228]. This high degree of bonding strength at the substrate-coating interface has been attributed to the chemical reaction occurring at high coating temperatures of about 1000 °C during the CVD coating process [80, 79].

It has been reported that the shear strain generated within the chip at tool/chip interface under seizure conditions is much higher, being in the order of 20 to 50, than that of primary shear zone where shear strain is approximately between 2 to 5 when machining nickel-based alloys [160]. As a result of high shear strain and the fact that nickel-based alloy possesses good high-temperature strength, a steep temperature rise is generated at the interface, a large portion of which is then conducted into the substrate. The heat diffused into the substrate will rapidly increase once the coating is removed. According to Trent [1], when cutting under seizure conditions, the heat generated within the flow zone, due to secondary shear, continuously flows into the same small volume of tool through the interface area. The strong bond between the tool and chip at this interface is often considered completely metallic in character whereby the temperature of the tool at the surface of contact will effectively be the same as that of the flow-zone, hence building up a stable temperature gradient within the tool. This constant heat source increases the tool's temperature and becomes one of the most important factors limiting the tool life when machining high temperature strength materials with work hardening tendency.

One explanation to the removal of coatings and the substrate material in this manner at an initial stage of cutting would be that under cyclic thermal and mechanical shocks

(which are inherent in the milling process), the interface between coating and substrate was disturbed due to differences in thermal expansion coefficients of the substrates (5.26 to 5.5 10^{-6}/K) and coatings (8.1 to 9.35 10^{-6}/K, Table 6.5 and 6.6) and due to fluctuating mechanical forces. On the other hand high shear forces in the flow zone under seizure condition will influence the interface by applying a stress in the direction of chip flow. Such shear stresses will be very high, considering a strain rate of 20 to 50, and hence leading to quick delamination of the coating layers in both PVD and CVD-coated tools. However, the occurrence of coating delamination (as shown in Figures 7.32, 7.98a and 7.100a), at the very beginning of cut, after ~11 cycles at the lowest cutting speed of 25 m/min suggests that it is more of a mechanically activated phenomenon than a thermal-fatigue related.

The second type of adhesion appears to be the welding of relatively bigger chip particles to the sharp section of the cutting edge and to the chipped or plucked areas, as shown in Figures 7.9, 7.11a, 7.26a, 7.45, 7.102a, 7.115, 7.144 and 8.2, when face milling both Inconel 718 and Waspaloy with CVD, PVD and uncoated tools. In general, this phenomenon became more pronounced at high cutting speeds of 75 and 100 m/min and feed rate of 0.14 mm/tooth. These Figures demonstrate that adhered workpiece material of this kind at the cutting edge had a structure that consists of several vertically stacked layers of workpiece material of unstable accumulation, resembling a kind of BUE. This structure indicates that the adhered material at the tool edge is most likely the end section of the chip which was left attached when the main body was broken away. This type of adhesion can also be very detrimental if it stays at the tip of the cutting edge, as it may act as a cutting edge hence adversely affecting initial transient contact configuration at entry and hence altering chip flow and shear pattern in the primary and secondary deformation zones. This in turn can cause micro chipping or substrate plucking at the time when adhered bulk of workpiece martial is removed.

Coating delamination, substrate plucking/pitting, micro chipping due to workpiece adhesion and detachment, resulted in an uneven rake face at the cutting edge. This would encourage further workpiece adhesion and loss of tool material by attrition wear through

stress raising effect of the rough, damaged areas within tool-chip interface as shown in Figures 7.25a, 7.45, 7.99a and 8.15.

8.2.1.2 Micro chipping at early cutting stage

Micro-chipping, having a length of less than 0.3 mm according to the ISO standard [124], was observed to occur in a discrete manner, at low cutting speeds of 25 and 50 m/min on CVD, PVD and uncoated tools along the cutting edge when examined after 5 seconds of cutting as shown in Figures 7.12a, 7.33a, 7.43, 7.116a, 7.128 and 7.130. However, the size and frequency of chipping were increased with increase in cutting speed and feed rate. This effect was more prominent at the cutting speeds of 75 and 100 m/min and feed rate of 0.14 mm/tooth when cutting both Inconel 718 and Waspaloy workpieces, as shown in Figures 7.34, 7.101, 7.103a, 7.118 and 7.146.

Of the two workpieces, Waspaloy induced more chipping and caused premature failure at identical cutting conditions. Short tool life (~3 minutes or less) similar to that obtained at the cutting speed of 75 m/min on Inconel 718, was observed at a lower cutting speed of 50 m/min when cutting Waspaloy. Furthermore, the occurrence of micro-chipping was relatively more in the case of the PVD-coated tools KC720 and KC730.

The formation of initial micro-chipping could be attributed to the following factors which were observed to occur to occur simultaneously.

a) Adhered workpiece material, for instance, as in Figures 7.9, 7.11a and 7.102a, could act as a BUE, whereby the primary shear pattern and chip flow pattern would be altered. Adhered workpiece material in such a manner could also result in high localised stresses along the cutting edge when considering its irregular nature. This effect is believed to be more pronounced in the case of the PVD-coated tools which possess a sharper cutting edge than that of the CVD-coated KC994M and uncoated KMF tools (Figure 8.16).

b) Removal of strongly adhered workpiece material is largely tensile in nature and can cause removal of the tool material by attrition (Figure 7.12a and 7.43) thereby encouraging further subsequent chipping and associated stress concentration.

c) Fatigue effect, due to inherent cyclic thermo-mechanical impacts can be another factor making the cutting edge susceptible to fracture in the form of chipping. Once chipping occurred, the original geometry of the cutting edge was altered and the edge was subjected to extreme compressive and shear stresses. In addition, the sharp sections of the chipped areas could act as stress raisers that could lead to plastic deformation, mechanical crack initiation and fracture. Initiated cracks are expected to propagate with ease under cyclic thermo-mechanical shocks.

Of the four different types of cutting tools tested, outstanding performance of the CVD-coated KC994M tools can be strongly associated with the micro-geometry of its cutting edge and with the CVD coating. These are the two most distinguishing factors which differentiate the CVD-coated KC994M tool from PVD-coated KC720 as both tools are of the same substrate (Table 6.5). The micro geometry of the cutting tools tested are shown Figure 8.16. As shown, CVD-coated KC994M posses a honed radius of ~ 0.03 mm at the cutting edge which would increase its strength and make it more resistant to mechanically induced stresses and provide better heat dissipation due to larger contact area compared to the sharp cutting edge of PVD-coated KC720 and KC730. These advantages of honed cutting edge also applies to the uncoated KMF tool which also features a radius of ~ 0.027 mm, as shown in Figure 8.16, and performed generally better than the sharp-edged PVD-coated KC720 and KC30 tools at the lowest cutting speed of 25 m/min when face milling both Inconel 718 and Waspaloy. During the face milling tests, much less frequent micro chipping was recorded with CVD-coated KC994M tools within a given time span at the beginning of cut for Inconel 718 and Waspaloy workpieces. As reported by previous workers [93, 229, 230, 231, 232], cutting edge with a radius reduces tool life scattering to fracture and with an optimum value of such a radius, longer tool lives were achieved. The second factor in CDV coated tool is the coating itself. Despite the fact that the top coating layer of Al_2O_3 seems to have been removed from the rake face through delamination (Figure 7.8a and 7.98a), the second layer of TiCN stayed intact for a longer period, due mainly to higher adhesion strength. TiCN has been reported to be superior to TiN owing to its higher hardness and heat transmission behaviour (Table 6.6), abrasion resistance, toughness and lower friction coefficient as a result of the lubrication effect of carbon presence in its structure [121,

178]. On the flank face however, the extent of coating delamination was not as severe as that of the rake face for both CVD and PVD-coated tools at the early stage of cutting (Figures 7.22 and 8.17). This suggests that the CVD-coated KC994M tool can still have advantage of possessing two coating layers (Al_2O_3 and TiCN) on its flank for a longer period at this initial stage. The presence of Al_2O_3 as the top layer further protects the substrate from the effect of high temperatures by acting as a thermal shield due to its extremely low thermal conductivity of 7.5 W/mK (70 % lower than TiN) and better chemical stability as reported previously [85, 129, 202].

It is an established fact that the temperature distribution in the tool-chip contact zones is influenced by the value of the thermal conductivity of the coating [1, 80, 135]. Thermal conductivity values for both coating layers of Al_2O_3 and TiCN (7.5 and 31 W/mK) are respectively 10 and 46 % of that of the substrate of KC994M tool (67 W/mK). This will reduce the amount of heat conduction into the substrate and cause more heat to remain in the chip and carried away by the chip flow. Thus, elevated temperatures so generated in the shear zones facilitate easy plastic deformation of the workpiece material to some extent and increases shear angle and chip velocity with consequent thinner chips. These factors in turn cause a reduction in the width of the contact zone as indicated by the measured values presented in Table 8.1. The measured contact zone width for CVD-coated KC994M tool were smaller at all cutting conditions than those observed for all the other cutting tools used. This proves the retention of high temperatures within the chip, when machining with CVD coated tools, based on the proposed analogy. The values presented in Table 8.1 were measured within first 5 to 20 seconds of cutting before any significant wear was developed. In the light of the foregoing discussions, it can be concluded that the two properties of the CVD-coated KC994M tools (nose radius and CVD coating) have compensated well known disadvantages, relative to PVD-coated tools, which are (a) up to 30 % reduction in transverse rupture strength (b) tensile residual stresses imposed upon tool surface and (c) presence of brittle eta phase at coating-substrate interface (Table 6.6) [1, 80, 82, 85, 88, 92, 93, 120, 233, 234], when machining Inconel 718 and Waspaloy workpiece materials.

Increased chipping observed on PVD-coated tools, KC720 in particular, could be attributed to its sharper cutting edge (Figure 8.16b). Tools with sharp cutting edge are

more sensitive to fracture due to the cyclic impacts and associated vibration generated during face milling process. As cutting continued, chipped areas progressed from micro level to macro and beyond by overlapping each other along the cutting edge. Progressive chipping of this kind results in severe breakage and plastic deformation of the cutting edge, sometimes accompanied with flaking on the rake face, towards the end of the tool life.

Analysis of the uncoated KMF tools under SEM at the initial stage of cutting (after 5 seconds as shown in Figures 7.42 and 7.47) showed that the thickness of adhered workpiece material was smaller compared with that of the CVD and PVD-coated tools. Thinner layer of workpiece adhesion can be related to the honed rake face of the KMF inserts contrary to the rougher ground substrate of the other tools. This could partly be attributed to the fact that higher amount of heat is dissipated in to the substrate as there is no coating and the thermal conductivity of the KMF inserts (85 W/mK) is significantly higher than that of coating layers of TiN and of other substrates as presented in Table 6.5 and 6.6. It has been reported that the thickness of the flow zone (secondary shear) will be less in the case of uncoated tools due to less heat concentration within the area and hence resulting in thinner smeared workpiece material on the rake face of the tool [1, 80, 135].

It was also observed that the pitted/plucked areas on the rake face of the KMF inserts (Figure 7.45) were not as deep and damaging as those on the coated tools as shown in Figure 7.7a, 7.22 and 7.25a. As mentioned earlier, micro chipping on KMF inserts at this early stage was less frequent than that observed on PVD-coated tools. This can be attributed to the strengthening effect provided by the generation of a honed cutting edge radius (~0.027 mm) on the KMF tools (Figure 8.16c). The transverse rupture strength of KMF insert (3.6 GPa), was 28 to 31 % greater than those of KC720 and KC730 (Table 6.5). This gives extra resistance to fracture and better toughness as reported by others [1, 79, 84, 235]. This effect combined with the cutting edge radius was probably the main factor for the KMF's better chipping resistance.

Less degree of plucking on the rake face of the KMF tools can be attributed to its finer grain size of 0.8 μm than those of KC720 and KC730, being 1 to 6 and 1 to 3 μm respectively. The rough texture of the plucked/pitted areas on the rake face suggest that

attrition wear mechanism is operative due to periodic workpiece adhesion and detachment. Trent [1] has reported that the most important factor affecting attrition wear in WC-Co tools is the grain size, fine grained tools being much more resistant than coarse grained ones. Results, similar to Trent's, were observed in this work and hardness of the tools was found to have no direct effect on attrition resistance.

8.2.2 Analysis of tool wear modes and mechanisms at tool failure

Experimental observations showed that all of the cutting tools tested exhibited a similar trend of progressive chipping/plucking/pitting-dominated wear pattern associated with the workpiece adhesion/detachment phenomenon at low cutting speeds of 25 and 50 m/min when face milling Inconel 718 (Figures 7.4, 7.18, 7.19, 7.31 and 7.38). In the case of Waspaloy, this type of progressive wear was observed generally at the lowest cutting speed of 25 m/min (Figures 7.91, 7.104, 7.105, 7.119, 7.120 and 7.132). Moreover, it was observed that the rate of wear was slower at the low feed rate of 0.08 mm/tooth.

8.2.2.1 Flank wear

All the cutting tools tested failed due to flank wear which was dominantly caused by a combination of plucking, pitting and chipping associated mainly with workpiece adhesion, and by diffusion and slight abrasion to a less degree of importance. As the sectioned through failed tools in Figures 8.18 to 8.22 show, the tool life criterion was mainly reached due to advancement of worn areas by plucking and/or chipping. It is for this reason that the wear at the flank was dominantly of non-uniform type, being more evident at high feed rate of 0.14 mm/tooth and at cutting speeds of 75 and 100 m/min for Inconel 718 and at 50 m/min and above for Waspaloy.

Figures 8.18, 8.23 and 8.24 suggest that previously worn uneven flank face by attrition or fracture was completely filled in with workpiece material, whereby a very strong bond of mechanical character along the interface is promoted owing to the high work hardening tendency. This results in a considerably large area of contact on the flank face whereby rubbing or seizure between flank and already-machined transient surface is encouraged with consequent increase in cutting forces and temperatures. Thus the extent

of the corresponding thermal and mechanical fatigue would also increase which is likely to initiate fine cracks within the tools as shown in Figure 8.25. When the adhered layer was forced to separate, it also picked up embedded WC grains and most probably caused enhanced wear by attrition and/or fracture as shown in Figures 8.18 and 8.23.

Failed tools as shown in Figures 7.4 and 7.105 and magnified view of sectioned areas in Figures 8.26, 8.27, 8.28 and smoothly worn regions in Figures 8.29, 8.30 and 8.31, strongly suggest that along the lower boundary of the worn flank faces, particularly at nose region, a combined diffusion and slight abrasion wear mechanism is operative when face milling Inconel 718 and Waspaloy with CVD-coated KC994M, PVD-coated KC720 and KC730 and uncoated KMF tools even at the lowest cutting speed of 25 m/min. However even in this region, sliding contact was often interrupted by adhering workpiece material thereby diminishing further diffusion/abrasion process. As shown in Figure 8.30 dislodged individual or small groups of WC grains from the tool surface due to detachment of adhered workpiece material, were among the possible causes of abrasion, in addition to the other hard dispersed carbide phases present in Inconel 718 and Waspaloy (such as TiC, NbC Cr_7C_3, referred in section 5.6.3) as reported previously by other researchers [1, 15, 162, 163, 166, 167].

In a study, Hanasaki and Fujiwara [176] have shown that by performing EPMA analysis on the sectioned tools, Ni and Cr from a high nickel alloy diffused into the flank of a P10 grade carbide to a depth of 5 micron. Ezugwu and Machado have also reported to find evidence of diffusion when face milling Nimonic 75 and Inconel 718 with carbide tools. Moreover, Trent [1] reports that temperatures over 850 °C is high enough to allow considerable amount of solid-state diffusion to take place when machining with WC-Co tools. He also states that the rate of diffusion increases rapidly with temperature, typically doubling for an increment of the order of 20 °C. Temperatures experienced by cutting tools when machining nickel alloys are much higher than conventional steels [7, 171]. The experiment by Smart and Trent [66] on cast iron and Nimonic 75 nickel-based alloy at a cutting speed of 10 m/min showed maximum rake face temperatures of 320 and 800 °C respectively. Further, tungsten and cobalt are amongst the effective alloying elements used for solid-solution hardening of nickel-based materials. This indicates the

presence of relative affinity between the atoms of tool (WC-Co) and workpiece materials [156, 236]. Based on such work, it has been established that machining of nickel-based workpiece materials generates diffusion wear even at extremely slow speeds, restricting tool life to low values [9]. Diffusion/abrasion related smooth wear was observed to occur mostly in the nose region of the flank. This can be associated with constant reduction of undeformed chip thickness towards the minor cutting edge, as a result of the nose radius (r_c) of 1 mm as depicted in Figure 6.17. Since the nickel based alloys have high tendency to work harden (Figure 5.6), work hardening and related rubbing tend to take place more readily in this particular section. Therefore generated temperatures are expected to be high enough to promote diffusion process. However, the effect of such diffusion wear was not as dominant as that of attrition and fracture mechanisms on tool life.

8.2.2.2 Rake face wear

Sectioned through failed tools as shown in Figures 8.19, 8.20, 8.32 and 8.33 demonstrate that a typical stair-form crater was formed on the rake face of worn CVD-coated KC994M and PVD-coated KC720 when machining both workpiece materials at the lowest cutting speed of 25 m/min. Figures 7.4, 7.18 and 7.105 also show the presence of such form of rake face on the failed insets. However, when milling with PVD-coated KC730 and uncoated KMF tools at the lowest speed of 25 m/min, rake face was not subjected to progressive plucking or fracture. It was either relatively less worn or fractured in a more brittle manner as shown in Figures 8.34, 8.35 and in Figures 7.31, 7.38, 7.119.

Generally the wear on the rake face contributed indirectly to the tool failure. The change in the original geometry of the rake due to chipping, plucking or pitting results in subsequent alteration of the shear pattern in the primary (shear angle reduces) and secondary shear zones. The deformed cutting edge acts as a negatively-raked tool with significant increases in cutting forces and temperatures. This may accelerate wear and deformation processes even further. During cutting tests, it was observed that chips were accumulated more on the entry side than on exit, towards the end of tool life. This

strongly indicates that the adhesion of the chip onto the rake face becomes stronger with prolonged machining due to the effect of increased cutting forces and corresponding stresses. Consequently this may have enhanced the plucking the tool material picked up by the root of the chip as was shown and discussed in section 8.2.1.

The irregular, unevenly worn rake face due to plucking or fracture becomes a susceptible source of crack initiation and fracture because of the stress concentration at sharp, irregular sections and cavities generated as shown in Figures 7.107, 7.122, 7.138, 8.15, 8.36 and 8.37. Cracking was found to intensify towards the end of tool life when the cutting edge was excessively damaged. Although cracking was observed at all cutting speeds, the occurrence was more evident at the cutting speeds of 50 to 100 m/min and high feed rate of 0.14 mm/tooth. The shape and location of the cracks were random suggesting that they were mechanically induced. Combined effect of localised high tensile stresses due to fracture-dominant wear modes, cutting edge deformation and cyclic thermo-mechanical stresses is believed to be the major factor in crack formation.

Adhesion of workpiece material to the rake and flank faces of the tool in the form of galling, may become a source of tool fracture. Shaw and Ramaraj [224] have reported that if strongly adhered patchy (isolated) workpiece material has high temperature, which is most likely the case under seizure condition, both the workpiece material and the tool contract upon cooling. This will induce localised tensile stresses in the tool face due to differences in thermal expansion coefficients of tool (5.2-5.5 10^{-6}/K) and workpiece materials (13-12.1 10^{-6}/K). This phenomenon could lead to crack initiation and hence tool fracture. Moreover, during chip flow, a tensile stress is induced on the trailing side (relative to chip flow) of the adhered workpiece material on tool faces. The magnitude of such a tensile stress may become extremely high at high coefficient of friction, which is the case under seizure conditions due to strong workpiece adhesion as reported by Takeyama et al. [171]. Figures 7.25, 8.15, 8.36 and 8.38 show the condition of CVD-coated KC994M and PVD-coated KC730 tools with adhered workpiece patches which are very likely to cause plucking or micro fracture due to the effect of such a mechanism.

Moreover, when the cutting speed was increased, a shear-localised (segmented) chip was produced due to periodic shear localisation being a characteristic feature of nickel

based alloys as shown in Figure 8.39. The longitudinal section of the chip produced at a cutting speed of 50 m/min, was almost continuos with no shear localisation unlike the one produced at 100 m/min which is highly shear localised. This type of chip subjects the tool to mechanical fatigue and induce chatter that could result in crack initiation and subsequent fracture [237, 238].

8.2.2.3 Brittle fracture

At higher cutting speeds premature chipping or breakage was found to be the life limiting factor for all the tools investigated as shown in Figures 7.2, 7.17, 7.30, 7.40, 7.90, 7.92, 7.106, 7.121 and 7.133.

Early fracture of the cutting tools was observed when face milling Inconel 718 at 75 and 100 m/min and Waspaloy at 50 to 100 m/min as shown in Figures 7.34, 7.101, 7.118 and 7.146. This happened even before a wear land was developed. Hence it is unlikely that early fracture is a fatigue-related phenomena, as the amount of cyclic thermal and mechanical shocks is far less than sufficient at the very beginning of the cutting process as proposed by Ai and Li [239]. Tool breakage occurs in interrupted cutting when the impact load is too large especially at high cutting speeds. Such breakage can even occur under properly selected cutting conditions due to the fatigue of tool material upon prolonged cutting [239]. In interrupted cutting operations, cutting speed is reported to have prevailing influence on tool fracture through its effect on the impact frequency and the rate of absorption and release of impact energy during engagement and disengagement [14, 224, 239]. Increasing the cutting speed results in a corresponding increase in impact energy at entry. Although the resultant static cutting force may decrease to a certain degree, rapid increase in dynamic force and the absorption rate of the impact energy at entry and the release rate at exit can cause early tool fracture. Moreover, increasing the cutting speed leads to proportional increase in thermal stresses imposed upon the tool because of the corresponding increase in temperature difference between cutting and idling cycles. It has been reported that the greater the difference in temperatures and the larger the thermal conductivity, the easier are the cracks to be initiated and propagated [239].

8.2.2.4 Coating delamination

Coating delamination has been found to occur in two distinctive manners. As discussed in section 8.2.1.1 concerning initial wear, the coating was removed by plucking effect of adhered workpiece material. This type of coating delamination occurred mainly on the rake face where intimate tool/chip contact took place.

The second type of coating delamination was seen towards the end of tool life occurring in the form of large detached pallets. The coating layer(s) has been separated as a whole bulk from the substrate. This was in a pealed manner with clear and smoother separation in PVD-TiN coated inserts (Figure 7.106). For CVD-coated tool, it happened in a fractured fashion leaving a rough surface with uneven texture as shown in Figure 8.40. The rough texture is a strong indication that adhesion strength of the coating in CVD-coated tool is much higher than that of PVD-coated tools. This could be due to better adhesion of coating, generated at high temperatures (~1000 °C) used for the CVD process [79, 87]. Delamination of this type generally occurs on the main rake face of the tool after being subjected to plastic deformation under excessive compressive and shear stresses imparted on heavily chipped cutting edges.

8.2.2.5 Plastic deformation

Plastic deformation was also found to occur on the rake face of all the cutting tools tested, becoming more pronounced towards the end of tool life, when face milling Inconel 718 at 75 and 100 m/min and Waspaloy at 50 to 100 m/min as shown in Figures 7.95, 7.110, 7.123, 8.41 and 8.42. Plastic deformation was generally observed as a consequence of chipping at the cutting edge and of subsequent temperature increases in the tool-chip contact zones. Plastic deformation was clearly visible along the borders of the chipped areas and causing the rake to deform upwards as shown in the above figures.

Increased cutting forces due to cutting edge deterioration by chipping and subsequent temperature rise resulting in softening of the cobalt binder phase are believed to be the main reasons for plastic deformation of the cutting edge, as reported by other researchers [1, 136, 137, 138].

8.3 Effect of cutting speed and feed rate on tool life

The effect of cutting speed and feed rate on tool life of all the tools used to machine Inconel 718 is shown in Figures 7.1, 7.48 and 7.49. Similarly, the effect of cutting speed and feed rate when machining Waspaloy is presented in Figures 7.89, 7.149 and 7.150.

In general increasing cutting speed from 25 to 75 m/min resulted in a steep reduction in tool life for all the coated tools tested on Inconel 718 as shown in Figures 7.1a, b and c. However, the plots in Figures 7.1a, b and c suggest that the rates of reduction in tool lives at the cutting speeds of 75 and 100 m/min were considerably lower for all the coated tools. Similar trends of steep and gradual decrease in tool lives were recorded at the cutting speeds of 25 to 40 m/min and 40 to 50 m/min respectively for the uncoated grade KMF when cutting Inconel 718 as shown in Figure 7.1d. For Waspaloy, the transition between steep and gradual reduction in tool lives appears to occur at the cutting speed of 50 m/min for the coated tools as suggested by the plots in Figures 7.89a, b and c. As for the uncoated KMF tool, the trends of the reduction in tool life for the low and high feed rates of 0.08 and 0.14 mm/tooth were significantly different. At low feed rate of 0.08 mm/tooth a transition was obvious at the cutting speed of 32 m/min between steep and gradual reduction in tool life, while there was no distinguishable difference in tool life reduction rate at high feed rate for the cutting speeds of 25 to 50 m/min. A common feature for both the workpiece materials when cutting with all the tool materials is that at the cutting speed where such a marked transition occurred in the rate of tool life reduction, tool life values were very low, being under 5 and 3 minutes respectively for Inconel 718 and Waspaloy. Therefore attempts will be made to compare the performance of the cutting tools with respect to tool life values obtained at the cutting speeds of 25 and 50 m/min.

At the lowest cutting speed of 25 m/min and feed rate of 0.08 mm/tooth, when machining Inconel 718, the tool life values obtained were 54, 32, 23 and 13 minutes for CVD-coated KC994M, uncoated KMF, PVD-coated KC730 and KC720 tools respectively. At high feed rate of 0.14 mm/tooth, tool life of 22 minutes each was recorded for CVD-coated KC994M and uncoated KMF inserts for the same cutting speed. Similarly PVD-coated KC730 and KC720 tools also showed an equal

performance by yielding a tool life of 14 minutes for the high feed rate of 0.14 mm/tooth at 25 m/min as shown in Figures 7.48 and 7.49.

When the cutting speed was increased to 50 m/min, reduced tool lives of 13, 10, 7 and 3 minutes were recorded for CVD-coated KC994M, PVD-coated KC730 and KC720 and uncoated KMF respectively for the low feed rate of 0.08 mm/tooth. When the feed rate was increased to 0.14 mm/tooth at the cutting speed of 50 m/min, a similar performance was recorded, with tool lives of 5, 4, 3 and 2.6 minutes respectively.

The results in Figures 7.149 and 7.150 indicate that, at the lowest cutting speed of 25 m/min and low feed rate of 0.08 mm/tooth, CVD-coated KC994M and uncoated KMF tools performed equally well, producing a tool life of 18 minutes, being the longest tool life achieved when cutting Waspaloy. PVD-coated tools KC730 and KC720 produced tool lives of 10 and 5 minutes respectively for the same cutting speed and feed rate. Increasing cutting speed to 50 m/min at lower feed rate of 0.08 mm/tooth, all the coated tools gave a similar low performance, yielding tool lives of 1 to 1.2 minutes. Uncoated KMF insert however lasted for 3.2 minutes. Considering these results, it is evident that the uncoated KMF grade performed and is followed by the CVD-coated KC994M, PVD-coated KC730 and KC720.

At higher feed rate of 0.14 mm/tooth and cutting speed of 25 m/min, tool lives of 9, 3, 2 and 1.8 minutes were recorded for KC994M, KC720, KMF and KC730 tools respectively when machining Waspaloy. When the cutting speed was increased to 50 m/min, a steep reduction in tool lives to 0.5 and 0.2 minutes was recorded, a reduction of 85 to 95 % . Figure 7.150 indicates that the performance of all the tools used at both the speed followed a similar pattern.

Steep reductions in tool lives, associated with the increase in cutting speed and feed rate, are shown in Figures 7.1 and 7.89 for Inconel 718 and Waspaloy respectively. The effect of cutting speed on tool life, in interrupted cutting operations, has been attributed to its prevailing influence on tool fracture through its effect on the impact frequency and the rate of absorption and release of the impact energy during engagement and disengagement [14, 224, 239]. Increasing the cutting speed results in a corresponding

increase in impact energy at entry and most importantly in cutting temperatures. Concentration of the highest temperature region at the cutting edge when machining nickel-based alloys, is another factor encouraging rapid deterioration of the cutting tools [7, 66, 160, 170]. Although the resultant static cutting force may decrease to a certain degree with increasing cutting speed, rapid increase in dynamic force and the absorption rate of the impact energy at entry and the releasing rate at exit can cause early tool fracture. Similarly, increasing the feed rate results in corresponding increase in impact forces at cutter entry and exit. Moreover, increasing the cutting speed leads to a proportional increase in thermal stresses (fatigue) by causing greater difference in temperatures between idling and cutting cycles [69, 239].

As the results indicate, CVD-coated KC994M tool gave the best overall performance in terms of tool life at cutting speeds of 25 and 50 m/min when milling Inconel 718 and Waspaloy. This can be attributed to the combined effect of its properties: (a) Possessing a cutting edge radius of 0.03 mm which provides increased structural strength, better stress distribution and resistance to mechanical impacts, (b) higher adhesion strength of the TiCN layer to the substrate and its superior properties to that of TiN as discussed in section 8.2, (c) higher cobalt content which provides increased toughness relative to PVD coated KC730 tools, (d) better resistance to wear of Al_2O_3+TiCN double coating at the flank face.

Considering its properties listed in Table 6.5, good performance of uncoated KMF tool relative to PVD-coated KC720 and KC730 tools, at the lowest cutting speed of 25 m/min, can be attributed to the combined effect of the following properties: (a) Better resistance to attrition wear, induced particularly by workpiece adhesion and detachment, due to sub-micron (0.8 micron) grain size, (b) featuring a honed cutting edge radius of ~ 0.027 mm which provides increased resistance to chipping, (c) higher transverse rupture strength and fracture toughness (3.6 GPa and 15 $MPa.m^{1/2}$ respectively) than the other tools, which provides grater resistance to fracture and crack propagation.

At the cutting speeds of 50 m/min, uncoated KMF tool gave the poorest average performance in terms of tool life when cutting both workpiece materials. At this cutting speed, cutting temperatures are expected to increase considerably in addition to rapid

increase in dynamic force and the absorption rate of the impact energy at entry and the releasing rate at exit. All the coated tools yielded longer tool lives by a factor of 2 to 4, than uncoated KMF insert, at the low feed rate of 0.08 mm/tooth and cutting speed of 50 m/min when milling Inconel 718. This strongly indicates that PVD-TiN coatings on KC720 and KC730 and CVD-TiCN+Al_2O_3 coatings on KC994M tools offered better wear resistance and lubricity particularly at the flank face, and provided some degree of thermal protection of the substrate at the cutting speed of 50 m/min. In addition, the presence of 2.5 % Ta(Nb)C (cubic carbide) in KC994M and KC720 substrate increases its hot hardness and resistance to diffusion/abrasion wear as reported by many researchers [1, 79, 84, 142]. Similarly KC730 has the highest room temperature and hot hardness values of 1830 and 760 HV respectively. These properties are reported to increase strength and give better resistance to wear at high cutting temperatures [1, 79].

At low feed rate of 0.08 mm/tooth, PVD-coated KC730 gave better performance than KC720, particularly at the cutting speed of 25 m/min when cutting both Inconel 718 and Waspaloy workpieces by producing 76 and 50 % longer tool lives respectively (Figures 7.48, 7.49 and 7.149, 7.150). This can be associated with: (a) KC730 has lower cobalt content approximately half that of KC720, (b) smaller grain size and (c) higher hot hardness by 180 HV units (Table 6.5 and 6.6). At the cutting speed of 50 m/min, the difference in performance reduced from 76 % to approximately 40 % for the low feed rate when machining Inconel 718. At high feed rate, both PVD-coated KC720 and KC730 gave similar performance with marginal differences in tool lives on both workpieces. This is most likely due to better toughness of the former and increased susceptibility to fracture of the latter at the high feed rate where the tools are subjected to increased mechanical impacts.

8.4 Effect of workpiece material

Both workpiece materials Inconel 718 and Waspaloy are regarded as difficult to machine nickel based alloys and therefore exhibit all of the respective machinability-related difficulties discussed in section 5.6 to a varying extent. Here attempts will be concentrated on the relative differences in properties between the two alloys which would affect their machinability behaviour.

The tool life results show that Waspaloy is more difficult to machine than Inconel 718, despite the fact that the former is of lower room-temperature hardness and tensile strength values than the latter (hardness of 454 and 486 HV_{30} and tensile strength of 1430 and 1280 MPa respectively). However, the amount of elongation, which is considered to be the measure of ductility [240], for Inconel 718 and Waspaloy at a temperature of 870 °C were reported be 88 and 37 % respectively [156, 241]. This considerable difference in the magnitudes of elongation at temperatures that are easily encountered during machining nickel-based alloys at relatively low cutting speeds (e.g. 20 m/min) [1, 66, 160], indicates that Inconel 718 is easier to machine than Waspaloy. The same conclusion can be drawn from the fact that high temperature tensile strength of the former at 870 °C is much lower (by ~ 35 %) than that of the latter, being 340 and 525 MPa respectively [156]. These properties suggest that high temperature strength of the material is of more impairing influence on the performance of the carbide tools than that of ductility. This also indicates that the behaviour of the material at high cutting temperatures is more crucial for metal cutting application than the room temperature properties alone.

In addition, the measured contact length widths on the rake face of the tools for all the cutting conditions tested, presented in Table 8.1, show that the values for Waspaloy are, in most of the cases, higher than those for Inconel 718 for the same cutting condition and tool material. As referred in the previous reports on nickel-based materials and steels [1, 135, 167], the cutting forces were higher, with smaller shear plane angle and thicker chips, when cutting Waspaloy than that of Inconel 718, showing superiority of the former in respect of high temperature strength.

Moreover, it has been reported that in the case of iron-containing nickel-based superalloys, the solubility temperatures of the precipitating phases, (primary strengthening phase of γ', Ni_3Nb) due to coarsening and transformation, are lower than that of other nickel based alloys which do not contain iron. Inconel 718 contains 18.5 wt. % iron, indicating that it is susceptible to softening at much lower temperatures than Waspaloy, as implied by the potential upper service temperature limits being 815 and 1150 °C respectively [236].

The fact that Waspaloy has 13.5% cobalt and more molybdenum (4.3%) than Inconel 718 (3%), raises the solubility temperature of gamma prime (γ') phase. The amount of gamma prime in the alloy increases with the content of Al and Ti. Hence Waspaloy is primarily strengthened by the γ' phase, as it contains about 3 times as much Al and Ti as does Inconel 718. This results in higher operating temperatures and strength at elevated temperatures. [156, 198]. As pointed out by Focke et al [159] that increasing the volume of γ' phase within the alloy matrix, generally accelerates the rate of tool wear. Similar results were recorded in this work as well.

8.5 Surface integrity

Importance and relevance of the surface integrity of the aerospace components employed in demanding applications has been emphasised in a detailed account given earlier in sections 2.2 and 5.10. The surface integrity aspects of face milling Inconel 718 and Waspaloy will now be discussed in relation to surface roughness and metallurgical condition of the surface and sub-surface of both the alloys.

8.5.1 Surface roughness

The surface roughness values (R_a) of the machined surfaces with all four types of cutting tools tested are presented in Figures 7.52 to 7.61 for Inconel 718 and Figures 7.153 to 7.160 for Waspaloy at various cutting conditions. These figures in general suggest that for both feed rates of 0.08 and 0.14 mm/tooth, a similar trend of surface roughness pattern was produced, which is more evident at the lower cutting speeds of 25 and 50 m/min.

In order to make a relative comparison of the surface finish results produced by each cutting tool tested, the surface roughness trends produced at the cutting speed of 25 m/min, are presented in Figures 7.60, 7.61 and 7.159, 7.160 for Inconel 718 and Waspaloy respectively.

The results show that surface roughness values were relatively high at the initial cutting stage and gradually dropping with prolonged cutting, mostly in a fluctuating fashion. The fluctuating nature of surface roughness values with the progress of machining can be associated with repetitive workpiece adherence to and detachment

from the cutting edge as reported by Conaway when machining nickel-based superalloys [162]. The second reason for this fluctuation can be the wear pattern of the cutting tools which involved progressive chipping at various degrees of severity depending on the cutting speed and feed rate employed. The sharp sections of the newly-chipped areas at the cutting edge may produce irregularities in the form of ploughing, scouring or tearing on machined surfaces which tend to increase surface roughness.

The high surface roughness values at the beginning of cut were probably due to the sharp cutting edge which is relatively more sensitive to interrupted cutting and associated vibration hence causing deeper cutting marks and irregularities on the machined surface. This shows that a correlation exists between the surface roughness produced and the tool wear/cutting edge condition [93]. Another notable common characteristics suggested by Figures 7.60, 7.61 and 7.159, 7.160, is that the difference in surface roughness values become marginal with prolonged machining regardless of the workpiece materials and cutting conditions employed.

The results also indicate that the effect of feed rate and cutting speed on the surface roughness were marginal. This is most likely due to the geometric configuration of the cutting edge which features a flat wiper edge of 2.4 mm length (minor cutting edge) as depicted in Figure 6.17. Such an edge theoretically eliminates the geometric effect of changing feed rate on surface roughness. All the cutting tools produced an average surface roughness within ranges of 0.44 to 0.65 and 0.54 to 0.67 micron on Inconel 718 and Waspaloy respectively for the cutting speed of 25 m/min and feed rate of 0.08 mm/min.

Figures 7.60, 7.61 and 7.159, 7.160 also indicate that, in most cases, slightly lower surface finish values were obtained when machining at low feed rate. However the difference was negligible when the initial fluctuations of the initial cutting stage were ignored. For example, a maximum difference of 0.12 micron was found in the average surface roughness values produced by KMF tool at low and high feed rate conditions when machining Inconel 718 at 25 m/min. This suggests that the effect of feed rate on the surface roughness produced was not significant at the low cutting speed range.

The fact that more uniform and consistent surface roughness readings were obtained with prolonged machining could be associated with the simultaneous development of a

uniform wear band on the minor cutting edge (wiper) flank and with the high work hardening tendency of the workpiece material. Because the more deteriorated the tool, the more work hardening effect is produced on the machined surface and the smoother the surface may become, a characteristic phenomenon which was also reported by others [13, 135, 163]. The presence of work hardening due to machining on the machined surfaces of Inconel 718 and Waspaloy was shown in Figures 7.62 to 7.65 and 7.161 to 7.164 respectively. This relationship is further supported by the fact that there was almost no measurable work hardening on the machined surface at the start of cutting (measured after 5 seconds of machining) due to insignificant amount of flank wear (~ 0.03 mm) on the minor cutting edge within this period. On the other hand, the width of flank wear on the minor cutting edge was approximately 0.10 to 0.15 mm when the tool was rejected, hence resulting in significant work hardening and associated relative improvement and consistency in surface roughness.

8.5.2 Variations in subsurface microhardness

The results of the subsurface microhardness measurements performed on the machined Inconel 718 and Waspaloy samples, using all four types of cutting tools are presented in Figures 7.62 to 7.65 and 7.161 to 7.164 respectively.

In order to compare the effect of worn tool with that of sharp, microhardness readings on the samples produced after 5 seconds of machining at the cutting speed of 25 m/min were also presented in the above figures.

In case of CVD and PVD coated tools, a similar trend of hardness pattern was observed on the machined surface samples as shown in Figures 7.62 to 7.64 and Figures 7.161 to 7.163 for Inconel 718 and Waspaloy workpieces respectively. The results show that the hardness of the top surface layer was always higher than that of the inner section of the workpiece materials. It followed a reduction pattern towards the nominal hardness values of the workpiece materials with increasing depth below the machined surface.

The results show that, a maximum increase in subsurface microhardness was produced by CVD-coated KC994M tools, measuring 607 and 586 HV (representing a maximum of 18 and 28 % increase) at the closest measurable depth of 0.020 mm, for Inconel 718 and Waspaloy respectively. This could be associated with the two notable

properties of KC994M tool, namely micro geometry of the cutting edge and CVD-TiCN+Al_2O_3 coating layers. The nose of the insert was a major influence on the state of the machined surface. The nose of the KC994M tool featured a radius of 1 mm and also a radius of ~ 0.03 mm at the cutting edge (between rake and flank face). The undeformed chip thickness gradually reduces to 0 at the point where nose and minor cutting edge (wiper) intersect. Because the workpiece materials have a high work-hardening tendency, rubbing and/or related plastic deformation, rather than cutting, is most likely to occur due to gradual reduction of undeformed chip thickness at a particular section of the nose/workpiece interface. This phenomenon is further encouraged by the presence of micro radius (0.03 mm). It is for this reason that many authors have drawn attention to the fact that too low a feed rate should not be used when cutting nickel based materials to prevent excessive work hardening that would otherwise lead to rapid tool failure [4, 46, 158, 162]. This rubbing and associated plastic deformation generates excessive temperatures within the nose area. Since the presence of TiCN+Al_2O_3 coating layers will diminish the rate of heat dissipation into the tool body, due to their low thermal conductivity (Table 6.6), heat concentration is expected to occur within the workpiece [16]. This subsequently increases the susceptibility of the workpiece to plastic deformation which results in a harder and deeper affected zone. This would also explain why uncoated KMF tools caused relatively less plastic deformation in the machined surface than the coated tools. The effect of this phenomenon will be more pronounced at higher cutting speeds due to consequent increases in temperatures. This effect is most likely to be responsible for relatively higher microhardness readings obtained when cutting speed was increased. In addition, a common characteristics of the surfaces produced by coated tools is that the microhardness readings up to the depth of 0.2 mm, produced at a cutting speed of 75 m/min were notably higher than that of the other cutting conditions. This suggests that the degree of hardening of the machined surface increases with increasing cutting speed.

Figures 7.62 to 7.65 show a particular plot which represents the effect of sharp tools on subsurface microhardness of Inconel 718 samples produced after 5 seconds of milling at a cutting speed of 25 m/min and feed rates of 0.08 and 0.14 mm/tooth., The figures suggest that there was no significant deviation from the nominal hardness value at the

early stage of machining. This indicates that there exists a strong correlation between the tool wear and the extent of surface hardening as a result of prolonged machining. However, micrographs showing the microstructures of the surface region, in sections 7.2.6.3 and 7.3.6.3, indicate that plastic deformation and associated strain hardening, occurred at this early stage of cutting within a narrow zone of approximately 10 to 15 μm depth beneath the surface.

When cutting Waspaloy however, the depth of affected layer at this initial stage of cutting was found to vary between 0.03 and 0.06 mm with regard to the cutting conditions and tool type. The plots in Figures 7.161 to 7.164, suggest that an increase in microhardness between 6 to 16 % was recorded at the closest measurable point of 0.02 mm depth. This could be attributed to the lower hardness (460HV) and higher ductility (20 % elongation) of Waspaloy workpiece than that of Inconel 718 (Table 6.4).

8.5.3 Subsurface metallurgical alterations

Figures 7.66 to 7.88 and 7.165 to 7.184 show respectively the state of subsurface microstructure on machined Inconel 718 and Waspaloy samples which were obtained from the initial and final stages of machining.

In the analyses of the subsurface microstructures, both of the workpiece materials tested showed similar types of microstructural alterations and surface damage pattern as they are of the same class of materials. These alterations include curved slip lines, in the direction of cutter rotation and/or feeding direction, and disturbed microstructure within the surface regions which indicate that the machined surfaces have been subjected to plastic deformation during the cutting process.

Micrographs showing the effect of initial machining indicate that the extent of plastic deformation was generally more when machining at the high feed rate of 0.14 mm/tooth than at the low feed rate of 0.08 mm/tooth. Plastic deformation is evidently the most common feature of all the surfaces generated at early and final stages of machining. The above figures suggest that the degree of plastic deformation increased with prolonged cutting and with increasing feed rate and cutting speed.

Plastic deformation observed within the machined surface layer can be attributed to localised high temperatures and high compressive stresses generated with prolonged

cutting. Temperatures up to 1000 °C [66, 136], generated during machining of nickel-based alloys, can cause softening of the machined surface to some extent. Hence, the surface is subjected to high compressive and shear stresses in excess of its yield strength under the combined action of high temperatures and cutting forces that results in plastic deformation of the machined surfaces. Moreover, the increased wear land on the minor edge and nose flank, as a result of prolonged cutting, promotes rubbing action that subsequently imposes higher stresses and temperatures onto the machined surfaces. At the same time, the rear section of the already-dull minor cutting edge induces a cold working action on the cooled regions of the machined surface. This will in turn intensify the plastic deformation and work hardening towards to he end of tool life.

It has been found that some physical damage in the form of surface tearing and embedded or dislodged hard particles (WC grains) occur which causes discontinuity and irregularity in the surface layer. Results also suggest that whenever the tool was subjected to severe chipping, surface tearing or irregularities on the machined surface occurred regardless of the machining stage and tool type. This effect was more evident at higher cutting speeds and feed rate where severe chipping was the dominant wear mode. Given that the chipping is one of the dominant wear modes of early cutting period at high cutting speeds, it is very likely that chipped and trapped tool particles (predominantly WC) are causes for such kind of surface damage. Although some surface irregularities are noticeable on the initial surface samples of low feed rate as shown in Figure 7.171, the difference between the two cases is markedly evident. This can be attributed to the difference in the scale of the chipping observed at both conditions.

8.6 Summary

All the coated tools experienced severe premature coating delamination at initial stage of machining. Cyclic adhesion and detachment of chip was mainly responsible for this. In addition, micro chipping became an important factor at higher cutting speeds and feed rate, diminishing tool performance. An adhesion/attrition dominant wear mechanism was found to be effective on all the tools particularly under low cutting conditions, causing progressive wear development. At higher cutting speeds, tool failure was due to severe chipping and/or breakage. CVD-coated KC994M tool gave better

performance than PVD coated and uncoated tools, due mainly to coating and stronger cutting edge micro geometry. KMF tool performed better than PVD coated tools at low cutting speed of 25 m/min due to its superior attrition resistance and stronger edge geometry. The presence of TiN coating on PVD coated tools provided a marginal increase in tool life when the cutting speed was increased. Shorter tool lives were obtained when milling Waspaloy workpiece material which possess higher elevated-temperature strength than Inconel 718. Machined surfaces were subjected to subsurface plastic deformation (work hardening), the degree of which increasing with the tool wear. Surface tearing was found to occur at initial as well as final stages of machining, associated with attrition wear and tool chipping.

CHAPTER 9

CONCLUSIONS

Following conclusions can be drawn from the face milling investigations of Inconel 718 and Waspaloy, using four different types of carbide inserts.

1. On the basis of tool life, CVD-coated KC994M tool gave generally better performance than all the other tools at the cutting speeds of 25 and 50 m/min when milling Inconel 718 and Waspaloy. This was due mainly to stronger cutting edge micro geometry, good substrate toughness and better adhesion between coating and substrate.
2. The uncoated KMF tool was generally the second best performing tool at the lowest cutting speed of 25 m/min on both the workpieces, giving an equal performance to that of CVD coated tool under some cutting conditions. This has been associated with its superior attrition wear resistance, stronger cutting edge micro-geometry and good toughness.
3. The tool life values were very low at high cutting speeds of 75 and 100 m/min, less than 2.3 minutes, due to rapid deterioration of the cutting edge by excessive chipping and/or breakage for both the workpieces.
4. PVD coated KC720 and KC730 gave longer tool lives than uncoated KMF tool at the cutting speed of 50 m/min when machining Inconel 718. KC730 outperformed KC720, by giving 44 to 100 % longer tool lives at low feed rate of 0.08 mm/tooth and cutting speed of 25 m/min when machining Inconel 718 and Waspaloy.
5. The TiN coating on KC720 and KC730 and TiCN+Al_2O_3 on KC994M tools were removed from the rake face contact zone by a cyclic chip adhesion/detachment process, at an early stage of cutting (within 5 seconds), regardless of cutting conditions and workpiece materials.
6. Coating delamination was much more severe on PVD coated KC720 and KC730 tools and was largely in a pealed manner, indicating an easy removal. Similarly, the top layer of Al_2O_3 on the rake face of the CVD-coated KC994M tool was observed to delaminate with ease. The second layer of TiCN on KC994M remained intact for a longer period than TiN coating on PVD-coated tools.

7. Coating on the flank face of the tools remained intact for a longer period than on the rake face. Premature large scale delamination, similar to that of the rake face, was not observed on the flank. Delamination on the flank was more gradual and discrete manner.
8. The tool life results indicate that Waspaloy alloy was more difficult to machine than Inconel 718. This was associated with the considerable differences in their high temperature tensile strength (by ~ 35 % at 870°C).
9. Tool failure at low cutting speeds of 25 and 50 m/min, was due to a combination of progressive chipping, plucking and flank wear whereby attrition and micro-fracture being the dominant wear mechanisms. Whereas at high cutting speeds tool failure was due to excessive chipping, breakage and plastic deformation.
10. The volume of metal removed was affected by the feed rate used. Comparing the results at 25 m/min, higher volumes of metal were removed at high feed rate when machining Inconel 718 with PVD-coated and uncoated tools. In case of Waspaloy, the volumes of material removed were higher at low feed rate with all the cutting tools tested.
11. The variations in surface roughness results produced by each cutting tool were insignificant, with average Ra values being generally under 1 micron. Each cutting tool produced an average surface roughness within a range of 0.44 to 0.67 micron on Inconel 718 and Waspaloy for the cutting speed of 25 m/min and feed rate of 0.08 mm/min where the longest tool lives were achieved.
12. The uncoated KMF tools caused relatively less plastic deformation on the machined surface than the coated tools. CVD-coated KC994M tool produced the maximum increase in the subsurface microhardness on both workpieces.
13. All the cutting tools produced an increase in the subsurface microhardness by 18 to 28 % at the closest measurable depth of 20 micron on the surfaces generated at the final stage of machining. It was observed that Waspaloy was more prone to subsurface microhardness alterations than Inconel 718.
14. Both workpieces were subjected to subsurface microstructural alterations in the form of plastic deformation that caused strain hardening to a depth of between 0.1 to 0.2 mm. In addition, physical damage in the form of surface tearing and embedded hard particles were found which caused discontinuity and irregularity in the surface layer.

FUTURE WORK

1. It would be a valuable contribution to study the effect of micro edge geometry on cutting tool performance in relation to face milling of nickel-based materials.

2. Tool life models should be established for those cutting tools which performed satisfactorily.

3. The effect of surface integrity on the functional and mechanical behaviour of the nickel-based materials tested would be of interest.

4. It has been proved that the adhesion strength between coating layer and substrate is of dramatic influence on tool performance. A study on the adhesion properties of coating/substrate would prove valuable.

5. Investigation of the effect of different cutter/workpiece relative position on tool life and wear behaviour is another important area of study as an extension to this work.

REFERENCES

1. Trent E. M., Metal Cutting, Butterworth-Heinemann, London, 1991.
2. Black Paul H., Theory of Metal Cutting, Mcgraw-Hill Book Company Inc., USA, 1961.
3. Taylor F. W., On the Art of Cutting Metals, Transaction of ASME, Vol. 28, 1907, pp. 31-57.
4. Shaw M. C., Metal Cutting Principles, Oxford University Press, New York, 1984.
5. Bradley E. F., (Edt), Superalloys; a Technical Guide, ASM Int. , Metals Park, Ohio, 1988.
6. Noaker Paula M., Taming Superalloy Tough Cuts, Manufacturing Engineering, October 1994, pp. 47-50.
7. Richard N. and Aspinwall D., Use of Ceramic Tools for Machining Nickel Based Alloys, Int. J. Machine Tools & Manufacture, Vol. 29, No. 4, 1989, pp. 575-588.
8. Drozda T. J. and Wick C., Tool and Manufacturing Engineers Handbook, Volume 1, Machining, SME, 1983.
9. Jawaid A., Phd Thesis, University of Warwick, UK, 1983.
10. Drozda T.J., Ion Implantation, Manufacturing Engineering., Vol. 94, No. 1, 1985, pp. 51-56.
11. Shook G. R. Jr., Face Milling of Hardened Inconel 718 With Whisker Reinforced Ceramic Composit Indexable Inserts, MSc Thesis, Purdue University, USA, 1986.
12. Tooher John F., Face Milling of a High-Stregth Temperature Resistant Cobalt Based Alloy, MSc Thesis, Trinity College, Dublin, 1986.
13. Ezugwu E.O. and Machado A.R., Face Milling of Aerospace Materials, 1. Int. Conf. on the Behaviour of Materials in Machining, Stratford-Upon-Avon, UK., 8-10 November 1988, pp.3/1-3/11.
14. Anon, Modern Metal Cutting, AB Sandvik Coromant, Sweden, 1994.
15. Alauddin M. and El-Baradie M.A., Hashmi M.S.J., End Milling Machinability of Inconel 718, Journal of Engineering Manufacture, Vol.210, 1996, pp.11-23.
16. El-Bestawi M.A., El-Wardany T.I., Yan Di, Tan Min, Performance of Whisker-Reinforced Ceramic Tools in Milling Nickel-Based Superalloy, Annals of the CIRP, Vol. 42/1, 1993, pp. 99-102.
17. Narutaki N. and Yamane Y., High Speed Machining of Inconel 718 With Ceramic Tools, Annals of the CIRP, Vol. 42/1, 1993, pp. 103-106.
18. Tonshoff H. K., Wobker H.-G. and Cassel C., Wear Characteristics of Cermet Cutting Tools, Annals of the CIRP, Vol. 43/1, 1994, pp. 89-92.
19. Kronenberg M., Analysis of Initial Contact of Milling Cutter and Work in Relation to Tool Life, Transactions of the American Society of Mechanical Engineers, Vol. 68, 1946, pp. 217-228.
20. Opitz H. and Beckhaus H., Influence of Initial Contact on Tool Life When Face Milling High Strength Materials, Annals of the CIRP, Vol. 18, 1970, pp. 257-264
21. Pekelharing A.J. , The Exit Failure in Interrupted Cutting, Annals of the CIRP, Vol. 27/1, 1978, pp. 5-10
22. Lindberg R. A., Processes and Materials of Manufacture, 4th. Edition, Allyn and Bacon, 1990.
23. Lambert B. K. (Edt.), Milling Methods and Machines, SME, Ohio, 1982

24. ISO 3002/1-1982-08-01(Second Editon), Basic Quantities in Cutting and Grinding-Part 1: Geometry of Active Part of Cutting Tools-General Terms, Reference Systems, Tool and Working Angles, Chip Breakers
25. Martellotti M.E., An Analysis of the Milling Process, Transactions of ASME, 1941, Vol. 63, pp. 667-700
26. Usiki H., Narutaki N. and Yamane Y., Face Milling of Beta Titanium Alloy, Proc. of 3. Int. Conf. on Progress of Cutting and Grinding, Japan Society for Precision Engineering (JSPE), November 19-22, 1996, pp. 57-62
27. Fowler David, Get More From Your Milling Cutter, Manufacturing Engineering, July 1996, pp. 74-81.
28. Gilbert W.W., Boston O.W. and Siekman H.J., Cutter Life for Face Milling Cast Iron, Transactions of ASME, Vol. Ol 76, 1954, pp. 607-703
29. Phillips P. K., Tool Wear and Tool Life Characteristics of Unconventional Sintered Carbides in Interrupted Cutting of Hardened Steel, Wear, Vol 47, No 1, 1978, pp. 45-51.
30. Ber A. and Heldman D., The Influence of Radial Location on the Wear Behaviour of Multi Tooth Face Milling Cutter, Annals of the CIRP, Vol. 25, N 1, 1977, pp. 1-4.
31. Venkatesh V.C., Raju A.S. and Srinivasan R., On the Aspects of Tool Wear Mechanism of Cemented Carbides Tools, Annals of the CIRP, Vol 25, No 1, 1977, pp. 27-33.
32. Asai T., Nakatani S. and Hara A., Study on the Early Fracture of Carbide Tools, Annals of the CIRP, Vol. 29, N 1, 1980, pp. 53-56.
33. Okushima K., and Hoshi T, The Effect of the Diameter of Carbide Face Milling Cutters on Their Failures, Bulletin of Japan Society for Manufacturing Engineering, Vol 6, No 22, 1963, pp. 308-314.
34. Yellowley Ian, Development of Machinability Testing Methods With Specific Reference to High Strength Thermal Resistant Work Material, Phd Thesis, Victoria University of Manchester, 1974.
35. Loladze T. N., Nature of Brittle Failure of Cutting Tool, Annals of the CIRP, Vol. 24, N 1, 1975, pp. 116-122.
36. Lat H. and Ber A., Investigation of Cemented Carbide Tool Behaviour in the Milling Operation, Proc. of the 6. North American Metalwork Res. Conf., Gainesville, April 16-19, 1978, pp. 270-275.
37. Pekelharing A.J., The Exit Failure of Cemented Carbide Face Milling Cutters, Part.1-Fundamentals and Phenomena, Annals of the CIRP, Vol. 33/1, 1984, pp. 47-50.
38. Pekelharing A.J., Van Luttervelt C.A. and Willemse H.R., The Exit Failure of Cemented Carbide Face Milling Cutters, Part. 2- Testing of Commercial Cutters, Annals of the CIRP, Vol. 33/1, 1984, pp. 51-54.
39. Shaw M. C., Fracture of Metal Cutting Tools, Annals of the CIRP, Vol. 28, No. 1, 1979, pp. 19-24.
40. Martellotti M.E., An Analysis of the Milling Process, Part II-Down Milling, Transactions of the ASME, 1945, Vol 67, pp. 670-690.
41. Heikkala J., Determining of Cutting Force Components in Face Milling, Journal of Materials Processing Technology, Vol. 52, 1995, pp. 1-8.
42. Abdou G., Yien J., Analysis of Force Patterns and Tool Life in Milling Operations, Int J. of Advanced Manufacturing Int. Journal of Advanced Manufacturing Technology, Vol. 10, 1995, pp. 11-18.
43. Field M., Kahles J.F., Rewiev of Surface Integrity of Machined Components, Annals of the CIRP, Vol 20/2, 1971, pp. 153-163.

44. Field Michael, Machining Aerospace Alloys, Proceedings of the Conference on Machinability, Iron and Steel Institute, 4-6 Oct. 1965, UK.
45. Klocke F., Konig W., Gerschwiler K., Advanced Machining of Titanium and Nickel-Based Alloys, in "Advanced Manufacturing Systems and Technology" E. Kuljanic (Edt), CISM Courses and Lectures No. 372, Springer Verlag, New York, 1996.
46. Warburton P., Problems of Machining Nickel-Based Alloys, Proc. of the Conf. on Machinability, Iron and Steel Institute, 4-6 Oct. 1965, UK.
47. Kalpakjian, S., Manufacturing Engineering and Technology, 3. Ed., Addison-Wesley Publishing Co., USA, 1995.
48. Boothroyd G and Knight W. A., Fundamentals of Machining and Machine Tool, 2. Ed., Marcel Dekker Inc., USA., 1989.
49. ISO 4288- 1985(E), Rules and Procedures for the Measurement of Surface Roughness Using Stylus Instruments.
50. Black J.T., Mechanics of Chip Formation, in "Metals Handbook, 9. Ed., Vol. 16, Machining, ASM Int., 1989.
51. Finnie I., Review of the Metal Cutting Analyses of the Past Hundred Years, Mechanical Engineering, Vol. 13, Part 1, August 1956, pp. 715-721.
52. Lee E. H. and Shaffer B. W., The Theory of Plasticity Applied to a Problem of Machining, Journal of Applied Mechanics, Transactions of ASME, Vol. 18, No 4, 1951, pp. 405-413.
53. Oxley P. L. B., Rate of Strain Effect in Metal Cutting, Journal of Engineering for Industry, ASME, Vol. 85, 1963, pp. 335-337.
54. Zorev N. N., Interrelationship Between Shear Processes Occurring Along Tool Face and on Shear Plane in Metal Cutting, Proc. of Int. Prod Res. Conf., Pittsburgh, USA, Sept. 9-12, 1963, pp. 42-49.
55. Trent E. M., Conditions of Seizure At the Tool-Work Interface . Proc. of the Conference on Machinability, Iron and Steel Institute, London, 4-6 Oct., 1965, pp. 11-18.
56. Schey Jhon A., Tribology in Metalworking: Friction, Lubrication and Wear, American Society for Metals (ASM), 1983.
57. Trent E. M., Metal Cutting and the Tribology of Seizure: 1- Seizure in Metal Cutting, Wear, Vol. 128, 1988, pp. 29-45.
58. Trent E. M., Metal Cutting and the Tribology of Seizure: II- Movement of Work Material Over the Tool in Metal Cutting, Wear, Vol. 128, 1988, pp. 47-64.
59. Trent E. M., Metal Cutting and the Tribology of Seizure: III- Temperature in Metal Cutting, Wear, Vol. 128, 1988, pp. 65-81.
60. Wright P. K., Frictional Interaction in Machining: Comparisons Between Transparent Sapp. Hire and Steel Cutting Tools, Metals Technology, Vol. 8, 1981, pp. 150-160.
61. Wright P. K., Horne J. G. and Tabor D, Boundary Conditions At the Chip-Tool Interface in Machining; Comparisons Between Seizure and Sliding Friction, Wear, Vol. 54, 1979, pp. 371-390.
62. Wallbank J, Structure of Built-Up Edge Formed in Metal Cutting, Metals Technology, Vol. 6, 1979, pp. 145-153.
63. Oishi K., Built-Up Edge Elimination in Mirror Cutting of Hardened Steel, Trans. ASME, J. Eng. Ind., Vol. 117, Feb. 1995, pp. 62-66.
64. Lenz E., Katz Z., Ber A., Investigation of the Flank Wear of Cemented Carbide Tools, Trans. ASME, J. Eng. for Ind., Vol. 98, Feb. 1976, pp. 246-251.
65. Juneja B. L. and Sekhon G. S., Fundamentals of Metal Cutting and Machine Tools, John Willey & Sons Inc., 1987.

66. Smart E. F., Trent E. M., Temperature Distributions in Tools When Cutting Titanium and Nickel, Int. J. of Production Research, Vol. 13, N3, 1975, pp. 265-290.
67. Wright P. K. and Trent E. M., Metallurgical App. Raisal of Wear Mechanisms and Processes on High Speed Steel Cutting Tools, Metals Technology, January 1974, pp. 13-23.
68. Lo Casto S., Lombardo A., Passannanti G., Relation Between Tool Life in Milling and in Interrupted Turning, Wear, Vol. 131, 1989, pp. 207-216.
69. Wayne S. F. and Buljan S. T., The Role of Thermal Shock on Tool Life of Selected Ceramic Cutting Tool Materials, J. Amer. Cer. Soc., Vol. 75, 1989, pp. 754-760.
70. Stephenson D. A., Ail A., Tool Temperature in Interrupted Metal Cutting, ASME Journal of Engineering for Industry, Vol. 114, May 1992, pp.. 127-136.
71. Chakraverti G., Analysis of Tool Temperature Fluctuation in Interrupted Cutting, Precision Engineering, Vol. . 6, No. 2, 1984. pp. 99-105.
72. Yellowley I. and Barrow G., Influence of Thermal Cycling on Tool Life in Peripheral Milling, Int. J. MTDR, Vol. 16/1, 1976, pp. 1-12.
73. Seco Milling Catalog, ST944739E, Seco Tools AB, Sweden, 1994
74. Komanduri R., and Desai J. D., Tool Materials for Machining: Part One of a Three-Part Series, The Carbide and Tool Journal, Sept.-Oct., 1983, pp. 3-10.
75. Trent E. M., Cutting Tool Materials, Metallurgical Review, No. 127, 1968, pp. 129-144.
76. Edwards R., Cutting Tools, The Institute of Materials, London, 1993.
77. Tlusty J., High-Speed Machining, Annals of the CIRP, Vol. 42, 1993, pp. 733-738.
78. Hoyle G., High Speed Steels, Butterworths, 1988.
79. Davis J. R., (Edt.), Tool Materials, ASM Speciality Handbook, ASM Int., 1995.
80. Konig W., Fritsch R., Kammermeier D., Physically Vapour Deposited Coatings on Tools; Performance and Wear Phenomena, Surface and Coating Technology, Vol. 49, 1991, pp. 316-324
81. Metals Handbook, Volume 16, Machining, 10. Edn., ASM Int., 1989.
82. Santhanam A.T., Grab G.P., Innovations in Coated Carbide Cutting Tools, Proc. of the 9. Conf. on Advances in Tool Materials for Use in High Speed Machining, 25-27 Feb. 1987, Arizona.
83. Kalish H. S. and August J. S., How Composition Affects the Properties and Performance of Cemented Carbide Cutting Tools, Metal Progress, June 1979, pp. 64-70.
84. Brookes Kenneth J.A., World Directory and Handbook of Hard Metals and Hard Materials, 1992, 5th Edn., Int. Carbide Data, UK.
85. Hunt J. L., Santhanam A. T., Coated Carbide Metal Cutting Tools: Development and Applications, Fundamental Issues in Machining, ASME, Production Engineering Division, PED. Vol. 43, 1990, pp. 139-155.
86. ISO 513: 1997 Classification of Carbides.
87. Santhanam A. T., Tierney P. and Hunt J. L., Cemented Carbides, in Metals Handbook, 9. Edn. Vol. 16, ASM, 1989.
88. Edwards Dean R., Coated Carbides Used for Milling, Proceedings of the 77th AESF Annual Technical Conference, Boston, July 9-12, 1990, pp. 823-833.
89. Spur Gunter and Lachmund Uwe, Application Properties of Diamond-Coated Carbides, Proc. of the 3. Int. Conf. on Progress of Cutting and Grinding, Japan Society for Precision Engineering (JSPE), November 19-22, 1996, pp. 108-113.
90. Katbi K., Thin Is in for Tool Coatings, American Machinist, October 1999, pp. 116-118.

91. Kohno Yuichiro, Recent Developments in Cutting Tools and Tool Materials, Proc. of 3. Int. Conf. on Progress of Cutting and Grinding, Japan Society for Precision Engineering (JSPE), November 19-22, 1996, pp. 14-19.
92. Beeghly Craig W., Get Your Shop Out of the Uncoated Age, in: "High Speed Machining; Solution for Productivity", ASM Int., Ohio, 1989.
93. Hunt J.L., Petrosky C.J. and Quinto D. T., Development of a PVD-Coated Carbide Grade for Milling, Carbide Tool Journal, Vol. 19, No. 5, 1987, pp. 5-9.
94. Kodama M., Bunshah R.F., Interrupted Cutting Tests of Cemented Carbide Tools Coated by Physical Vapor Deposition and Chemical Vapour Deposition Techniques, Thin Solid Films, Vol. 96, 1982, pp. 53-58.
95. Forrest J.H., The Use of Titanium Nitride Coated Tools, in: "High Speed Machining; Solution for Productivity", ASM Int., Ohio, 1989.
96. John B. W., and Malcolm G. M., Advanced Ceramics; Structural Materials With a Hot Feature, Manufacturing Engineering, Feb. 1985, pp. 56-63.
97. North B., Ceramics Cutting Tool, Carbide and Tool Journal, Vol. 18, No. 15, 1986, pp. 23-28.
98. Momper F. J., Ceramic on the Line, Production Engineer, Vol. 68, 1989, pp. 13-15.
99. Li Xing Sheng and Low It-Meng (Edt.), Advanced Ceramic Tools for Machining Applications-1, Trans Tech Pub. Ltd., Switzerland, 1994.
100. Clinton D. J., Lay L. A. and Morrell R., The Microstructure Dependence of Hardness in High-Purity Alumina Ceramics, British Ceramic Proceedings, Vol. 37, 1986, pp. 217-227.
101. Furukawa M., Nakano O., Takashima Y., Fracture Toughness of Al_2O_3-Tic Ceramics, Int. Journal of Refractory and Hard Metals, Vol. 7, No. 1, 1988, pp. 37-40.
102. Li X. S. and Low I. M., Evaluation of Zirconia-Toughened Alumina Cutting Inserts During Machining of High Strength Steel, Journal of Material Science Letters, Vol. 12, No. 24., 1993, pp. 1916-1919.
103. Claussen N., Fracture Toughness of Al_2O_3 With An Unstabilised Zro_2 Dispersed Phase, Journal of the American Ceramic Society, Vol. 59, 1976, pp. 49-51.
104. Wei G. C. and Becher P. F., Development of Sic Whisker-Reinforced Ceramics, American Ceramic Society Bulletin, Vol. 64, No.2, 1985, pp. 296-304.
105. Billman B. R., Mehrotra P. K., Shuster A. F. and Beeghly C. W., Machining With Al_2O_3-Sic Whisker Cutting Tools, American Ceramic Society Bulletin, Vol. 67, No.6, 1988, pp. 1016-1019.
106. Fukuhara M., Fukazawa K., Fukawa A., Physical Properties and Cutting Performance of Silicon Nitride Ceramic, Wear, Vol. 102. 1985, pp. 195-210.
107. Aucote J. and Foster S. R., Performance of Sialon Tools When Machining Nickel Based Aerospace Alloys, Material Science and Technology, Vol. 2, 1986, pp. 700-708.
108. Hampshire S., Engineering Properties of Nitrides Ceramics and Glasses, Engineered Materials Handbook, ASM Int. , Vol. 4, 1991, pp. 812-820.
109. Aspinwall D. K., Superhard Tooling Ten Years on , Metalworking Production, Vol. 129, No. 11, 1984, pp. 90-98.
110. Brookes C. A. and Lambert W. A., Ultrahard Material Application Technology. (De Beers), Hornbeam Press Ltd, 1982.
111. Field J. E. Strength and Fracture Properties of Diamond, in: "The Properties of Diamond", Field J. E. (Edt.), Academic Press, London, 1979.

112. Hay R. A., The New Diamond Technology and Its Application in Cutting Tools, In: "Ceramic Cutting Tools Materials Development and Performance", Whitney E. Dow (Edt.), Noyes Publications, USA, 1994.
113. Krar S. F. and Ratterman E., Superabrasives, in "Grinding and Machining With CBN and Diamond", Zollo S. M., (Edt.), Mcgraw-Hill Inc., New York, 1990.
114. Lammer A., Mechanical Properties of Polycrystalline Diamond (PCD), Material Science and Technology, Vol. 4, Nov. 1988, pp. 949-955.
115. Peter J. H., Structure, Properties and Application of Polycrystalline Cubic Boron Nitride, Proc. of 14. NAMRC, May 1986, pp. 66-80.
116. Heath P. J., Ultrahard Tool Materials, Metals Handbook, 10th Edt., Vol. 16, ASM Int., Metals Park, Ohio, 1989.
117. Focke A., Wear of Superhard Materials When Cutting Superalloys, Wear, Vol. 46, 1978, pp. 65-79.
118. Ratterman E. and Bovenkerk H. P., Polycrystalline Diamond and Cubic Boron Nitride, In: "Ceramic Cutting Tools Materials, Development and Performance", Whitney E. Dow (Edt.), Noyes Publications, USA, 1994.
119. Christopher J. D., Selection of Tool Materials, In "Ceramic Cutting Tools Materials Development and Performance", Whitney E. Dow (Edt.), Noyes Publications, USA, 1994.
120. Katayama S., Hashimura M., Effect of Micro Cracks in Layer on Performance of CVD Coating Carbide Cutting Tool, Journal of the Japan Society for Precision Engineering, Vol. 60, N 1, Jan. 1994, pp. 124-127.
121. Takadoum J. Friction and Wear Characteristics of TiN, TiCN and Diamond-Like Carbon Films, Surface and Coatings Technology, Vol. 88, 1996, pp. 232-238
122. Kim S., Material Properties of Ceramic Cutting Tools, Key Engineering Materials, Vol. 96, 1994, pp. 33-78.
123. Stephenson D. A., Agapiou J. S., Metal Cutting Theory and Practice, Marcel Dekker Inc., 1997.
124. ISO 8688-1:1989 (E), Tool Life Testing in Milling-Part 1: Face Milling, First Edition, 1989-05-01
125. Quinto D. T., Thecnology Perspective on CVD and PVD Coated Metal Cutting Tools, Int. J. of Refractory Metals and Hard Materials, Vol 14, 1996, pp. 7-20.
126. Floyd Tom, Diagnose Insert Failure, Manufacturing Engineering, Oct.1992, pp. 37-38.
127. Dearnley P. A., Trent E. M., Wear Mechanisms of Coated Carbide Tools, Metals Technology, Vol. 9, 1982, pp. 60-75.
128. Dearnley P.A., Rake and Flank Wear Mechanisms of Coated and Uncoated Cemented Carbides, Journal of Engineering Materials and Technology, Vol. 107, 1985, pp. 68-82.
129. Kramer B.M., On Tool Materials for High Speed Machining, Journal of Engineering for Industry, Vol. 109, 1987, pp. 87-91.
130. Bhatia S. M., Pandey P. C., Shan H. S., Thermal Cracking of Carbide Tools During Intermittent Cutting, Wear, Vol. 51, 1978, pp. 201-211.
131. Mills B., Redford A. H., Machinability of Engineering Materials, Applied Science Publishers Ltd., 1983.
132. Uehara K., Kanda Y., Kobayashi A. On the Chipp. Ing Phenomena of Carbide Cutting Tools, Annals of the CIRP, Vol. 25, N 1, 1977, pp. 11-16.
133. Al-Tornachi M.J. Kadhim, Dugdale D.C., Fracture of Cemented Carbide Tools in Face Milling, Proc. 18th Int. MTDR Conf., 1977, P 523-527

134. Kramer B.M., Requirements for Wear Resistant Coatings, Thin Solid Films, Vol. 108, 1983, pp. 117-125.
135. Venkatesh V. C., Ye C. T., Quinto D. T., Hoy D. E. P., Performance Studies of Uncoated, CVD-Coated and PVD-Coated Carbides in Turning and Milling, Annals of the CIRP, Vol. 40/1, 1991, pp. 545-550.
136. Kramer B.M., On Tool Materials for High Speed Machining, ASME Production Engineering Division, PED Vol. 12, 1984.
137. Graham D. E., Aluminum Oxide Coatings for Cemented Carbide Cutting Tools, In: "Ceramic Cutting Tools Materials Development and Performance", Whitney E. Dow (Edt.), Noyes Publications, USA, 1994.
138. Trent E.M., Evolution of Tool Materials for Metal Cutting, Tools and Dies for Industry, The Metals Society, London, 1977, pp. 374-387.
139. Kuljanic Elso, An Investigation of Wear in Single-Tooth and Multi-Tooth Milling, Int. J. of Mach. Tool Des. Res., Vol. 14, 1974, pp. 95-109.
140. Kopac J., Influence of Cutting Material and Coating on Tool Quality and Tool Life, Journal of Materials Processing Technology, Vol. 78, 1998. pp. 95-103.
141. Ezugwu E. O., Pashby I. R., The Milling of Titanium and Nickel Base Superalloys With Tin/Steel Composite End Mills, 2nd Int. Conf. on Behaviour of Materials in Machining, Organised by Institue of Metals, UK, 14-15 Nov. 1991, pp. 96-102.
142. Kramer Bruce M. and Hartung Paul D., Theoretical Considerations in the Machining of Nickel-Based Alloys, Cutting Tool Materials, American Society for Metals, Metal Park, OH., 1981, pp. 57-74.
143. Venkatesh V. C., and Chandrasekaran H., Experimental Techniques in Metal Cutting, Prentice Hall of India, New Delhi, 1987.
144. Ezugwu E. O., Jawaid A., The Effect of Coatings on the Performance of Carbide Cutting Tools When Machining a Nickel Base, Inconel 718, Superalloy, Proceeding of 5th Int. Manufacturing Conference With China (IMCC'91), April 1991. pp. A286-A296
145. Bhattacharyya S. K. and Jawaid A., Tool Life and Wear Mechanism of Sylon Ceramic Tools When Machining Nickel-Based Materials, Proc. 5th Int. Conf. on Production Engineering, 1984, pp. 203-208.
146. Armarego E.J.A. and Brown R.H., The Machining of Metals, Prentice-Hall Inc., USA, 1969.
147. Shaw M. C., Tool Life, In: "Ceramic Cutting Tools; Materials, Development and Performance", Whitney E. Dow (Edt.), Noyes Publications, USA, 1994.
148. Sabberwal A.J.P., Fleischer P., The Effect of Material and Geometry on the Wear Characteristics of Cutting Tools During Face Milling, Int. J. of Machine Tool Design and Research, Vol. . 4, 1964, pp. 47-71.
149. ISO 8688-2, Tool Life Testing in Milling-Part 2: End Milling, First Edn., 1989-05-01.
150. Inco Alloys Int. Ltd., Publication No: IAI-140, 1995.
151. Inco Alloys Int. Ltd., Publication No: IAI-150, Inco Alloys News, No. 1, 1996.
152. Metals Handbook, Properties and Selection of Nonferrous Alloys and Special-Purpose Materials, ASM Int. , 10th Edt. Vol. 2, 1990, P429-445.
153. Flower M. Harvey (Edt.), High Performance Materials in Aerospace, Chapman Hall, 1995.
154. Betteridge W., Nickel and Its Alloys, Ellis Horwood Ltd., UK, 1984.
155. Gessinger G.H., Recent Developments in Powder Metallurgy of Superalloys, In: "Superalloys Source Book", Donachie Jr. M. (Edt.), ASM, 1984.

156. Donachie Jr. Matthew J (Editor)., Superalloys Source Book, American Society for Metal (ASM), 1984.
157. Westbrook J. H., Bellows G., Field M. and Kahles J. F., Machining the Superalloys, In: "The Superalloys", Sims C. T. and Hagel W. C., (Edt), John Wiley & Sons Inc., 1972.
158. Inco Alloys Int. Ltd., Publication No: IAI-130, Machining, 1964.
159. Focke A.E., Westermann F.E., Ermi A., Yavelak J., Hoch M., Deformation of Tungsten Carbide Tools When Cutting Inconel 718, Proc. of 16th Int. Machine Tool Design and Research Conf., Manchester, England, 1975, pp. 565-572.
160. Wright P.K., Chow J.G., Deformation Characteristics of Nickel Alloys During Machining, Journal of Engineering Materials and Technology, Vol. 104, April 1982, pp. 85-93.
161. Komanduri R., Brown R.H., On the Mechanics of Chip Segmentation in Machining, Journal of Engineering for Industry, Vol. 103, 1981, pp. 33-51.
162. Conaway H. R., 1975, Machining the High-Nickel Alloys, In: "Influence of Metallurgy on Machinability", Tipnis Vijay A., (Edt), ASM, 1975.
163. Zlatin N. and Christopher J., Machining Characteristics of Difficult to Machine Materials, In: "Influence of Metallurgy on Machinability", Tipnis Vijay A., (Edt), ASM, 1975.
164. Howard J.J., Tools for Cutting Nickel Alloys, Tools and Dies for Industry, The Metals Society, London, 1977, pp. 105-121.
165. Russell J. E., Machinability As Affected By the Metallurgy and Size of the Workpiece, Proc. of the Conf. on Machinability, Iron and Steel Institute, 4-6 Oct. 1965, UK.
166. Anon, Machining Difficult Alloys, a Compendium on the Machining of High-Strength Steels and Heat-Resistant Alloys, American Society for Metals, Metals Park Ohio, 1962.
167. Ezugwu E.O. and Pashby I.R., High Speed Milling of Nickel-Based Superalloys, Journal of Materials Processing Technology, Vol. 33, 1992, pp. 429-437.
168. Addhoum H. and Broussaud D., Interaction of Ceramic Cutting Tools With Nickel-Based Alloys, Materials Science and Engineering, A 109, 1989, pp. 379-387.
169. Bhattacharyya S.K., Jawaid A., Lewis M.H., Wallbank J., Wear Mechanisnms of Syalon Ceramic Tools When Machining Nickel-Based Materials, Metals Technology, December 1983, Vol. 10, pp. 482-489.
170. Focke A.E., Grooving on Flank of Cemented Carbide Tools When Cutting Inconel 718, Proc. of the 4th North American Manufacturing Researh Conf., NAMRC-IV, 1976, pp. 45-51.
171. Takeyama H., Yamamoto Y., Surface-Technological Analysis of Metal Adhesion on Tungsten Carbide Tool and Prevention of Brittle Fracture Due to Metal Adhesion, Annals of the CIRP, Vol. 36, N 1, 1987, pp. 421-424.
172. Inco Alloys Publication No. IAI-38, 1994.
173. Christopher J. D., Machinability of Materials; An Overwiev, Proc. of the SCTE'89 'Society of Carbide and Tool Engineers' Conference, San Diego, California, 13-15 Nov. 1989, pp. 138-143.
174. Ezugwu E.O., Wang Z.M., Machado A.R., The Machinability of Nickel-Based Allloys; a Review, Journal of Material Processing Technology, Vol. 86, 1999, pp. 1-16.
175. Gorsler Frank W., High Speed Machining of Aircraft Engine Alloys, Proc. of the Int. Conf. on High Productivity Machining Materials and Processing, New Orleans, Louisiana, 7-9 May 1985, pp. 76-82.
176. Hanasaki S. and Fujiwara J., Ceramic-Coated Cutting Tools, Key Engineering Materials, Vol. 96, 1994, pp. 197-220.

177. Quigley O., Monaghan J., The Performance of Coated Carbide Cutting Tools in Turning a Nickel-Iron Base Superalloy, Proc. of the 10th. Conf. of the Irish Manufacturing Committee (IMC-10), 8-10 Sep. 1993, University College Galway, Ireland, pp. 337-349.
178. Ezugwu E.O., Wang Z.M., Performance of PVD and CVD Coated Carbide Tools When Machining Nickel Based Inconel 718, Proc. of the 3. Int. Conf. on Progress of Cutting and Grinding, Japan Society for Precision Engineering (JSPE), November 19-22, 1996, pp. 102-107.
179. Rahman M., Seah W.K.H., Teo T.T., The Machinability of Inconel 718, Journal of Material Processing Technology, Vol. 63, 1997, pp. 199-204.
180. Rahman M., Seah W.K.H., Teo T.T., The Machinability of Inconel 718, Journal of Material Processing Technology, Vol. 63, 1997, pp. 199-204.
181. Choudhury I. A. and El-Baradie M. A., Machining Nickel Base Superalloy, Journal of Engineering Manufacture, Proceeding of the Institution of Mechanical Engineers, Vol. 212, Part B3, 1998, pp. 195-206.
182. Yeomans J. A. and Page T. F., The Chemical Stability of Ceramic Cutting Tool Materials Exposed to Liquid Metals, Wear, Vol 131, 1989, pp. 163-175.
183. Jun C. K., and Smith K. H., Alumina-Silicon Carbide Whisker Composite Tools, In: "Ceramic Cutting Tools; Materials, Development and Performance", Whitney E. Dow (Edt.), Noyes Publications, USA, 1994.
184. Baker R. D., Ceramic Cutting Tools: Application Guidelines, Carbide and Tool Journal, Vol. 13, Sept. 1981, pp. 28-35.
185. El-Wardany T. I., E. Mohammed, Elbestawi M. A., Cutting Temperature of Ceramic Tools in High Speed Machining of Difficult-To-Cut Materials , Int. J. Machine Tools & Manufacture, Vol. 36, No. 5, 1996, pp. 611-634.
186. Baker R. D., Kyon 2000: A New World of High Performance, Carbide and Tool Journal, Vol. 12, May 1982, pp. 10-18.
187. Bhattacharyya S. K., Wallbank, J. and Jawaid A., Metalworking Production, Vol. 126, 1982, pp. 104-110.
188. Baldoni J. G. and Buljan S. T., Silicon Nitride Cutting Tools, In: "Ceramic Cutting Tools; Materials, Development and Performance", Whitney E. Dow (Edt.), Noyes Publications, USA, 1994.
189. Brandt G., Gerendas A., Mikus M., Wear Mechanizm of Ceramic Cutting Tools When Machining Ferrous and Non-Ferrousn Alloys, Journal of Eurpean Ceramic Society, Vol. 6,1990, pp. 273-290.
190. Szeszulski K. J., Thangaraj A. R., Weinmann K. J., On the Cutting Performance of Whisker-Reinforced Ceramics Machining Inconel, In: "Fundamental Issues in Machining" Klamecki B. E. and Weinmann K. J., (Edt), ASME, Production Engineering Division, PED. Vol. 43, 1990, pp. 97-113.
191. Vigneau J., Bordel P., Leonard A., Influence of the Microstructure of the Composite Ceramic Tools on Their Performance When Machining Nickel Alloys, Annals of the CIRP, Vol. 36/1, 1987, pp. 13-16.
192. Jackson D., The Cutting Materials of Tomorrow: Building on the Capabilities of Today, In: "High Speed Machining; Solution for Productivity", Schneider G. Jr., (Edt.), ASM Int., Ohio, 1989, pp. 34-38.
193. Mehrotra P. K., Beeghly C. W., Advanced Ceramic Tools for High Productivity Machining of Superalloys, In: "High Speed Machining; Solution for Productivity", Schneider G. Jr., (Edt.), ASM Int., Ohio, 1989, pp. 11-19.

194. Koelsch James R., Cutting Exotic Materials, Machine and Tool BLUE BOOK, Feb. 1990, pp. 31-33.
195. Richards N., Currie E.M., Aspinwall D.K., Smith D.J.M. and Dewes R. C., Tool Life Data When Machining Nickel Based Alloys With Ceramic Cutting Tools, Proc. of the 13th. Conf. of the Irish Manufacturing Committee (IMC-13), 4-6 Sept. 1996, pp 153-158.
196. Dailey James H., PCBN Tools Take off on Hard Surfaces, American Machinist, Vol. 140, N11, Nov. 1996, pp. 39-41.
197. Kato Hideharu, Cutting Performance of Pcbn Endmill on Machining of Nickel Based Superalloy : Effect of High Pressure Coolant Supply on Tool Wear, Proc. of the 3. Int. Conf. on Progress of Cutting and Grinding, Japan Society for Precision Engineering (JSPE), November 19-22, 1996, pp. 142-147.
198. Kirk D.C., Cutting Aerospace Materials (Nickel-, Cobalt-, and Titanium-Based Alloys), Tools and Dies for Industry,The Metals Society, London, 1977, pp. 374-387.
199. Chandrasekaran H., Nordgren A., Role of Tool Microstructure and Stress-State Upon the Wear Mechanisms in Milling, Annals of the CIRP, Vol. 39, N 1, 1990, pp. 65-69.
200. Ohtani Toshiaki, Fujjse Kenryo, Face Milling of Inconel 718 With Cemented Carbides Tools, Int. Jr. of the Japan Society for Precision Engineering, Vol. 29, N1, 1995, pp. 48-49.
201. Schreiber Rita R., Cut a Path to Productivity, Manufacturing Engineering, Feb.1992, pp. 29-32.
202. Coll B.F. and Sathrum P., Optimisation of Arc Evaporated (Ti,Al)N Film Composition for Cutting Tool Applications, Surface and Coatings Technology, Vol. 52, 1992, pp. 57-64.
203. Konig W., Cronjager L., Spur G., Tonshoff H. K., Hannover U., Vigneau M., Zdeplick W. J., Machining of New Materials, Annals of the CIRP, Vol. 39, N 2, 1990, pp. 673-681
204. Novak J. W., Shin Y.C. and Incropera F.P., Assessment of Plasma Enhanced Machining for Improved Machinability of Inconel 718, Journal of Manufacturing Science and Engineering, Vol. 119, Feb. 1997, pp. 125-129.
205. Komanduri R., Flom D.G., Lee M., Highlights of DARPA, Advanced Machining Research Program, Journal of Engineering for Industry, Nov. 1985, Vol. 107, pp. 325-335.
206. Wang Z., Machining of Aerospace Superalloys With Coated Carbides and Self-Propelled Rotary Tools, Phd Thesis, South Bank University, London, 1997.
207. Bhattacharyya S.K., Pashby I. R., Ezugwu E. O. and Khamsehzadeh H., Machining of Inco 718 and Inco 910 Superalloys With Sic Whisker Reinforced AL2O3 Composite Ceramic Tools, Proc. of 6th Int. Con. on Prodution Engineering, Nov. 1987, Osaka, Japan. pp. 43-47.
208. Vigneau J., Boulanger J.J., Behaviour of Ceramic Tools During the Machining of Nickel Base Alloys, Annals of the CIRP, Vol. 31/1, 1982, pp. 35-39.
209. Blazinski Marek, Fortin C., Mondalski K., Slomski J., Study of the Influence of Feed Variation on Tool Wear, In: "Fundamental Issues in Machining" Klamecki B. E. and Weinmann K. J (Edt.), ASME, Production Engineering Division, PED. Vol. 43, 1990, pp. 115-122.
210. Blazinski M., Songmene V., Improvement of Tool Life Through Variable Feed Milling of Inconel 600, Annals of the CIRP, Vol. 44/1, 1995, pp. 55-58.
211. Field Michael, Kahles John F., Cammet J.T., A Review of Measuring Method for Surface Integrity, CIRP, Vol. 21/2, 1972, pp. 219-238.

212. Tonshoff H.K., Bringsmier E., Determination of the Mechanical and Thermal Influences on Machined Surfaces By Microhardness and Residual Stress Analysis, Annals of the CIRP, Vol 29, No 2, 1980, pp. 519-530.
213. Huang Q. and Ren J. X., Surface Integrity and Its Effect on the Fatigue Life of the Nickel-Base Superalloy GH33A, Int. Journal of Fatigue, Vol. 13, Pt. 4, 1991, pp. 322-326.
214. Gatto L.R., Dilullo T.D., Metallographic Techniques for Determining Surface Alterations in Machining, SME Technical Paper, IQ71-225, 1971, pp. 1-25.
215. Field M., Koster W.P., Surface Integrity in Conventional Machining-Chip Removal Processes, SME Technical Paper, EM68-516, 1968, pp. 1-36.
216. Morral F.R., (Ed.) Wrought Superalloys, In: Donachie Jr. Matthew J (Ed.)., Superalloys Source Book, American Society for Metal (ASM), 1984.
217. Smith William F., Foundation of Materials Science and Engineering, Mcgraw-Hill Inc., 1993.
218. Kennametal Milling Catalog, Pub. No: 301.00 GB, 1995.
219. Ham Inyong, Computerised Machinability Study for Inconel 718, In: "Influence of Metallurgy on Machinability", Tipnis Vijay A., (Edt), American Society for Metals (ASM), 1975.
220. Tipnis Vijay A., (Edt), Influence of Metallurgy on Machinability, American Society for Metals (ASM), 1975.
221. Inco Alloy UK Limited, Private Communication.
222. Anon, Product Handbook, Inco Alloys Int., Pub. No: IAI-19/4M, 1994.
223. Bradley Elihu F. Editor, Source Book on Materials for Elevated-Temperature App. Lication, American Society for Metals, 1979.
224. Shaw M. C. and Ramaraj T. C., Brittle Fracture of Cutting Tools, Annals of the CIRP, Vol. 38, N 1, 1989, pp. 59-63.
225. Barrow G., Ghani A.K. and Ma Y.S., The Role of Workpiece Material in Brittle Tool Failure During Interrupted Cutting, Proc. of 6. Int. Manufacturing Conference With China, 10-12 March 1993, Hong Kong, Vol. 2, pp. 45-54.
226. Bhattacharyya S. K., Ezugwu E. O., Jawaid A., The Performance of Ceramic Tool Materials for the Machining of Cast Iron, Wear, Vol. 135, 1989, pp. 147-159.
227. Konig W., Fritsch R., Kammermeier D., New App. Roaches to Characterising the Performance of Coated Cutting Tools, Annals of the CIRP, Vol. 41, N1, 1992, pp. 49-54.
228. Jawaid A., Koksal S. and Sharif S., "Wear Behavior of PVD and CVD-Coated Carbide Tools When Face Milling Inconel 718", Tribology Transactions, Vol. 43, No 2, 2000, pp. 325 331.
229. Ber A, Kaldor S., The First Seconds of Cutting Wear Behaviour, Annals of the CIRP, Vol. 31, N 1, 1982, pp. 13-17.
230. Lo Casto S., Passannanti G., On the Influence of the Radius Between Face and Flank on the Tool Life of Sintered Carbides, Annals of the CIRP, Vol. 34, N 1, 1985, pp. 83-85.
231. Sikdar C., Paul S., Chattopadhyay A. B., Effect of Variation in Edge Geometry on Wear and Life of Coated Carbide Face Milling Inserts, Wear, Vol. 157, 1992, pp. 111-126.
232. Paul S., Sikdar C., Venkatesh V.C., Chattopadhyay A.B., Geometrical Modification of Coated Carbide Inserts for Improved Performance in High Production Face Milling, Int. J. Machine Tools & Manufacture, Vol. 34, N2, 1994, pp. 169-182.
233. Porat R. and Cassuto Y., A Comparison Between CVD and PVD Coated Cemented Carbide Cutting Tools, Journal of Physics C, Vol. 22, Part C5, 1989, pp. 803-810.

234. Quinto D.T., Santhanam A.T., Jindal P.C., Mechanical Properties, Structure and Perfromance of Chemically Vapor-Deposited and Physically Vapor-Diposited Coated Carbide Tools, Material Science and Engineering, A 105/106, 1988, pp. 443-452.
235. Karl Hertel Ltd., Machining of Aerospace Materials, (Perfromance of a Fine Grain Size Carbide), Aircraft Engineering, May 1986, pp. 6-7.
236. Sims C. T. and Hagel W. C., (Edt.), The Superalloys, John Wiley & Sons Inc., USA, 1972.
237. Komanduri R., Schroeder T.A., On Shear Instability in Machining a Nickel-Iron Base Superalloy, Journal of Engineering for Industry, May 1986, Vol. 108, pp. 93-100.
238. Xie J.Q., Bayoumi A.E. and Zbib H.M., A Study on Shear Banding in Chip Formation of Orthogonal Machining, Int. Journal of Machine Tools and Manufacture, Vol. 36, N 7, 1996, pp. 835-847.
239. Ai X. and Li Z. Characteristics of Ceramic Tool Fracture, Key Engineering Materials, Vol. 96, 1994, pp. 165-196.
240. William D. Callister, Material Science and Engineering, John Wiley & Sons Inc. USA. 1997.
241. Metals Handbook, 9.Ed., Vol 3, Superalloys, pp. 219-221, ASM Int. Metals Park OH, 1980.

APPENDIX I: PUBLICATIONS

1. A. Jawaid and S. Koksal, "Face milling of Inconel 718 with PVD and CVD coated carbide tools", Proceeding of the 8th Int. Manufacturing Conf. (IMCC'98), Singapore 12-14 May 1998.

2. A. Jawaid, S. Sharif and S. Koksal, "Study Of Cutter Location In Face Milling Of Aerospace Materials", Int. Conf. on 'Advances in materials and processing technologies, AMPT'98, Kuala Lumpur, Malaysia, 24-28 August 1998.

3. A. Jawaid, S. Koksal and S. Sharif, "Wear Behaviour Of PVD And CVD Coated Carbide Tools When Face Milling Inconel 718", Society of Tribologists and Lubrication Engineers 54th Annual meeting, Las Vegas, USA, 23-27 May 1999.

4. A. Jawaid, S. Koksal and S. Sharif, "Wear Behaviour Of PVD And CVD Coated Carbide Tools When Face Milling Inconel 718", Society of Tribologists and Lubrication Engineers, Tribology Transactions, Vol. 43, No 2,, April 2000, pp 325 331.

5. A. Jawaid, S. Koksal And S. Sharif, "Cutting Performance And Wear Characteristics Of PVD Coated And Uncoated Carbide Tools In Face Milling Inconel 718 Aerospace Material''. International Conference on Advanced Manufacturing Technology (ICAMT-2000), 16 – 17 August 2000, Universiti Teknologi Malaysia (UTM), Malaysia.

APPENDIX II: TABLES

Table 3. 1 Some of the important properties of tool and coating materials [79, 85, 99, 120, 121, 122]

Coating materials ⇒ Properties⇓	**TiN**	**TiC**	**TaC**	**Al_2O_3**	**WC**	**WC-Co** 94-6%
Hardness HV	2100	3200	1800	2100	2100	1800
Hot hardness at 1000 °C	400	250	600	900	200	
Thermal conductivity. W/m.K, (100 /1000 °C)	21-26	33-41		28-6	120	38-80
Thermal exp. coef. 10^{-6}/K	9.4	8.4	6.3	7.5	3.9	5-6
Melting point	2950	3100	3800	2050	2776	
Modulus of elasticity GPa	590	470	285	420	696	648
Free energy kcal/g at 1000 °C	-55	-40		-98	-5	
Fracture toughness. K_{ic} MPa $m^{1/2}$				4	16	

Table 3. 2 ISO classification of carbide cutting tools [86]

ISO Carbide Tool Classification Table (summarized)					
Symbol	Color code	Broad categories of materials to be machined	Designation	Change in characteristics of cut	of tool
P	Blue	Ferrous metals with long chip	P01	Increasing speed ---->> <<------ Increasing feed	Increasing wear resistance ---->> <<------ Increasing toughness
			P10		
			P20		
			P30		
			P40		
			P50		
M	Yellow	Ferrous and non-ferrous metals with long or short chips	M10		
			M20		
			M30		
			M40		
K	Red	Ferrous metals with short chips, non-ferrous metals and non-metallic materials	K01		
			K10		
			K20		
			K30		
			K40		

Table 3. 3 Salient physical and mechanical properties of ultrahard tool materials and their comparison with carbides and ceramics [74, 79, 118].

Tool Materials ⇒ Properties ⇓	Al_2O_3-based ceramics	Tungsten carbide, K10	Cermets finish grd.	Single-crystal diamond	PCD	PCBN
Density g/cm^3	3.2-4.3	14.7	8.1	3.52	3.43	3.1
Comp. strength GPa	1.8	4.5	4.4	8.68	4.74	3.8
Fracture toughness MPa m$^{1/2}$	1.9-8.0	10.8	8.5	3.4	6.89	10
Hardness HV at 20°C	1500-2450	800-2400	1700	8000-12000	6500-10000	3500-4000
Young's Modulus GPa	300-420	620	500	1141	925	680
Thermal exp. coef. x10^{-6}/K	3.2-8.5	5.4	7.9	1.5-4.8	3.8	4.9
Thermal conduc. W/mK	8-23	80-120	10	500-2000	120	100

Table 5. 1 The nominal chemical composition of Inconel 718 and Waspaloy with the effects of alloying elements in the microstructure [216].

Comp. w%	**Inconel 718**	**Waspaloy**	**The main functions of the alloying elements**
Cr	19	19.5	solid solution strengtheners, oxidation and sulfidation resistance, $M_{23}C_6$ type carbide former
Ni	52.5	57	FCC matrix stabiliser, γ' and γ'' phase former
Fe	18.5	2 max.	solid solution strengtheners
Mo	3	4.3	solid solution strengtheners, $M_{23}C_6$, M_6C and MC type carbide former
Nb	5.1	-	principle γ'' phase former (Ni_3Nb) MC type carbide former,
Ti	0.9	3	γ' phase former, MC type carbide former,
Al	0.5	1.3	γ' phase former, oxidation resistance
C	0.08 max.	0.08	matrix carbides and carbonitride former, causes grain boundary segregation
S	0.015 max.	-	If present at high percentages, reduces workability and damages properties
B	0.006 max.	0.006	Improves creep-rupture properties by grain boundary morphology changes
Zr	-	0.09	Improves creep-rupture properties by grain boundary morphology changes

Table 6. 1 The cutting parameters

Cutting speed m/min		Feed rate mm/tooth	Depth of cut mm	
Coated tools	Uncoated tool		Axial	Radial
100	50	0.08 and 0.14	1	40
75	40			
50	32			
25	25			

Table 6. 2 Chemical composition of Inconel 718 [222].

Inconel 718 Composition w %										
Ni	Cr	Al	Mn	C	Mo	Ti	Si	Cu	Nb	Fe
53.3	19	0.56	0.1	0.03	3.03	0.94	0.1	0.04	4.98	18.5

Table 6. 3 Nominal chemical composition of Waspaloy [223].

Composition of Waspaloy (w %)										
Ni	Cr	Al	Mn	C	Mo	Ti	Si	Zr	B	Co
57	19.5	1.3	0.5	0.08	4.3	3	0.3	0.06	0.006	13.5

Table 6. 4 Physical and mechanical properties of Inconel 718 and Waspaloy [156, 222, 223]

Properties	**Inconel 718**	**Waspaloy**
Hardness HV	486	454
Tensile strength MPa (at 20 and 870 °C)	1430 / 340	1280 / 525
Yield strength MPa (at 20 and 870 °C)	1190 / 330	795 / 515
Modulus of elasticity GPa (at 20 and 870 °C)	200 / 139	211 / 157
Elongation % (at 20 and 870 °C)	15 / 88	20 / 35
Reduction of area % 20°C	24	24
Density g/cm^3	8.19	8.19
Coefficient of thermal expansion (10^{-6}/°C) (at 21 and 760 ▪C)	13 14.4	12.1 18.5
Thermal conductivity W/m °C (at 20 and 760 ▪C)	11.4 23.2	

Table 6. 5 Physical properties of the substrates of the tools

Properties of the substrates of the inserts			
Grades	**KC720 and KC994M**	**KC730**	**KMF**
Composition	86 % WC 11.5% Co 2.5 % Ta(Nb)C	93.5 % WC 6.0 % Co 0.5 % Cr_3C_2	90.1 % WC 9.5 % Co 0.4 % VC
Grain size (micron)	1-6	1-3 (aver. 1)	0.8
Hardness at 25°C (HV)	1460	1830	1550
Hot hardness at 800°C	580	760	-
Porosity	A06	A04	<A02
Thermal conduc. (W/mK)	67.4	78.8	85
Thermal expansion coef. (10^{-6}/K)	5.26	5.31	5.5
Compressive strength (GPa)	4.84	6.71	4
Impact strength (Joule)	7.8	11.4	0.3
Fracture toughness (MPa.$m^{1/2}$)	12.6	8.7	15
Transverse rupture strength (GPa) (Modulus of rupture)	2.61	2.77	3.6

Table 6. 6 Physical properties of the coatings

Properties of the coatings		
Coating	PVD / TiN	CVD / TiNC- Al_2O_3
Thickness (micron)	2-3.5	2 / 1.5
Hardness (HV)	2200	2300/2000
Hot hardness	800	600/900
Adhesion strength	45 kg, indent	60 N, scratch
Residual stress (GPa)	- 3.5	0.5
Thermal conductivity (W/mK)	25	31 / 7.5
Thermal exp. coef. (10^{-6}/K)	9.35	8.65 / 8.1
Eta-phase	none	< 2 micron

Table 7. 1 Tool life and tool failure modes when face milling Inconel 718 with KC994M tools

Insert: KC994M, Workpiece: Inconel 718				
Cutting speed m/min.	Feed : 0.08 mm/tooth		Feed : 0.14 mm/tooth	
	Tool life min.	Failure modes	Tool life min.	Failure modes
100	0.5	ANW/ Ch/Gl/Pt/Pd	0.3	ANW/ Ch/Gl
75	1.5	ANW/ Ch/Fl/Cf	1	ANW/ Ch/Gl/Fl
50	13	ANW/ Ch/Gl/Pd/Pt	5	ANW/ Ch/Gl
25	54	ANW/ Gl/Pt/Ch	22	ANW/ Gl/Pt/Ch
Abbreviations used in the tables presented herein				
ANW: Average nose wear, AFW: Average flank wear, Gl: Workpiece galling or adhesion, Ch: Chipping, Fl: Flaking, Pt: Pitting/Plucking Cf: Catastrophic failure, Pd: Plastic deformation, Br: Breakage, Ab: Abrasion				

Table 7. 2 Tool life and tool failure modes when face milling Inconel 718 with KC720 tools

Insert: KC720, Workpiece: Inconel 718				
Cutting speed m/min.	Feed : 0.08 mm/tooth		Feed : 0.14 mm/tooth	
	Tool life min.	Failure modes	Tool life min.	Failure modes
100	0.1	ANW/ Ch/Gl/Pd	0.1	ANW/ Ch/Fl/Gl/Pd
75	0.5	ANW/ Br/Cf	0.3	ANW/ Ch/Gl/Pd
50	7	ANW/ Cp/Gl/Fl/Pd	3	ANW/ Ch/Gl/Pd
25	13	AFW/ Gl/Ch/Pd	14	AFW/ Ch/Gl/Pd

Table 7. 3 Tool life and tool failure modes when face milling Inconel 718 with KC730 tools

Insert: KC730, Workpiece: Inconel 718				
Cutting speed m/min.	Feed : 0.08 mm/tooth		Feed : 0.14 mm/tooth	
	Tool life min.	Failure modes	Tool life min.	Failure modes
100	0.7	AFW/ Ch/Gl/Pd/Fl	0.4	AFW/ Cf
75	2.3	MFW/ Ch/Fl/Gl	0.5	AFW/ Ch/Fl/Gl
50	10	ANW/ Cp/Gl/Fl/Pd	4	AFW/ Ch/Gl/Pd
25	23	AFW/ Gl/Pt/Ch	14	AFW/ Gl/Ch/Pt

Table 7. 4 Tool life and tool failure modes when face milling Inconel 718 with KMF tools

Insert: KMF, Workpiece: Inconel 718				
Cutting speed m/min.	Feed : 0.08 mm/tooth		Feed : 0.14 mm/tooth	
	Tool life min.	Failure modes	Tool life min.	Failure modes
50	3	AFW/ Gl/Ch/Pt/Pd	2.6	ANW/ Ch/Gl/Pd
40	6	AFW/ Gl/Ch/Pd	7.5	AFW/ Gl/Ch/Pt/Pd
32	25	ANW/ Gl/Ch/Pd	18	ANW/ Gl/Ch/Pt/Ab
25	32	ANW/ Gl/Pt/Ch	22	ANW/ Gl/Pt/Ch/Ab

Table 7. 5 Tool life and tool failure modes when face milling Waspaloy with KC994M tools

Insert: KC994M, Workpiece: Waspaloy				
Cutting speed m/min.	Feed : 0.08 mm/tooth		Feed : 0.14 mm/tooth	
	Tool life min.	Failure modes	Tool life min.	Failure modes
100	0.1	ANW/ Gl/Ch/Pd	0.06	ANW/ Ch/Gl/Pd
75	0.3	ANW/ Gl/Ch/Pd	0.1	ANW/ Ch/Gl/Pd
50	1	ANW/ Gl/Ch/Pd	0.5	ANW/ Ch/Gl/Pd
25	18	ANW/ Gl/Ch/Pt/Pd	9	ANW/ Ch/Gl/Pt/Pd

Table 7. 6 Tool life and tool failure modes when face milling Waspaloy with KC720 tools

Insert: KC720, Workpiece: Waspaloy				
Cutting speed m/min.	Feed : 0.08 mm/tooth		Feed : 0.14 mm/tooth	
	Tool life min.	Failure modes	Tool life min.	Failure modes
100	0.1	ANW/ Ch/Gl/Pd	0.05	ANW/ Ch/Gl
75	0.2	ANW/ Ch/Gl/Pd	0.08	ANW/ Ch/Gl
50	1.2	AFW/ Ch/Gl	0.4	AFW/ Ch/Gl
25	5	AFW/ Gl/Ch/Pt	3	ANW/ Gl/Ch/Pt

Table 7. 7 Tool life and tool failure modes when face milling Waspaloy with KC730 tools

Insert: KC730, Workpiece: Waspaloy				
Cutting speed m/min.	Feed : 0.08 mm/tooth		Feed : 0.14 mm/tooth	
	Tool life min.	Failure modes	Tool life min.	Failure modes
100	0.2	AFW/ Ch/Fl/Pd	0.05	AFW/ Ch/Gl/Fl
75	0.3	AFW/ Ch/Fl/	0.08	AFW/ Ch/Gl
50	1	ANW/ Ch/Fl	0.2	AFW/ Ch/Gl/Pt
25	10	ANW/ Gl/Ch/Pt	1.8	AFW/ Ch/Gl/Pt

Table 7. 8 Tool life and tool failure modes when face milling Waspaloy with KMF tools

Insert: KMF, Workpiece: Waspaloy				
Cutting speed m/min.	Feed : 0.08 mm/tooth		Feed : 0.14 mm/tooth	
	Tool life min.	Failure modes	Tool life min.	Failure modes
50	3.2	AFW/ Ch/Gl/Pd	0.2	AFW/ Ch/Gl
40	5.2	AFW/ Ch/Gl/Pd	0.6	AFW/ Ch/Gl
32	8	AFW/ Ch/Gl/Pt	1.6	AFW/ Ch/Gl
25	18	AFW/ Gl/Pt/Ab	2	AFW/ Ch/Gl

Table 8. 1 Measured average width of the rake face contact zone on each cutting tool when face milling Inconel 718 and Waspaloy

Measured average width of rake face contact zone (mm)									
Feed rate mm/tooth	Cutting sp. m/min	Inconel 718				Waspaloy			
		KC994M	KC720	KC730	KMF	KC994M	KC720	KC730	KMF
0.14	25	0.22	0.28	0.29	0.31	0.31	0.34	0.33	0.29
	50	0.19	0.22	0.23	0.29	0.27	0.3	0.27	0.3
	75	0.15	0.18	0.19	NA	0.24	NA	NA	NA
0.08	25	0.17	0.19	0.22	0.23	0.19	0.24	0.22	0.21
	50	0.13	0.18	0.18	0.2	0.17	0.23	0.2	0.18
	75	0.13	0.14	0.15	NA	0.16	0.2	0.19	NA

Table 8.2 Summary of the results

SUMMARY OF THE RESULTS			
	Inserts	**Workpiece**	
		Inconel 718	**Waspaloy**
Maximum tool lives (minute) (at 25 m/min and 0.08 mm/tooth)	KC994M	54	18
	KC720	13	5
	KC730	23	10
	KMF	32	18
Maximum volume of material removed (cm^3) with the cutting condition	KC994M	65.3, at 25 m/min, 0.08 mm/tooth	21.7, at 25 m/min, 0.08 mm/tooth
	KC720	29.6, at 25 m/min, 0.14 mm/tooth	6.3, at 25 m/min, 0.14 mm/tooth
	KC730	29.6, at 25 m/min, 0.14 mm/tooth	12, at 25 m/min, 0.08 mm/tooth
	KMF	46.5, at 25 m/min, 0.14 mm/tooth	21.7, at 25 m/min, 0.08 mm/tooth
Increase in subsurface micro hardness (at 20 µm depth and where tool life is maximum)	KC994M	18 %	28 %
	KC720	9.7 %	21.7 %
	KC730	8.7 %	19.5 %
	KMF	3.5 %	13 %
Average surface roughness (at condition where tool life is maximum)		0.44 to 0.65 µm	0.54 to 0.67 µm
Initial tool wear modes (after cutting for 5 seconds	KC994M	a) Premature delamination of Al2O3 and TiCN layers, b) Plucked/pitted rake face due to workpiece adhesion, c) Workpiece galling and seizure	
	KC720 and KC730	a) Premature delamination of TiN layer on the rake, b) Workpiece galling and seizure, c) Micro chipping	
	KMF	a) Rake face pitting/plucking associated with workpiece adhesion, b) Workpiece galling and seizure	
Predominant wear modes at tool failure	50 to 100 m/min	Severe chipping, breakage	
	25 to 50 m/min	Progressive wear; combination of progressive chipping, plucking and pitting	

APPENDIX III: FIGURES

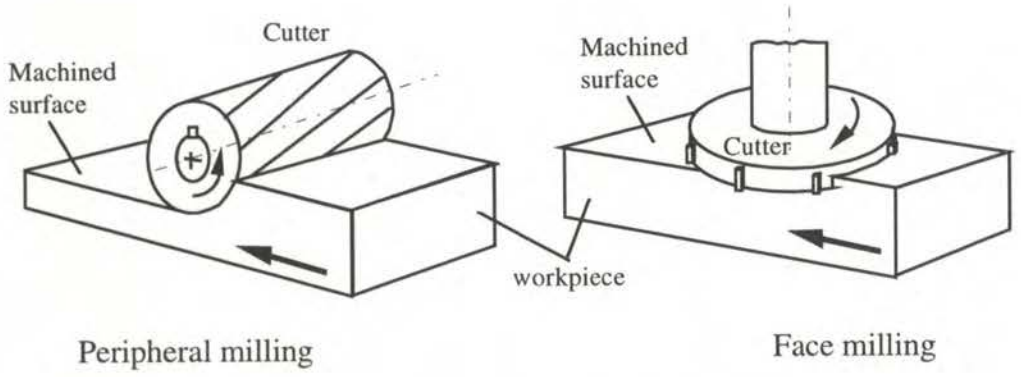

Figure 2.1 Relative motion of cutter and workpiece in peripheral and face milling.

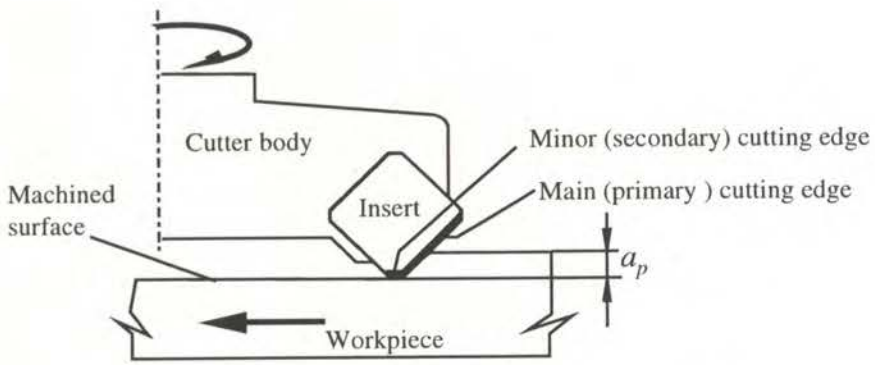

Figure 2.2 The location of primary and secondary cutting edges of a face milling cutter

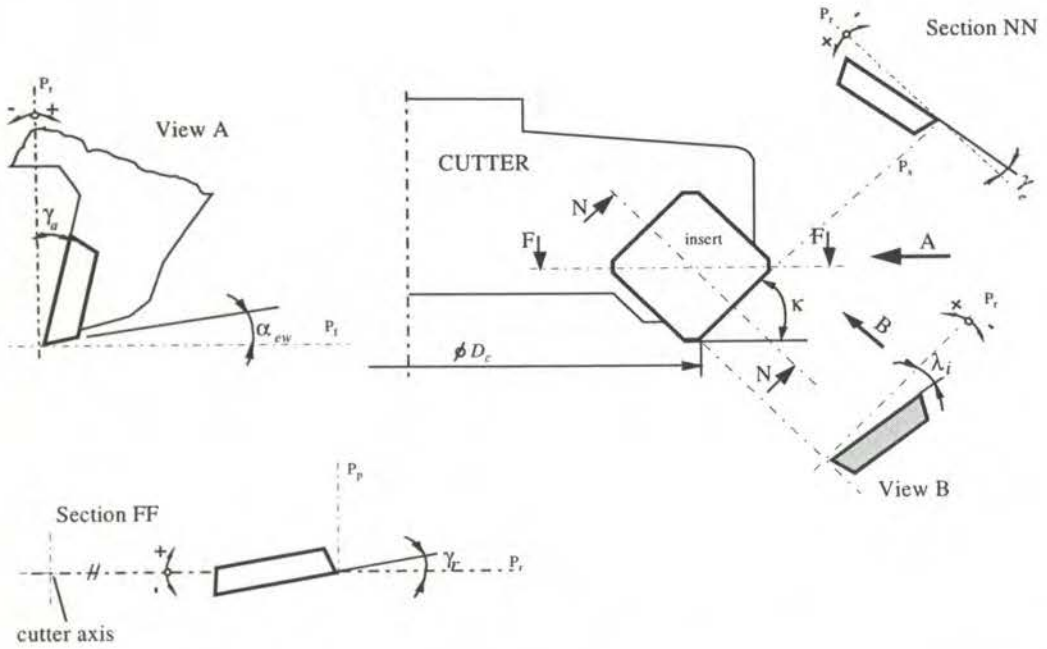

Geometric properties of the milling cutter			
Nominal cutter diameter	D_c	Inclination angle	λ_i
Number of insert	Z_i	Wiper edge clearance angle	α_{ew}
Radial rake angle	γ_r	Tool reference plane	P_r
Axial „ „	γ_a	Assumed working plane	P_f
Effective rake angle	γ_e	Tool back plane	P_p
Approach angle	κ	Tool cutting edge plane	P_s

Figure 2.3 Geometric properties of a face milling cutter

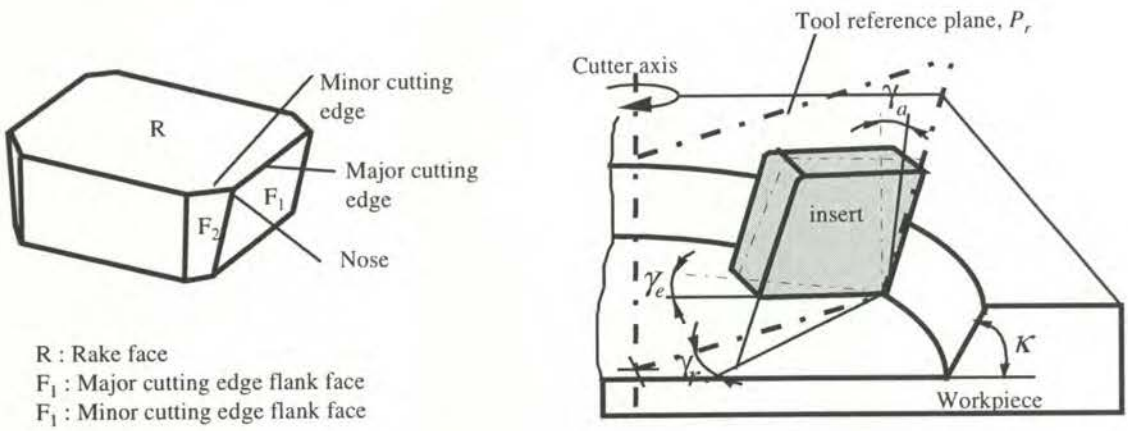

Figure 2.4 a) Important geometric features of the cutting insert, b) 3-D illustration of important operating angles of a face milling cutter. [73]

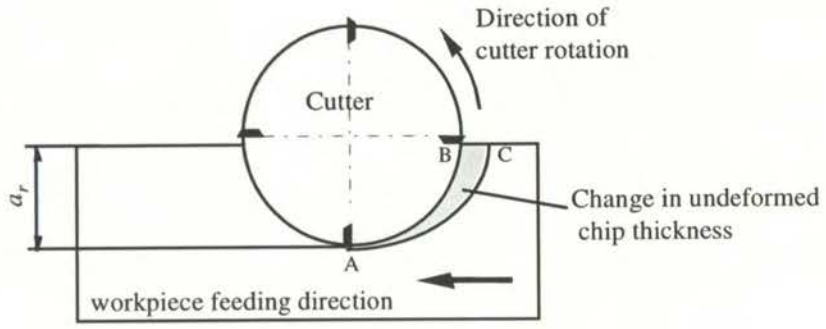

Up milling (a)

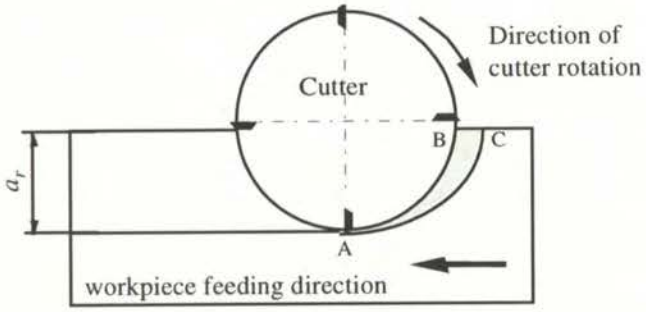

Down milling (b)

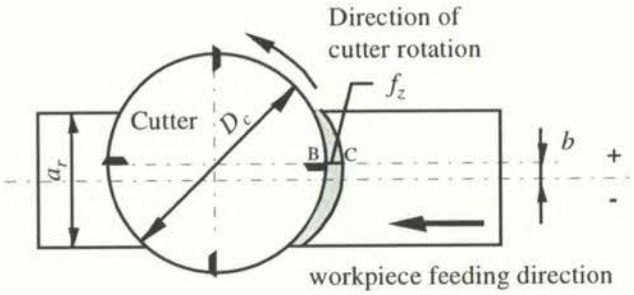

Combination of up and down milling (c)

Figure 2.5 Modes of face milling operation

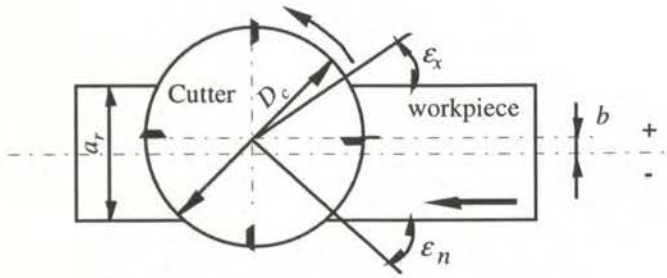

Cutter-workpiece offset, b, in face milling

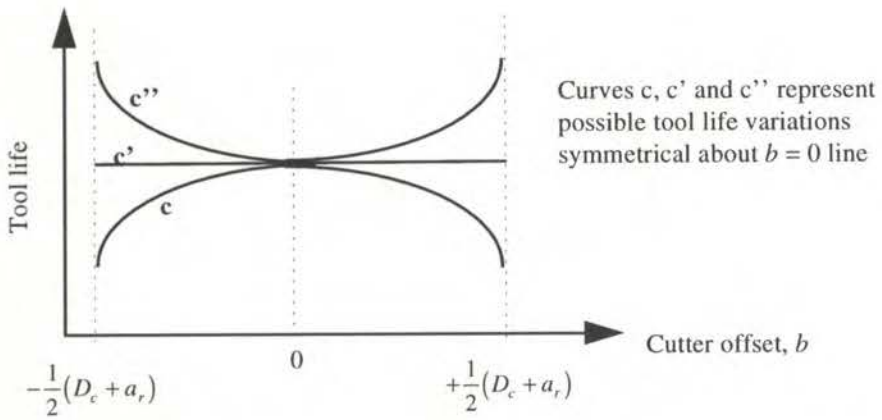

Figure 2.6 Plots of possible tool life trends versus cutter offset

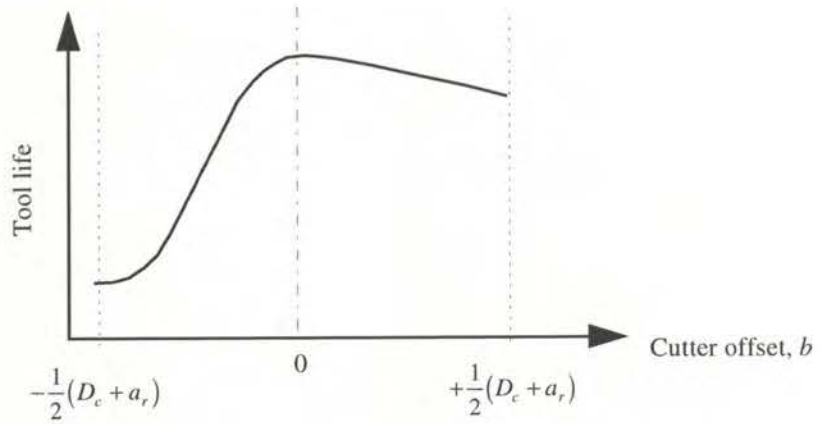

Figure 2.7 A typical plot of tool life against cutter-workpiece offset when milling hard and extremely work-hardening materials [34].

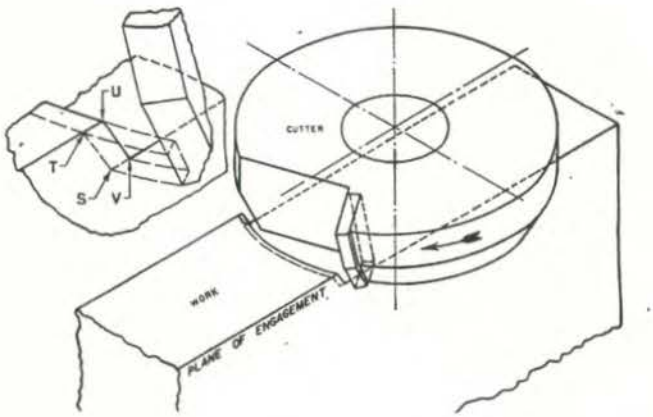

Figure 2.8 The definition of the area of initial tool contact [19]

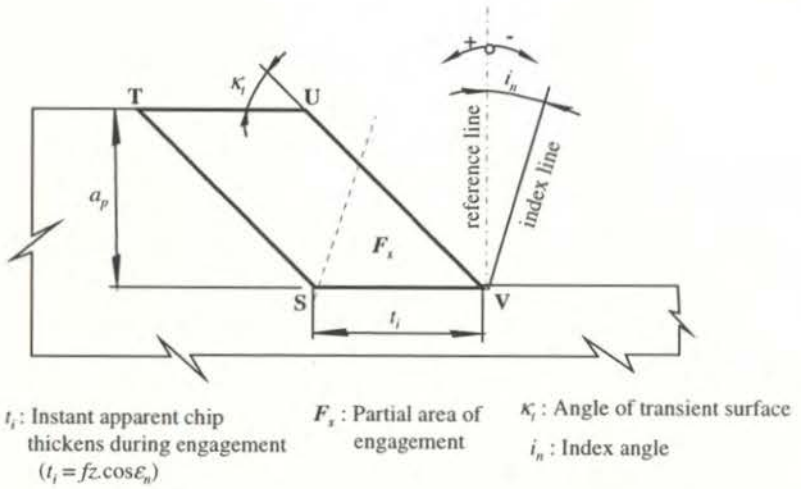

Figure 2.9 Description of the 'partial area of engagement'

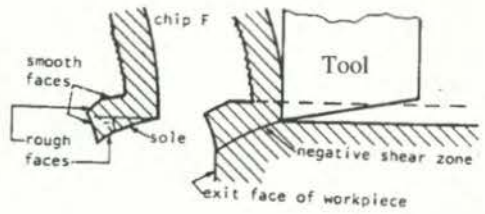

Figure 2.10 Depiction of 'negative shearing' and footed-chip formation [37]

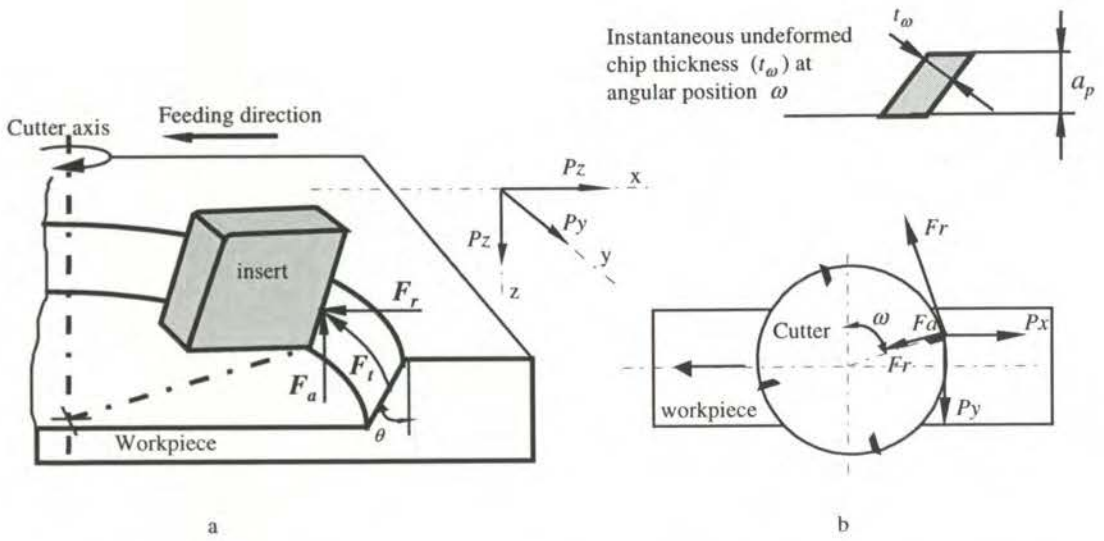

Figure 2.11 Schematic representation of the cutting force system in face milling; a) Cutter system, b) Table system

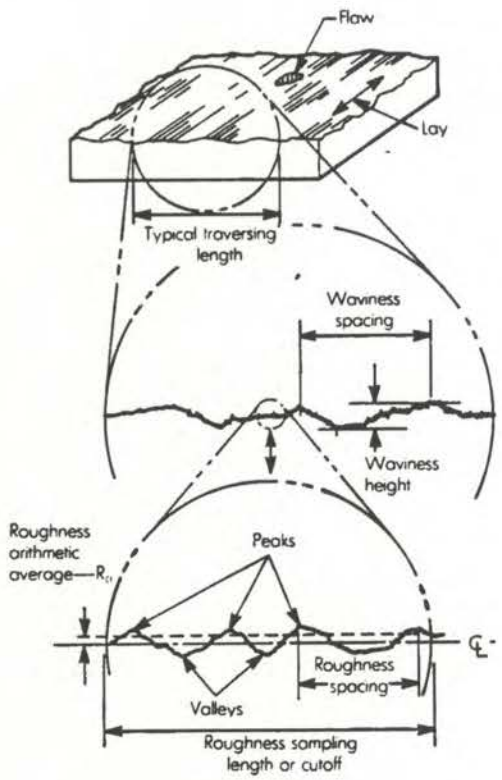

Figure 2.12 Description of the elements of surface finish [8]

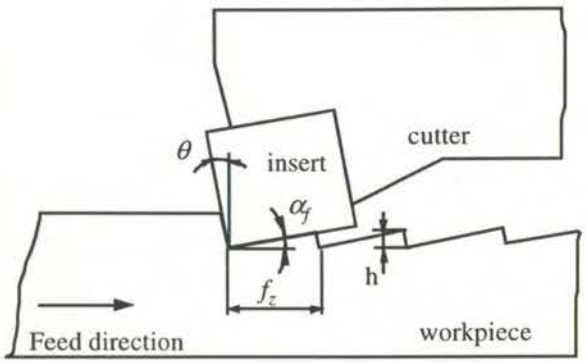

Figure 2.13 Elements used to calculate surface roughness in face milling with sharp tools [8].

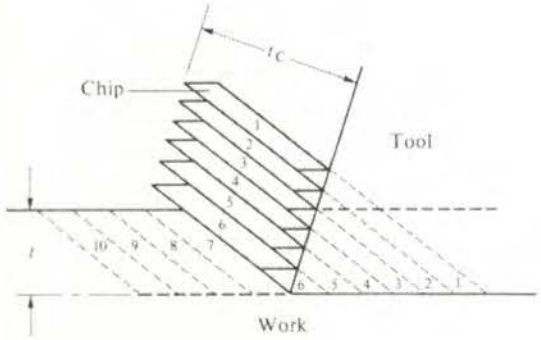

Figure 2.14 Piispanen's chip formation model [4]

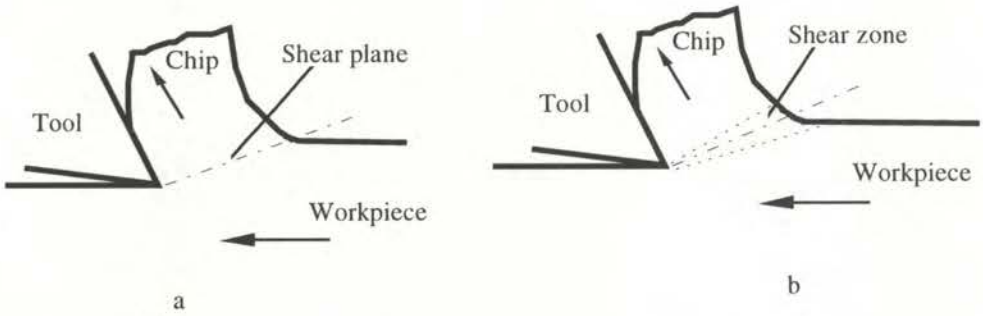

Figure 2.15 Chip formation (a) along the shear plane and (b) within a shear zone

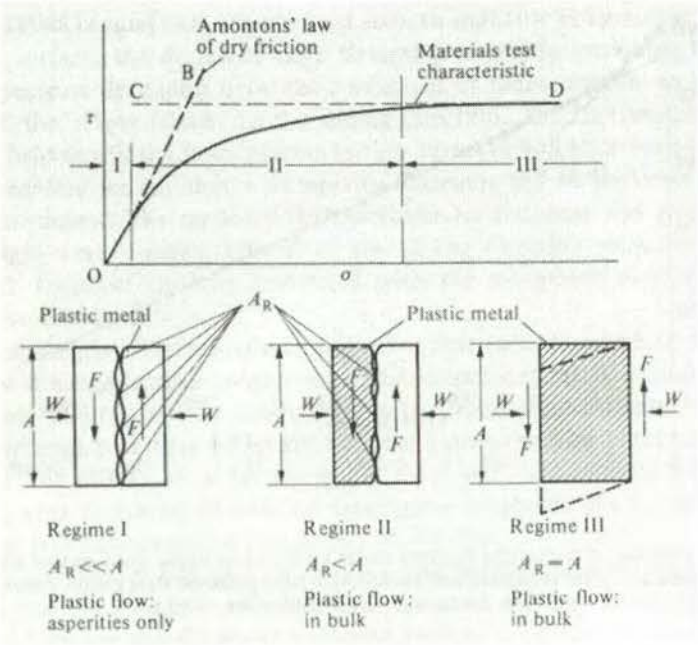

Figure 2.16 The stages of solid friction [4].

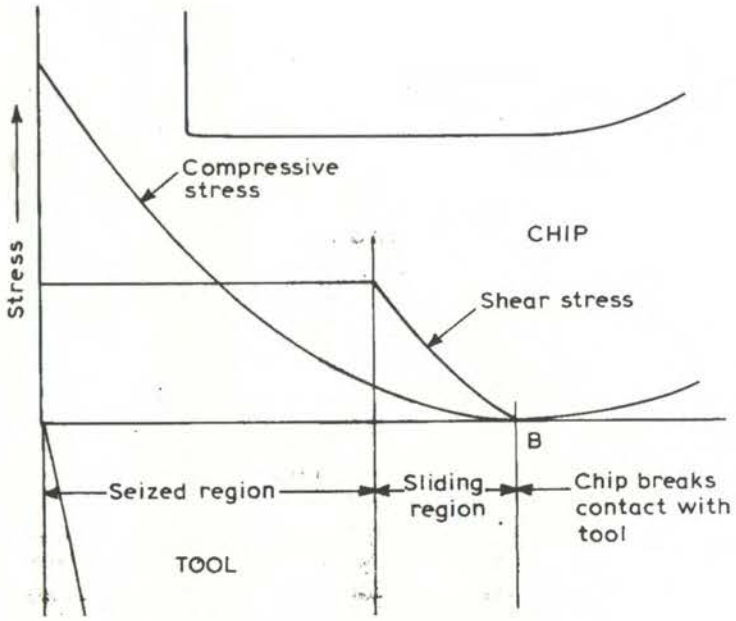

Figure 2.17 Model of stress distribution at tool-chip interface [54]

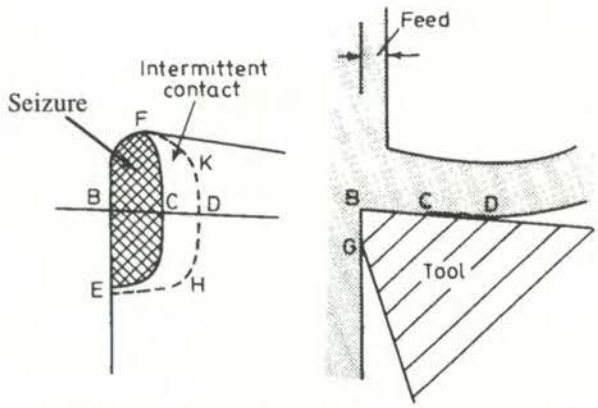

Figure 2.18 The area where seizure occurs [1]

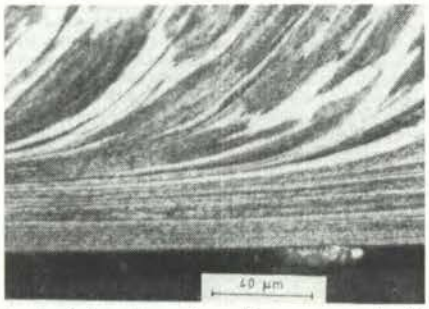

Figure 2.19 Sectioned steel chip showing flow zone indication of seizure at tool-chip interface [1]

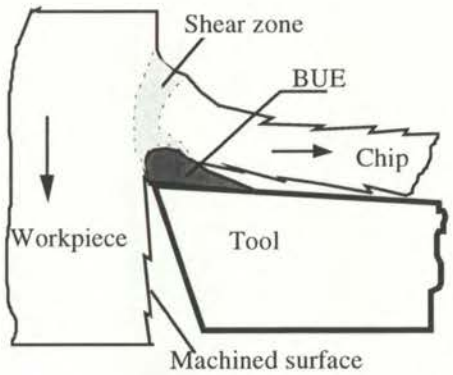

Figure 2.20 Depiction of BUE

Figure 2.21 Schematic illustration of the types of BUE [62]

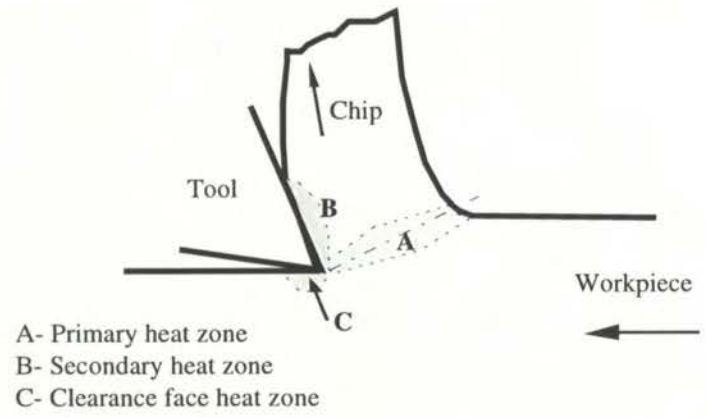

Figure 2.22 Principle regions of heat generation during cutting [48]

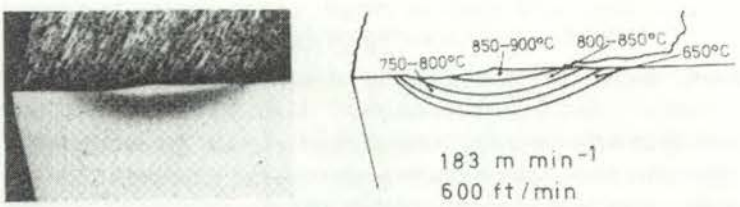

Figure 2.23 Temperature contours in a HSS tool used to cut a low carbon steel [66].

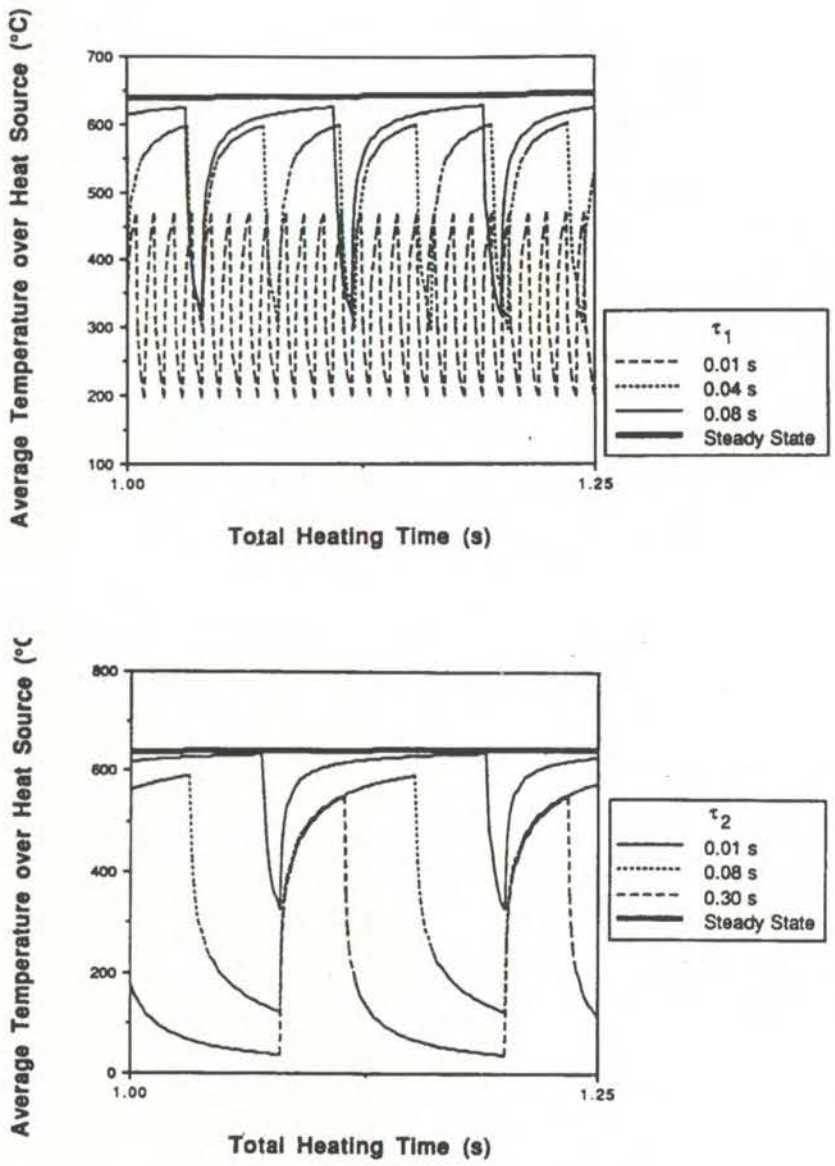

Figure 2.24 Average tool temperature variations in interrupted cutting in relation to the changes in the duration of heating cycle (τ_1) and cooling cycle (τ_2) [70].

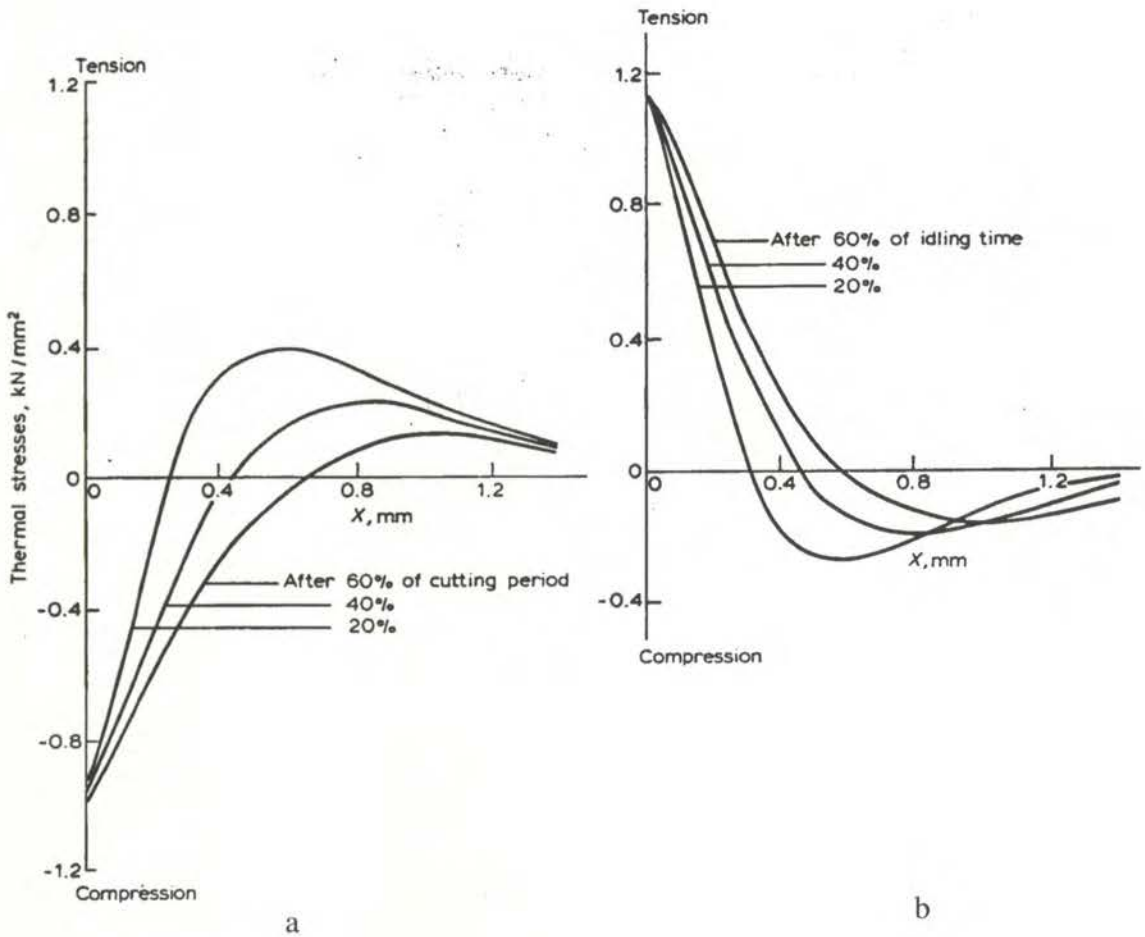

Figure 2.25 The type and variation of thermal stresses within tool body induced during cutting (a) and non-cutting (b) cycles in interrupted cutting [71].

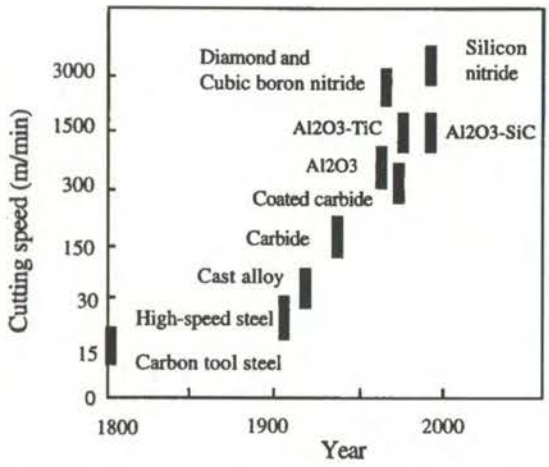

Figure 3.1 Introduction of new cutting tool materials and their relative comparison [99].

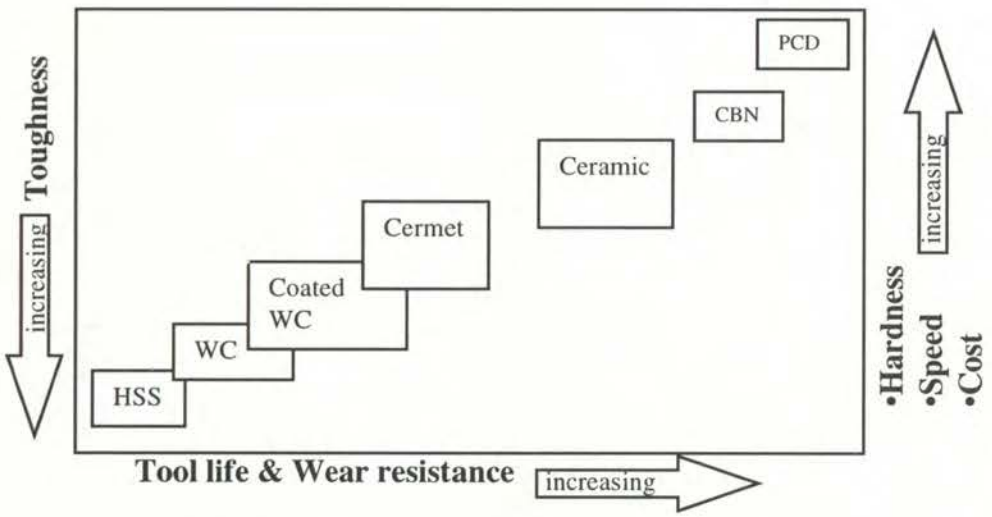

Figure 3.2 Relative comparison of some important properties of various tool materials [122].

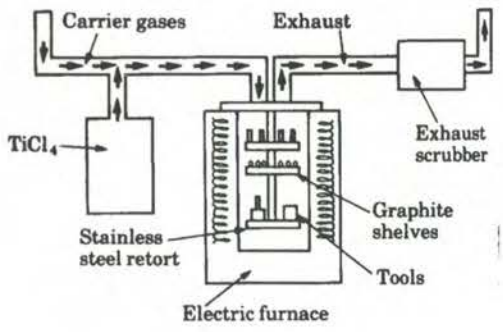

Figure 3.3 Schematic illustration of CVD coating process [47].

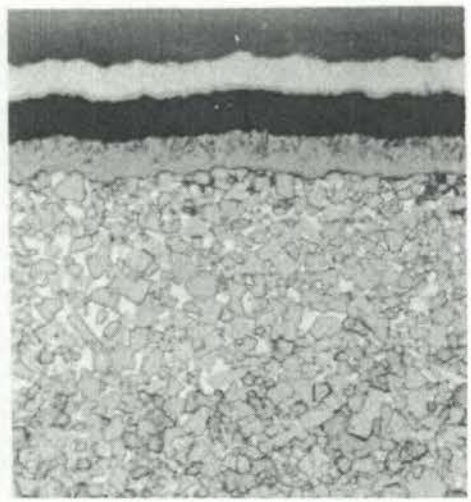

Figure 3.4 CVD-TiC/Al_2O_3/TiN multi layer coating of tungsten carbide with cobalt-enriched zone [79].

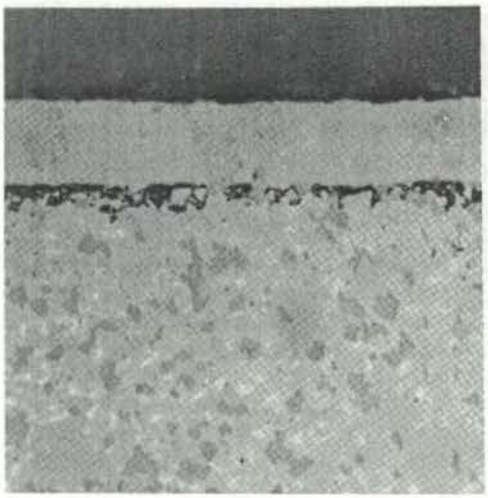

Figure 3.5 Eta-phase formed at the interface of CVD-TiC coated tungsten carbide substrate [79]

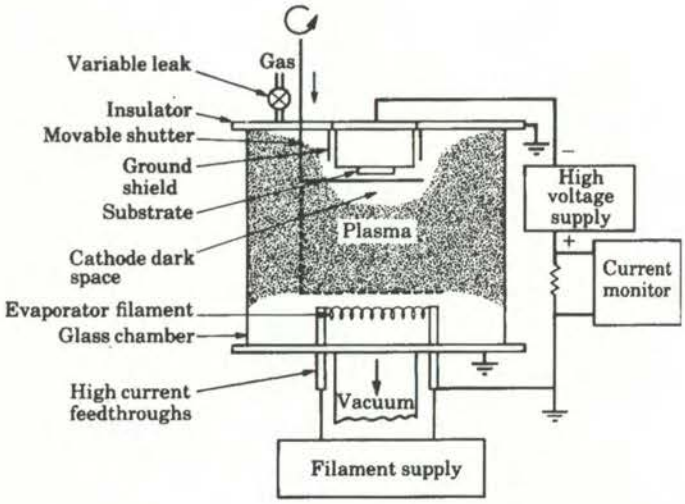

Figure 3.6 Schematic illustration of PVD ion-plating coating process [47].

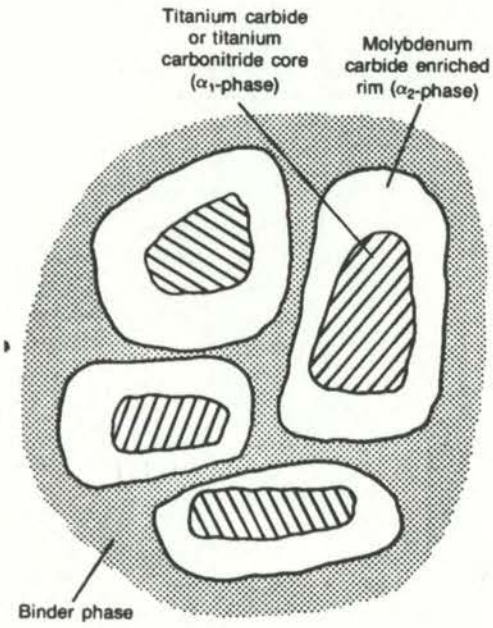

Figure 3.7 Schematic of the microstructure of a titanium carbonitride cermet tool [79].

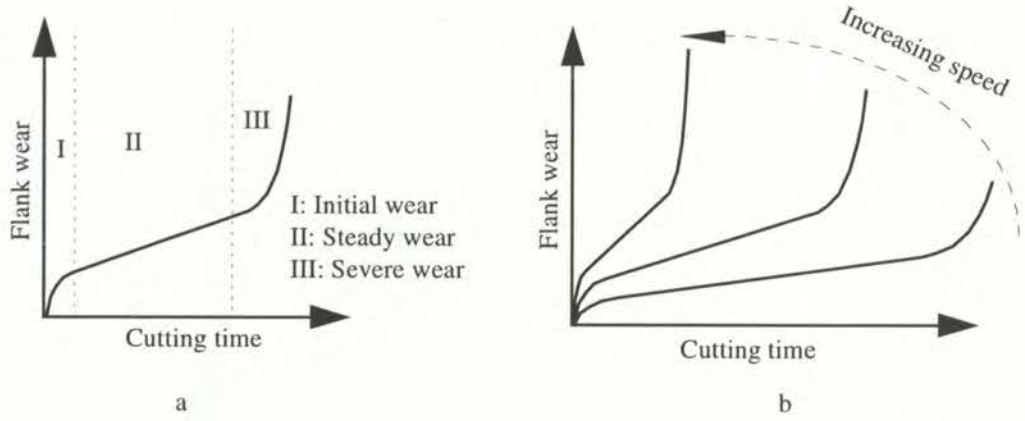

Figure 4.1 Typical development of flank wear as function of (a) cutting time and (b) cutting speed.

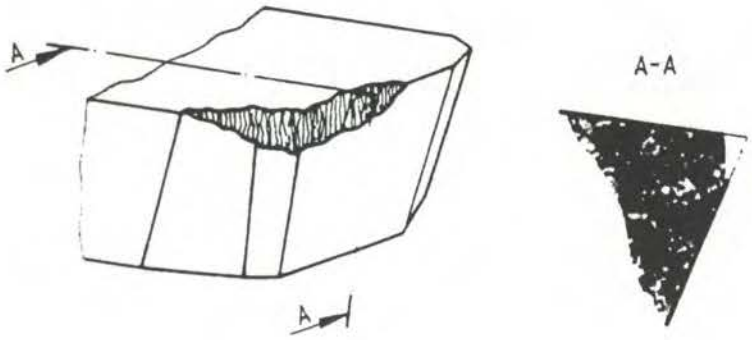

Figure 4.2 Illustration of uniform flank wear [124]

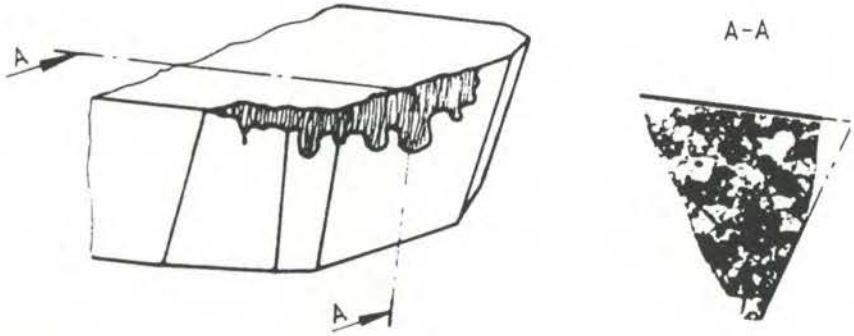

Figure 4.3 Illustration of non-uniform flank wear [124]

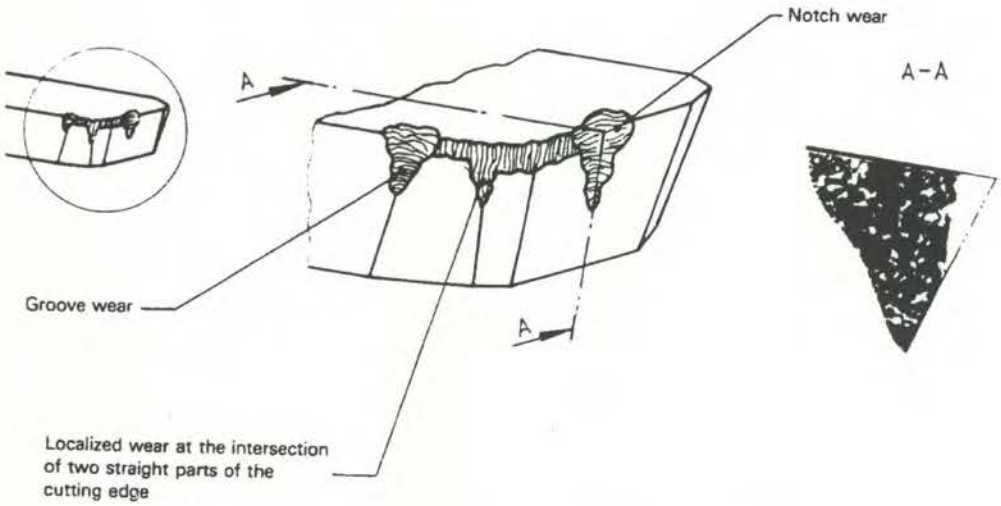

Figure 4.4 Illustration of localised flank wear [124]

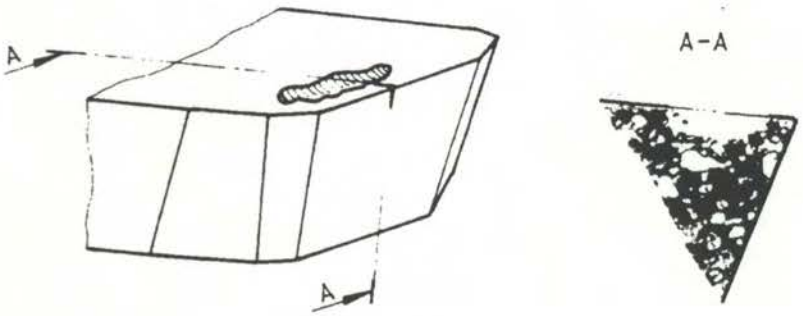

(a)

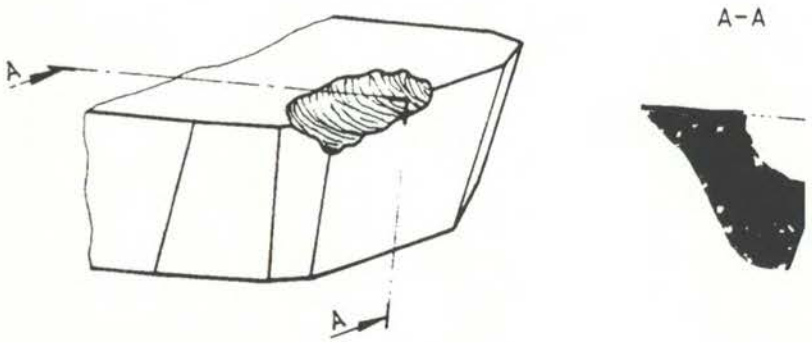

(b)

Figure 4.5 Depiction of crater wear (a) and stair-formed wear (b) on the rake face of the tool [124]

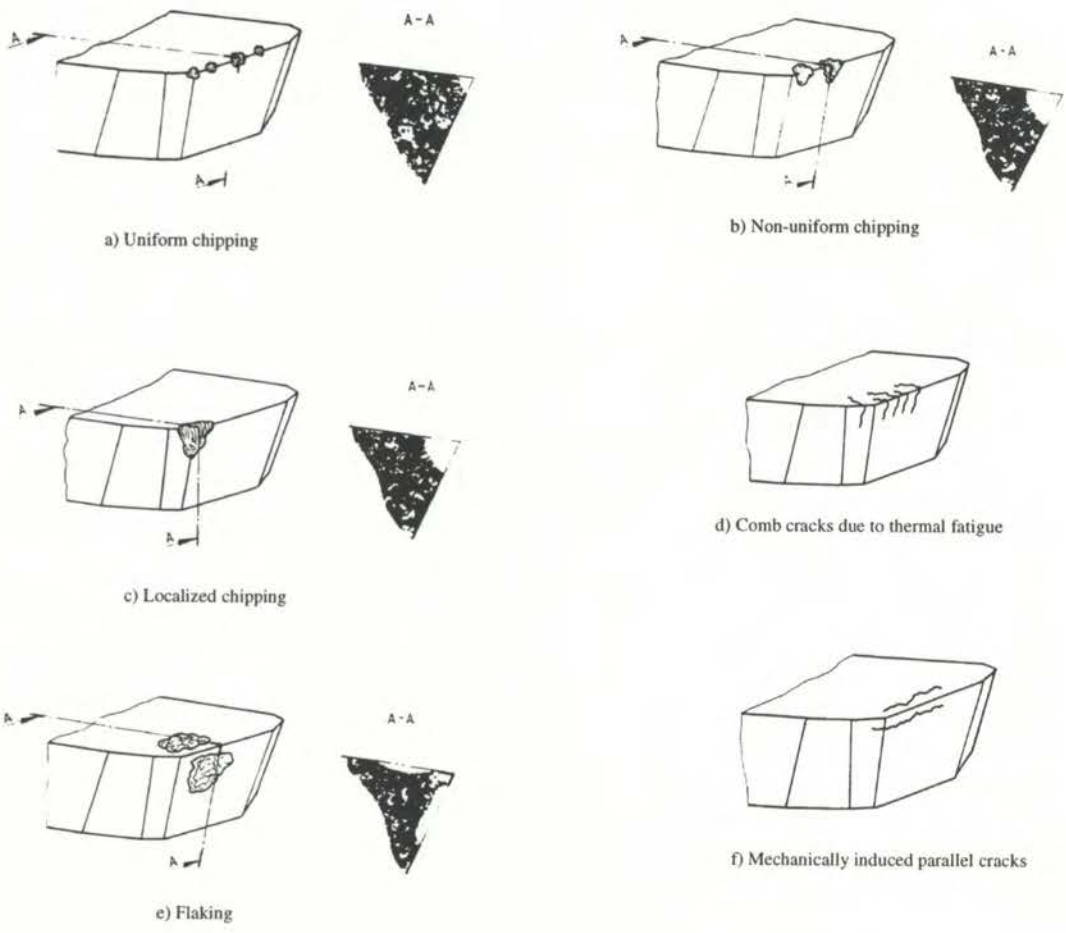

Figure 4.6 Definition of chipping, flaking and tool cracks according to ISO 8688-1 [124].

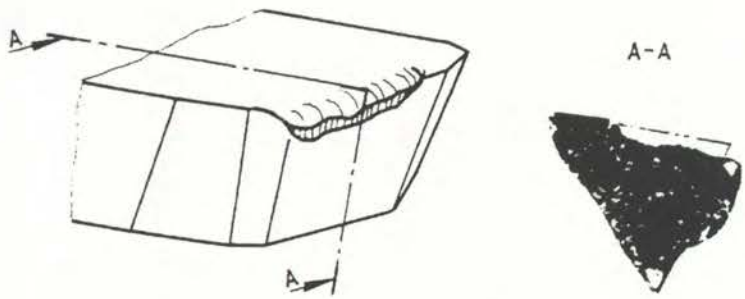

Figure 4.7 Schematic illustration of cutting edge plastic deformation [124].

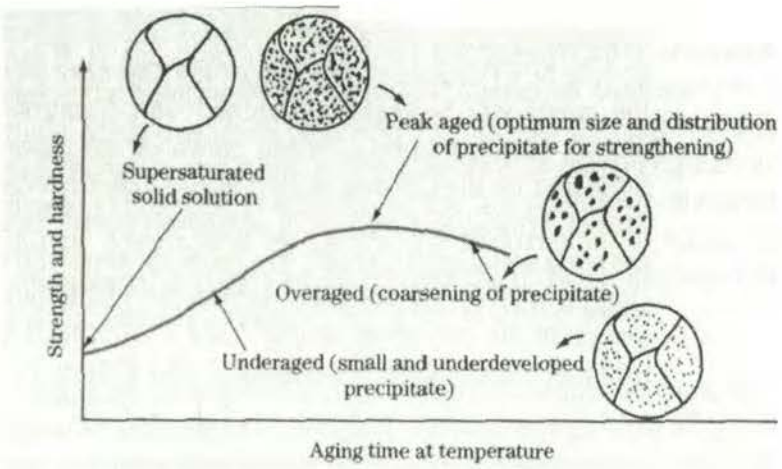

Figure 5.1. Formation of γ' precipitates within the main matrix [217]

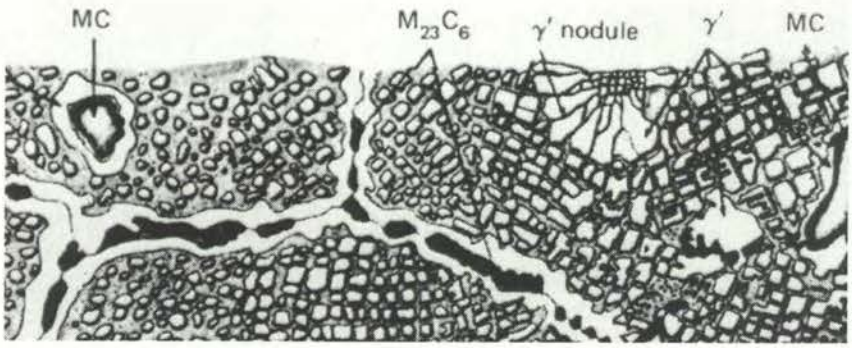

Figure 5.2 Micro structure of a nickel-based superalloy showing γ' and γ phases and metal matrix carbides formed within the grains and at the grain boundaries [156].

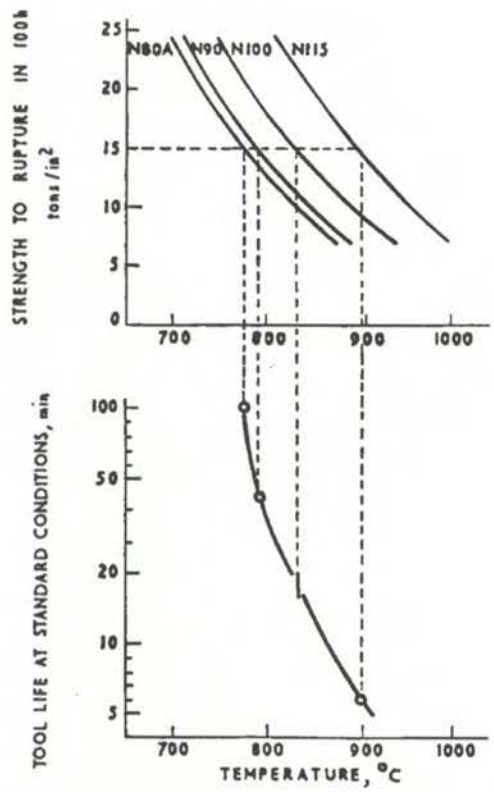

Figure 5.3 The effect of creep-rupture strength on tool life [46]

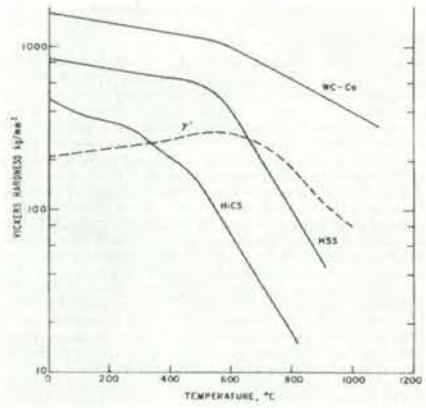

Figure 5.4 The temperature dependence of hardness of strengthening phase, γ', of creep-resistant nickel alloys compared with that for common tool materials [157].

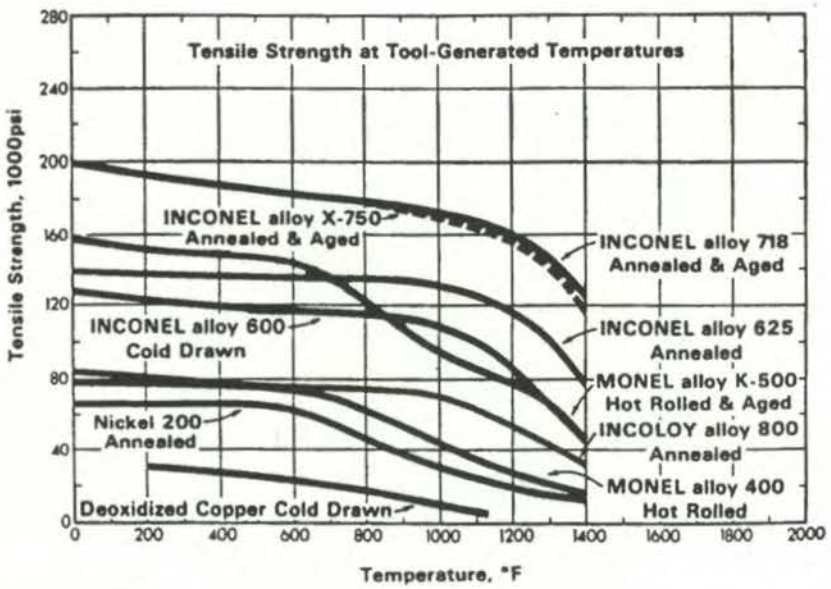

Figure 5.5 Tensile strength of nickel alloys at high temperature [162].

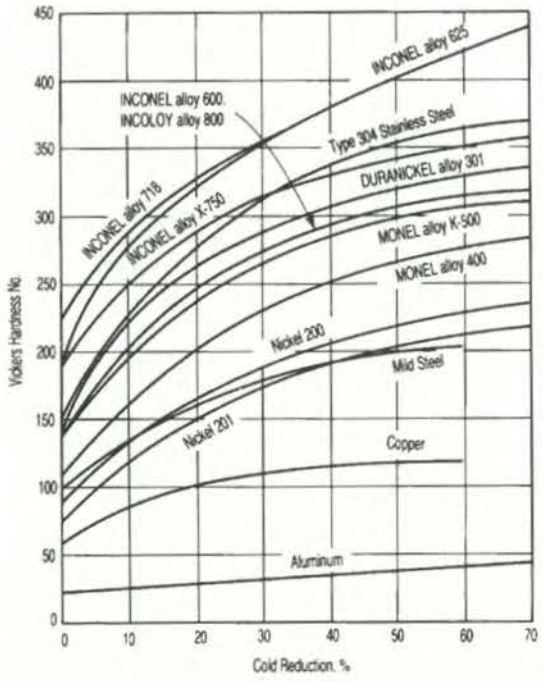

Figure 5.6 The effect of cold reduction on hardness indicating the degree of work-hardening of selected nickel alloys and other materials [158].

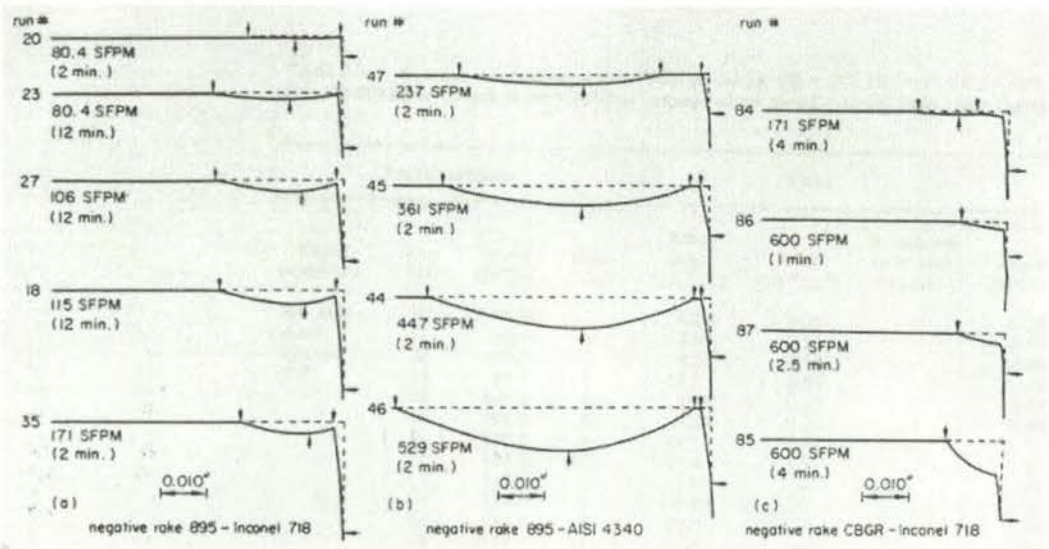

Figure 5.7 The profile of the worn rake face of a carbide tool used to machine Inconel 718 and AISI 4340, showing the absence of the 'cool region' in the case of Inconel 718 [170].

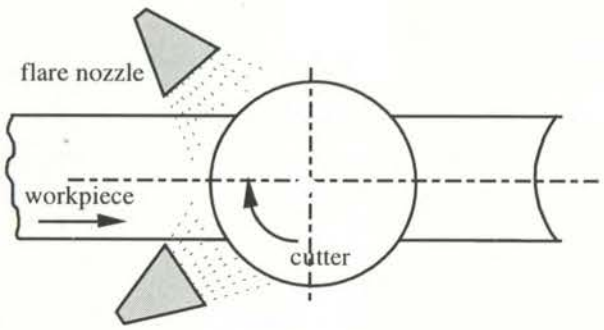

Figure 6.1 Illustration of the coolant application method

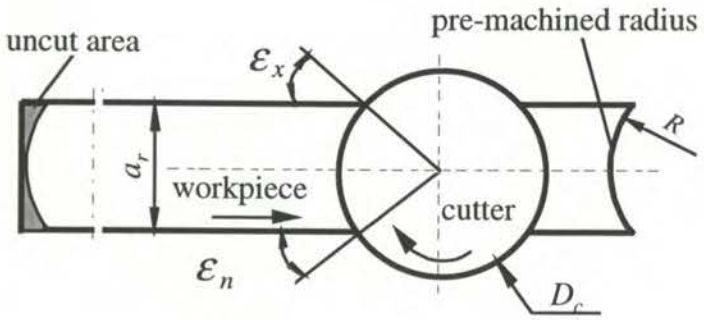

$D_c = 63$ mm; cutter diameter
$R_w = 31.5$ mm; radius of the pre-machined curve
$\varepsilon_n = 39^o$; angle of engagement
$\varepsilon_x = 40^o$; angle of exit
$a_r = 40$ mm; radial depth of cut (workpiece width)

Figure 6.2 Geometric detail of the cutter/workpiece relative position

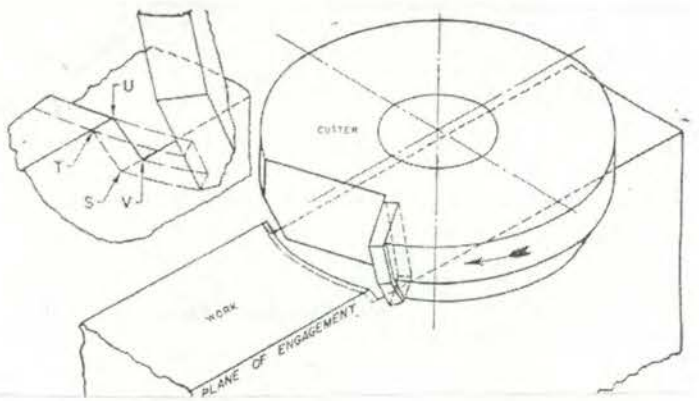

Figure 6.3 Definition of the initial contact of face milling cutter with the workpiece [19]

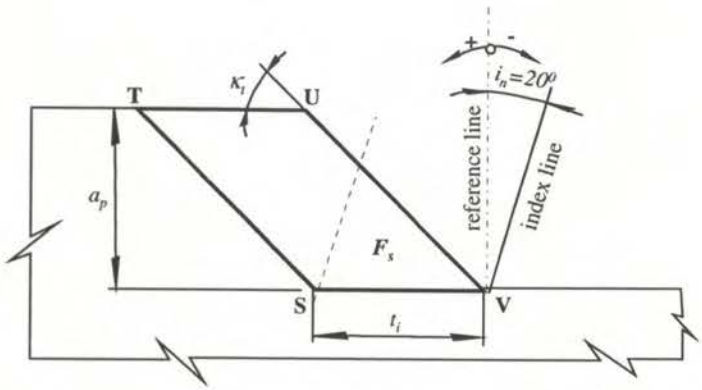

t_i : Instant apparent chip thickens during engagement ($t_i = fz.\cos\varepsilon_n$)

F_s : Partial area of engagement

κ_r : Angle of transient surface

i_n : Index angle

Figure 6.4 Definition of index line [20]

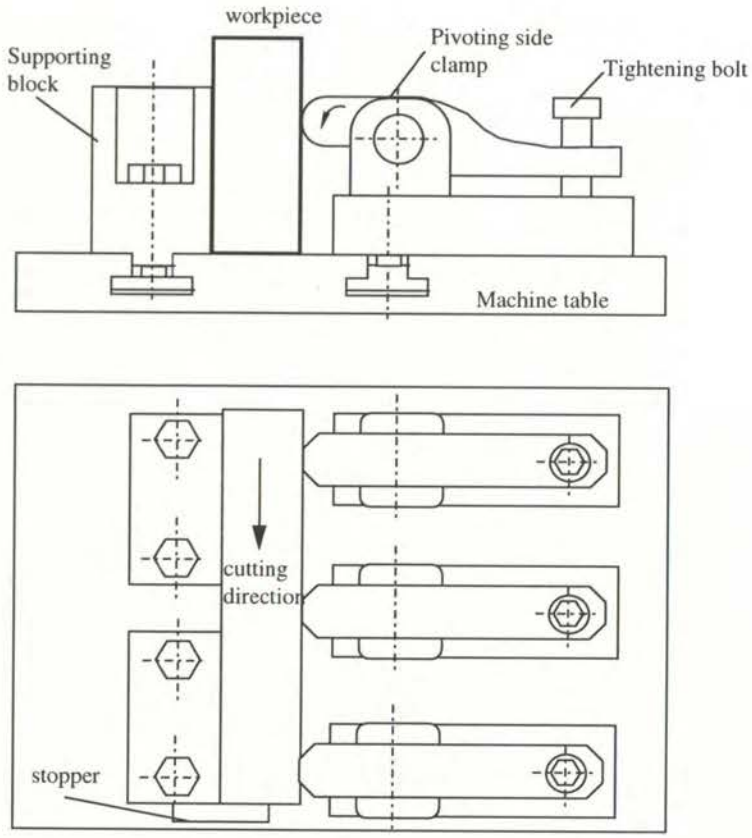

Figure 6.5 Description of the workpiece holding system

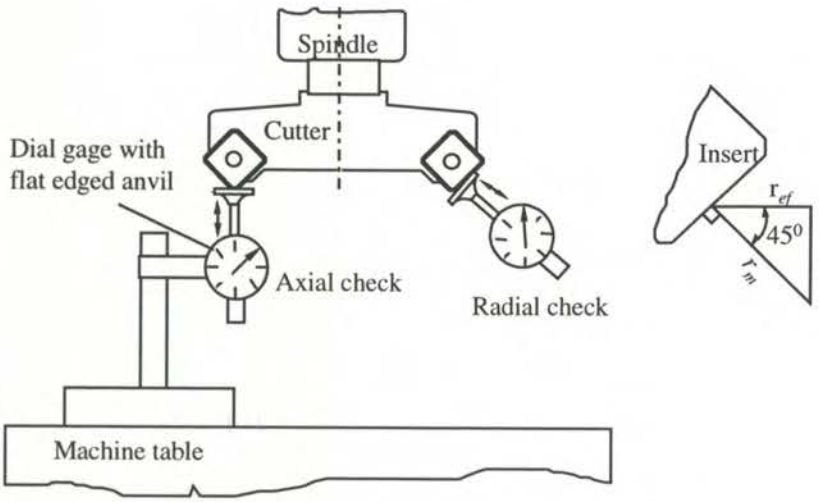

Figure 6.6 Axial and radial runout check

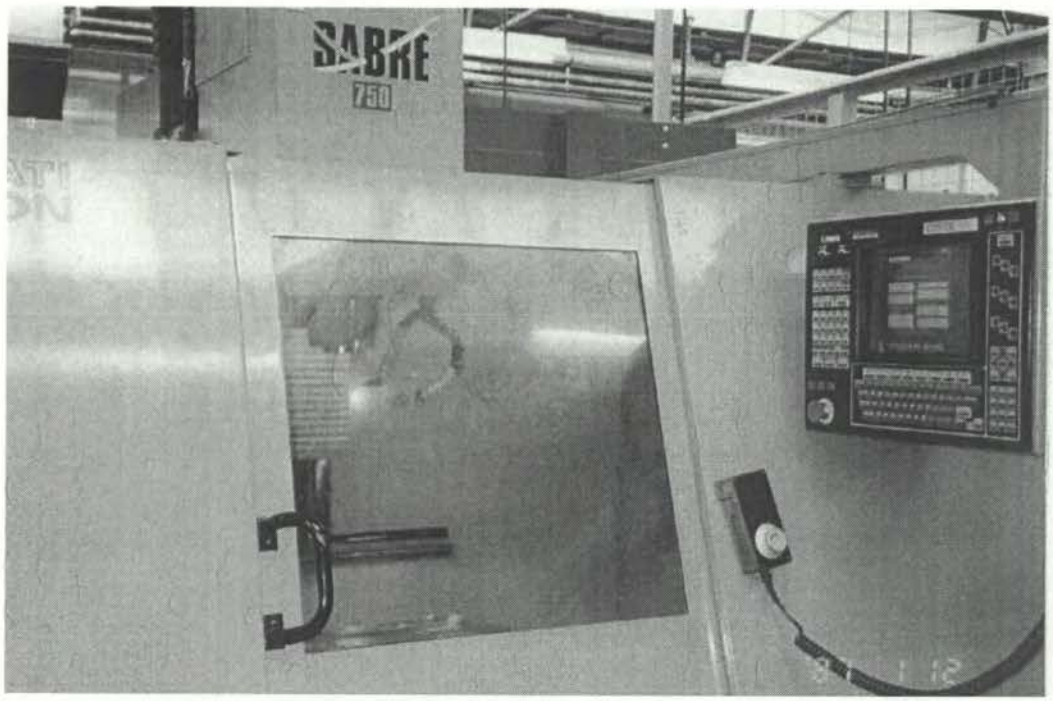

Figure 6.7 CNC controlled vertical machining centre (Cincinnati Milacron-Sabre 750)

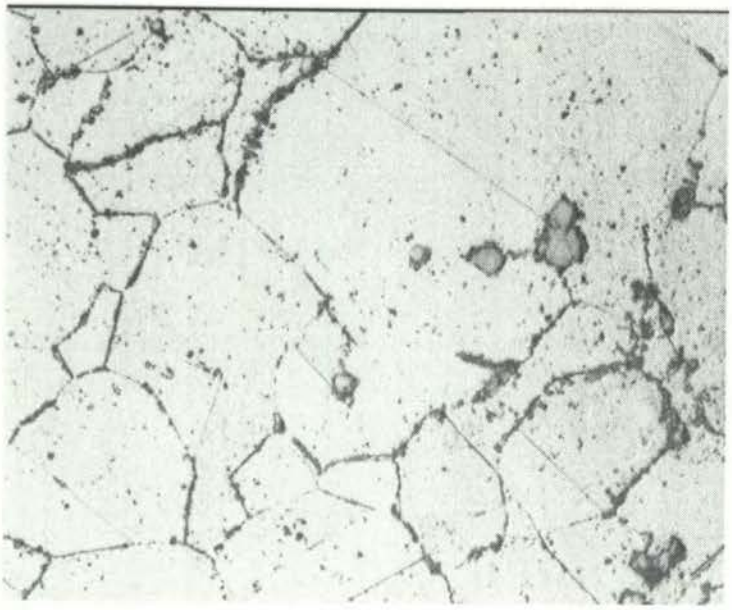

Figure 6.8 Microstructure of Inconel 718 (500x)

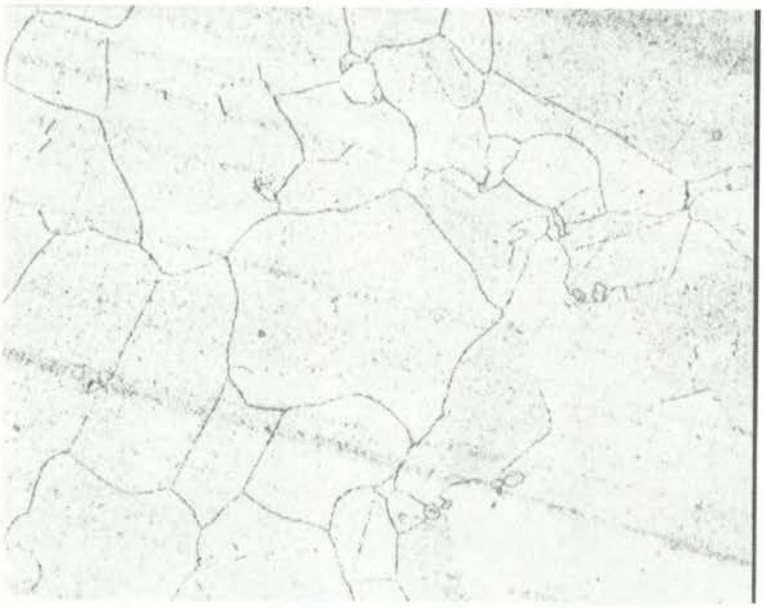

Figure 6.9 Microstructure of Waspaloy (243x)

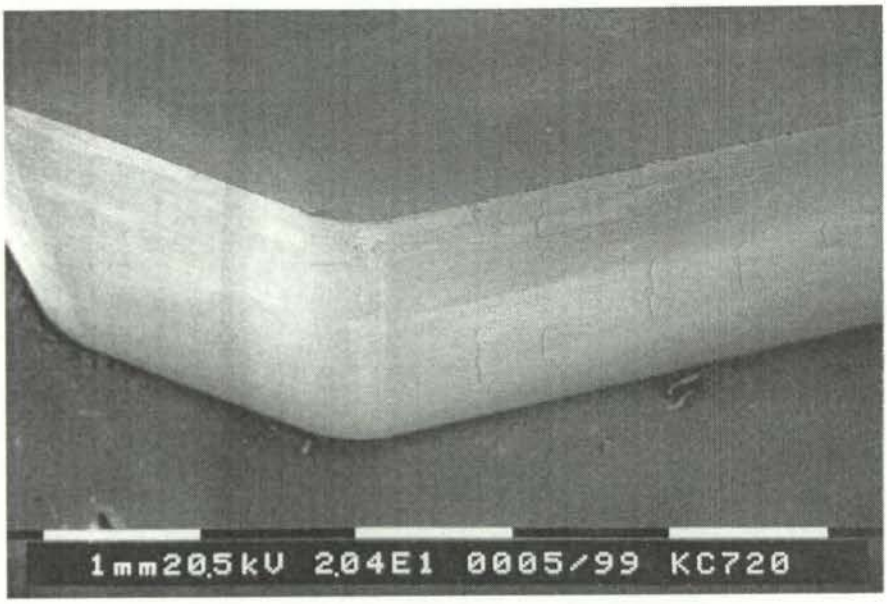

Figure 6.10 Sharp cutting edge of the PVD-TiN coated KC720 and KC730 insert

Figure 6.11: Sharp cutting edge of the CVD-TiCN+Al_2O_3 coated KC994M insert

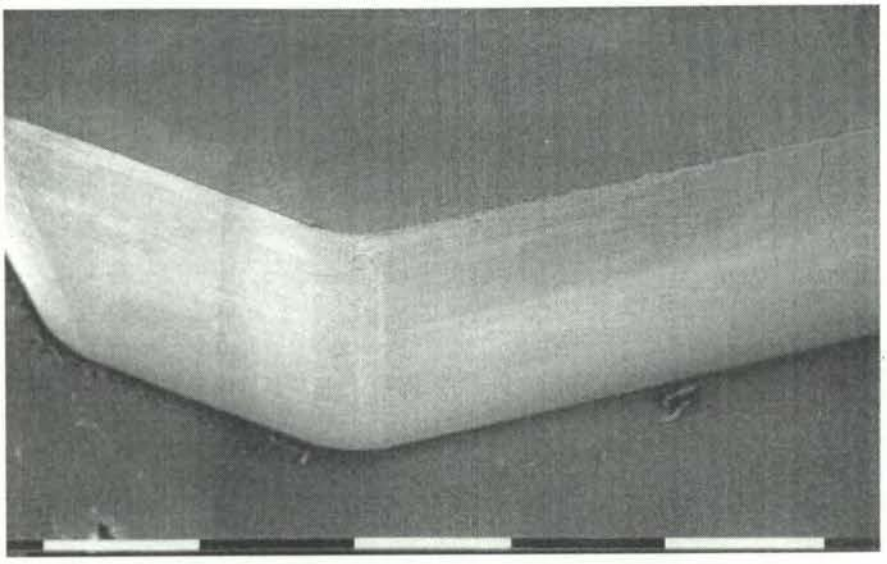

Figure 6.12: Sharp cutting edge of the KMF grade uncoated insert

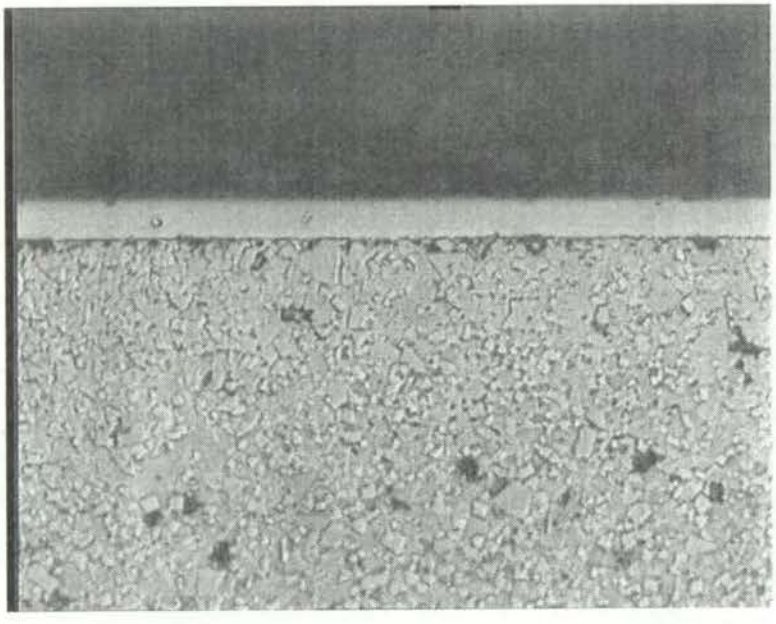

Figure 6.13: Microstructure of the of the PVD-TiN coated KC720 carbide insert

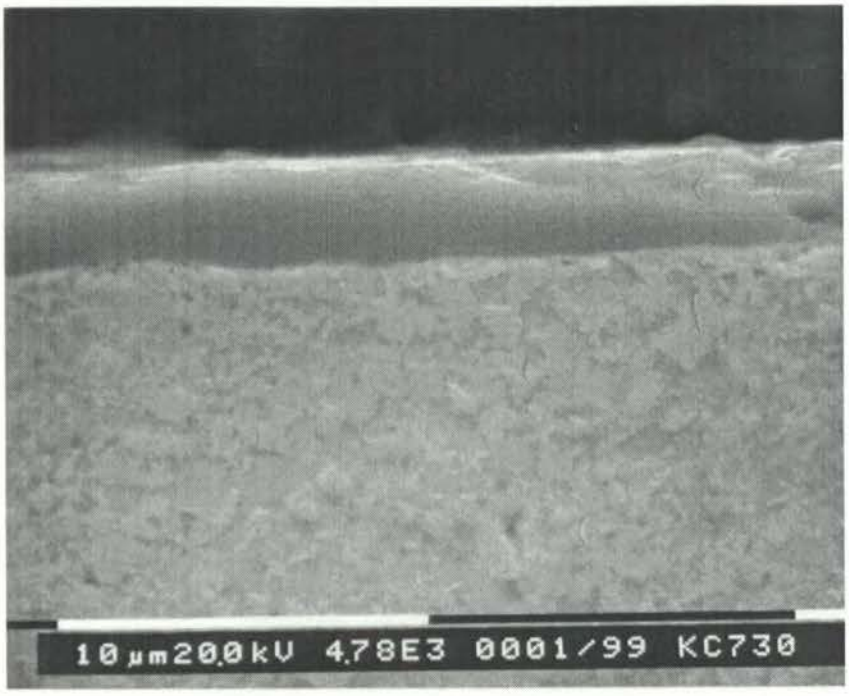

Figure 6.14 Microstructure of the of the PVD-TiN coated KC730 carbide insert

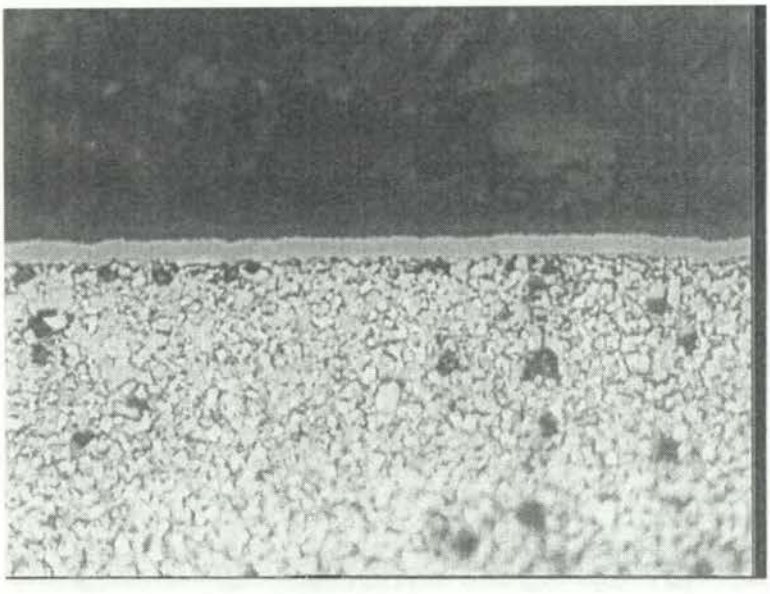

Figure 6.15: Microstructure of the CVD-TiCN+Al_2O_3 coated KC994M insert

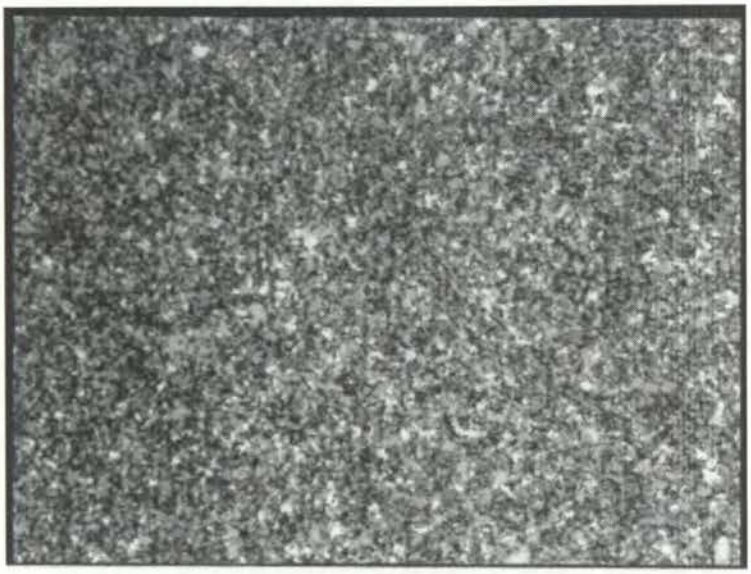

Figure 6.16 Microstructure of the KMF grade uncoated insert

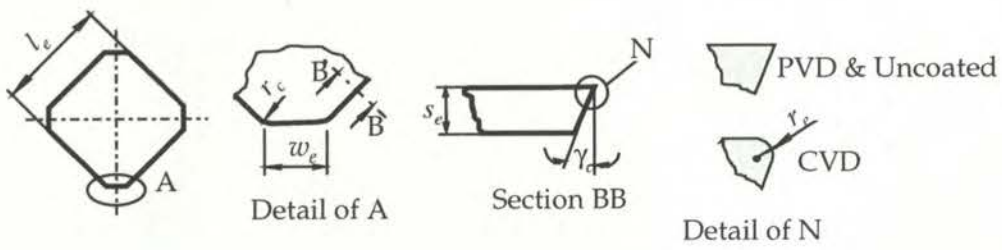

Geometric properties of the insert		
Edge length	l_e	12.7 mm
Thickness (coated & uncoated)	s_e	4.7 & 3.18 mm
Wiper length	w_e	2.4 mm
Edge clearance angle	γ_c	20°
Corner radius	r_c	1 mm
Edge radius	r_e	~ 0.025 mm

Figure 6.17 Geometric detail of the cutting inserts

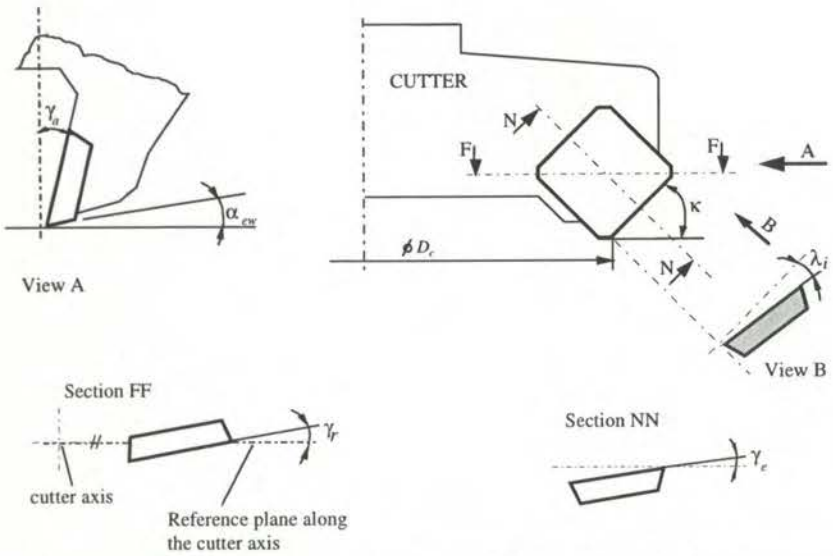

Geometric properties of the face milling cutter used			
Nominal cutter diameter D_c	63 mm	Effective rake angle γ_e	8°6'
Number of insert Z_i	3	Approach angle κ	45°
Radial rake angle γ_r	- 8°	Inclination angle λ_i	14°
Axial rake angle γ_a	20°	Wiper edge clearance angle α_{ew}	~ 5°

Figure 6.18 Geometric properties of the cutter

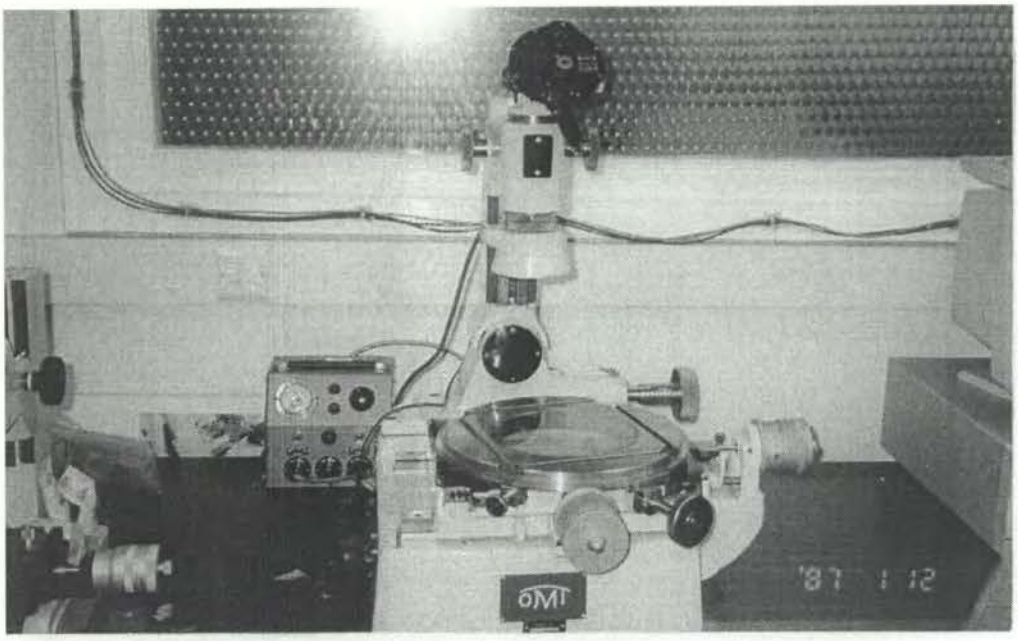

Figure 6.19 Travelling optical microscope used to measure the tool wear

Figure 6.20 Special jig used to hold and position the face milling cutter

Figure 6.21 Scanning electron microscope (Philips-SEM505)

Figure 6.22 Energy dispersive x-ray analyser, EDAX (PV-9100)

Figure 6.23 Optical microscope used to examine subsurface microstructure (Nikkon-LABOHOT)

Figure 6.24 Automatic grinding and polishing machine
(Buehler Metaserv-Motopol 12)

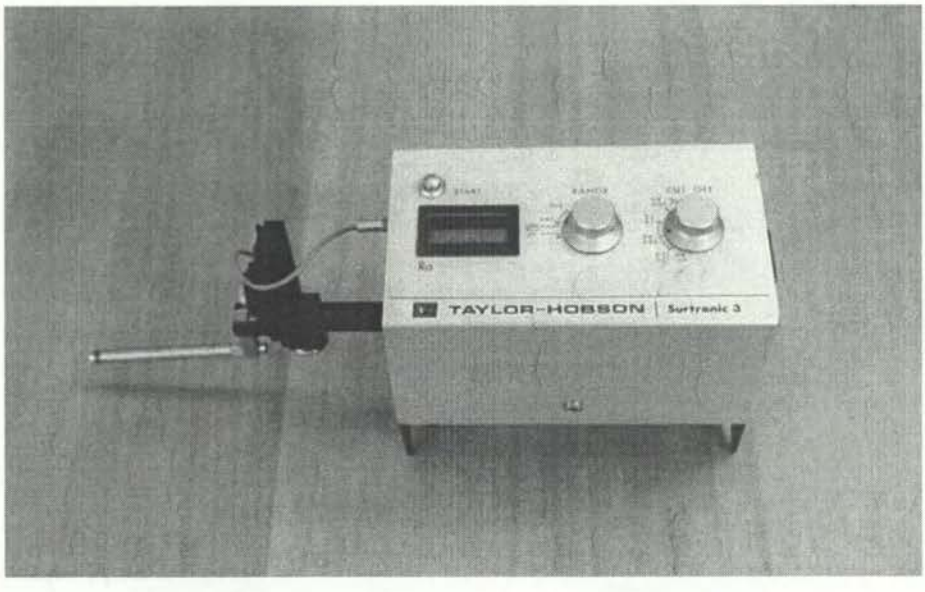

Figure 6.25 Surface roughness tester (Taylor-Hobson/Surtronic 3)

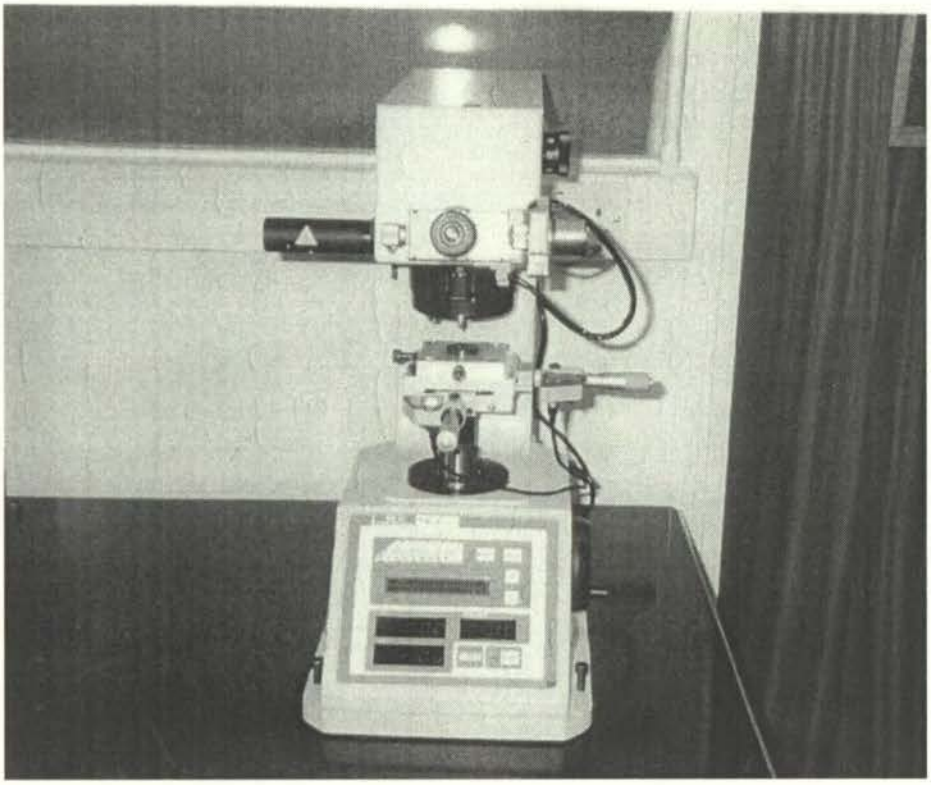

Figure 6.26 Microhardness testing machine (Mitutoyo MVK-H1)

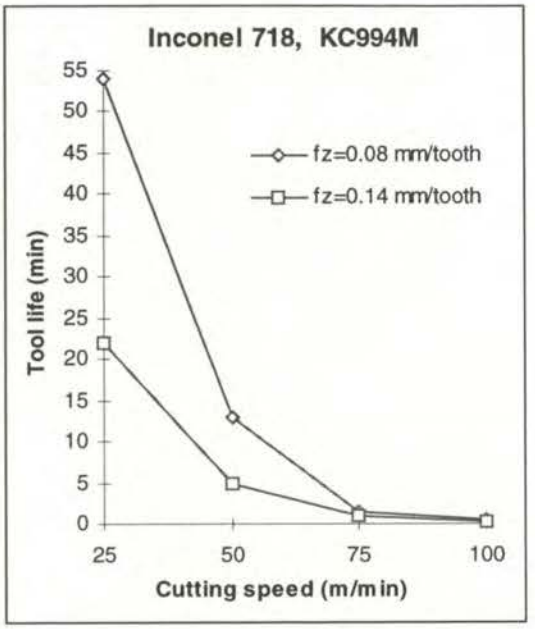

(a) Tool: KC994M

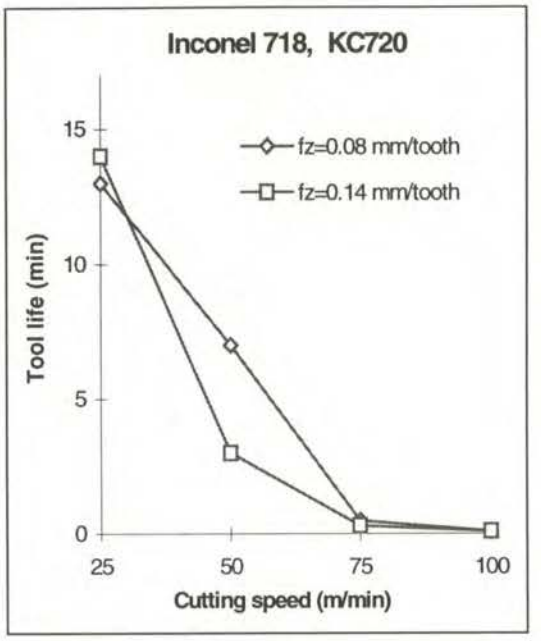

(b) Tool: KC720

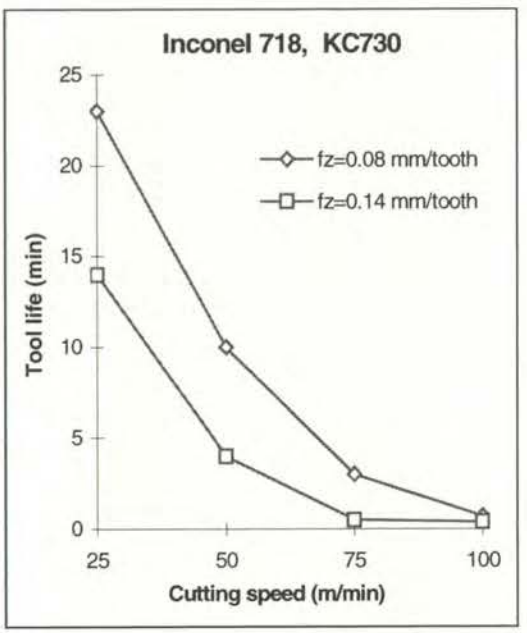

(c) Tool: KC730

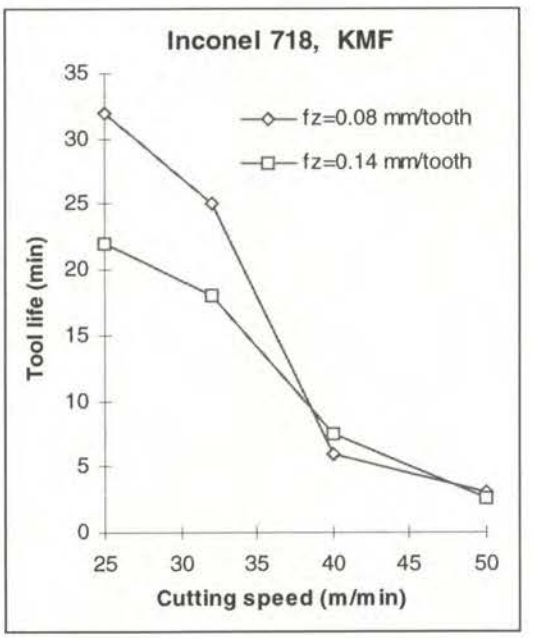

(d) Tool: KMF

Figure 7. 1 The effect of cutting speed and feed rate when face milling Inconel 718 with coated and uncoated tools

Figure 7. 2 Premature catastrophic failure with severe flaking of KC994M tool after 1 minute machining of Inconel 718 at 75 m/min and 0.14 mm/tooth

Figure 7. 3 Severe breakage at the cutting edge of KC994M tool failed prematurely after 20 seconds when face milling Inconel 718 at 100 m/min and 0.14 mm/tooth

Figure 7. 4 Failed KC994M tool due to combination of progressive wear by plucking, workpiece adhesion, pitting and chipping at the lowest cutting speed of 25 m/min and 0.08 mm/tooth

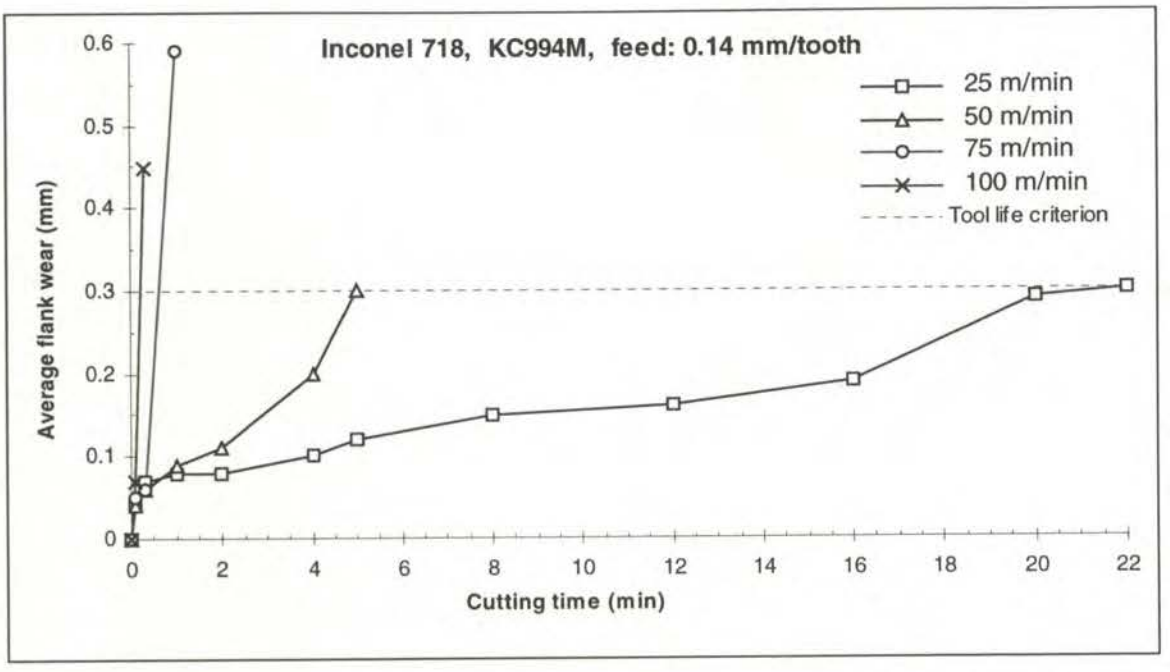

Figure 7. 5 Average flank wear versus cutting time when face milling Inconel 718 with KC994M at a feed rate of 0.14 mm/tooth

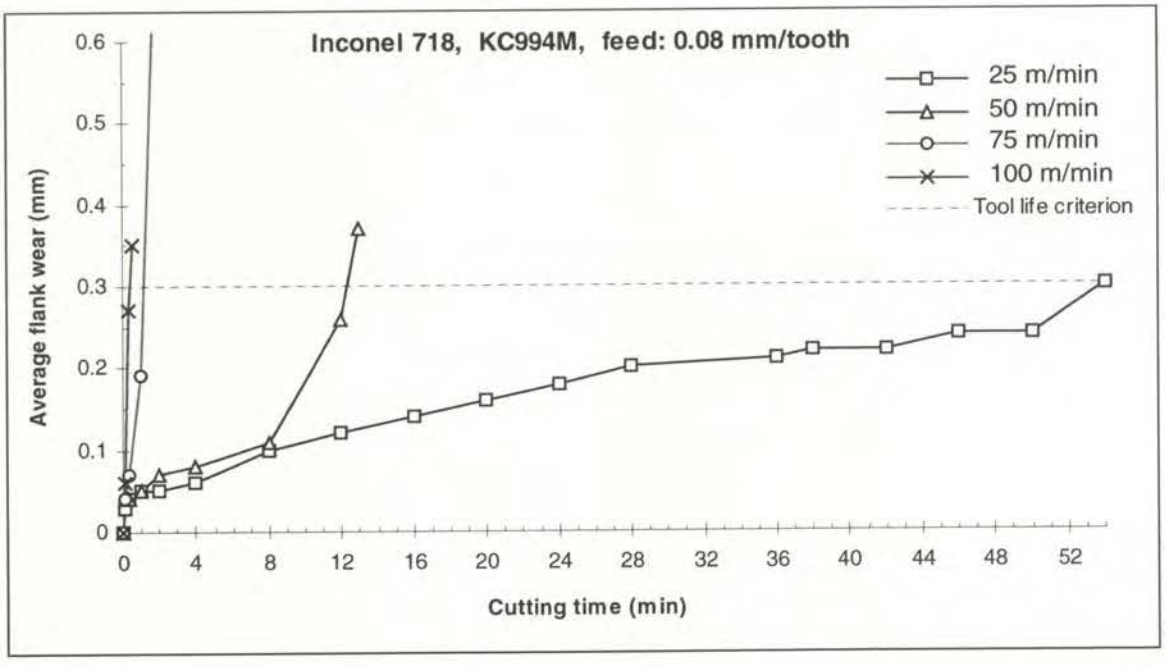

Figure 7. 6 Average flank wear versus cutting time when face milling Inconel 718 with KC994M at a feed rate of 0.08 mm/tooth

(a)

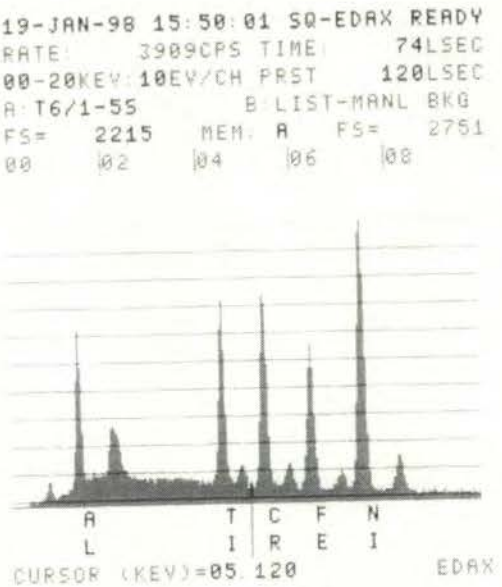

(b)

Figure 7. 7 (a) Severe workpiece galling and coating delamination at an initial stage of 5 seconds of face milling Inconel 718 with KC994M tool at 25 m/min and 0.08 mm/tooth. (b) EDAX analysis showing the presence of workpiece material adhesion on the rake face of KC994M tool

(a)

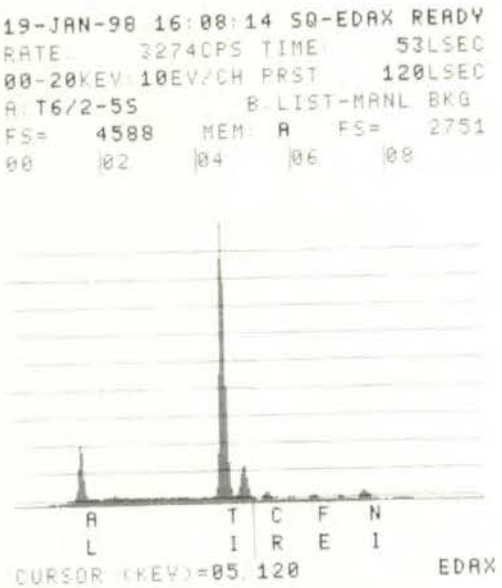

(b)

Figure 7. 8 (a) Delamination of the top coating layer at an initial stage of 5 seconds of cutting Inconel 718 with KC994M tool at 50 m/min and 0.14 mm/tooth. (b) EDAX analysis showing evidence of delamination of the top layer on the rake face of KC994M

Figure 7. 9 Galling and adhesion of relatively large workpiece material at the cutting edge of KC994M tool, occurring within first 5 seconds of cutting when machining Inconel 718 at 74 m/min and 0.14 mm/tooth

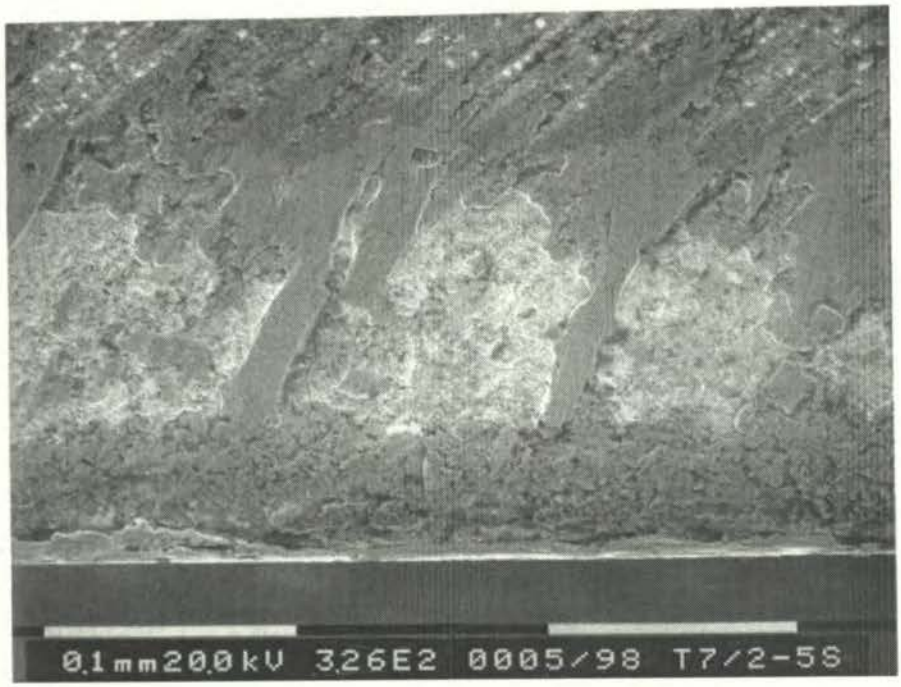

(a)

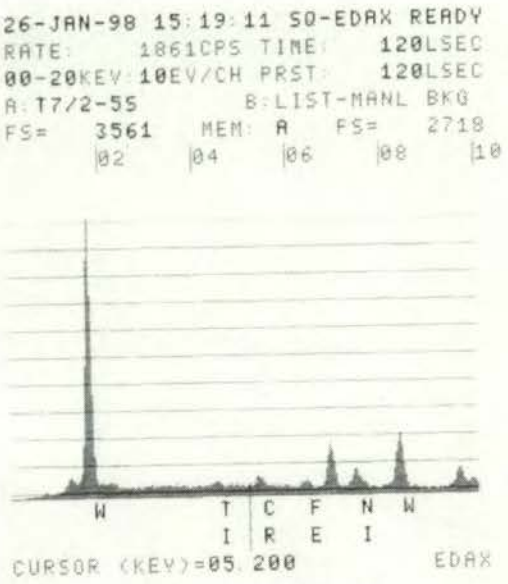

(b)

Figure 7. 10 (a) Workpiece galling and associated substrate plucking on the rake face of KC994M tool within first 5 seconds of machining Inconel 718 at 50 m/min and 0.08 mm/tooth. (b) Corresponding EDAX analysis showing evidence of substrate plucking and workpiece galling

(a)

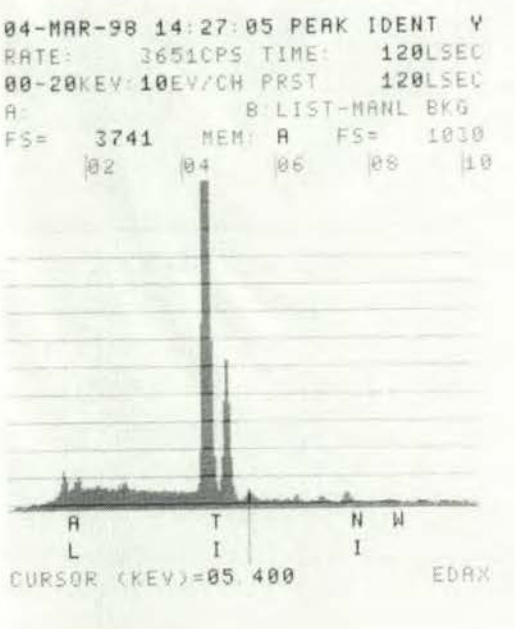

(b)

Figure 7. 11 (a) Collective presence of coating delamination (top layer of Al2O3), workpiece galling and adhesion, pitting on the rake face and microchipping at the cutting edge of KC994M tool occurring within the first 5 seconds of machining Inconel 718 at 75 m/min and 0.08 mm/tooth. (b) EDAX analysis showing evidence of the removal of the top coating layer

(a)

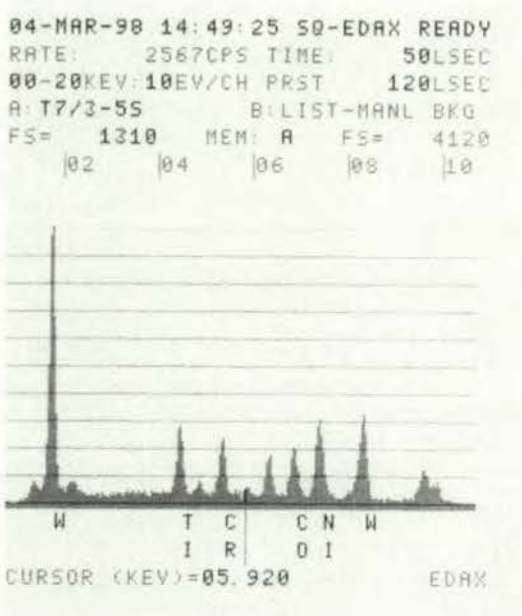

(b)

Figure 7. 12 (a) Cutting edge microchipping and workpiece adhesion on the flank face of KC994M tool, occurring within 5 seconds when machining Inconel 718 at 75 m/min and 0.08 mm/tooth. (b) Corresponding EDAX analysis of the above area showing evidence for the mentioned wear modes

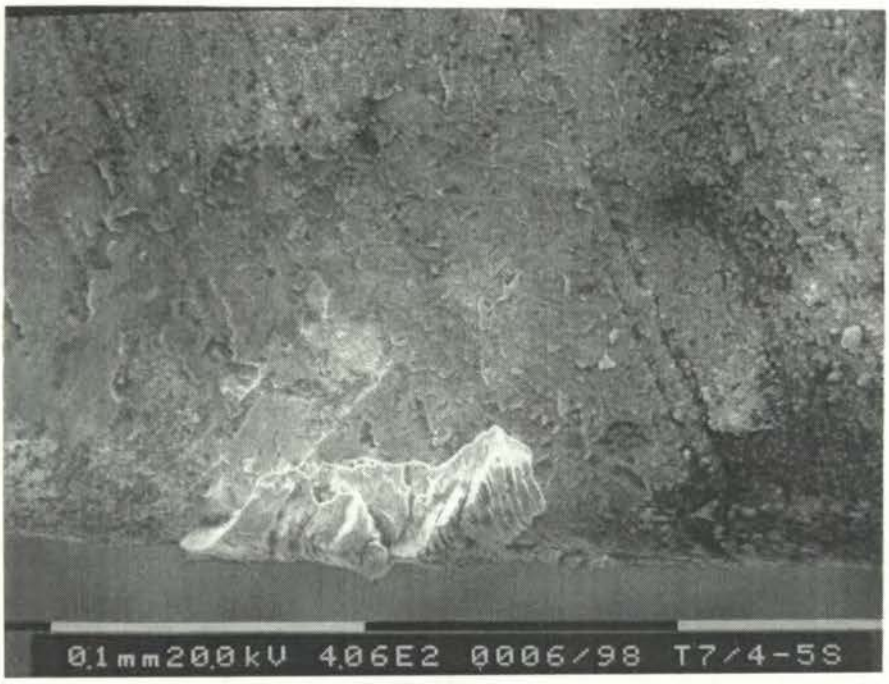

Figure 7. 13 Occurrence of coating delamination, workpiece adhesion and galling and associated substrate pitting at the highest cutting speed of 100 m/min and 0.08 mm/tooth, when machining Inconel 718 with KC994M tool, after cutting for 5 seconds.

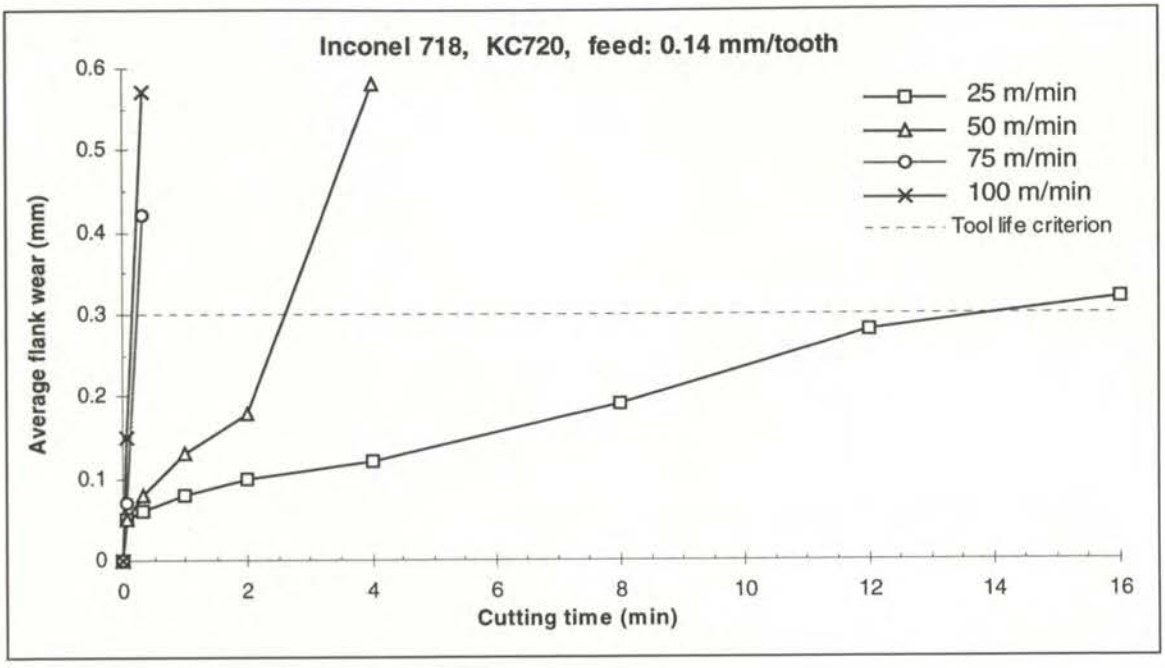

Figure 7. 14 Average flank wear versus cutting time when face milling Inconel 718 with KC720 at a feed rate of 0.14 mm/tooth

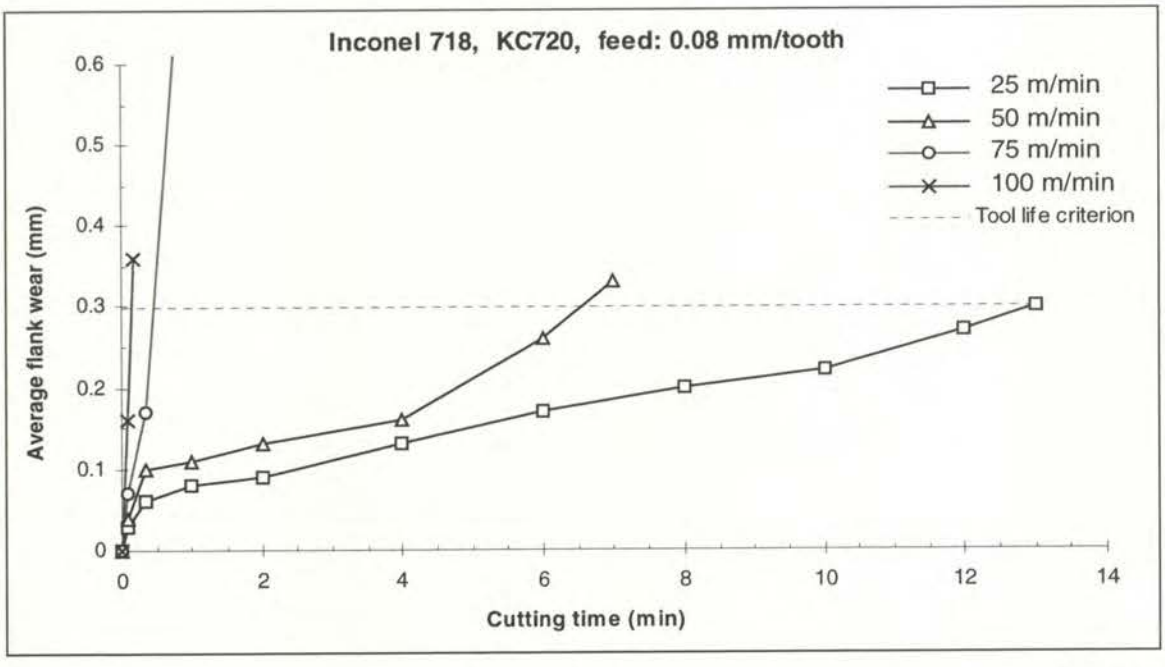

Figure 7. 15 Average flank wear versus cutting time when face milling Inconel 718 with KC720 at a feed rate of 0.08 mm/tooth

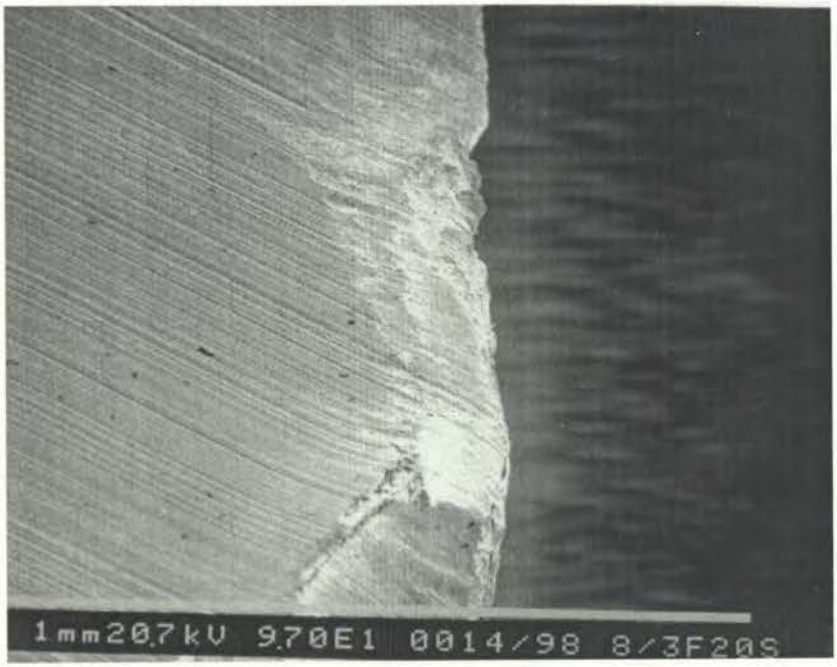

Figure 7. 16 Premature failure of KC720 tool by severe chipping/breakage and plastic deformation on the rake face after 20 seconds when machining Inconel 718 at 75 m/min and 0.14 mm/tooth

Figure 7. 17 Premature failure of KC720 tool after 5 seconds by severe breakage and workpiece adhesion when machining Inconel 718 at 100 m/min and 0.08 mm/tooth

Figure 7. 18 Plucking, microchipping and workpiece adhesion on the failed KC720 tool cutting Inconel 718 for 16 minutes at 25 m/min and 0.14 mm/tooth

Figure 7. 19 Plucking, microchipping and workpiece galling on the failed KC720 tool cutting Inconel 718 for 13 minutes at 25 m/min and 0.08 mm/tooth

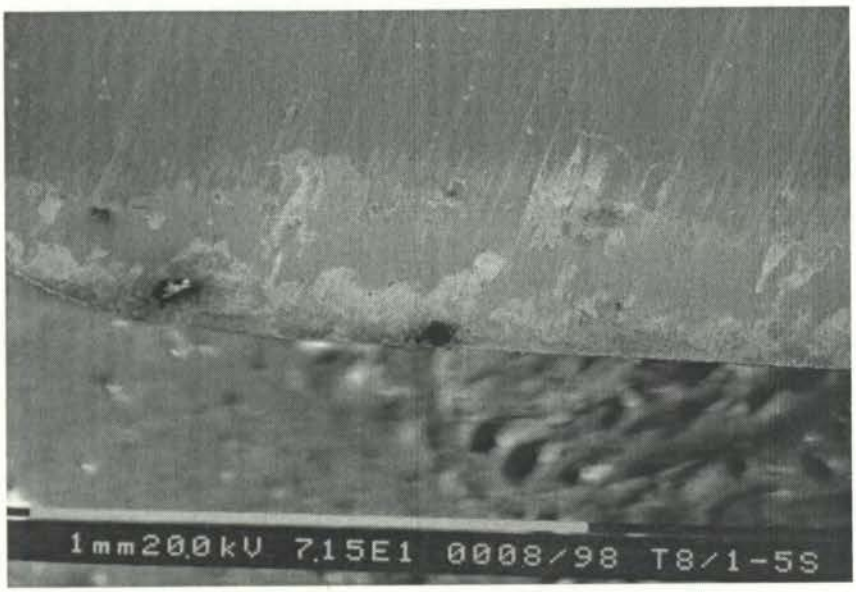

Figure 7. 20 Magnified view of the rake face of KC720 tool showing severe workpiece galling, coating delamination and substrate plucking after 5 seconds when machining Inconel 718 at 25 m/min and 0.14 mm/tooth

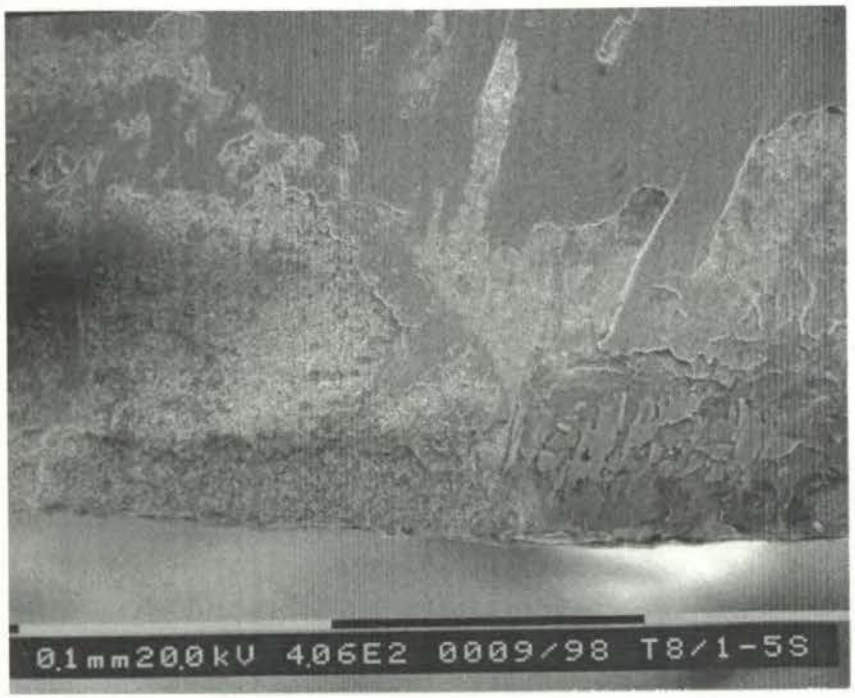

(a)

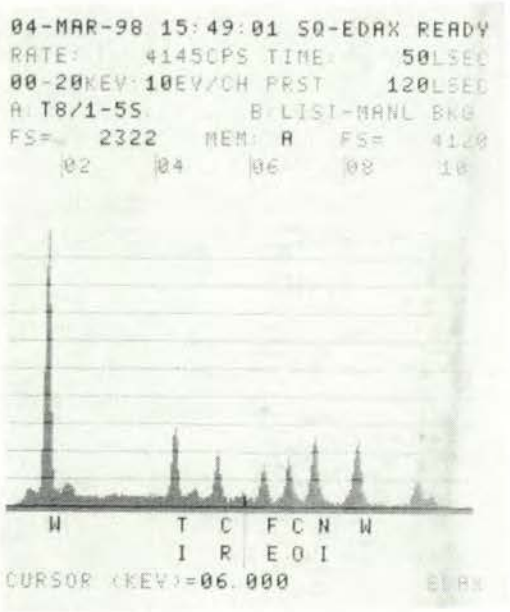

(b)

Figure 7. 21 (a) A focused view of the rake face of KC720 tool (Figure 7.20) at a higher magnification clearly showing microchipping, plucking, coating delamination and galling after 5 seconds when machining Inconel 718 at 25 m/min and 0.14 mm/tooth. (b) Corresponding EDAX analysis supporting the presence of these phenomena

Figure 7. 22 The condition of flank and rake face of the nose section of KC720 tool after cutting Inconel 718 for 5 seconds at 25 m/min and 0.14 mm/tooth, showing plucked areas on the rake face while flank face remaining relatively intact

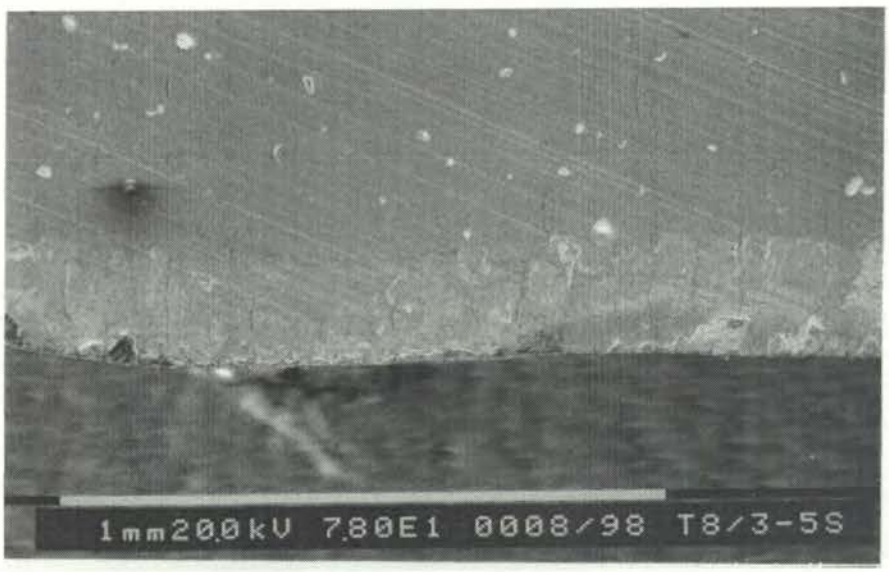

Figure 7. 23 SEM image showing coating delamination, chipping and workpiece adhesion on the rake face of KC720 tool after cutting Inconel 718 for 5 seconds at 75 m/min and 0.14 mm/tooth

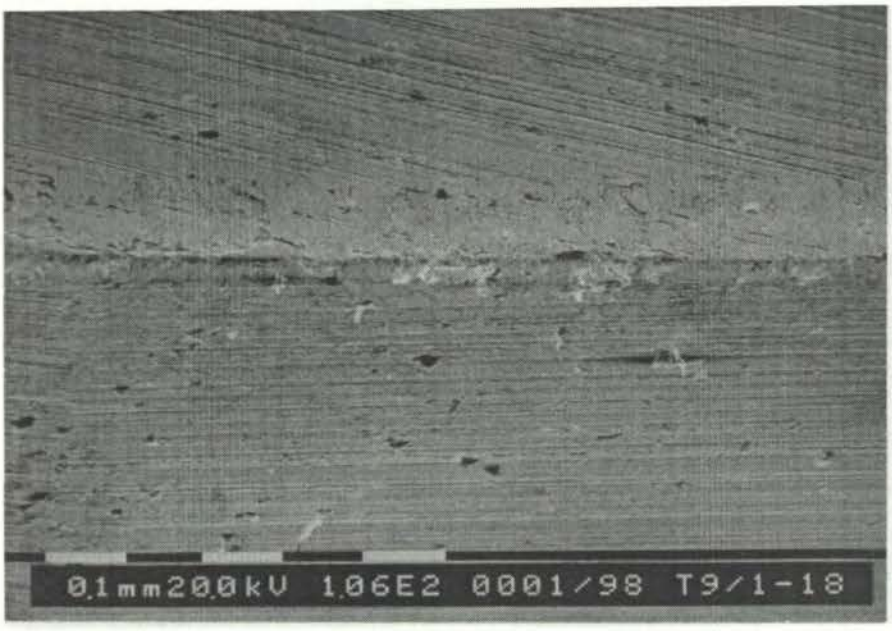

Figure 7. 24 A broad view of the cutting edge of KC720 tool showing dominance of workpiece galling on the rake and flank face galling after 18 seconds when cutting Inconel 718 at 25 m/min and 0.08 mm/tooth

(a)

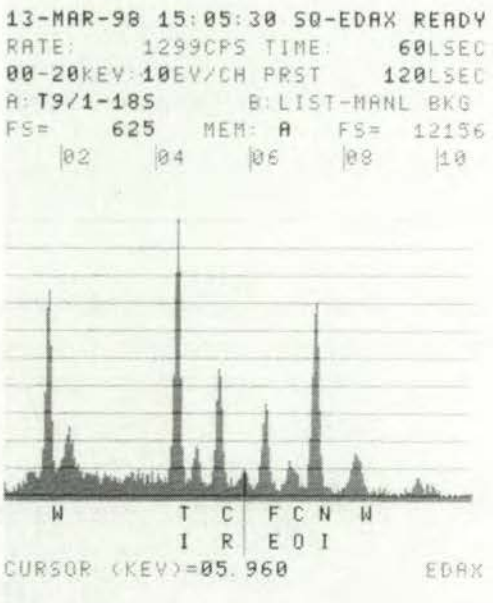

(b)

Figure 7. 25 (a) Magnified view of Figure 7.24 showing already pitted areas and initiation of plucking on the rake face. (b) EDAX analysis proving the substrate exposure on KC720 tool

(a)

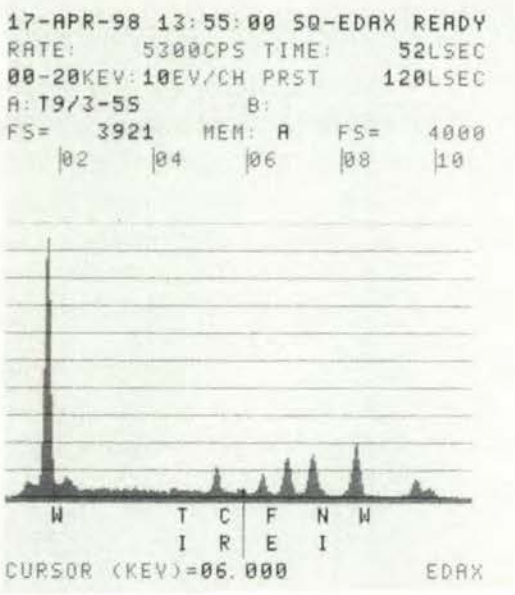

(b)

Figure 7. 26 (a) Severe workpiece adhesion, chipping and plucking on KC720 tool after 5 seconds of cutting Inconel 718 at 75 m/min and 0.08 mm/tooth. (b) EDAX analysis proving substrate exposure on the rake face of the above tool

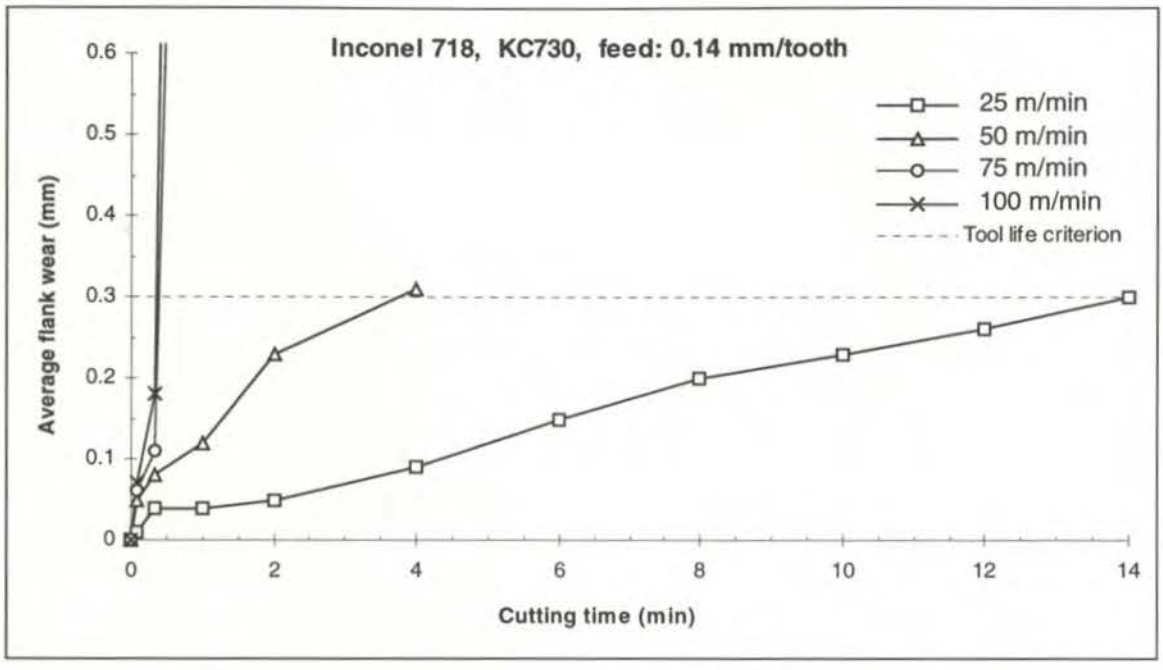

Figure 7. 27 Average flank wear versus cutting time when face milling Inconel 718 with KC730 at a feed rate of 0.14 mm/tooth

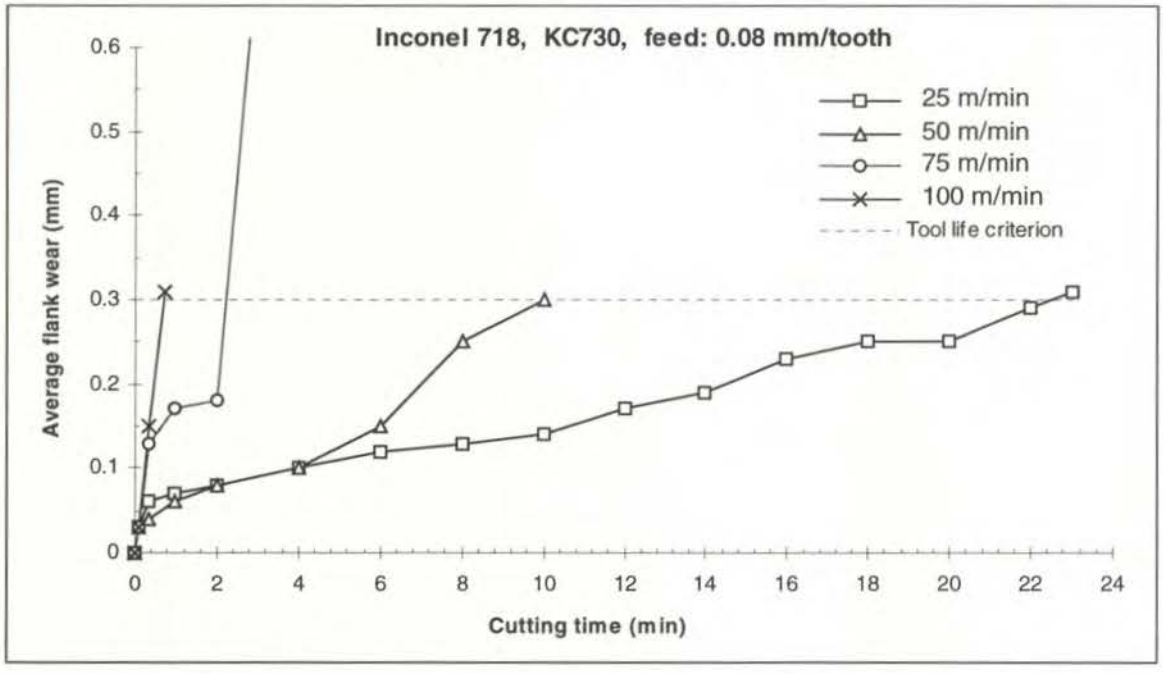

Figure 7. 28 Average flank wear versus cutting time when face milling Inconel 718 with KC730 at a feed rate of 0.08 mm/tooth

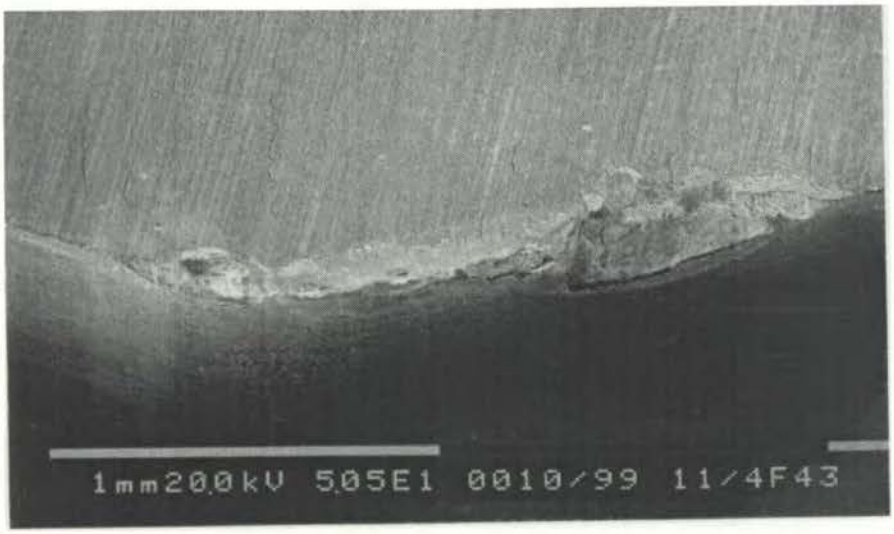

Figure 7. 29 Severe chipping at the cutting edge of KC730 tool, failed after 43 seconds at 100 m/min and 0.08 mm/tooth when cutting Inconel 718

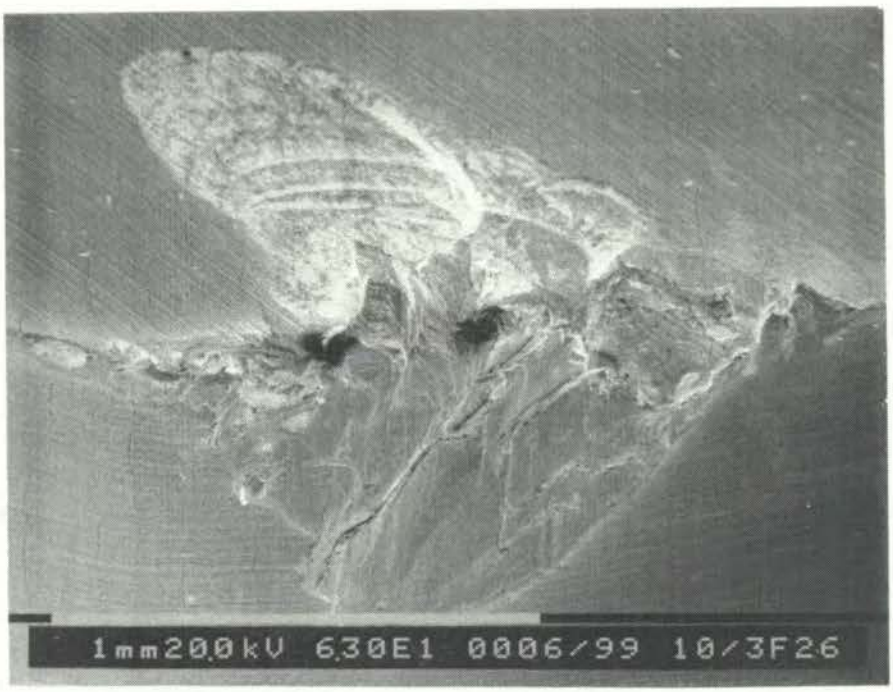

Figure 7. 30 Catastrophic failure of KC730 tool due to severe breakage and flaking at 75 m/min and 0.14 m/min after cutting Inconel 718 for 26 seconds

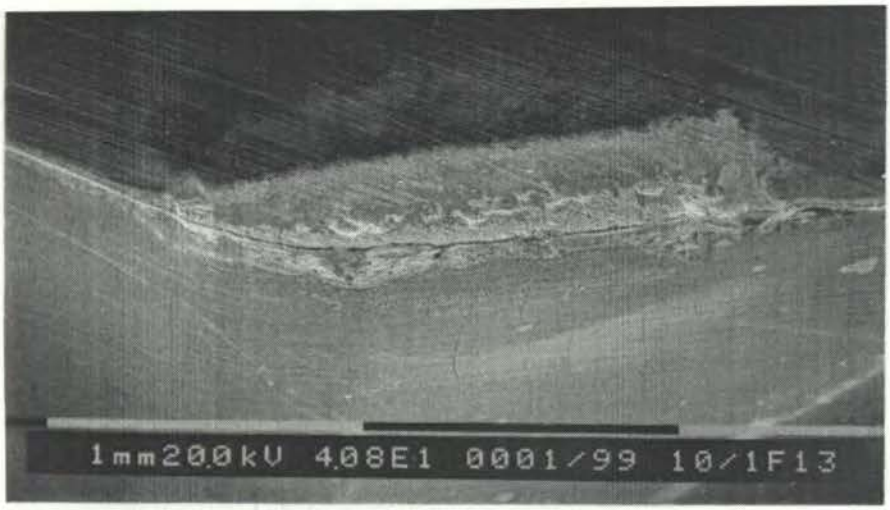

Figure 7. 31 General view of the entire cutting edge of KC730 tool after cutting Inconel 718 for 13 minutes at 25 m/min and 0.14 mm/tooth

Figure 7. 32 Coating delamination and workpiece adhesion on the rake face of KC730 tool after cutting Inconel 718 for 5 seconds at 25 m/min and 0.08 mm/tooth

(a)

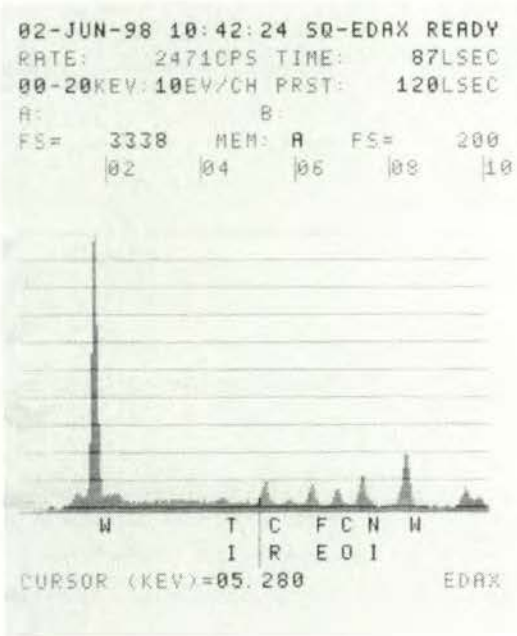

(b)

Figure 7. 33 (a) Early microchipping at the nose section of the cutting edge and substrate exposure on the rake face after cutting for 5 seconds (same tool and condition as in Figure 7.32). (b) EDAX analysis confirming substrate exposure

Figure 7. 34 Premature severe chipping of cutting edge and workpiece adhesion on KC730 after cutting Inconel 718 for 5 seconds at 75 m/min and 0.14 mm/tooth

(a)

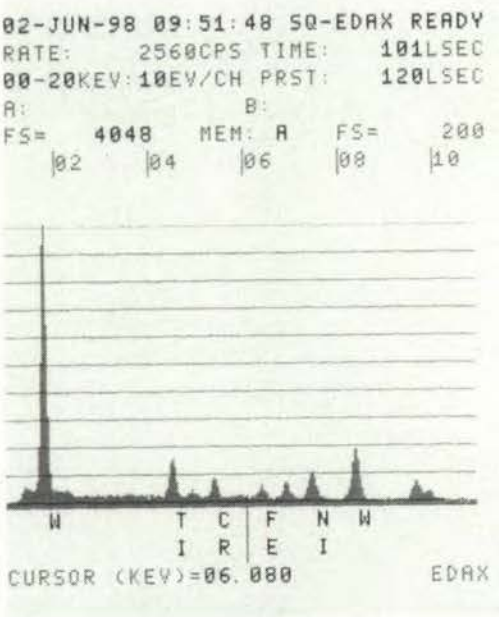

(b)

Figure 7. 35 (a) Early delamination of TiN coating layer in a fractured fashion at DOC region on the rake face of KC730 tool where intermittent chip flow takes palace, at 75 m/min and 0.14 mm/tooth. (b) EDAX analysis proving substrate exposure on KC730

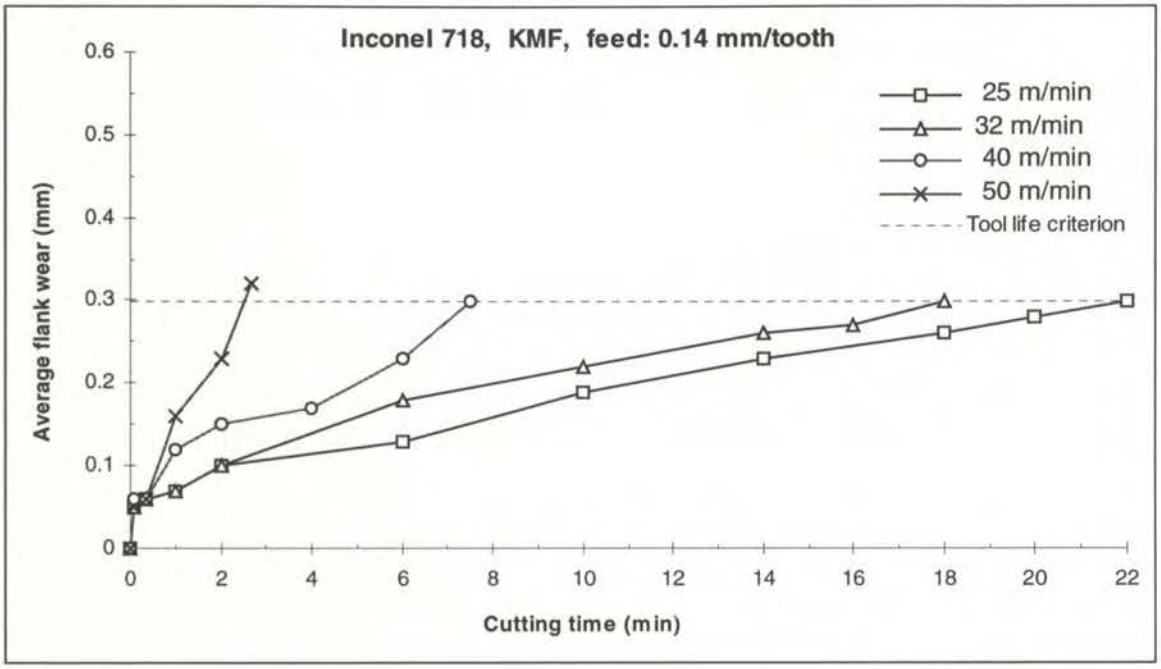

Figure 7. 36 Average flank wear versus cutting time when face milling Inconel 718 with KMF at a feed rate of 0.14 mm/tooth

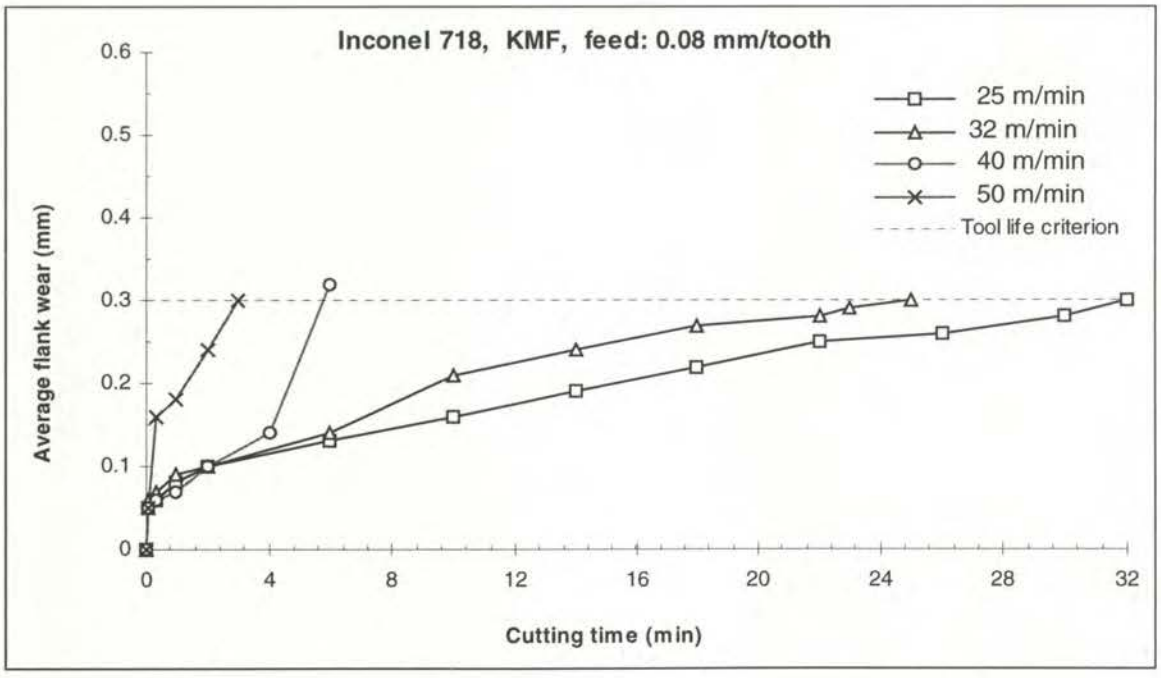

Figure 7. 37 Average flank wear versus cutting time when face milling Inconel 718 with KMF at a feed rate of 0.08 mm/tooth

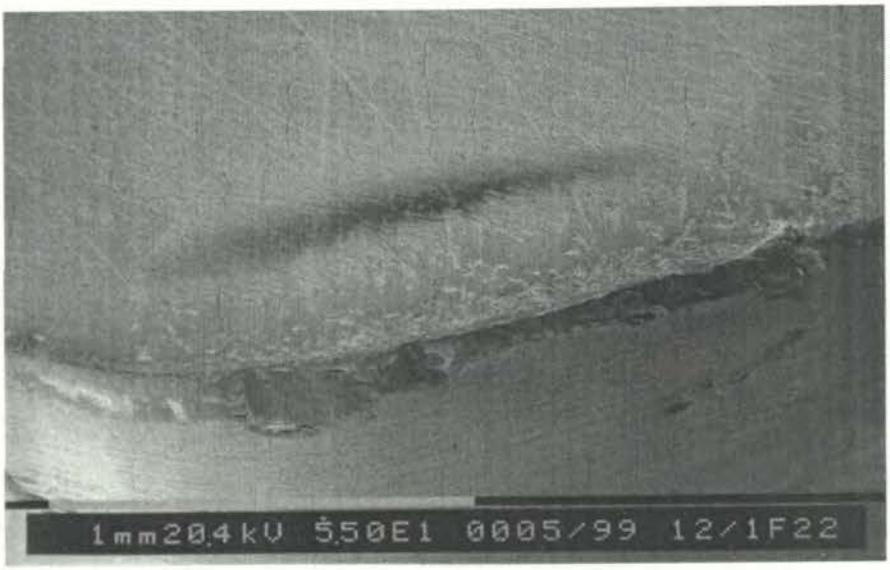

Figure 7. 38 A general view of KMF tool failed due to progressive chipping and workpiece adhesion after cutting Inconel 718 for 22 minutes at 25 m/min and 0.14 mm/tooth

Figure 7. 39 A general view of KMF tool failed due to progressive chipping/plucking, workpiece adhesion and smooth flank wear after cutting Inconel 718 for 32 minutes at 25 m/min and 0.08 mm/tooth

Figure 7. 40 Severe breakage along the entire cutting edge of a KMF tool after 3 minutes cutting of Inconel 718 at 50 m/min and 0.14 mm/tooth

Figure 7. 41 Workpiece material adhesion on the rake of KMF tool cutting Inconel 718 for 5 seconds at 25 m/min and 0.14 mm/tooth

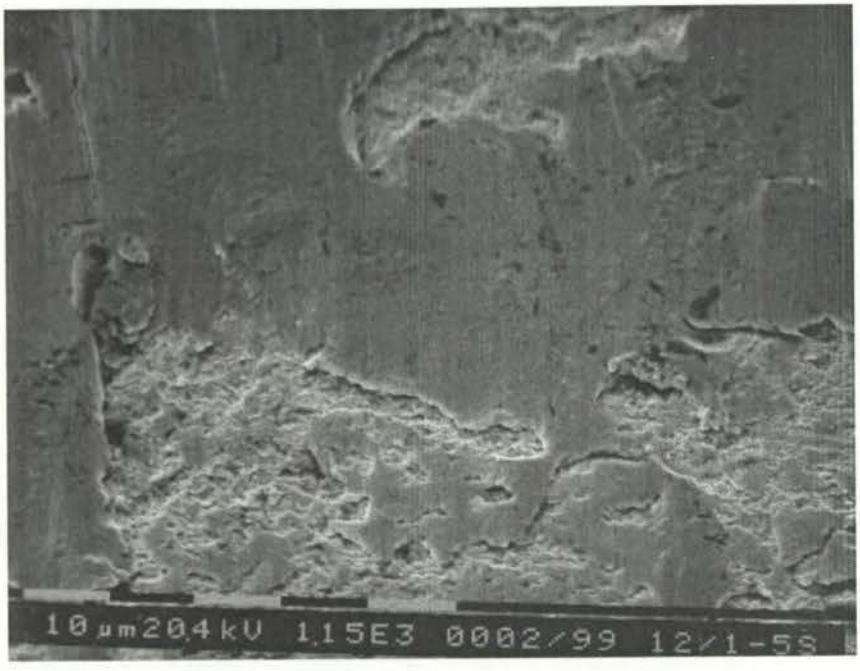

Figure 7. 42 Initial pitting and plucking of the rake face of KMF tool due to detachment of adhered workpiece material (same tool as in Figure 7.40 at a higher magnification)

Figure 7. 43 Initial microchipping at the very cutting edge of KMF tool (same tool as in Figure 7.40 at a higher magnification)

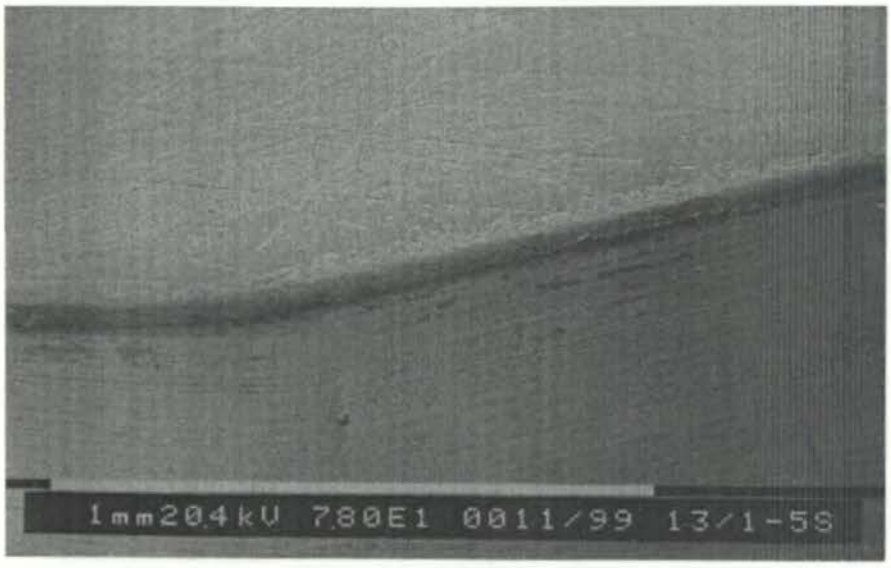

Figure 7. 44 Early workpiece galling and associated pitting of the rake face of KMF tool after cutting Inconel 718 for 5 seconds at 25 m/min and 0.08 mm/tooth

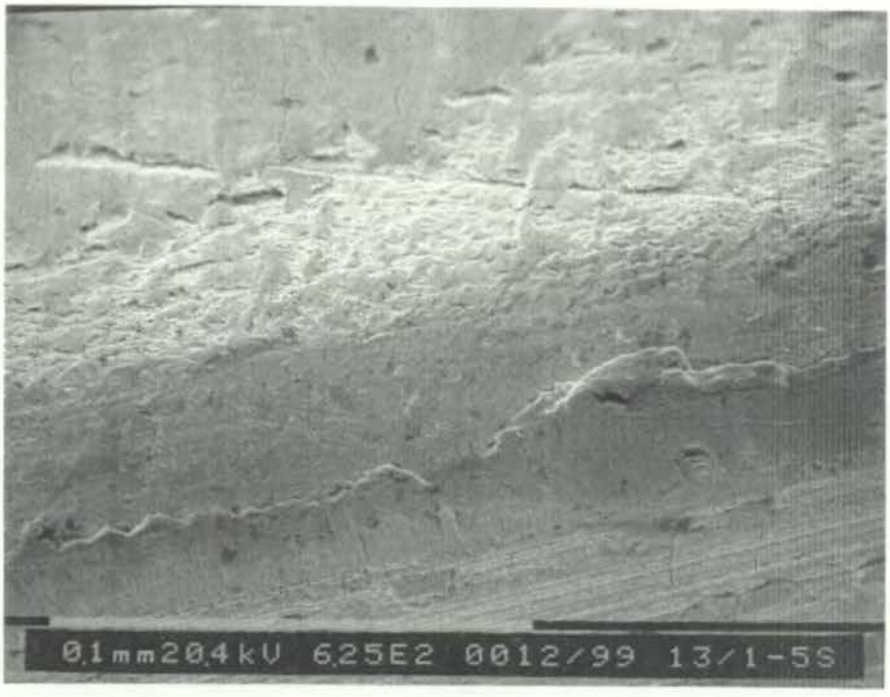

Figure 7. 45 Magnified view of the rake face of KMF tool in Figure 7.44, showing rake face pitting and adhered workpiece material

Figure 7. 46 General view of the entire cutting edge after cutting for 5 seconds, showing smeared and adhered large workpiece material when cutting Inconel 718 at 50 m/min and 0.14 mm/tooth

Figure 7. 47 Magnified view of the KMF tool in Figure 7.46, showing relatively thin layer of galled and adhered workpiece material and rake face pitting

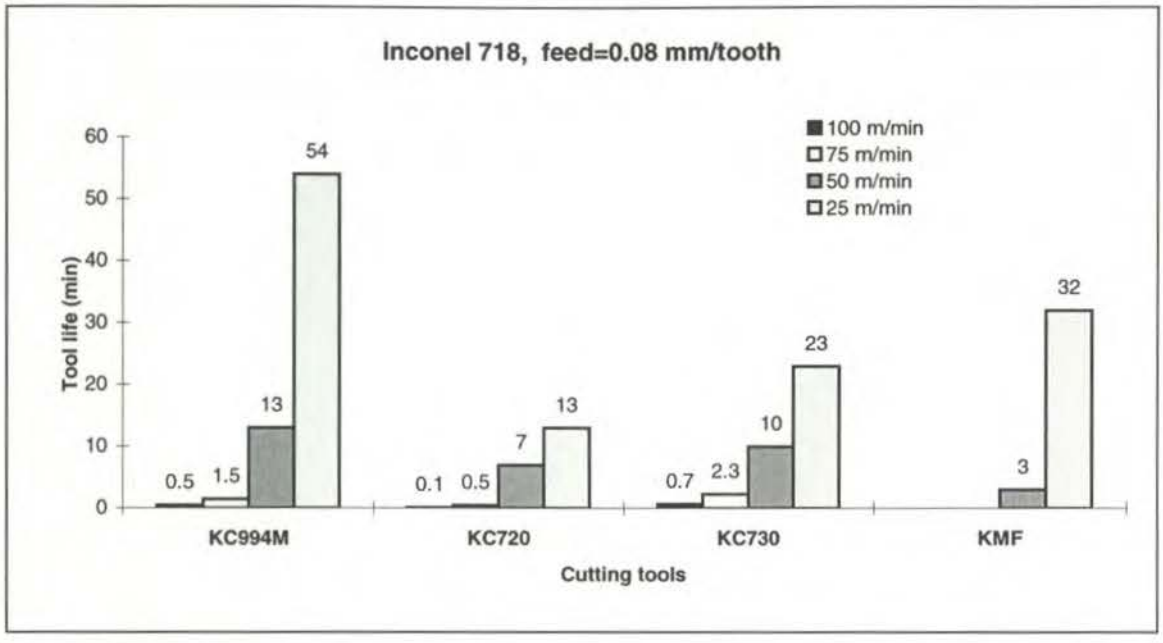

Figure 7. 48 Tool life comparison of coated and uncoated tools used for face milling Inconel 718 at various cutting speed with a feed rate of 0.08 mm/tooth

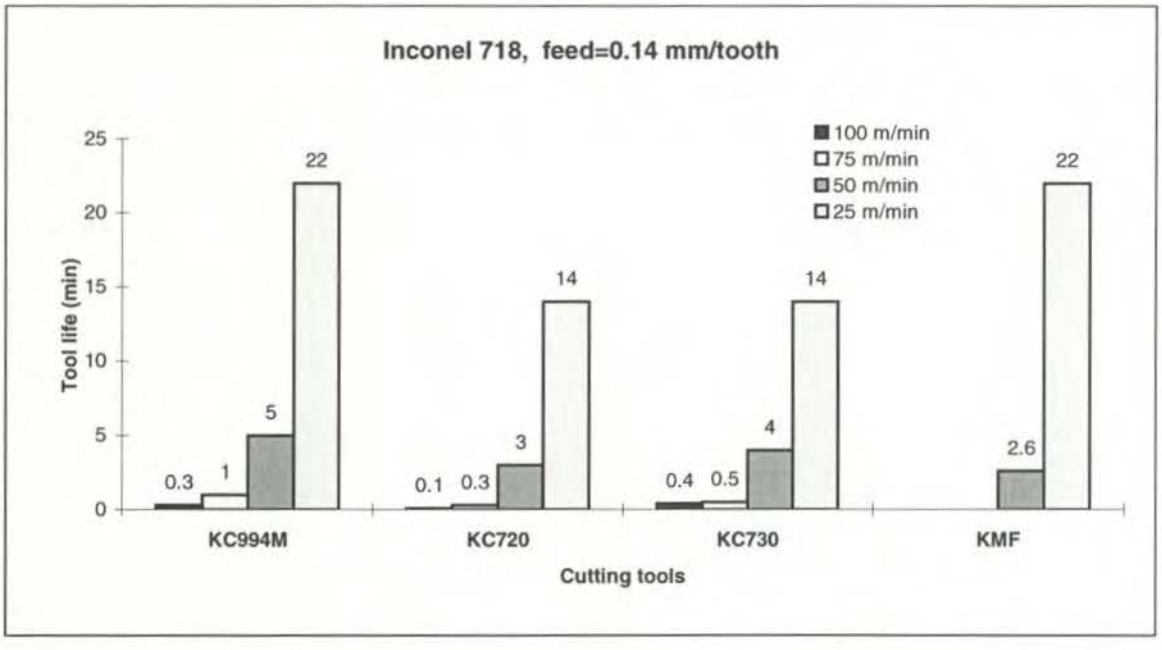

Figure 7. 49 Tool life comparison of coated and uncoated tools used for face milling Inconel 718 at various cutting speed with a feed rate of 0.14 mm/tooth

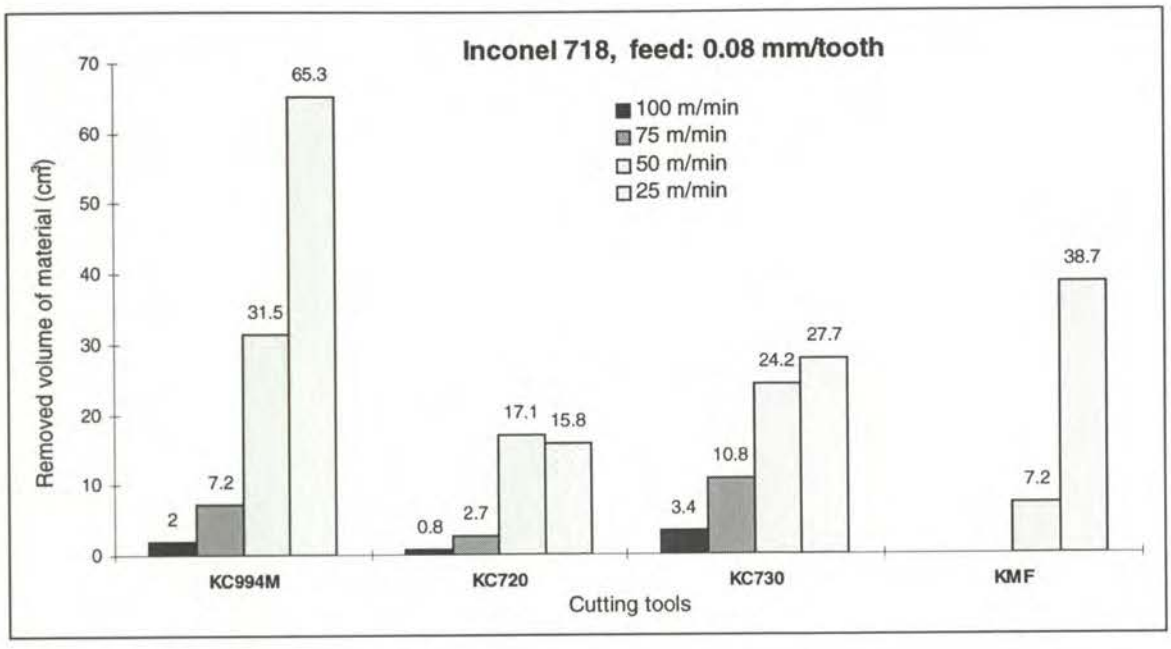

Figure 7. 50 Comparison of the volume of material removed with various types of coated and uncoated tools when face milling Inconel 718 at various cutting speed and a feed rate of 0.08 mm/tooth

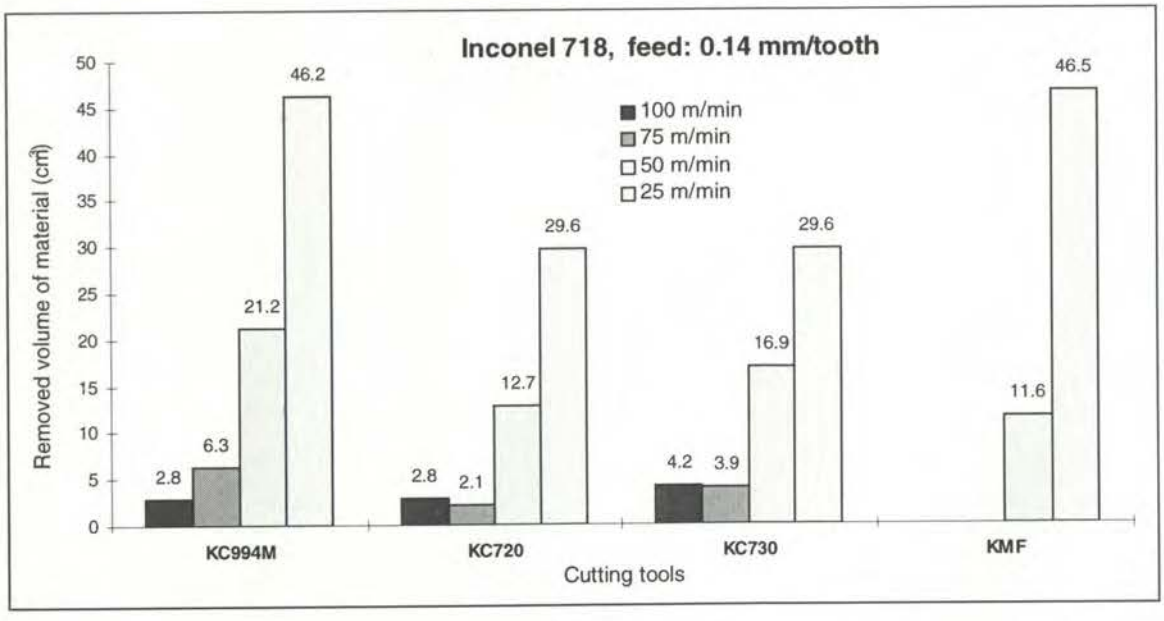

Figure 7. 51 Comparison of the volume of material removed with various types of coated and uncoated tools when face milling Inconel 718 at various cutting speed and feed rate of 0.14 mm/tooth

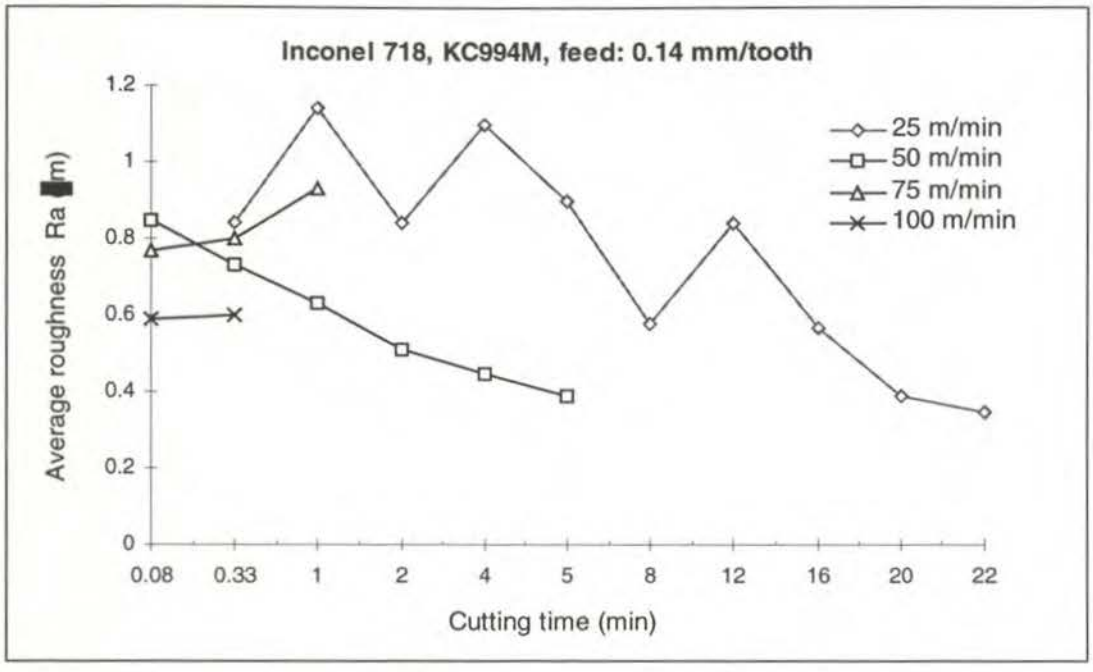

Figure 7. 52 Surface roughness versus cutting time when face milling Inconel 718 with KC994M tool at various cutting speeds and feed rate of 0.14 mm/tooth

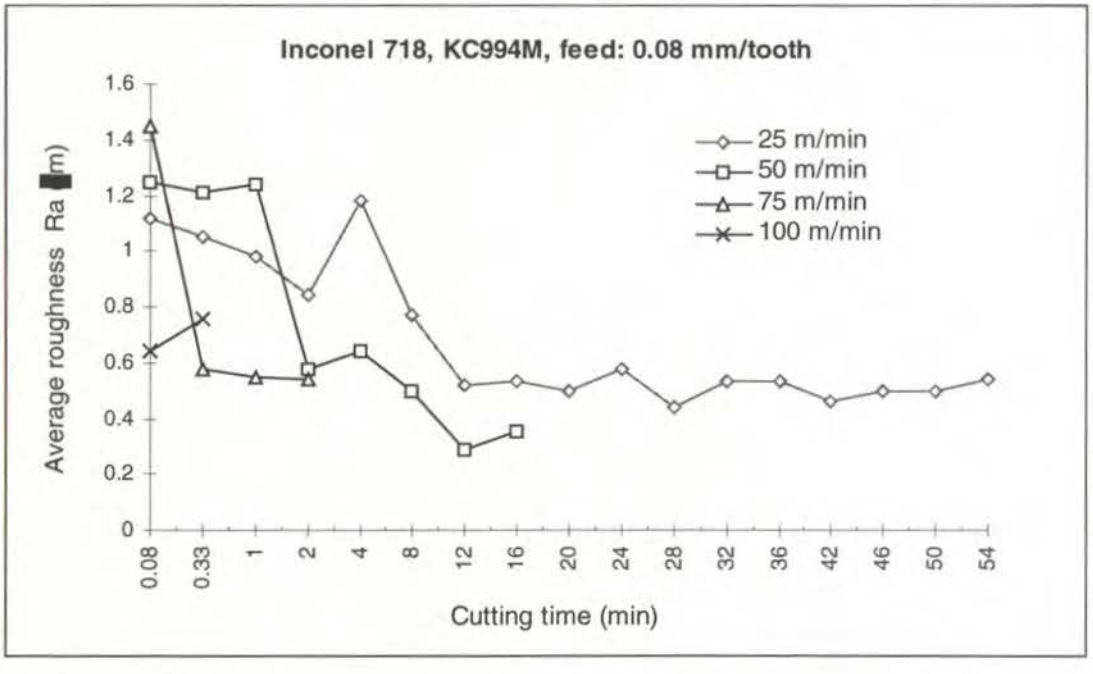

Figure 7. 53 Surface roughness versus cutting time when face milling Inconel 718 with KC994M tool at various cutting speeds and feed rate of 0.08 mm/tooth

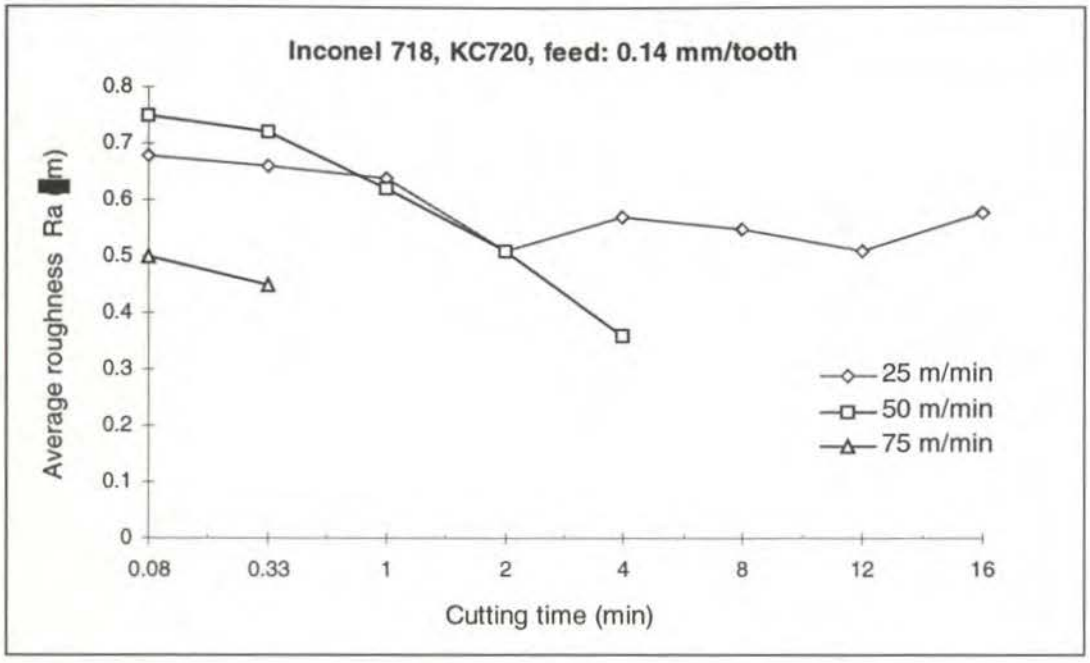

Figure 7. 54 Surface roughness versus cutting time when face milling Inconel 718 with KC720 tool at various cutting speeds and feed rate of 0.14 mm/tooth

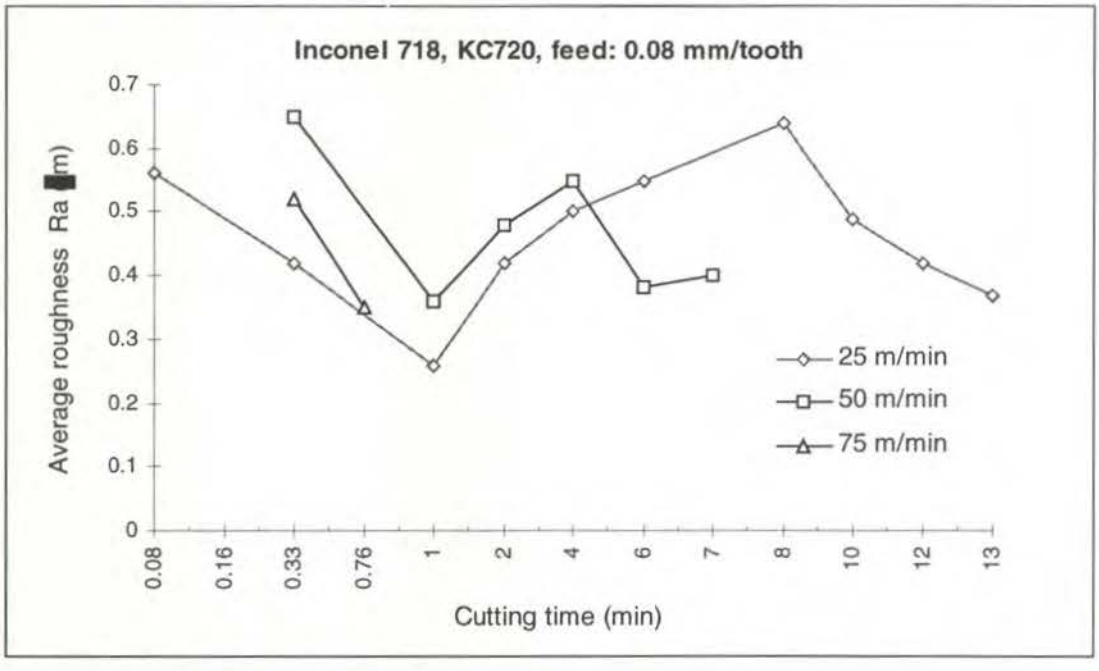

Figure 7. 55 Surface roughness versus cutting time when face milling Inconel 718 with KC720 tool at various cutting speeds and feed rate of 0.08 mm/tooth

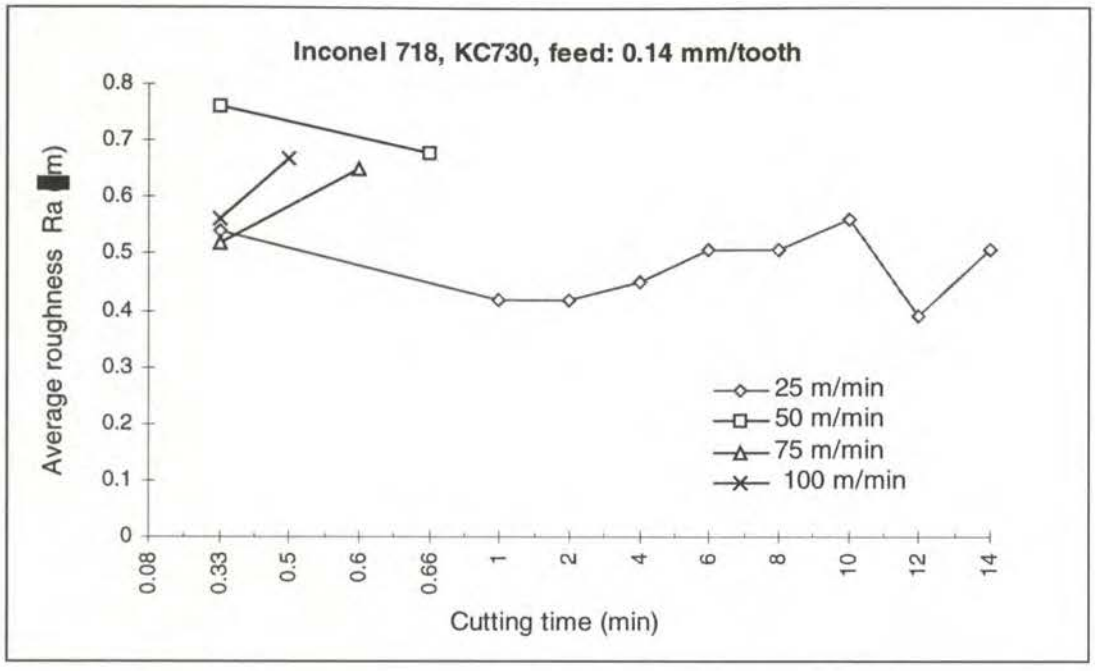

Figure 7. 56 Surface roughness versus cutting time when face milling Inconel 718 with KC730 tool at various cutting speeds and feed rate of 0.14 mm/tooth

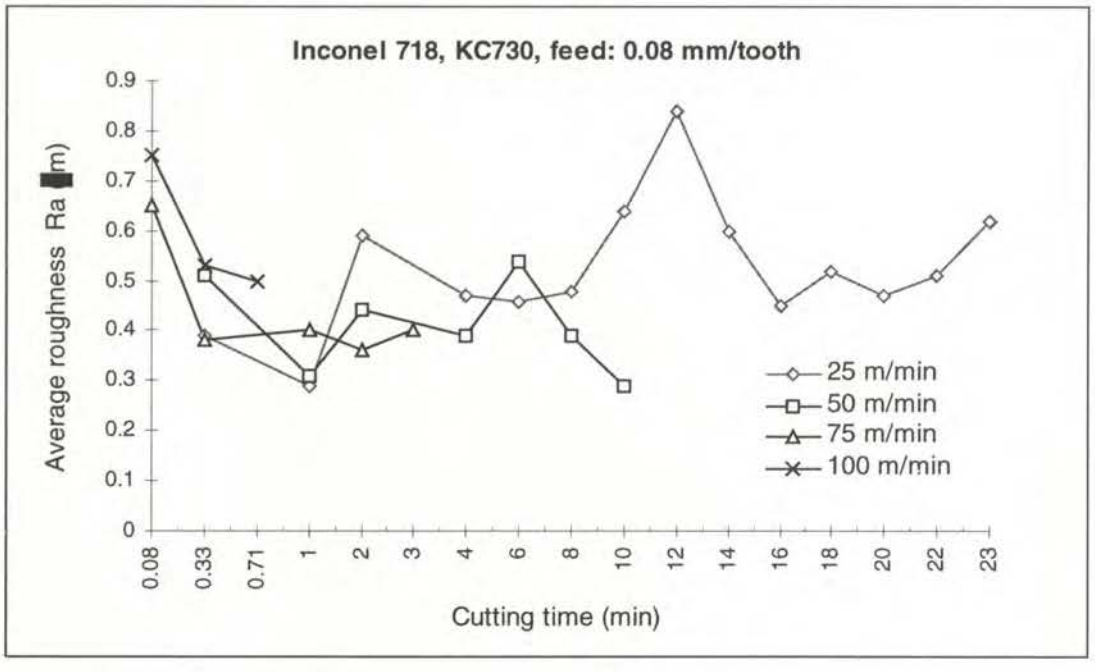

Figure 7. 57 Surface roughness versus cutting time when face milling Inconel 718 with KC730 tool at various cutting speeds and feed rate of 0.08 mm/tooth

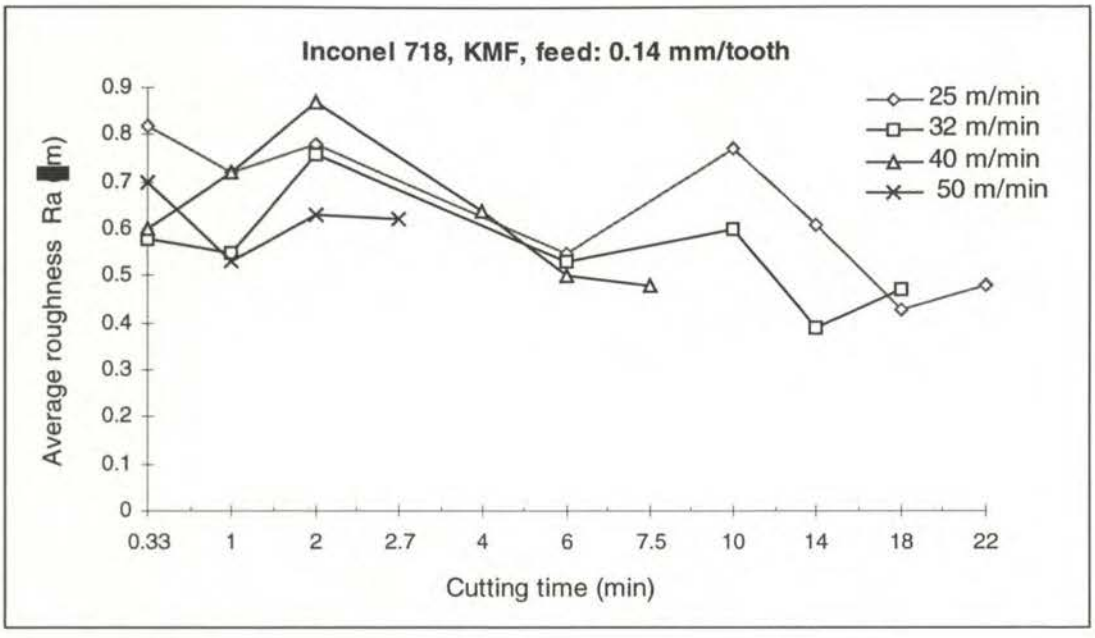

Figure 7. 58 Surface roughness versus cutting time when face milling Inconel 718 with KMF tool at various cutting speeds and feed rate of 0.14 mm/tooth

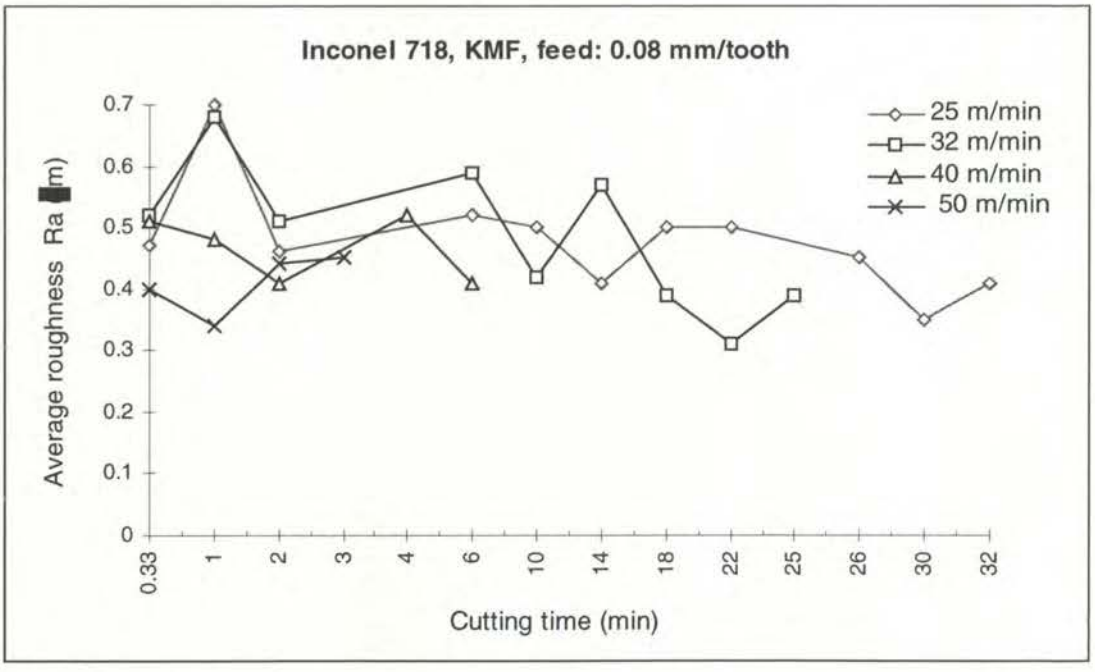

Figure 7. 59 Surface roughness versus cutting time when face milling Inconel 718 with KMF tool at various cutting speeds and feed rate of 0.08 mm/tooth

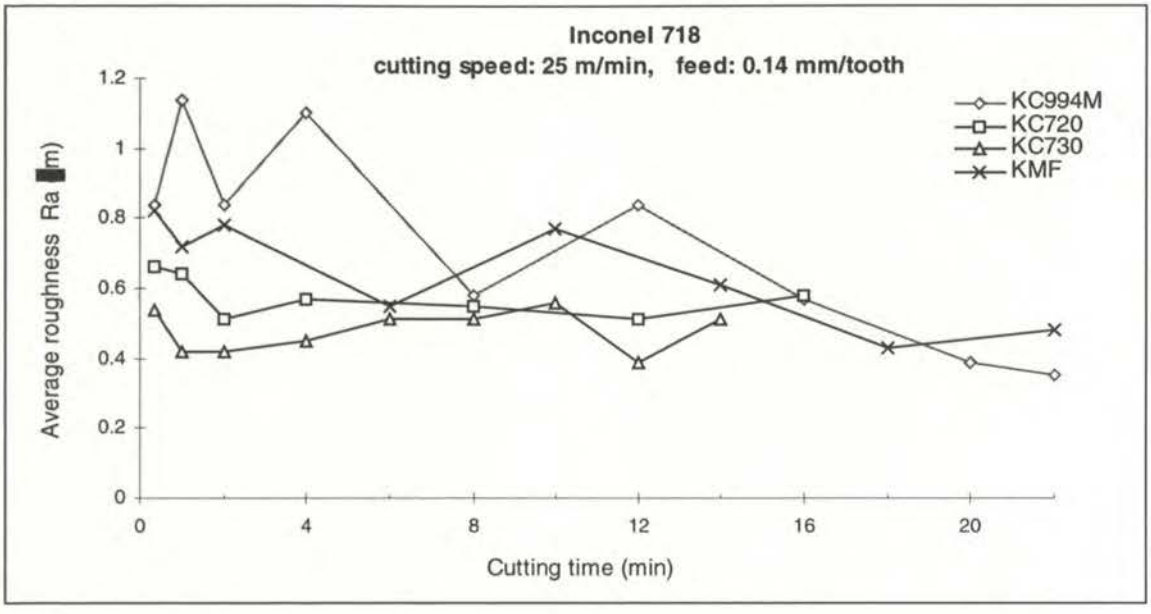

Figure 7. 60 Comparison of surface roughness when face milling Inconel 718 with different types cutting tools at a cutting speed of 25 m/min and feed rate of 0.14 mm/tooth

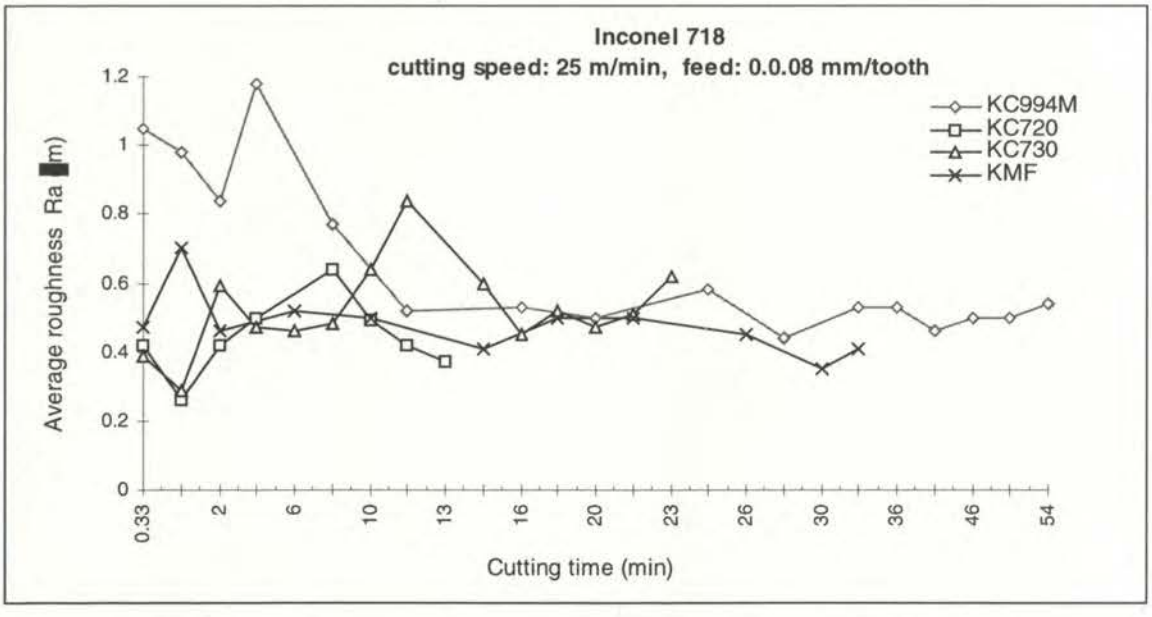

Figure 7. 61 Comparison of surface roughness when face milling Inconel 718 with different types cutting tools at a cutting speed of 25 m/min and feed rate of 0.08 mm/tooth

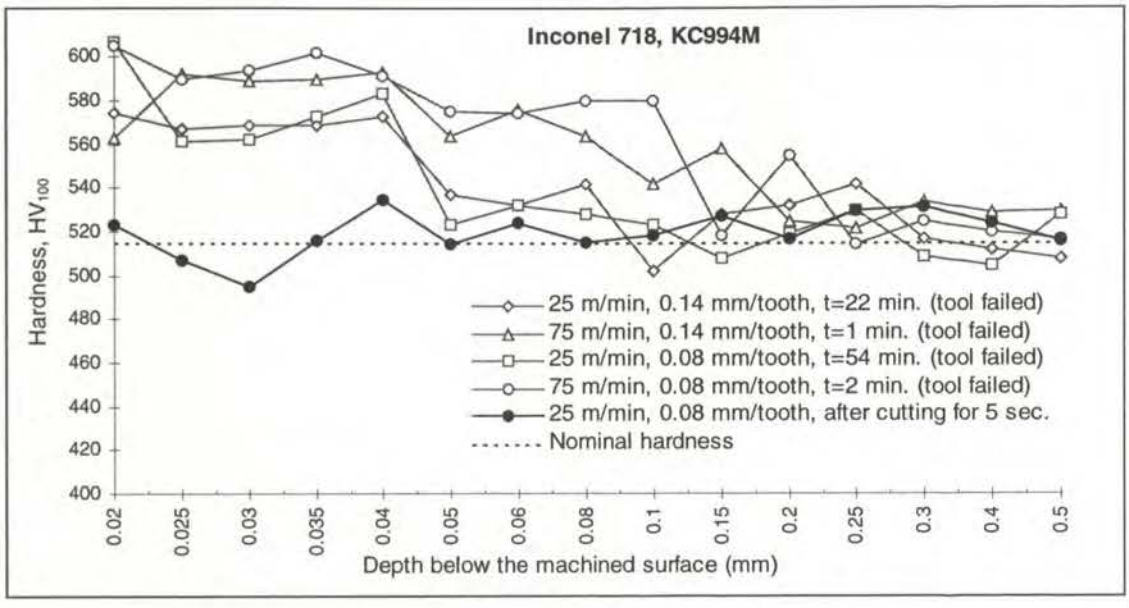

Figure 7. 62 Subsurface microhardness trends of Inconel 718 when face milling with KC994M tool at various cutting conditions

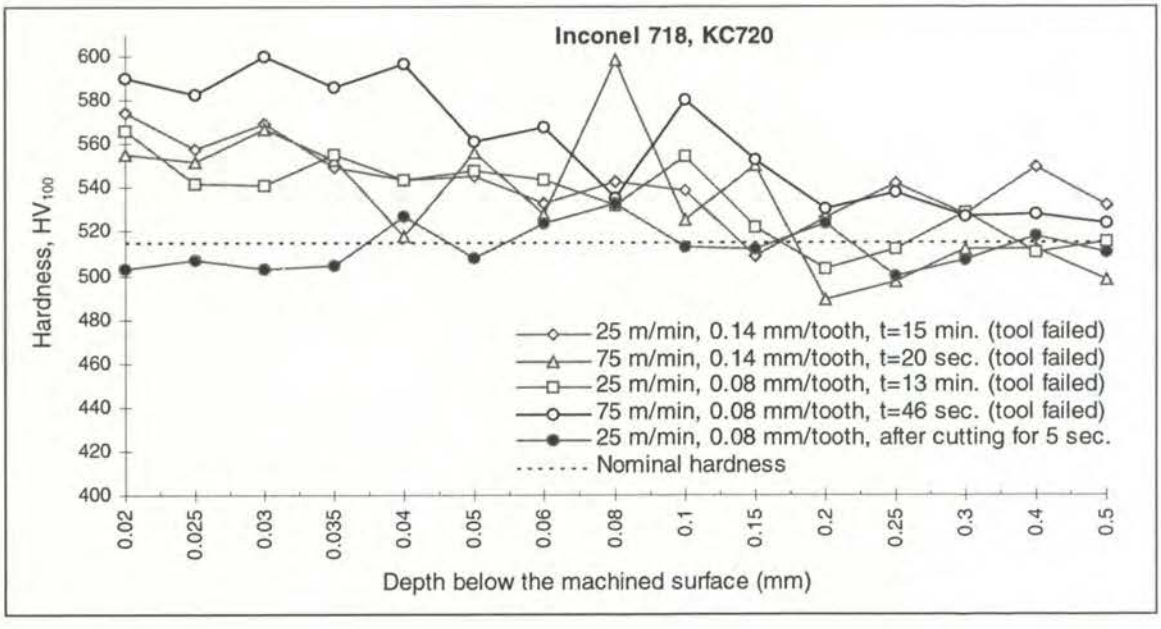

Figure 7. 63 Subsurface microhardness trends of Inconel 718 when face milling with KC720 tool at various cutting conditions

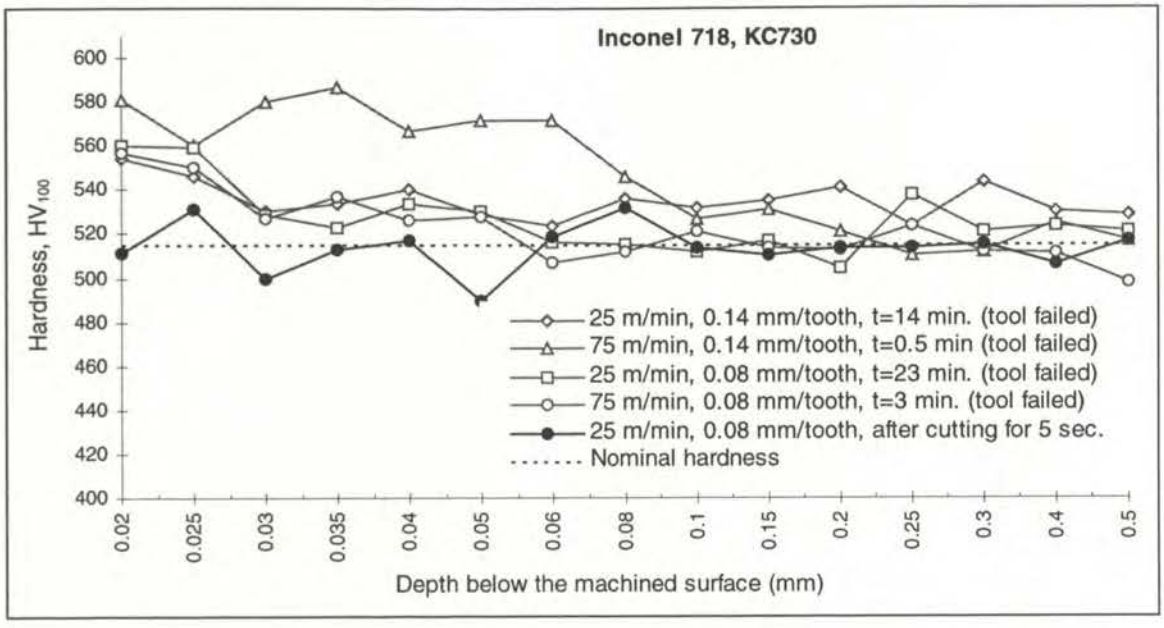

Figure 7. 64 Subsurface microhardness trends of Inconel 718 when face milling with KC730 tool at various cutting conditions

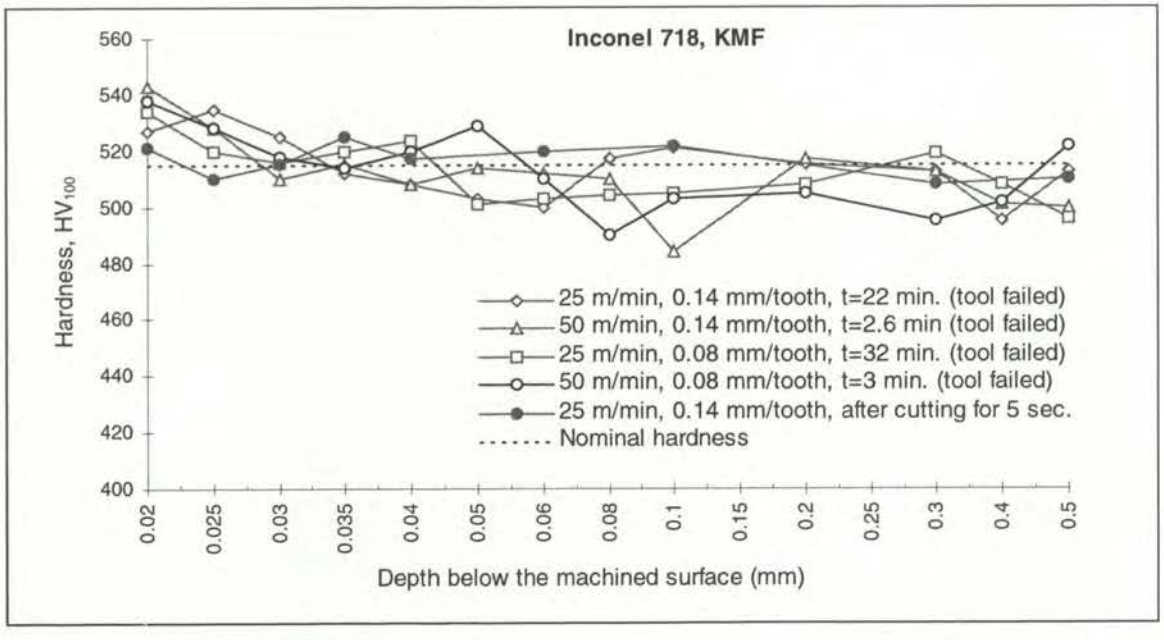

Figure 7. 65 Subsurface microhardness trends of Inconel 718 when face milling with KMF tool at various cutting conditions

Figure 7. 66 Evidence of plastic flow and disturbed layer after face milling Inconel 718 with KC994M tool for 22 minutes at 25 m/min and 0.14 mm/tooth

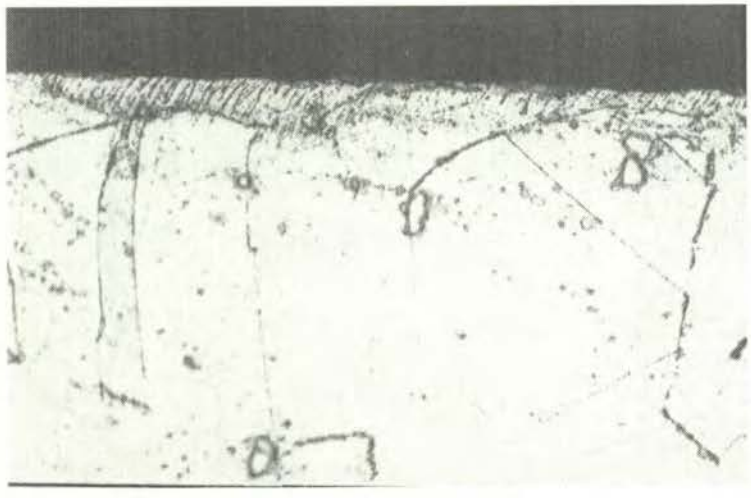

Figure 7. 67 Evidence of initial plastic flow after milling Inconel 718 with KC994M tool for 5 seconds at 25 m/min and 0.14 mm/tooth

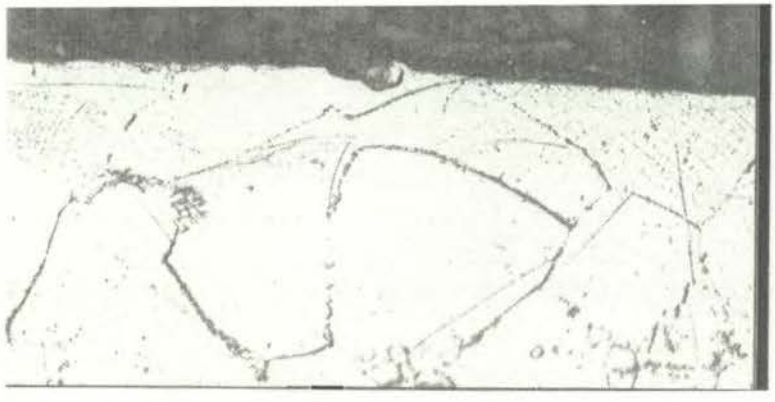

Figure 7. 68 Surface damage caused by an embedded hard particles after face milling Inconel 718 with KC994M tool for 1 minute at 75 m/min and 0.14 mm/tooth

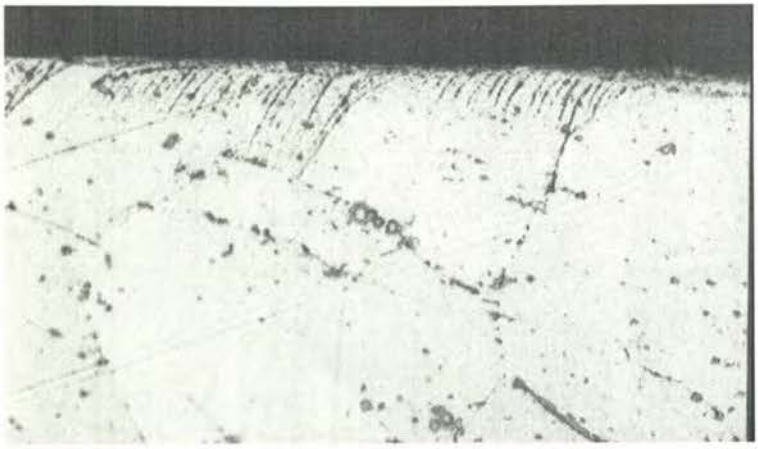

Figure 7. 69 Evidence of plastic flow and disturbed layer after milling Inconel 718 with KC994M tool for 54 minutes at 25 m/min and 0.08 mm/tooth

Figure 7. 70 Slight initial plastic flow after milling Inconel 718 with KC994M tool for 5 seconds at 25 m/min and 0.08 mm/tooth

Figure 7. 71 Evidence of severe surface tearing after milling Inconel 718 with KC994M tool for 2 minutes at 75 m/min and 0.08 mm/tooth (243X)

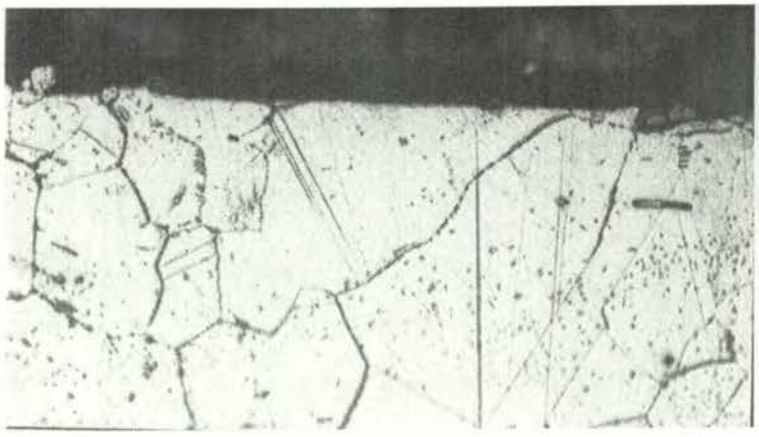

Figure 7. 72 Surface tearing of initial cutting stage after milling Inconel 718 with KC994M tool for 5 seconds at 75 m/min and 0.08 mm/tooth

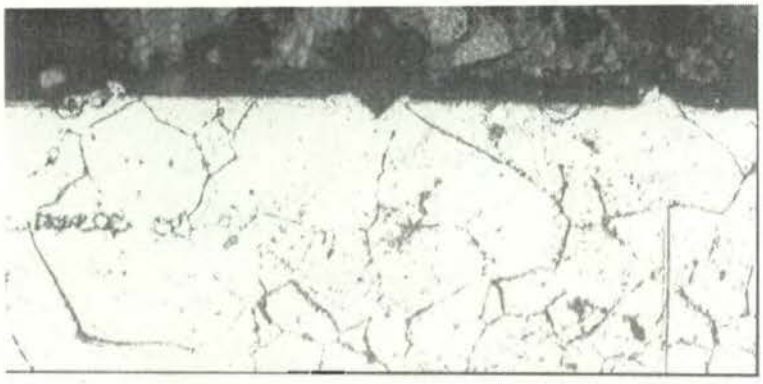

Figure 7. 73 Evidence of surface damage of initial cutting stage after milling Inconel 718 with KC720 tool for 5 seconds at 25 m/min and 0.14 mm/tooth (243X)

Figure 7. 74 Surface irregularity and slightly disturbed layer after face milling Inconel 718 with KC720 tool for 14 minutes at 25 m/min and 0.14 mm/tooth

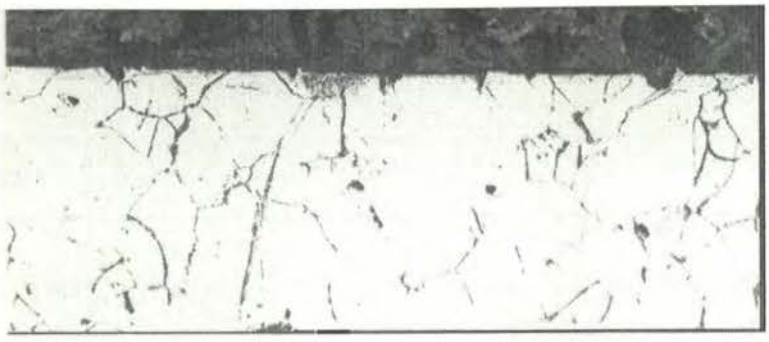

Figure 7. 75 Evidence of surface tearing after face milling Inconel 718 with KC720 tool for 5 seconds at 75 m/min and 0.14 mm/tooth (243X)

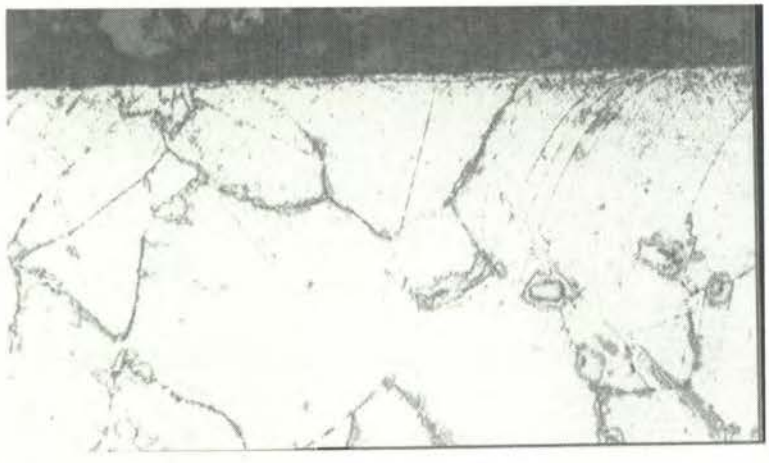

Figure 7. 76 Evidence of plastic flow and disturbed layer after face milling Inconel 718 with KC720 tool for 13 minutes at 25 m/min and 0.08 mm/tooth

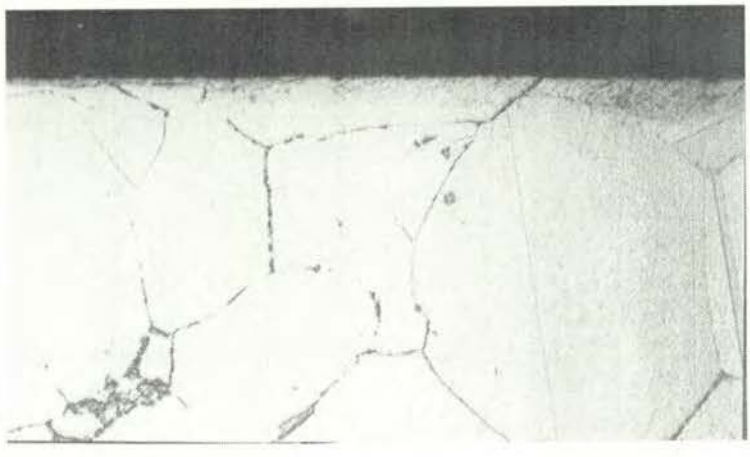

Figure 7. 77 Slight plastic flow of initial cutting stage after face milling Inconel 718 with KC720 tool for 5 seconds at 25 m/min and 0.08 mm/tooth

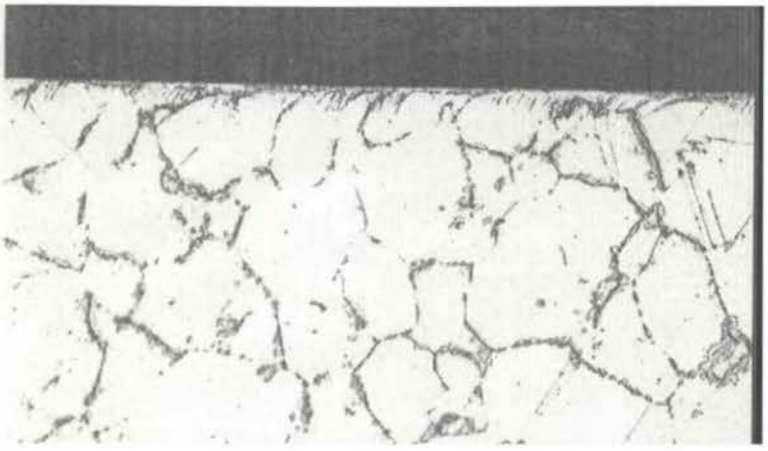

Figure 7. 78 Surface plastic flow after face milling Inconel 718 with KC730 tool for 14 minutes at 25 m/min and 0.14 mm/tooth

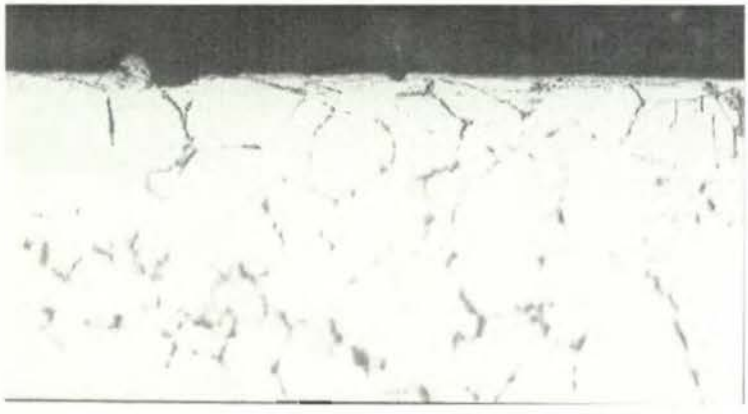

Figure 7. 79 Damaged and plastically disturbed surface layer after face milling Inconel 718 with KC730 tool for 14 minutes at 25 m/min and 0.14 mm/tooth

Figure 7. 80 Occasional surface damage occurred after face milling Inconel 718 with KC730 tool for 5 seconds at 25 m/min and 0.14 mm/tooth

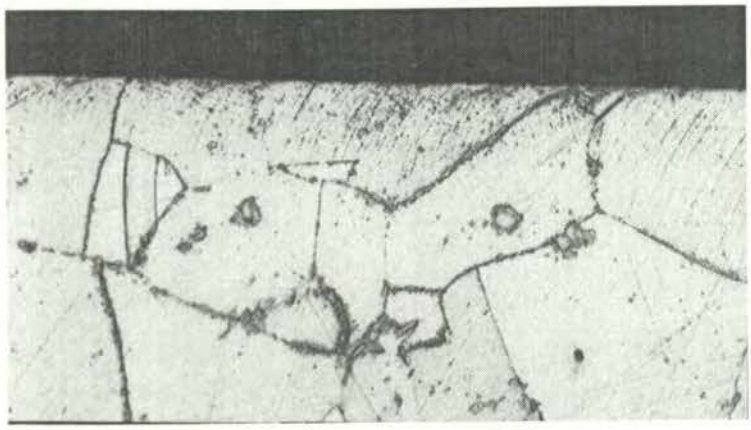

Figure 7. 81 Evidence of plastic flow after face milling Inconel 718 with KC730 tool for 23 minutes at 25 m/min and 0.08 mm/tooth

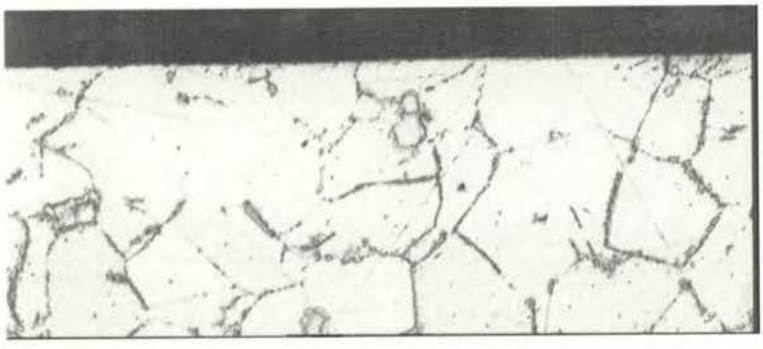

Figure 7. 82 Initial surface with no significant defect after face milling Inconel 718 with KC730 tool for 5 seconds at 25 m/min and 0.08 mm/tooth

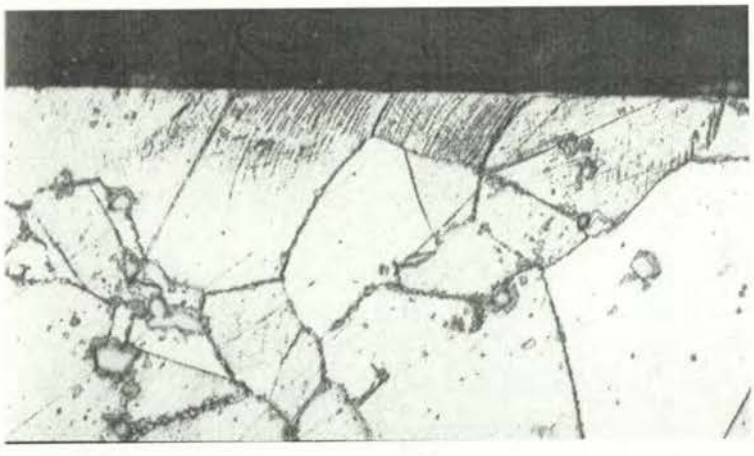

Figure 7. 83 Evidence of plastic flow after face milling Inconel 718 with KC730 tool for 3 minutes at 75 m/min and 0.08 mm/tooth

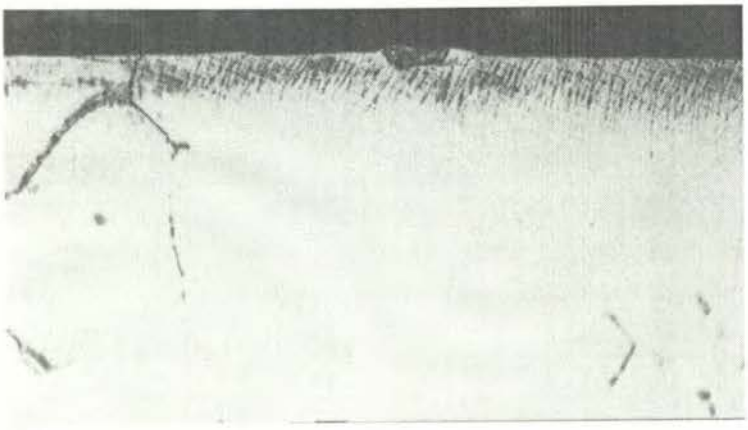

Figure 7. 84 Surface with an embedded hard particle (possibly from tool material) and plastic flow after face milling Inconel 718 with KC730 tool for 3 minutes at 75 m/min and 0.08 mm/tooth

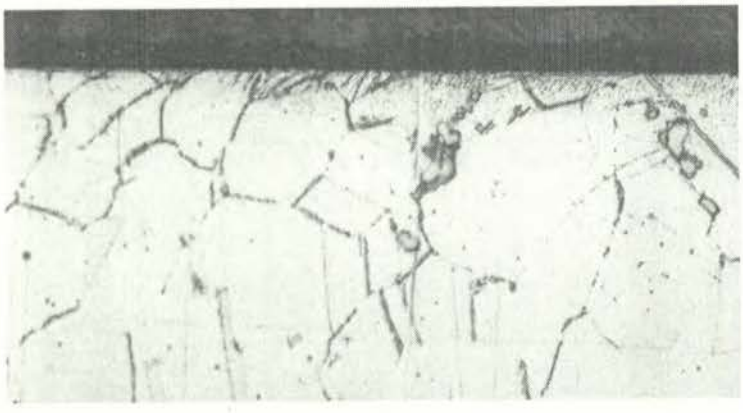

Figure 7. 85 Evidence of plastic flow after face milling Inconel 718 with KMF tool for 32 minutes at 25 m/min and 0.08 mm/tooth

Figure 7. 86 Evidence of plastic flow after face milling Inconel 718 with KMF tool for 22 minutes at 25 m/min and 0.14 mm/tooth

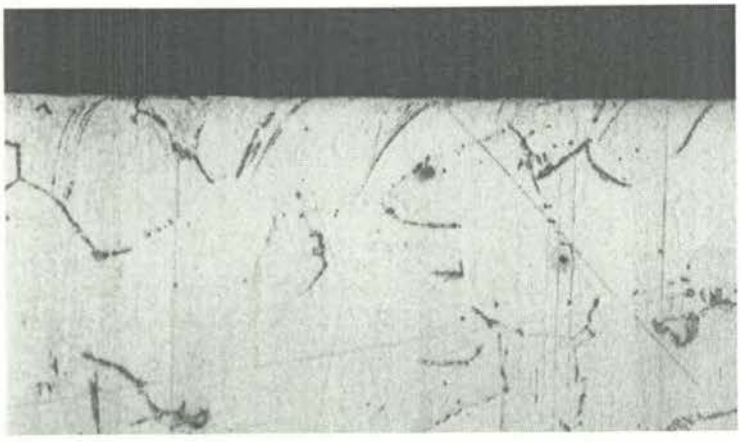

Figure 7. 87 Minor plastic flow of the subsurface after face milling Inconel 718 with KMF tool for 3 minutes at 50 m/min and 0.08 mm/tooth

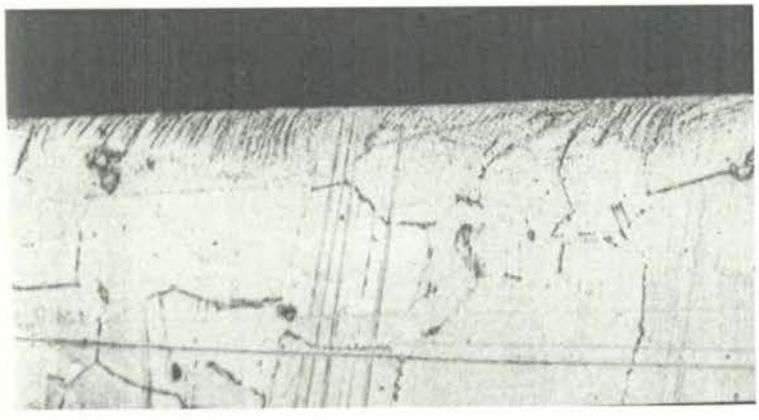

Figure 7. 88 Evidence of plastic flow after face milling Inconel 718 with KMF tool for 3 minutes at 50 m/min and 0.14 mm/tooth

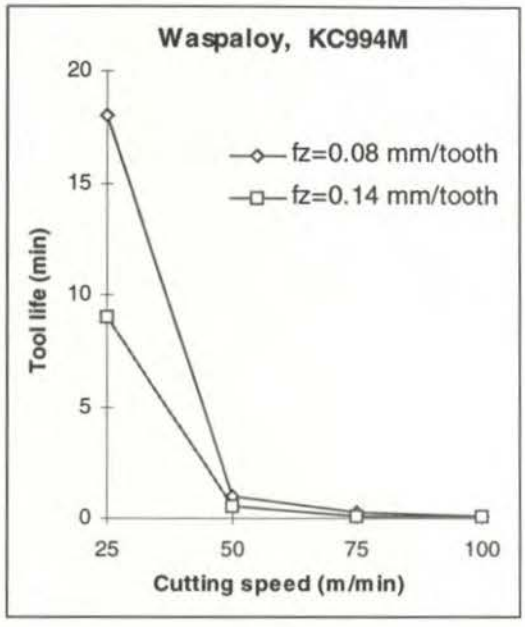

(a) Tool: KC994M

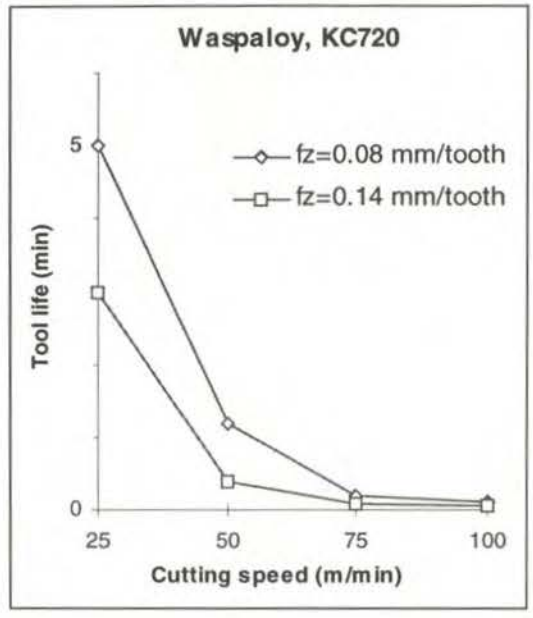

(b) Tool: KC720

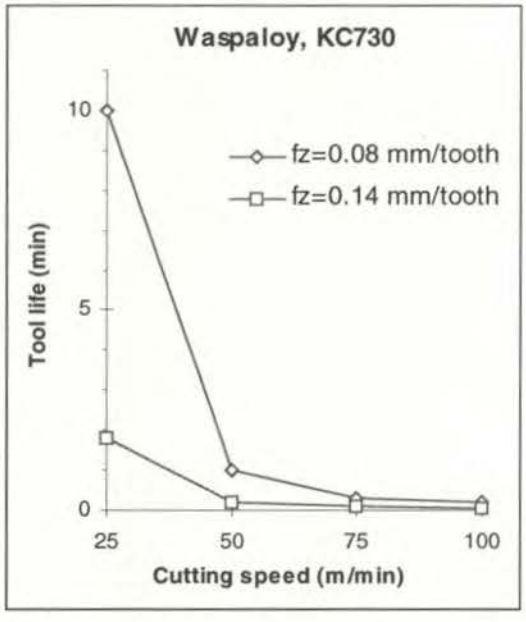

(c) Tool: KC730

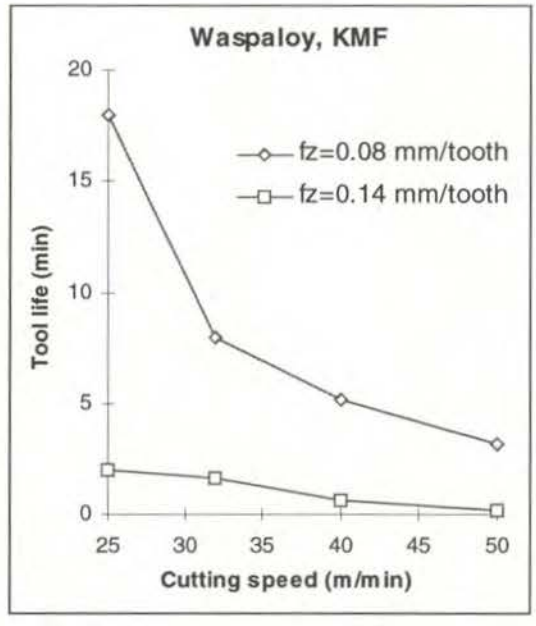

(d) Tool: KMF

Figure 7. 89 The effect of cutting speed and feed rate when face milling Waspaloy with coated and uncoated tools

Figure 7. 90 Premature failure by severe breakage and chipping, and resultant workpiece adhesion and coating delamination on the plastically deformed rake of KC994M tool after 10 seconds cutting Waspaloy at 75 m/min and 0.14 mm/tooth

Figure 7. 91 Progressive chipping, plucking, galling and plastic deformation-related coating delamination on KC994M tool after 18 minutes when cutting Waspaloy at 25 m/min and 0.08 mm/tooth

Figure 7. 92 Premature failure due to severe breakage of KC994M tool after 1 minute when cutting Waspaloy at 50 m/min and 0.08 mm/tooth

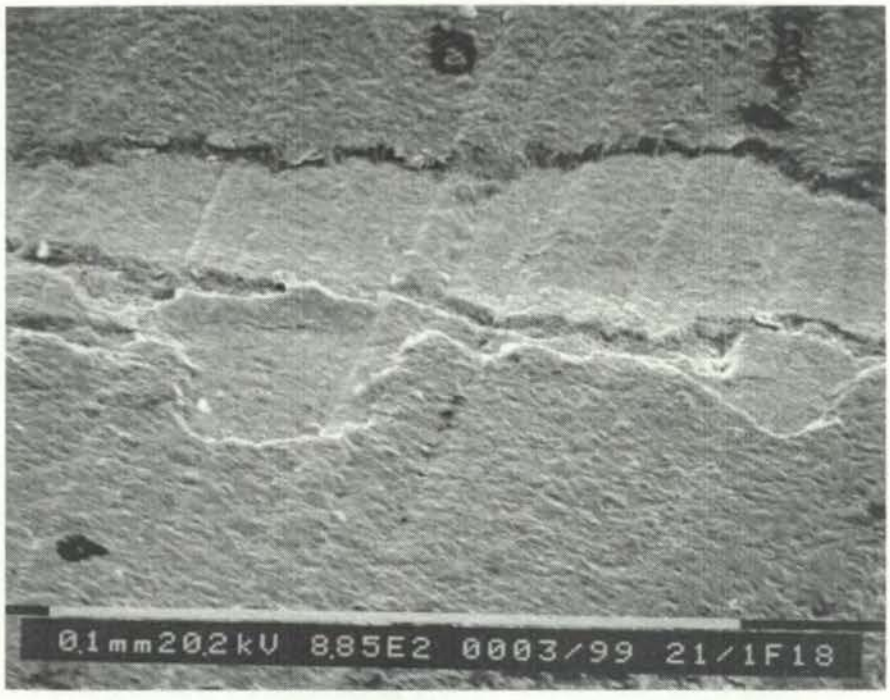

Figure 7. 93 Magnified view of Figure 7.91 showing pealed Al_2O_3 top coating layer due to deformation of the rake face of KC994M tool

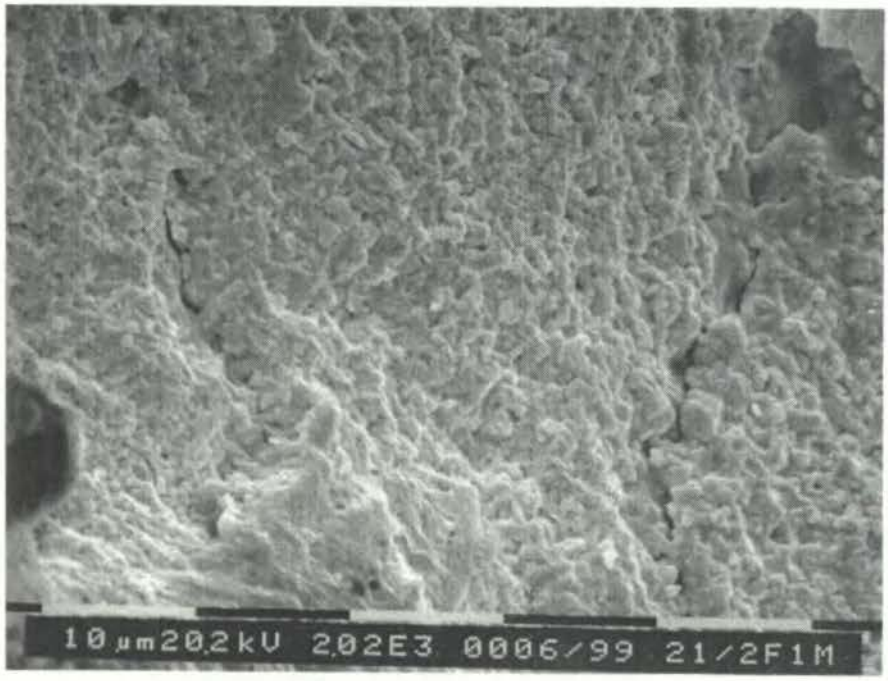

Figure 7. 94 Magnified view of Figure 7.92 showing cracks in the substrate of failed KC994M tool

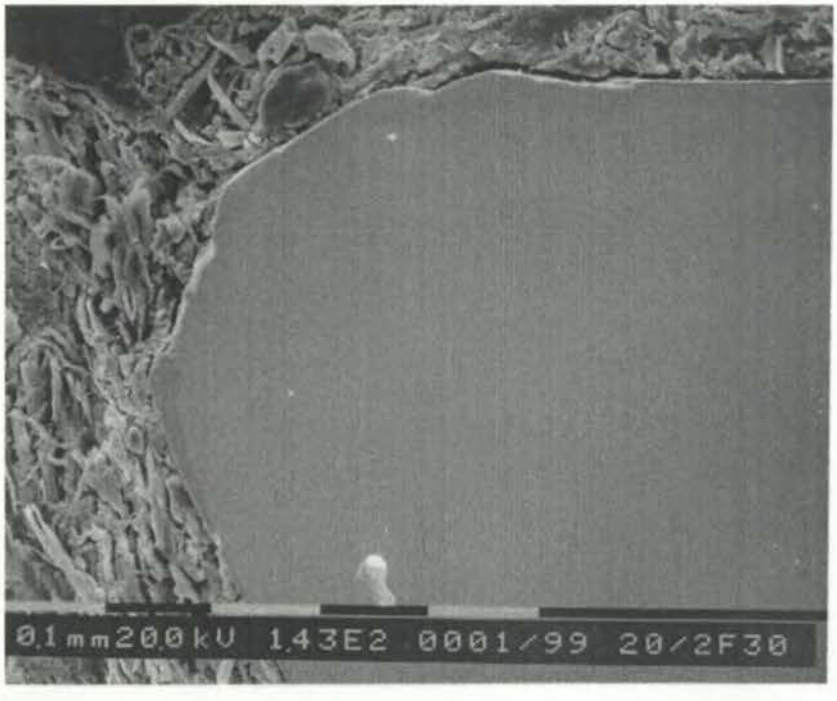

Figure 7. 95 Section trough failed KC994M tool showing plastic deformation on the rake face and adhered workpiece material on the flank after cutting Waspaloy for 30 seconds at 50 m/min and 0.14 mm/tooth

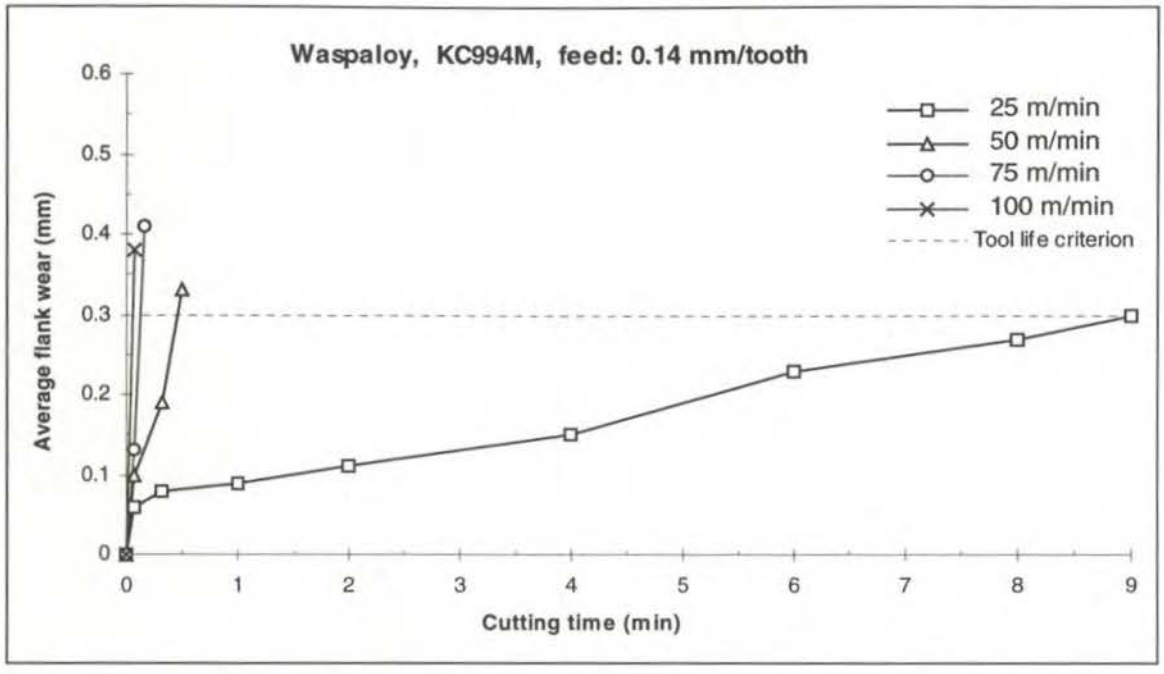

Figure 7. 96 Average flank wear versus cutting time when face milling Waspaloy with KC994M tool at a feed rate of 0.14 mm/tooth

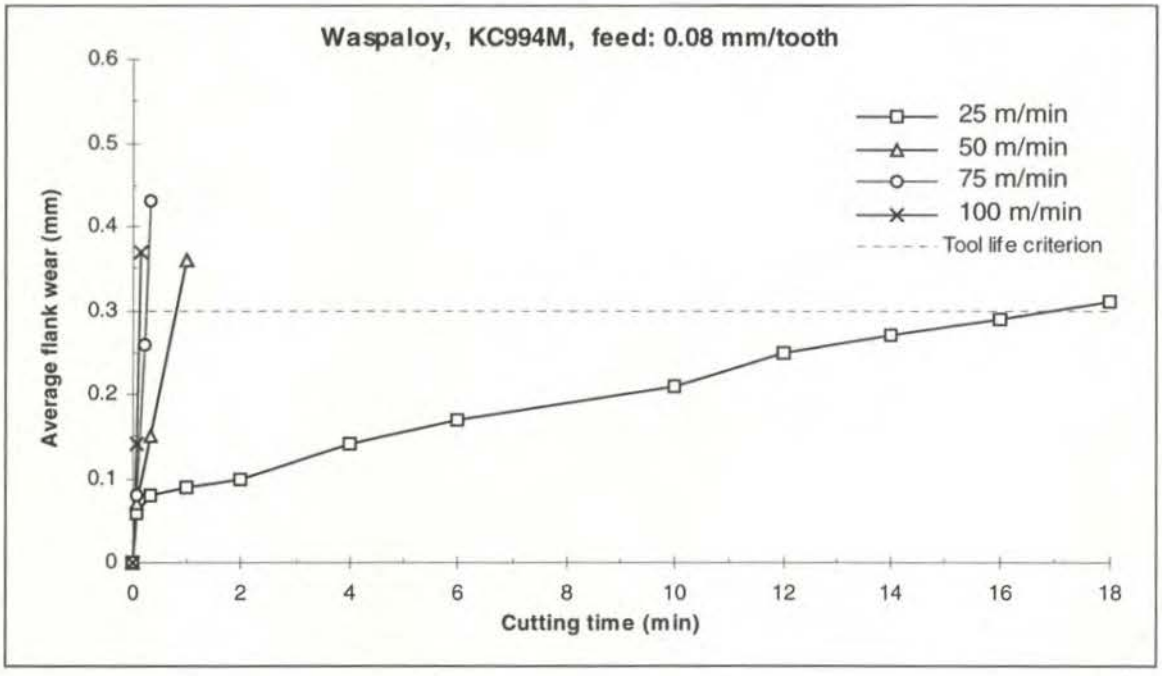

Figure 7. 97 Average flank wear versus cutting time when face milling Waspaloy with KC994M tool at a feed rate of 0.08 mm/tooth

(a)

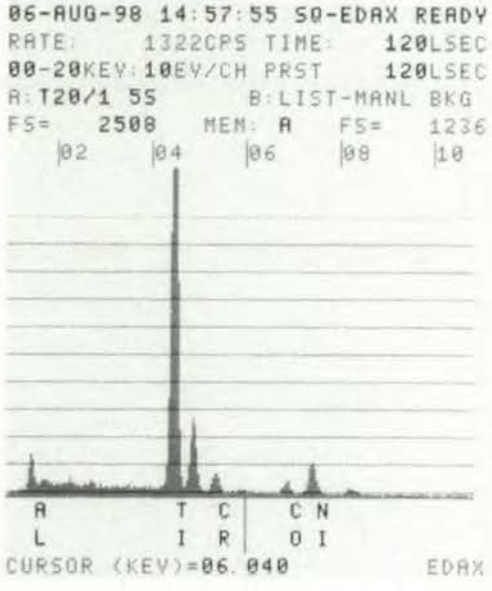

(b)

Figure 7. 98 (a) Premature delamination of Al_2O_3 top coating layer on the rake face of KC994M tool after machining Waspaloy for 5 seconds at 25 m/min and 0.14 mm/tooth. (b) EDAX analysis showing the exposure of second coating layer of TiCN on the rake face of KC994M tool

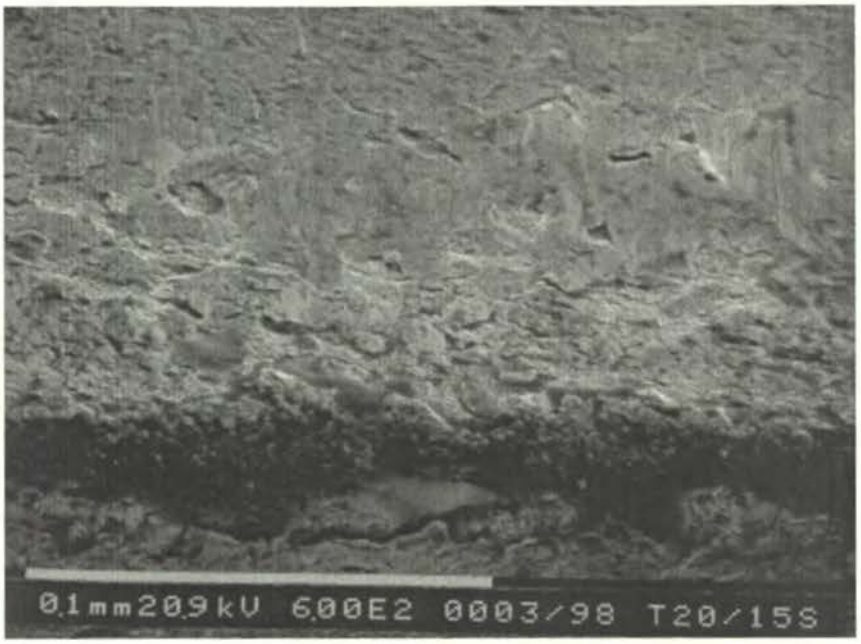

(a)

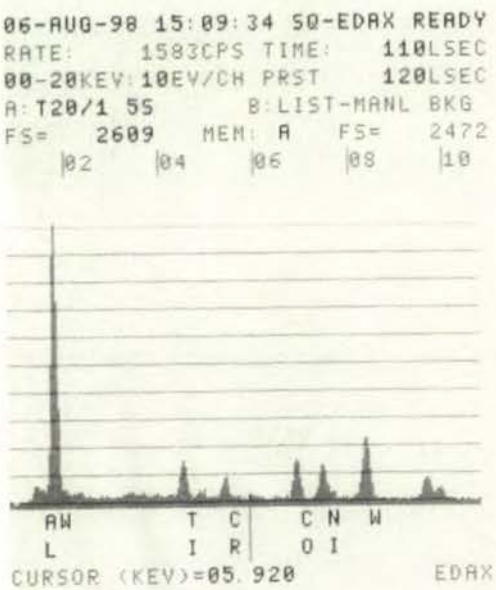

(b)

Figure 7. 99 (a) Workpiece galling and substrate pitting at the cutting edge (rake face) of KC994M tool after machining Waspaloy for 5 seconds at 25 m/min and 0.14 mm/tooth. (b) EDAX analysis showing the exposure of tool substrate in the pitted areas

(a)

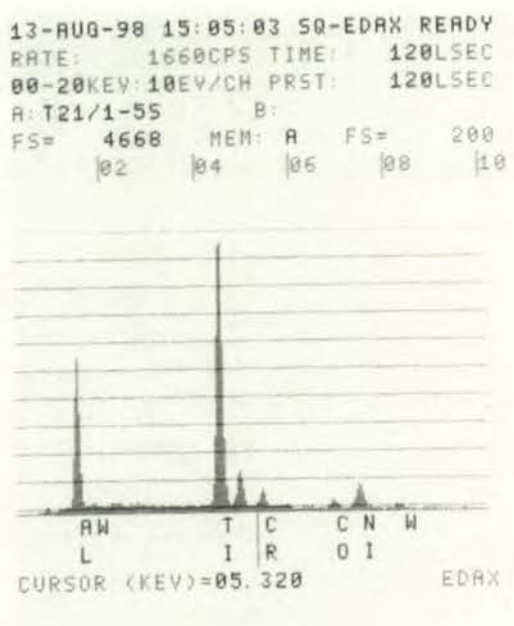

(b)

Figure 7. 100 (a) Workpiece galling and premature delamination of Al_2O_3 top coating layer on the nose rake and flank face of KC994M tool after machining Waspaloy for 5 seconds at 25 m/min and 0.08 mm/tooth. (b) EDAX analysis confirming the exposure of the second coating layer of TiCN on KC994M tool

Figure 7. 101 Excessive premature chipping of entire cutting edge and workpiece adhesion on KC994M tool after machining Waspaloy for 5 seconds at 75 m/min and 0.14 mm/tooth

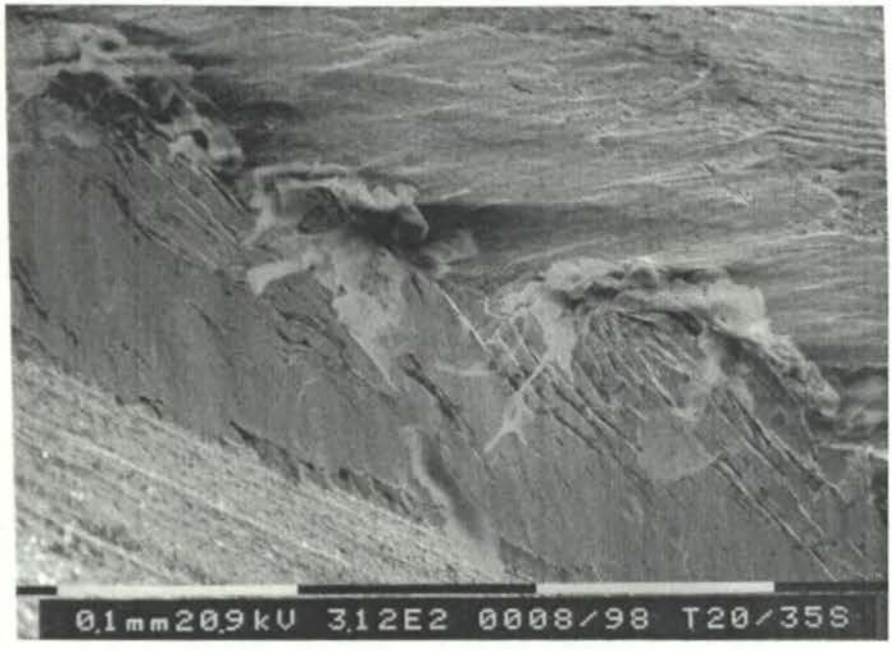

(a)

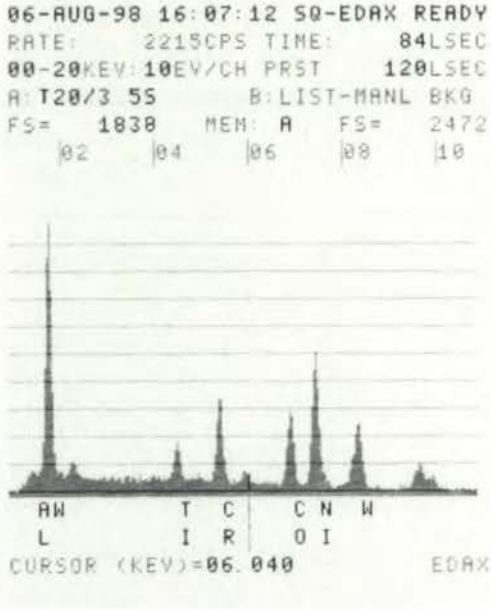

(b)

Figure 7. 102 (a) Excessive initial workpiece adhesion in the form of lumps and galling on KC994M tool after machining Waspaloy for 5 seconds at 75 m/min and 0.14 mm/tooth. (b) Respective EDAX analysis on KC994M tool indicating adhesion and substrate exposure

(a)

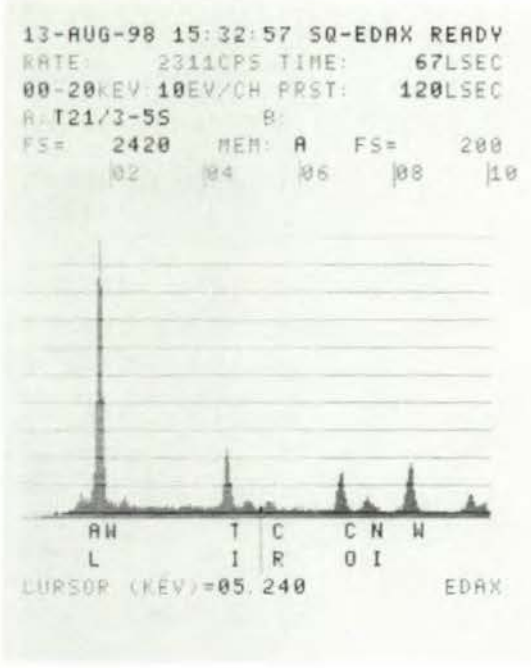

(b)

Figure 7. 103 (a) Initial microchipping, coating delamination and galling on KC994M tool after machining Waspaloy for 5 seconds at 75 m/min and 0.08 mm/tooth. (b)EDAX analysis showing the exposure of substrate of KC994M tool shown in Figure 7.103a

Figure 7. 104 Combination of chipping, plucking, coating delamination and galling on a failed KC720 tool after cutting Waspaloy for 3 minutes at 50 m/min and 0.14 mm/tooth

Figure 7. 105 Combination of chipping, plucking, coating delamination and galling on a failed KC720 tool after cutting Waspaloy for 5 minutes at 25 m/min and 0.08 mm/tooth

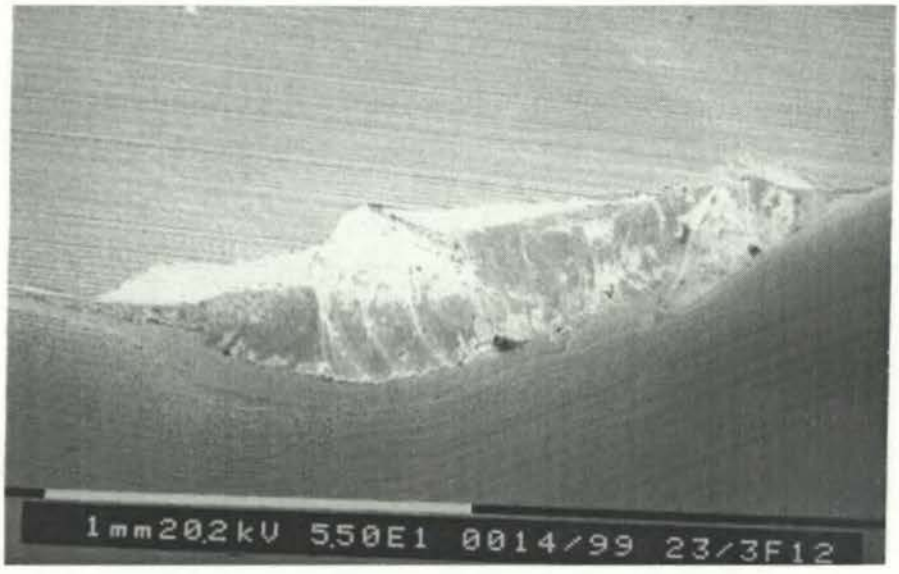

Figure 7. 106 Severe breakage, galling and coating delamination on a prematurely failed KC720 tool after cutting Waspaloy for 12 seconds at 75 m/min and 0.08 mm/tooth

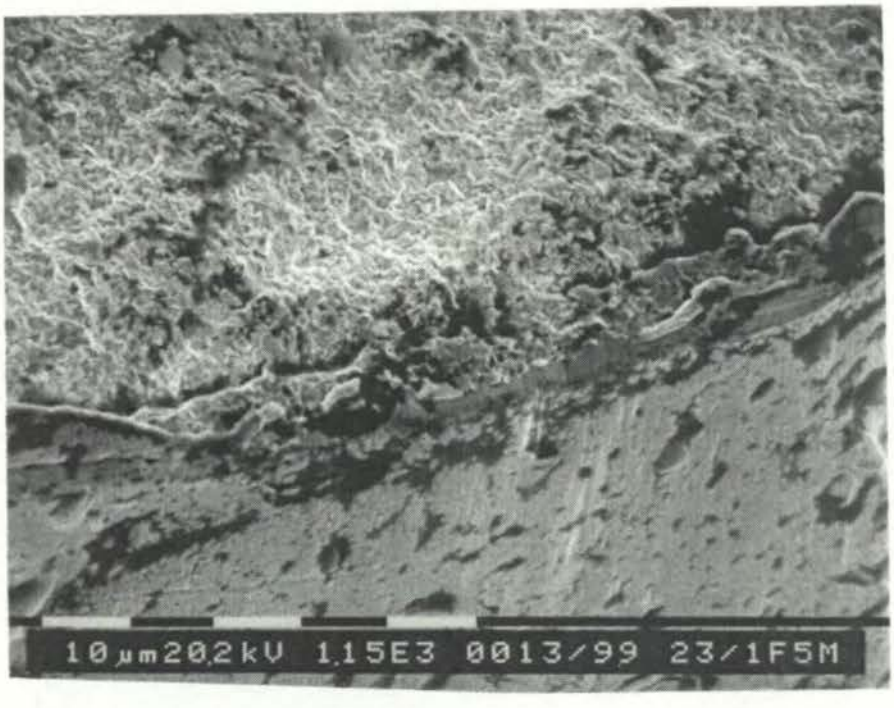

Figure 7. 107 Crack running parallel to the cutting edge of a failed KC720 tool with smooth flank wear after cutting Waspaloy for 5 minutes at 25 m/min and 0.08 mm/tooth

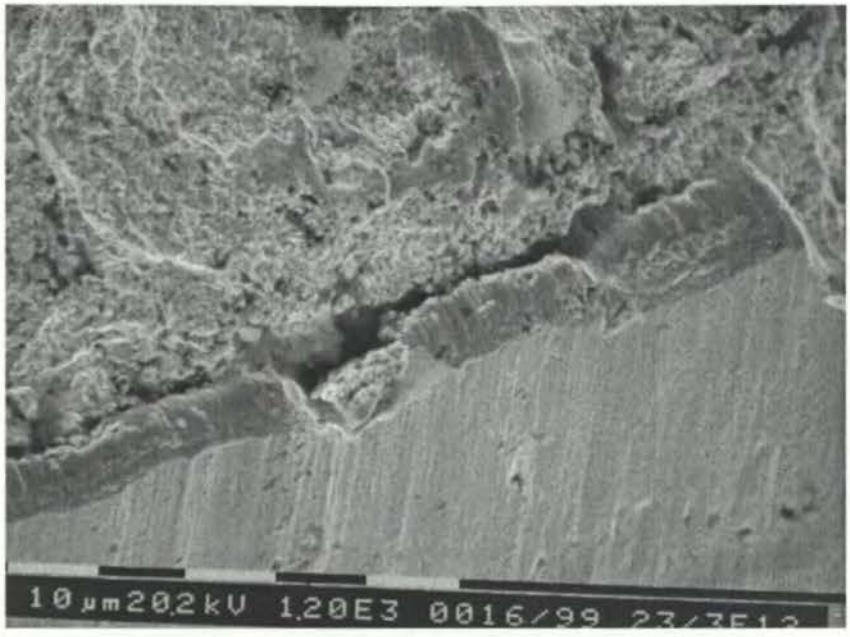

Figure 7. 108 Crack running parallel to the cutting edge of a failed KC720 tool with smooth flank wear after cutting Waspaloy for 5 minutes at 75 m/min and 0.08 mm/tooth

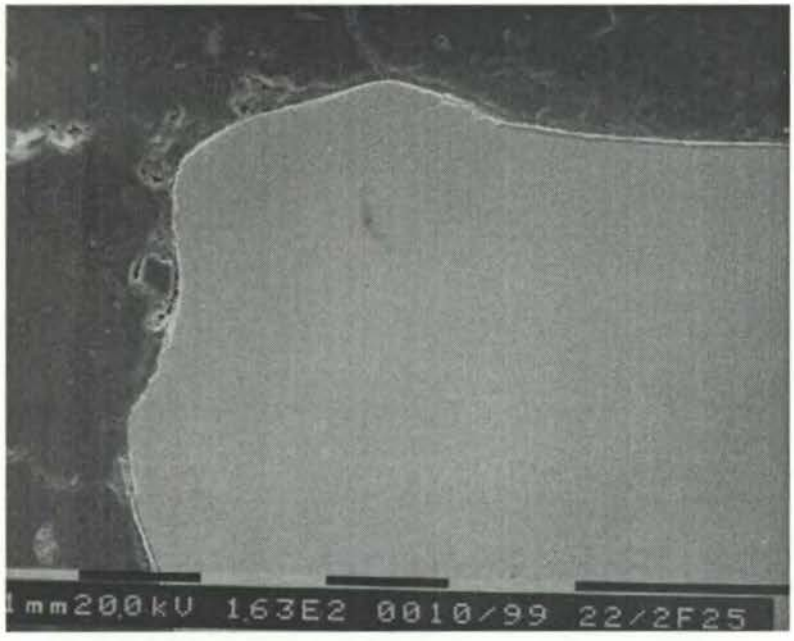

Figure 7. 109 Chipping and plastic deformation of the rake face of a failed KC720 tool after cutting Waspaloy for 25 seconds at 50 m/min and 0.14 mm/tooth

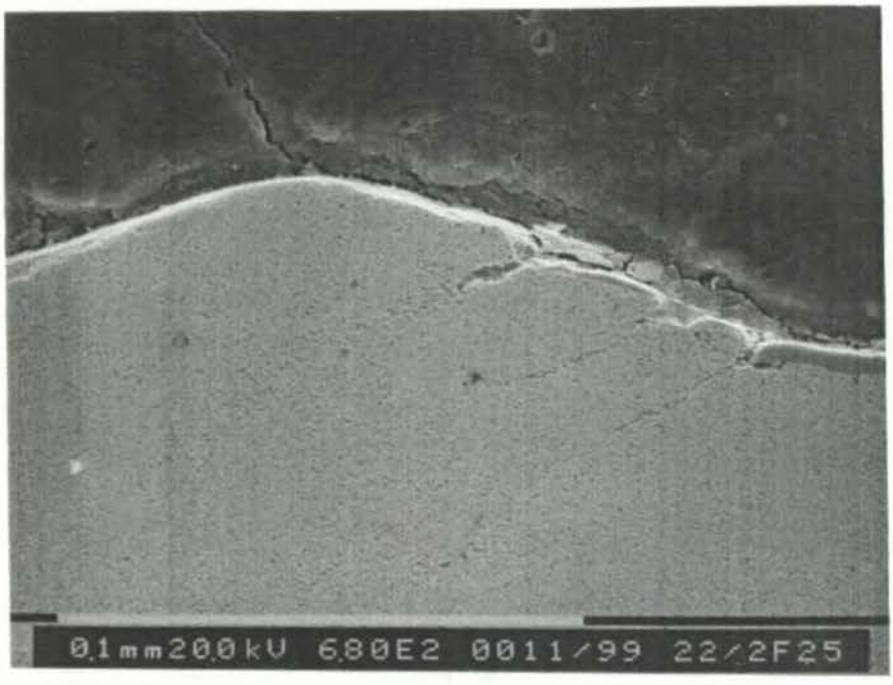

Figure 7. 110 Magnified view of plastically deformed area in Figure 7.109 showing associated crack formation

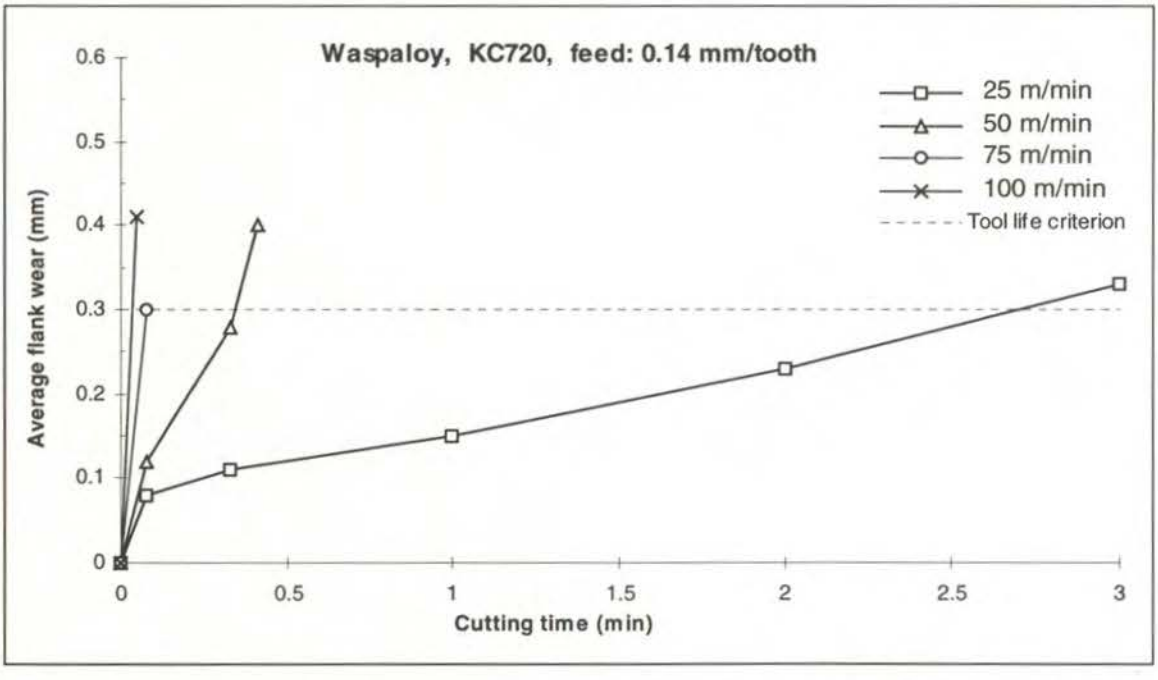

Figure 7. 111 Average flank wear versus cutting time when face milling Waspaloy with KC720 at a feed rate of 0.14 mm/tooth

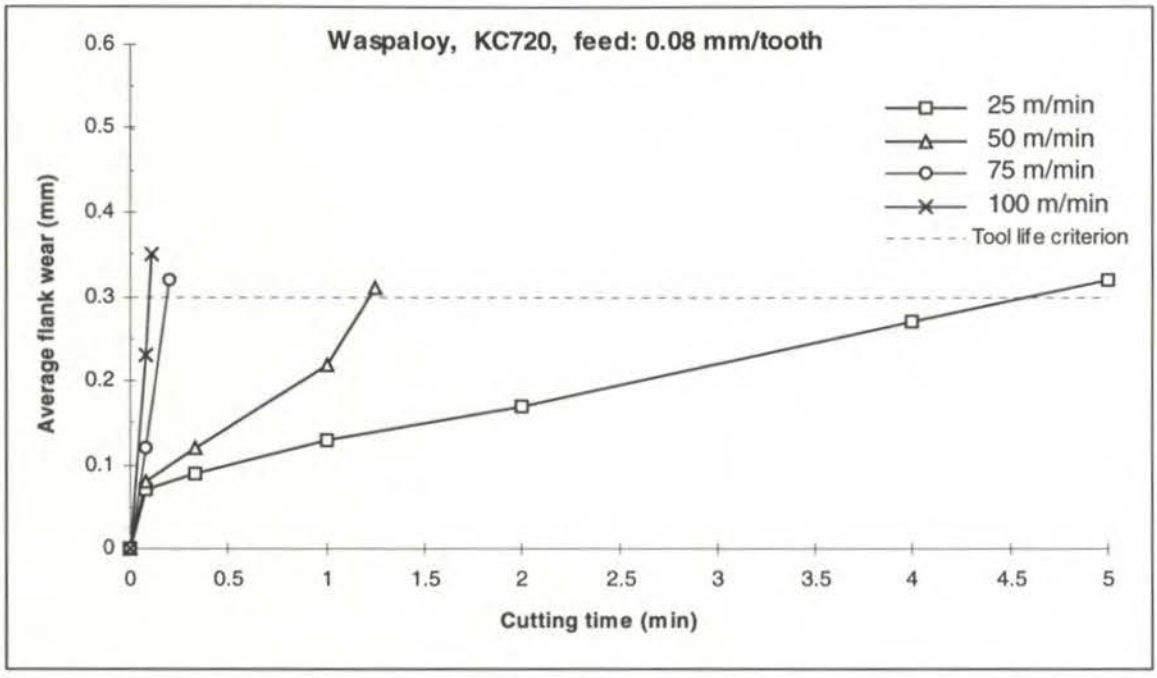

Figure 7. 112 Average flank wear versus cutting time when face milling Waspaloy with KC720 at a feed rate of 0.08 mm/tooth

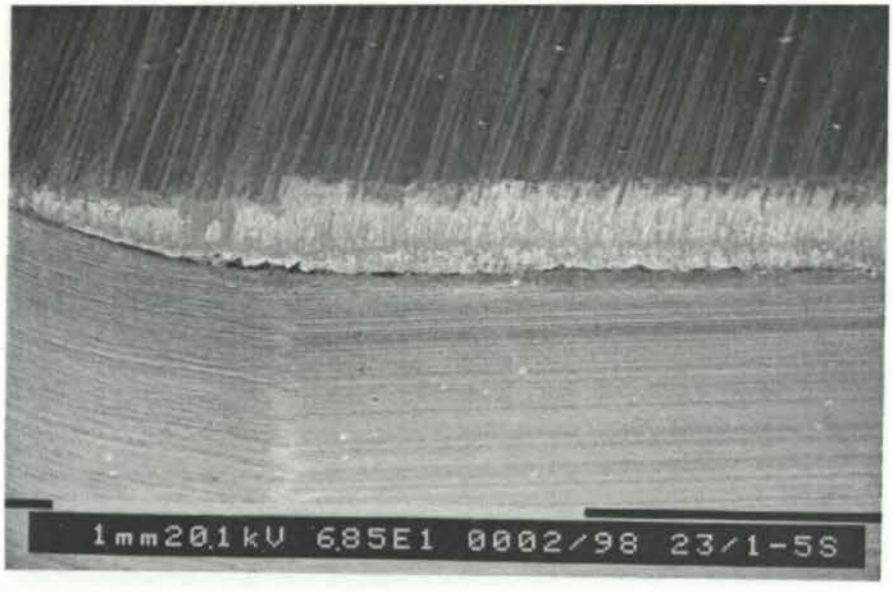

Figure 7. 113 Overall view of KC720 tool showing coating delamination, adhered and smeared workpiece material after cutting Waspaloy for 5 seconds at 25 m/min and 0.08 mm/tooth

Figure 7. 114 Magnified view of the rake face of KC720 tool in Figure 7.113 showing pealed coating, substrate pitting and galling on the rake face

Figure 7. 115 Magnified view of the KC720 tool in Figure 7.113 showing coating delamination, substrate pitting and galling on the rake face with adhered bulks of workpiece at the cutting edge

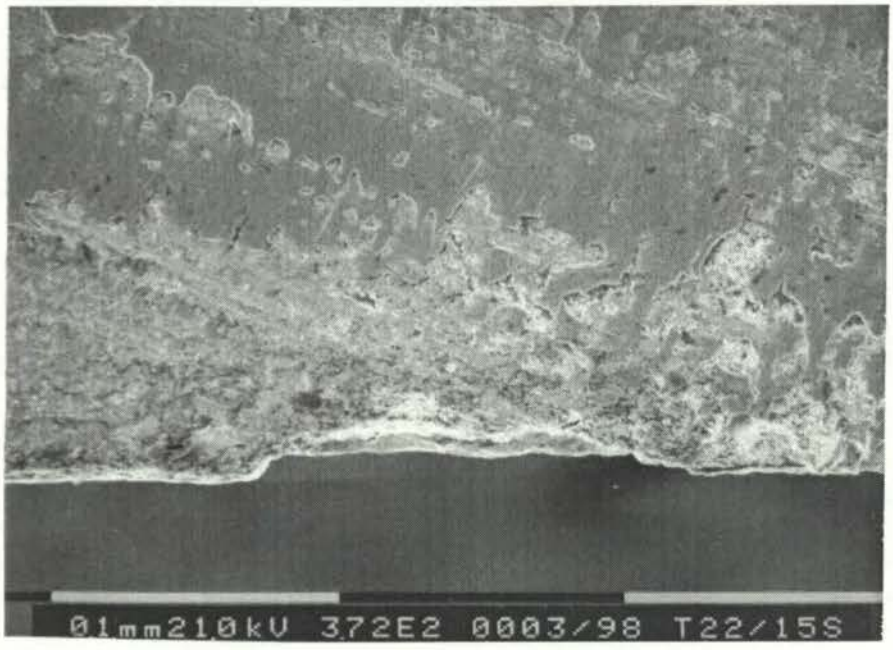

(a)

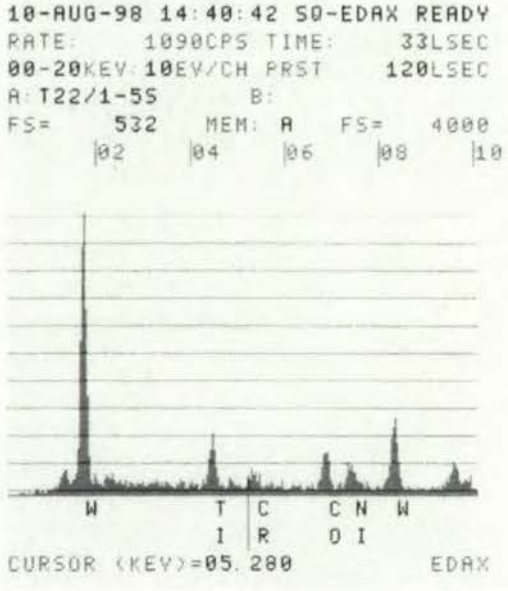

(b)

Figure 7. 116 (a) Initial microchipping, coating delamination and galling on rake face of a KC720 tool after cutting Waspaloy for 5 seconds at 25 m/min and 0.14 mm/tooth. (b) EDAX analysis proving premature substrate exposure on KC720 tool

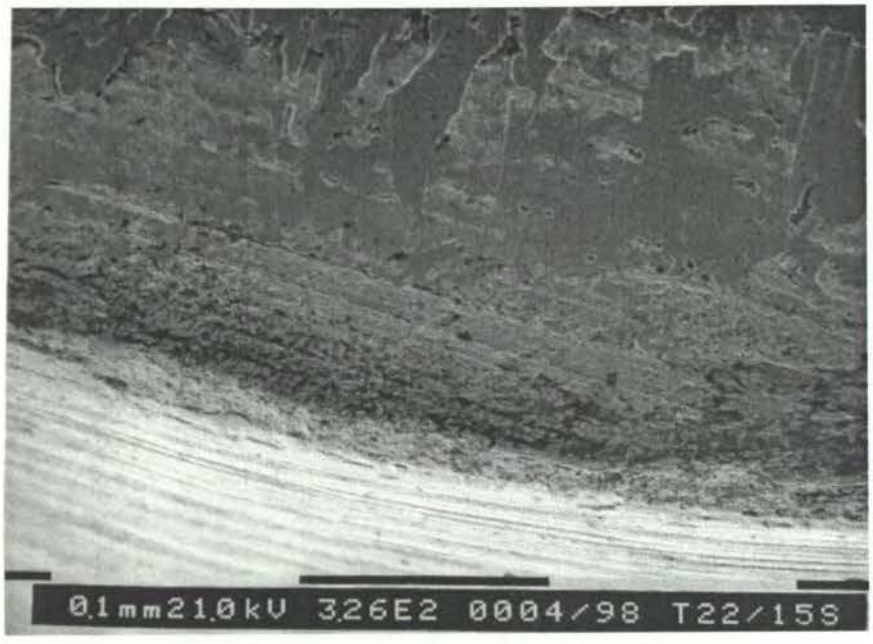

(a)

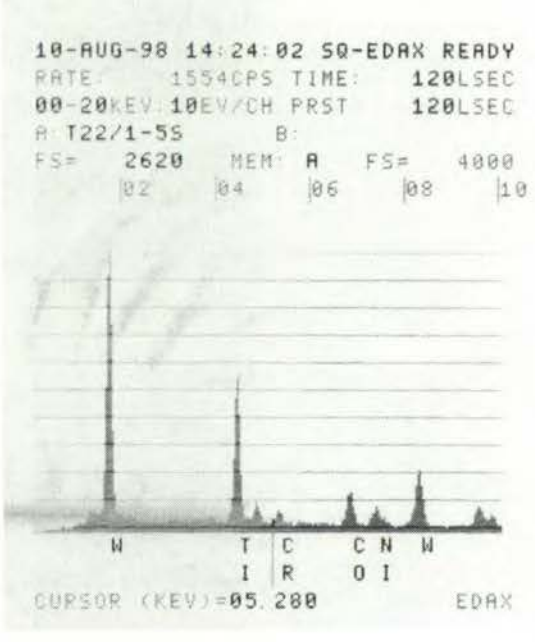

(b)

Figure 7. 117 (a) Initial microchipping of the cutting edge at tool nose with coating delamination and galling on the rake face of the KC720 tool in Figure 7.116. (b) EDAX analysis proving substrate exposure

Figure 7. 118 Severe premature chipping on a KC720 tool after cutting Waspaloy for 5 seconds at 50 m/min and 0.14 mm/tooth

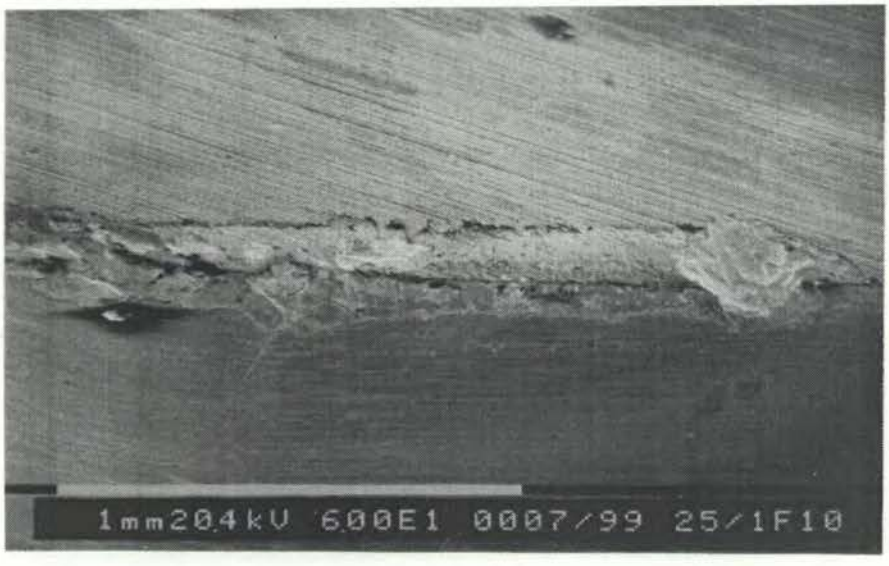

Figure 7. 119 Combination chipping, plucking, coating delamination and workpiece adhesion on a failed KC730 tool after cutting Waspaloy for 10 minutes at 25 m/min and 0.08 mm/tooth

Figure 7. 120 Severe chipping, plucking, coating delamination and workpiece adhesion on a failed KC730 tool after cutting Waspaloy for 110 seconds at 25 m/min and 0.14 mm/tooth

Figure 7. 121 Severe premature breakage of the cutting edge of a failed KC730 tool after cutting Waspaloy for 11 seconds at 50 m/min and 0.14 mm/tooth

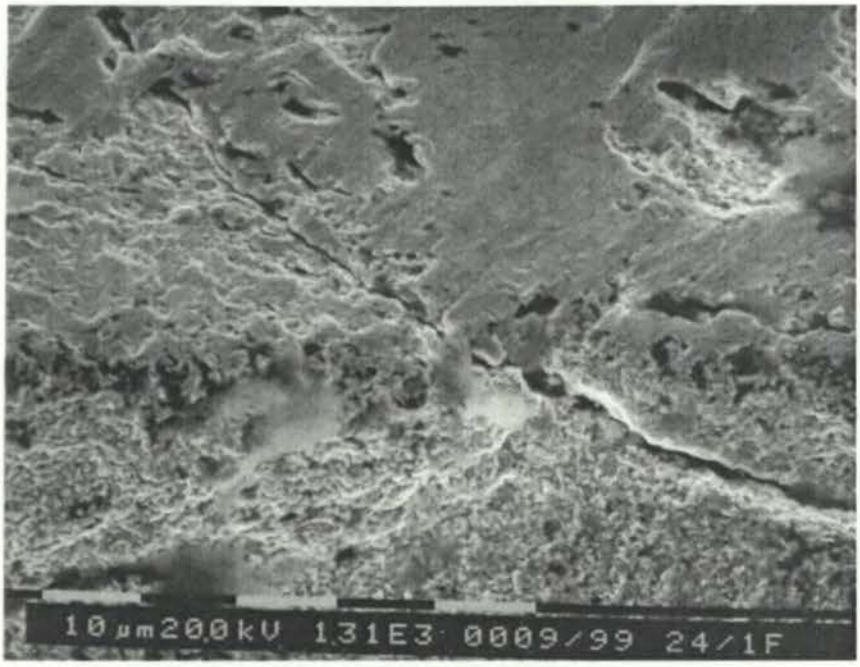

Figure 7. 122 Magnified view of the cutting edge of failed KC730 tool in Figure 7.120 showing cracking

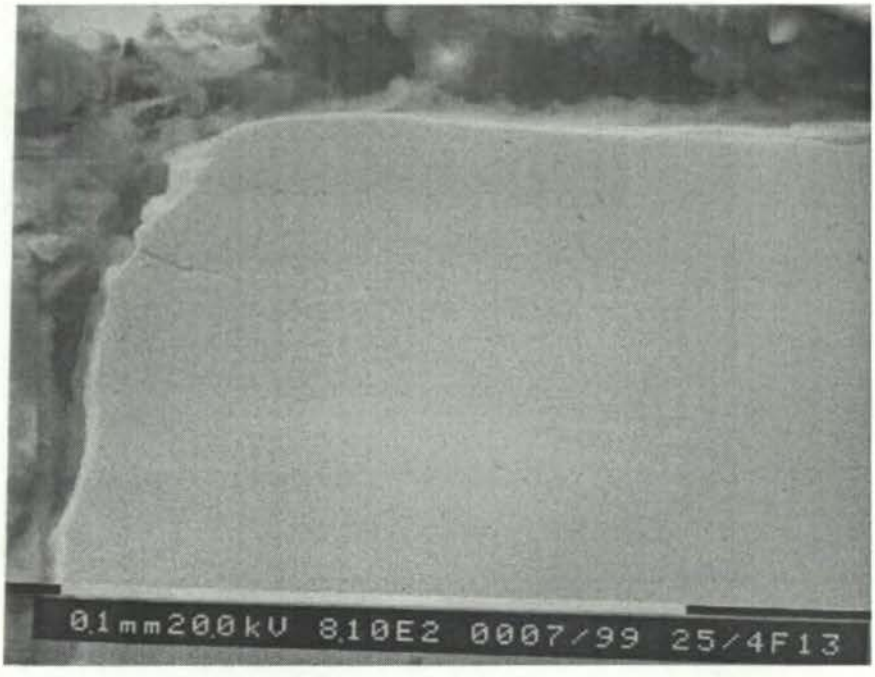

Figure 7. 123 Sectioned KC730 tool showing plastic deformation on the rake face and propagated cracks from the chipped area on the flank, after cutting Waspaloy for 13 seconds at 100 m/min and 0.08 mm/tooth

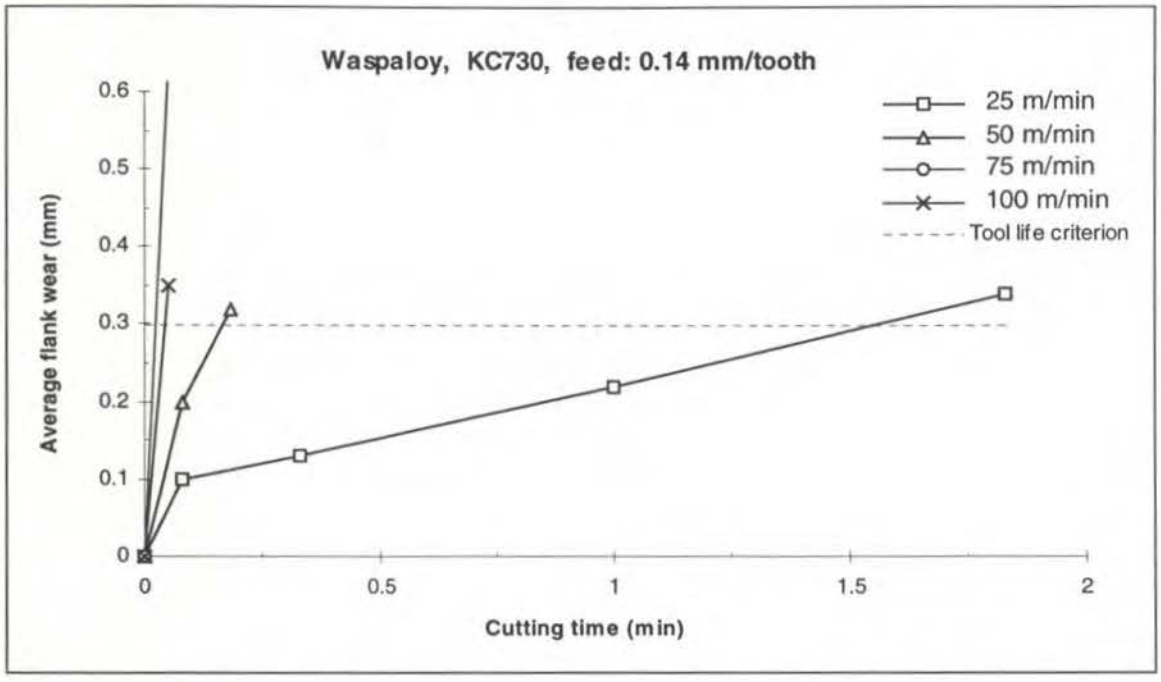

Figure 7. 124 Average flank wear versus cutting time when face milling Waspaloy with KC730 tool at a feed rate of 0.14 mm/tooth

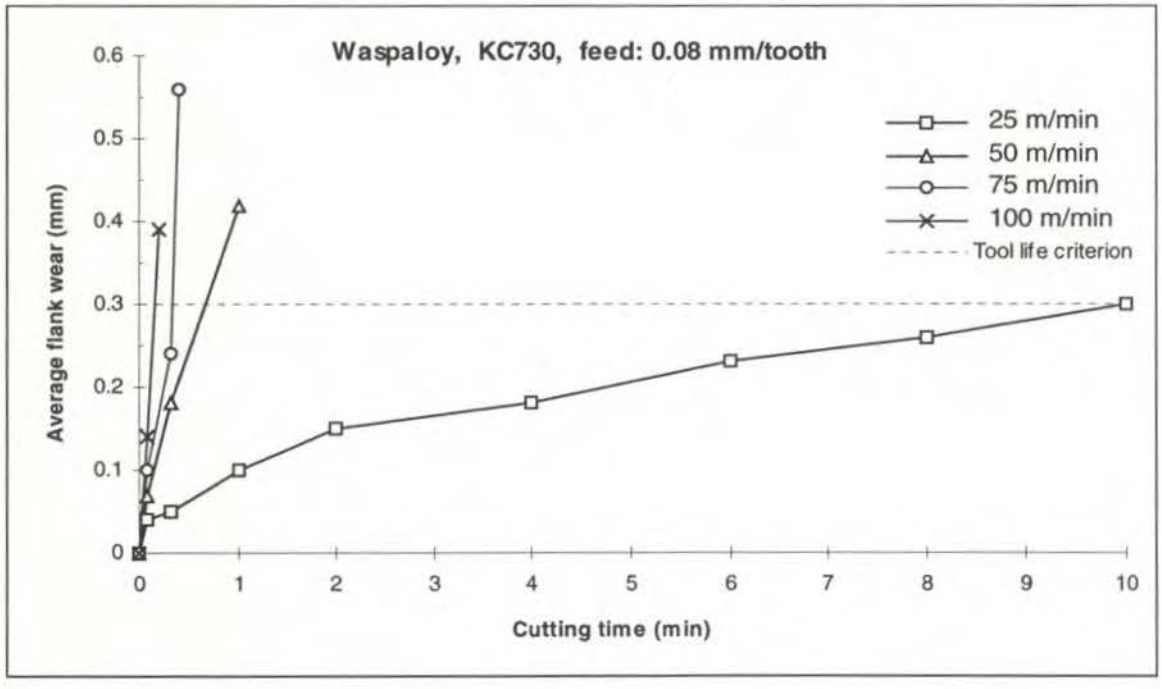

Figure 7. 125 Average flank wear versus cutting time when face milling Waspaloy with KC730 tool at a feed rate of 0.08 mm/tooth

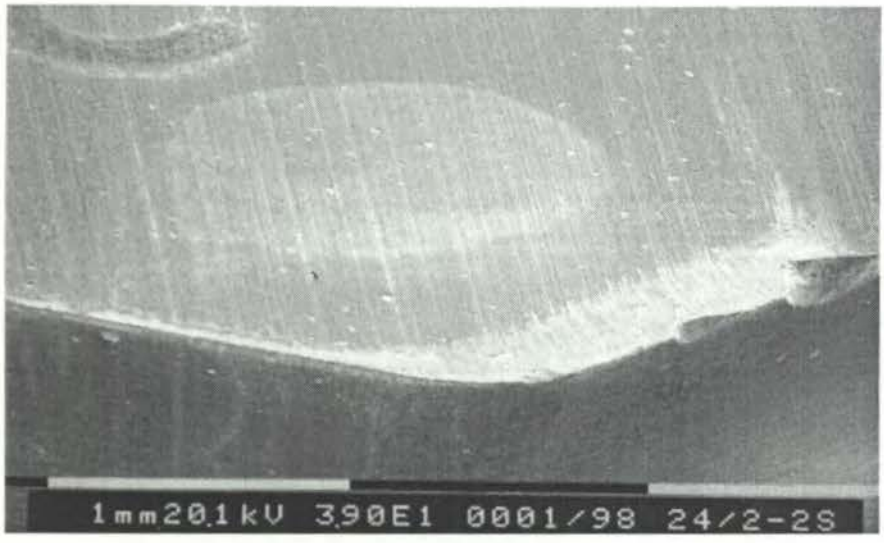

(a)

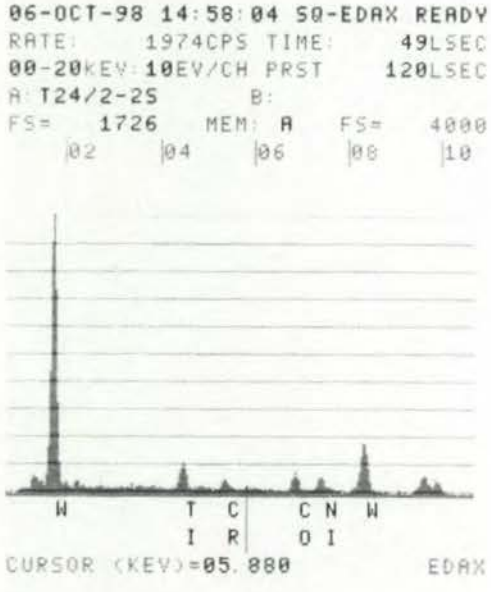

(b)

Figure 7. 126 (a) Premature chipping and coating delamination on KC730 tool after 2 seconds when machining Waspaloy at 50 m/min and 0.14 mm/tooth. (b) EDAX analysis indicating substrate exposure on the rake face

Figure 7. 127 Early coating delamination and galling on KC730 tool after 5 seconds when machining Waspaloy at 25 m/min and 0.08 mm/tooth

Figure 7. 128 Premature microchipping, coating delamination and galling on KC730 tool after 5 seconds of machining Waspaloy at 25 m/min and 0.14 mm/tooth

(a)

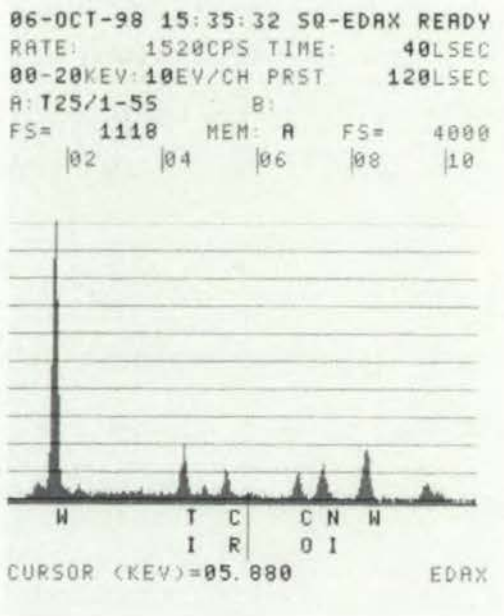

(b)

Figure 7. 129 (a) Magnified view of KC730 in Figure 7.127 showing exposed grinding marks of the substrate indicating easy coating delamination and discrete plucking on the rake face after 5 seconds of machining. (b) EDAX analysis confirming coating delamination

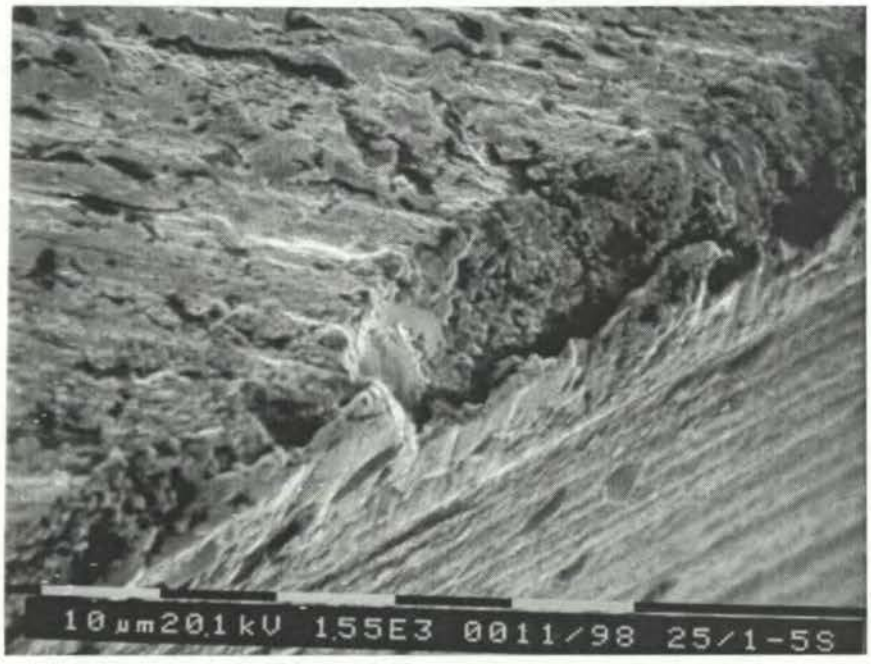

Figure 7. 130 Magnified view of KC730 in Figure 7.127 showing initial microchipping of the cutting edge after 5 seconds of machining Waspaloy at 25 m/min and 0.14 mm/tooth

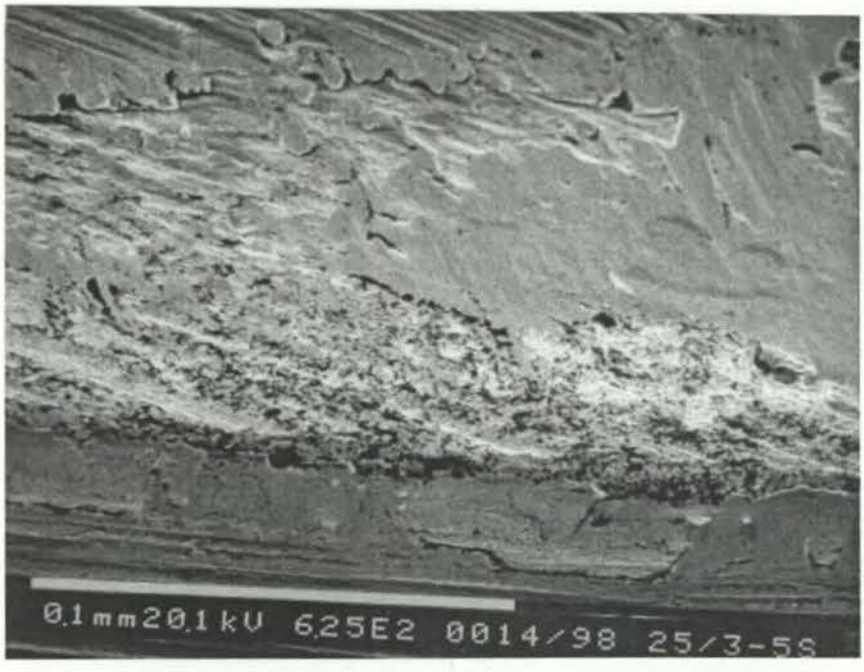

Figure 7. 131 Discrete delamination and galling on the flank with completely delaminated and pitted rake face of KC730 tool after 5 seconds when machining Waspaloy at 75 m/min and 0.08 mm/tooth

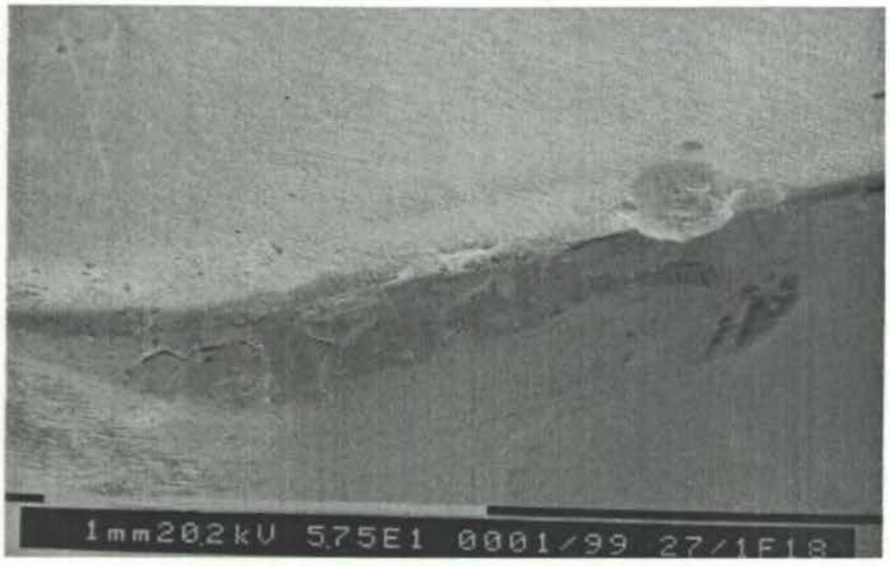

Figure 7. 132 Overall view of a failed KMF tool showing chipping, flaking and workpiece adhesion after cutting Waspaloy for 18 minutes at 25 m/min and 0.08 mm/tooth

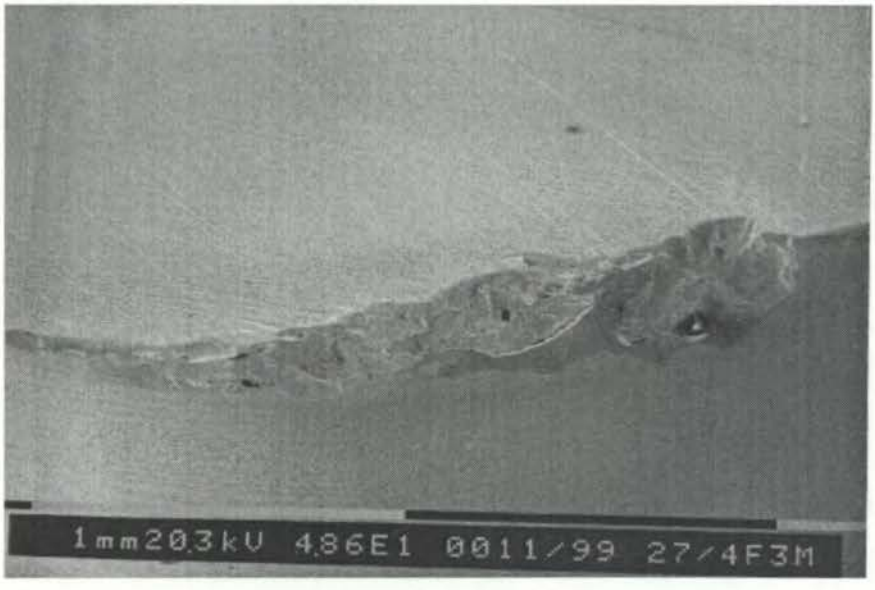

Figure 7. 133 Severe chipping on a failed KMF tool after cutting Waspaloy for 3 minutes at 50 m/min and 0.08 mm/tooth

Figure 7. 134 Catastrophic failure of a KMF tool after cutting Waspaloy for 2 minutes at 25 m/min and 0.14 mm/tooth

Figure 7. 135 Premature failure due to severe breakage on a KMF tool after 15 seconds when machining Waspaloy for at 50 m/min and 0.14 mm/tooth

Figure 7. 136 Magnified view of the failed KMF tool in Figure 7.132 showing flaking and associated cracking on the rake face

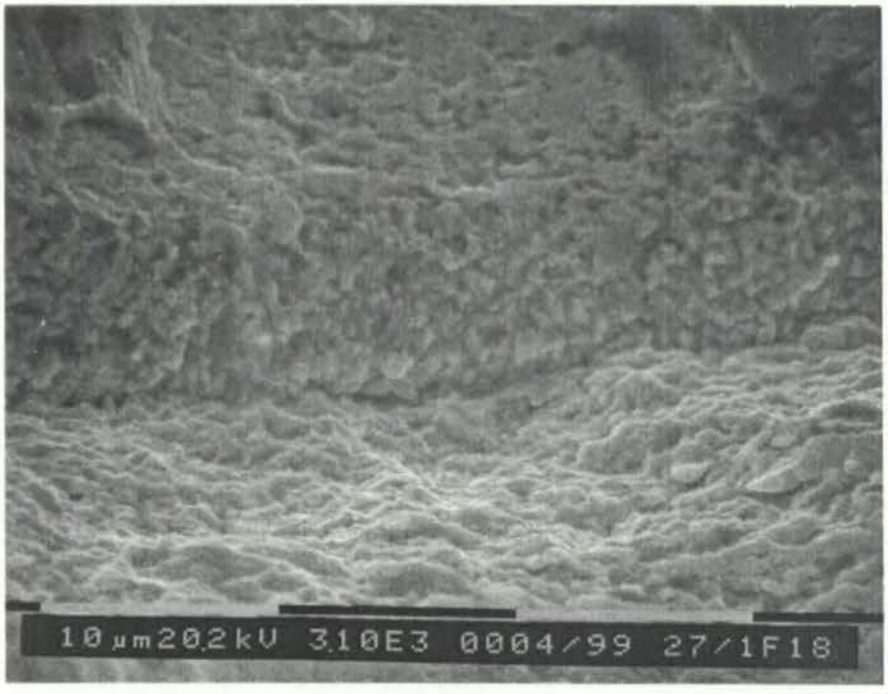

Figure 7. 137 Magnified view of the crack in Figure 7.136

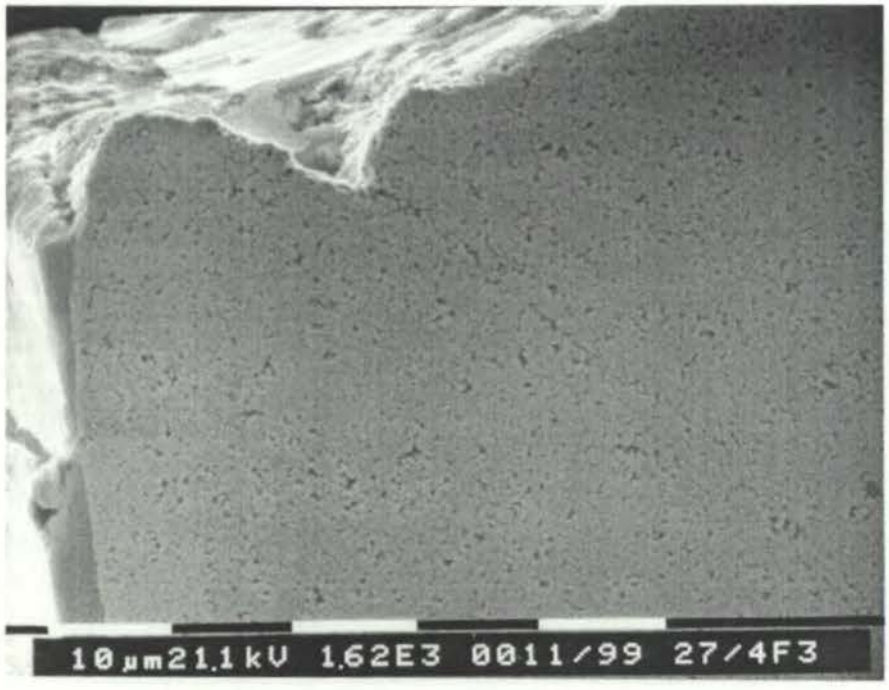

Figure 7. 138 Section through of a KMF tool showing propagated cracks with point of initiation and workpiece adhesion on smoothly worn flank face, after cutting Waspaloy for 3 minutes at 50 m/min and 0.08 mm/tooth

Figure 7. 139 Magnified view of the failed KMF tool in Figure 7.134 showing crack in the fractured region after cutting Waspaloy for 2 minutes at 25 m/min and 0.14 mm/tooth

Figure 7. 140 Enlarged view of a fractured area with crack on a KMF tool after 5 seconds of cutting Waspaloy at 50 m/min and 0.14/tooth

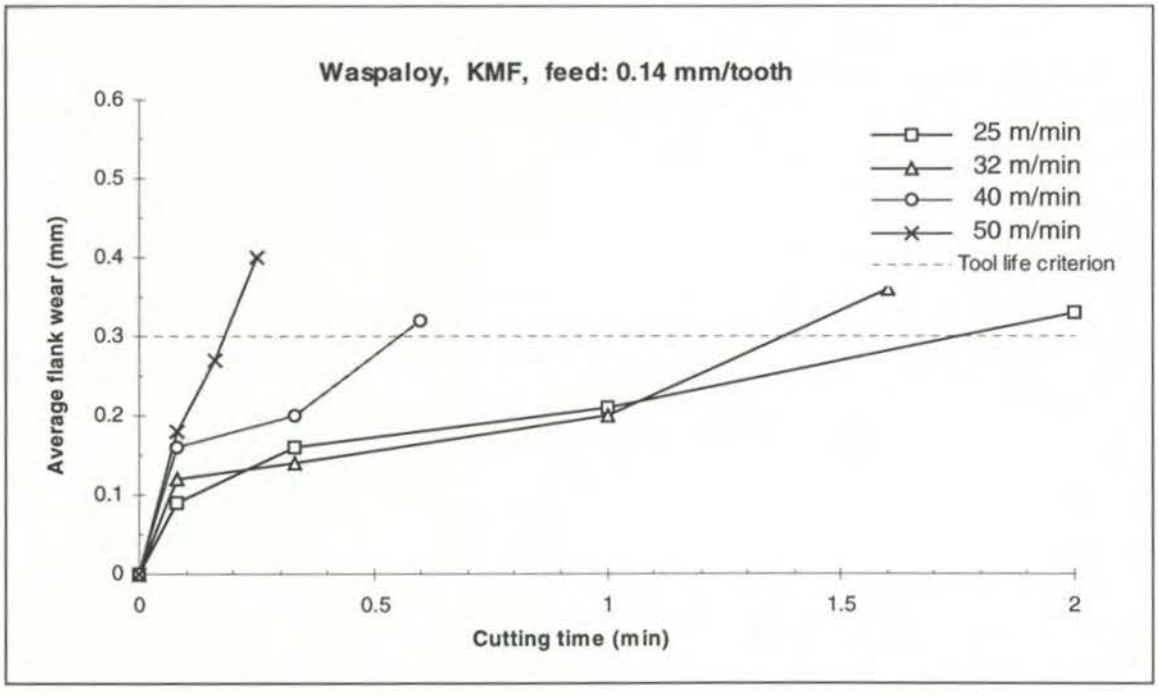

Figure 7. 141 Average flank wear versus cutting time when face milling Waspaloy with KMF tool at a feed rate of 0.14 mm/tooth

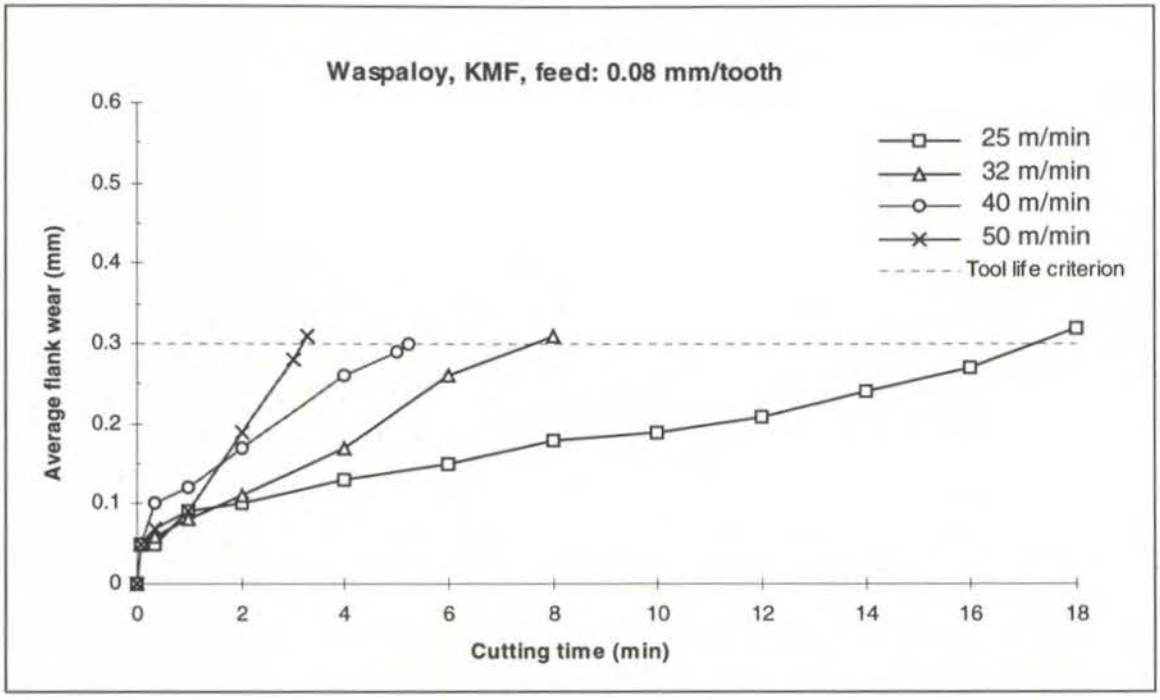

Figure 7. 142 Average flank wear versus cutting time when face milling Waspaloy with KMF tool at a feed rate of 0.08 mm/tooth

Figure 7. 143 Overall view of a KMF tool showing initial workpiece adhesion and pitted rake face after machining Waspaloy for 5 seconds at 25 m/min and 0.14 mm/tooth

Figure 7. 144 Enlarged view of the KMF tool in Figure 7.143 showing adhered bulk of workpiece material and initial pitting on the rake

Figure 7. 145 Enlarged view of the KMF tool in Figure 7.143 showing pitted area caused by attrition after 5 seconds when machining Waspaloy at 25 m/min and 0.14 mm/tooth

Figure 7. 146 Premature breakage of the entire cutting edge of a KMF tool after 5 seconds when machining Waspaloy at 50 m/min and 0.14 mm/tooth

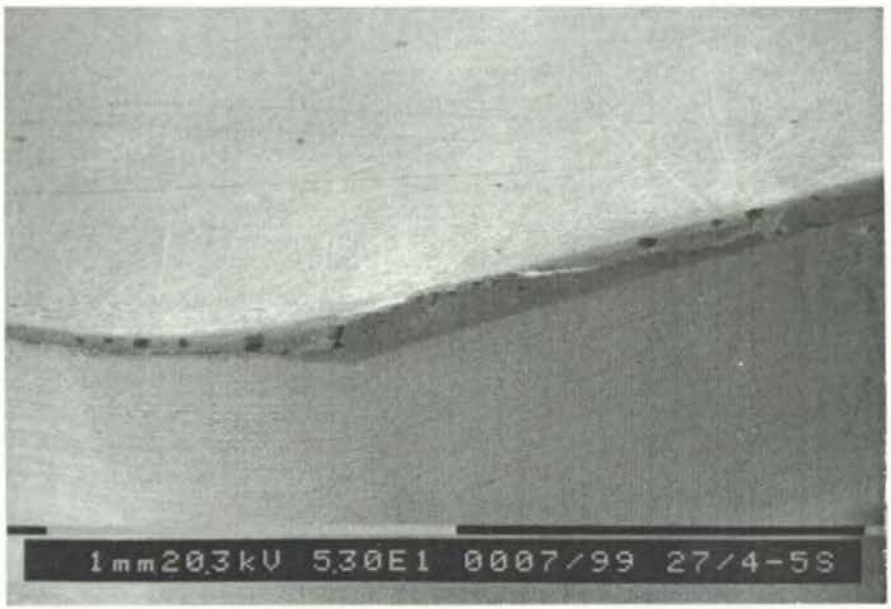

Figure 7. 147 Overall view of a KMF tool showing adhered bulk of workpiece material, most likely on microchipped chipped areas after machining Waspaloy for 5 seconds at 50 m/min and 0.08 mm/tooth

Figure 7. 148 Magnified view of the KMF tool in Figure 7.147 showing initial microchipping and workpiece adhesion after 5 seconds when machining Waspaloy at 50 m/min and 0.08 mm/tooth

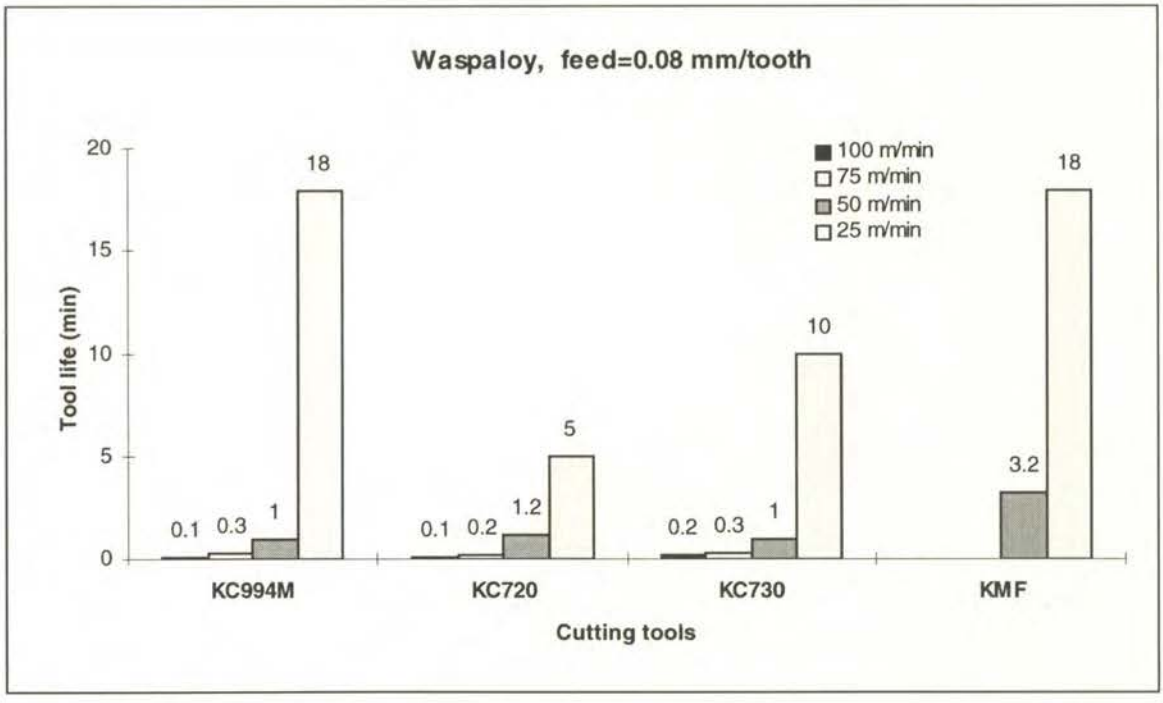

Figure 7. 149 Tool life comparison of coated and uncoated tools used for face milling Waspaloy at various cutting speeds and a feed rate of 0.08 mm/tooth

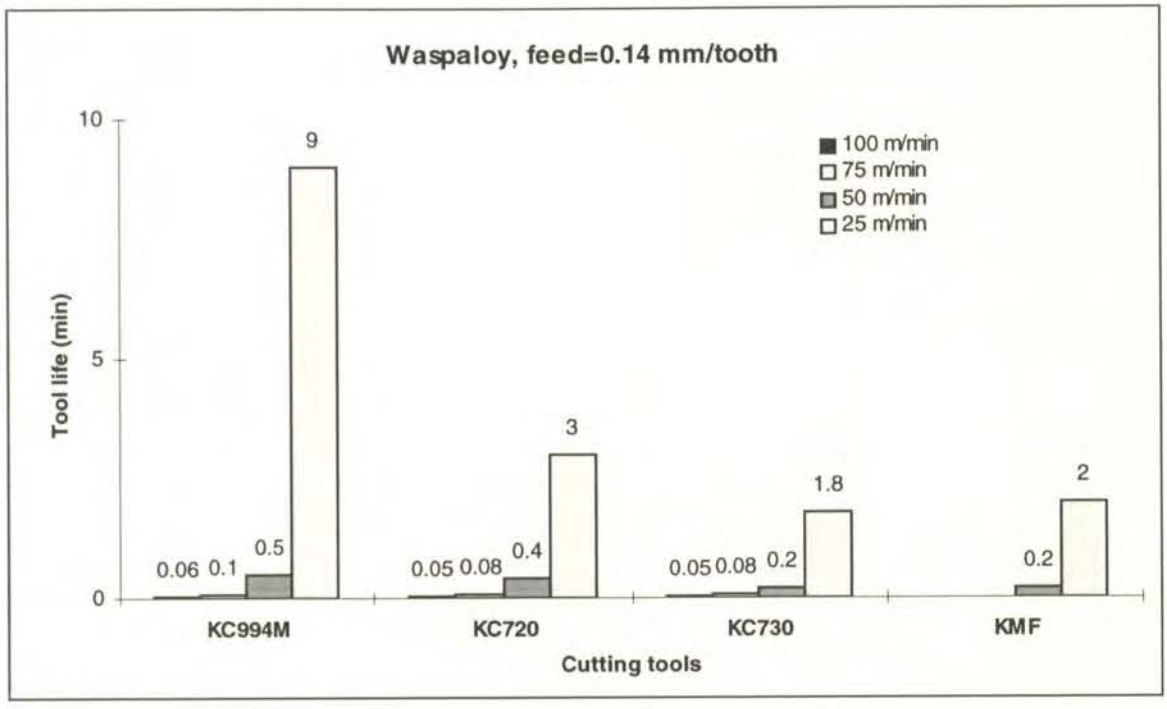

Figure 7. 150 Tool life comparison of coated and uncoated tools used for face milling Waspaloy at various cutting speeds and a feed rate of 0.14 mm/tooth

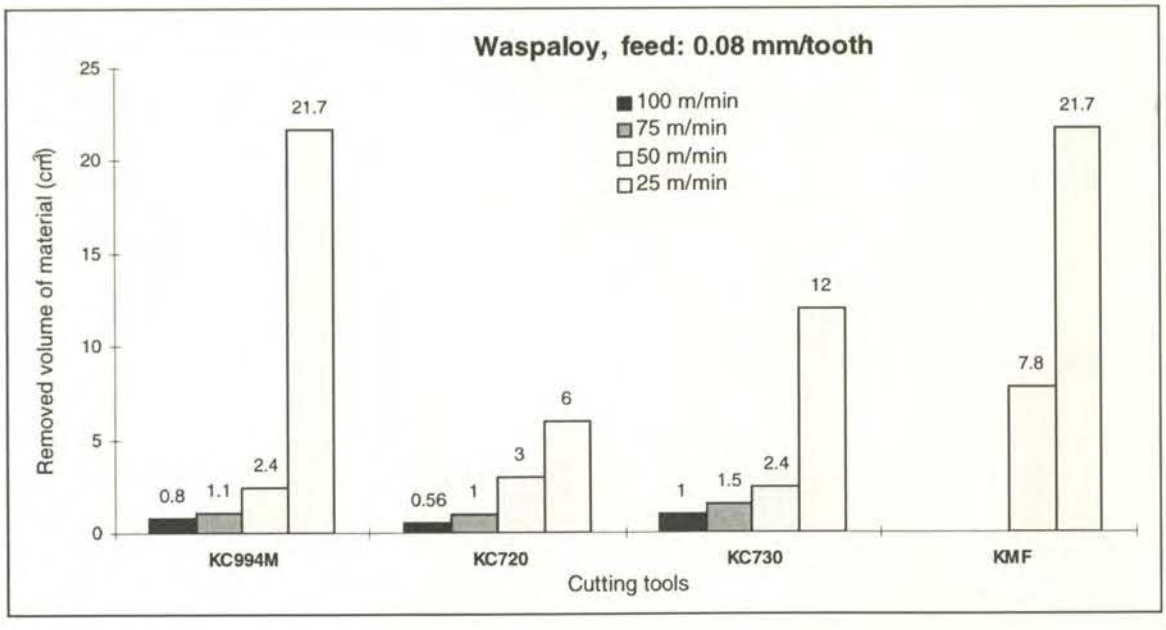

Figure 7. 151 Comparison of the volume of material removed with various types of coated and uncoated tools when face milling Waspaloy at various cutting speeds and a feed rate of 0.08 mm/tooth

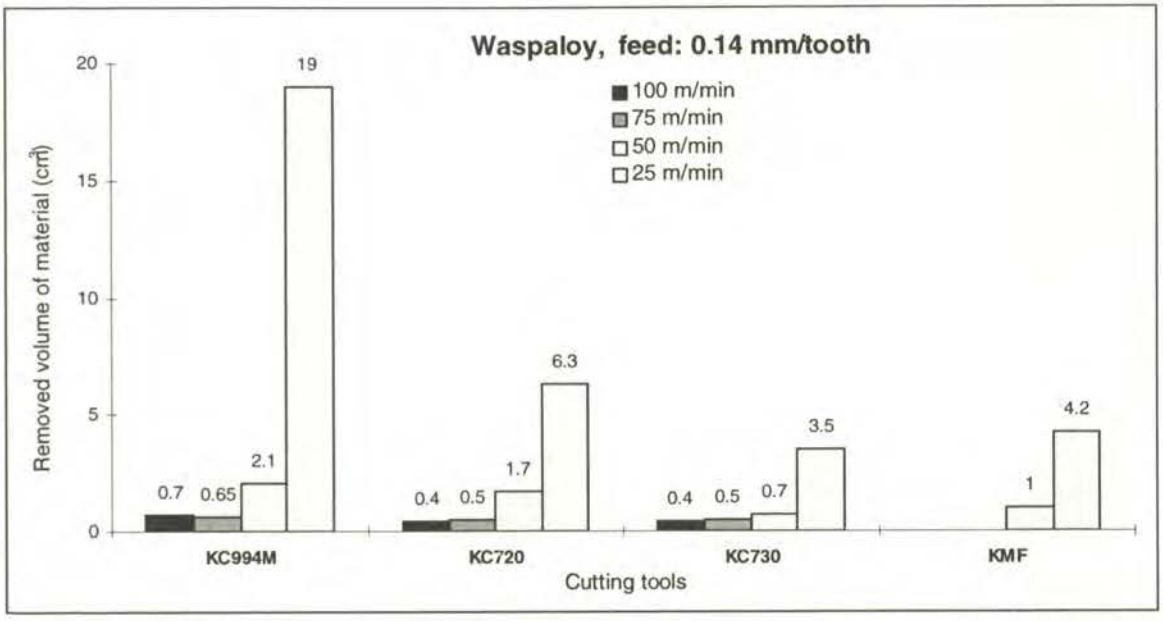

Figure 7. 152 Comparison of the volume of material removed with various types of coated and uncoated tools when face milling Waspaloy at various cutting speeds and a feed rate of 0.14 mm/tooth

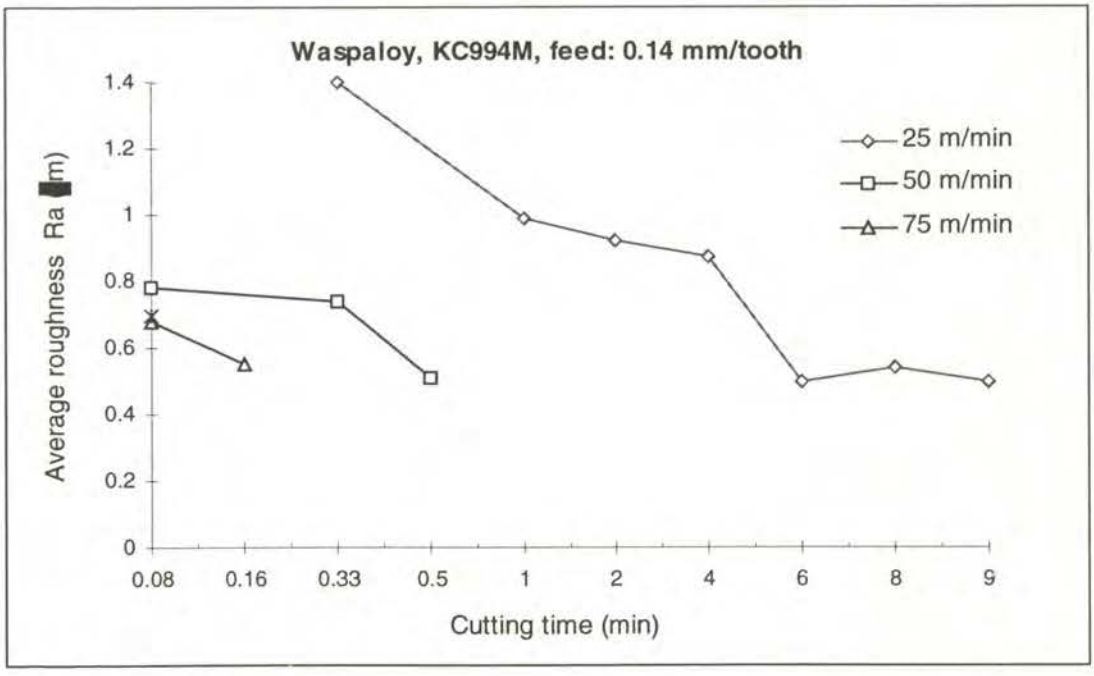

Figure 7. 153 Surface roughness versus cutting time when face milling Waspaloy with KC994M tool at various cutting speeds and feed rate of 0.14 mm/tooth

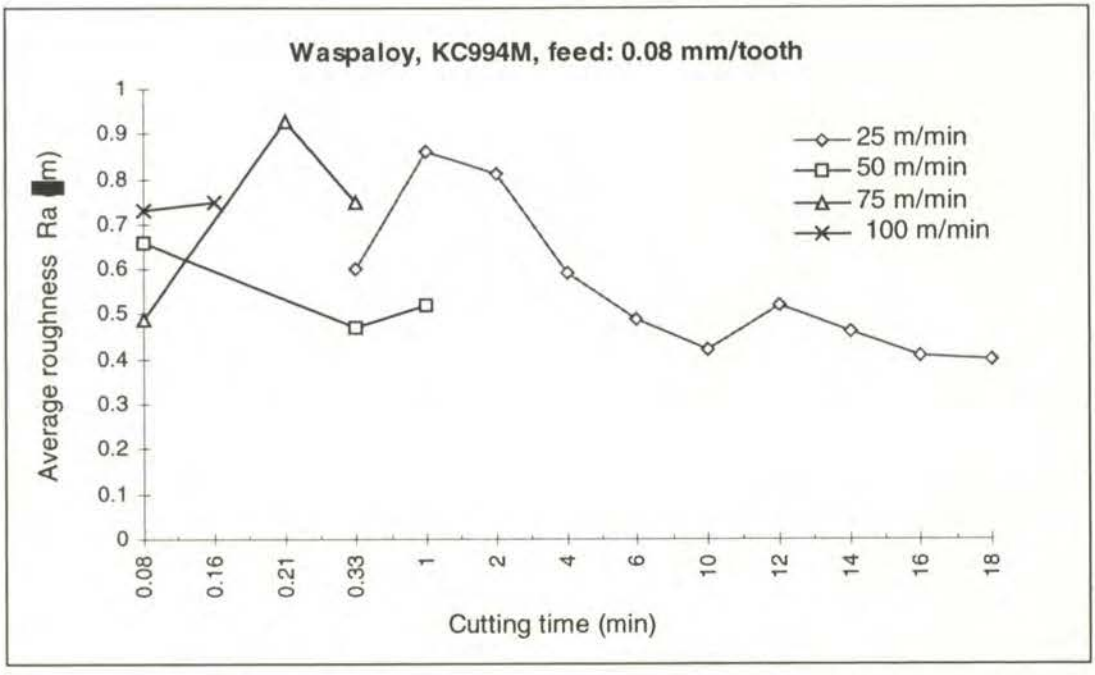

Figure 7. 154 Surface roughness versus cutting time when face milling Waspaloy with KC994M tool at various cutting speeds and a feed rate of 0.08 mm/tooth

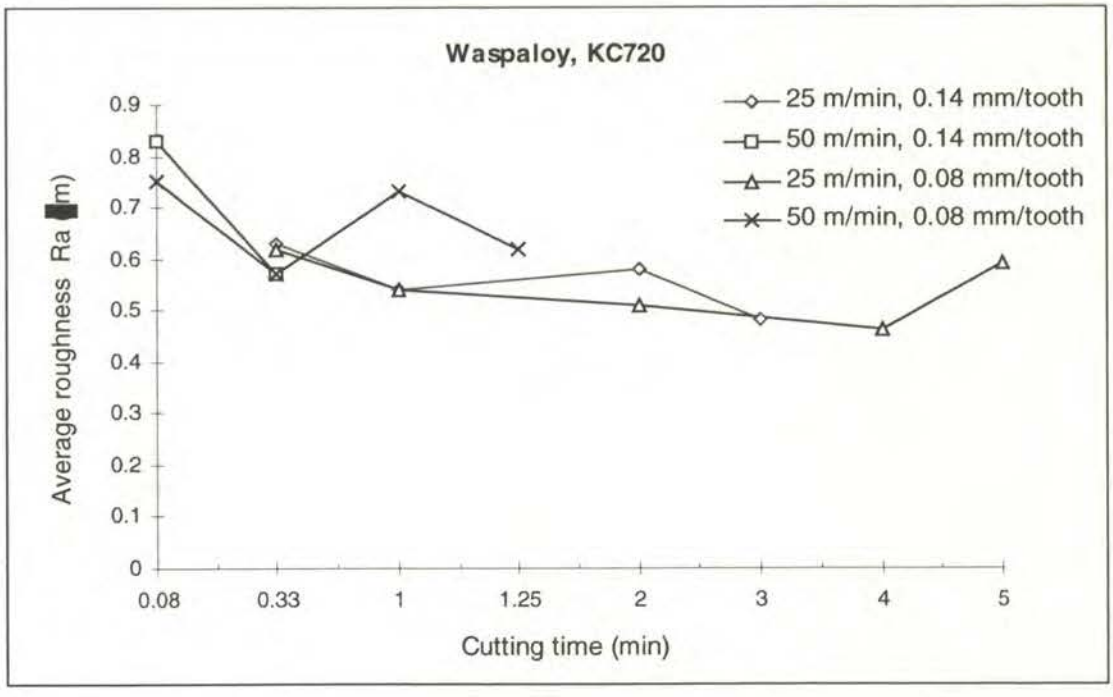

Figure 7. 155 Surface roughness versus cutting time when face milling Waspaloy with KC720 tool at various cutting speeds and feed rates

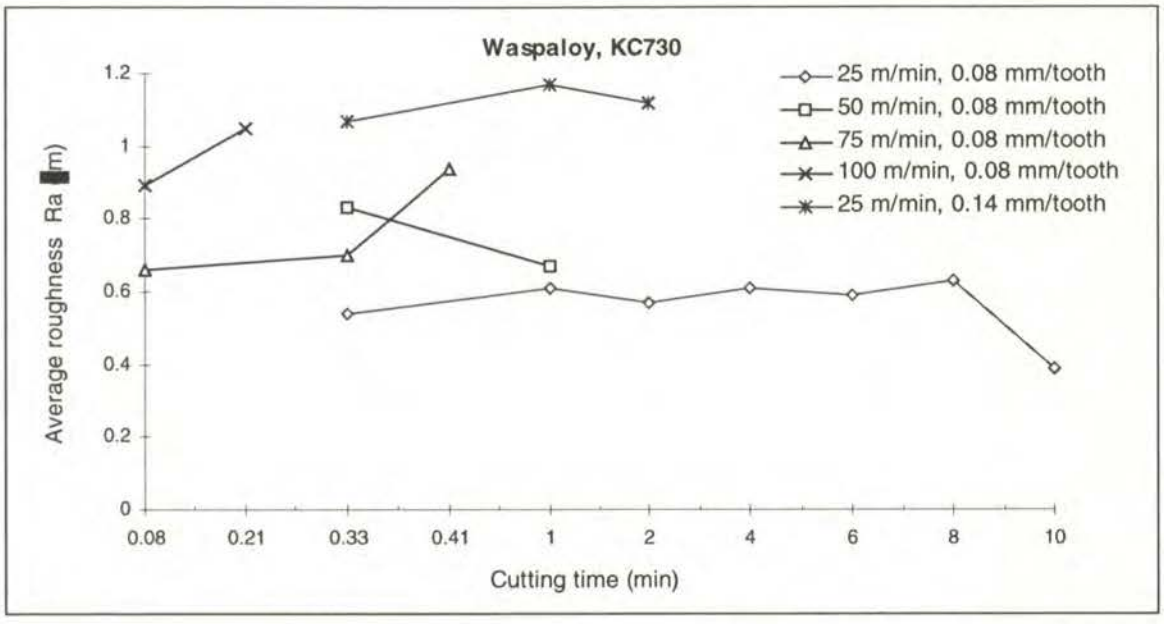

Figure 7. 156 Surface roughness versus cutting time when face milling Waspaloy with KC730 tool at various cutting speeds and feed rates

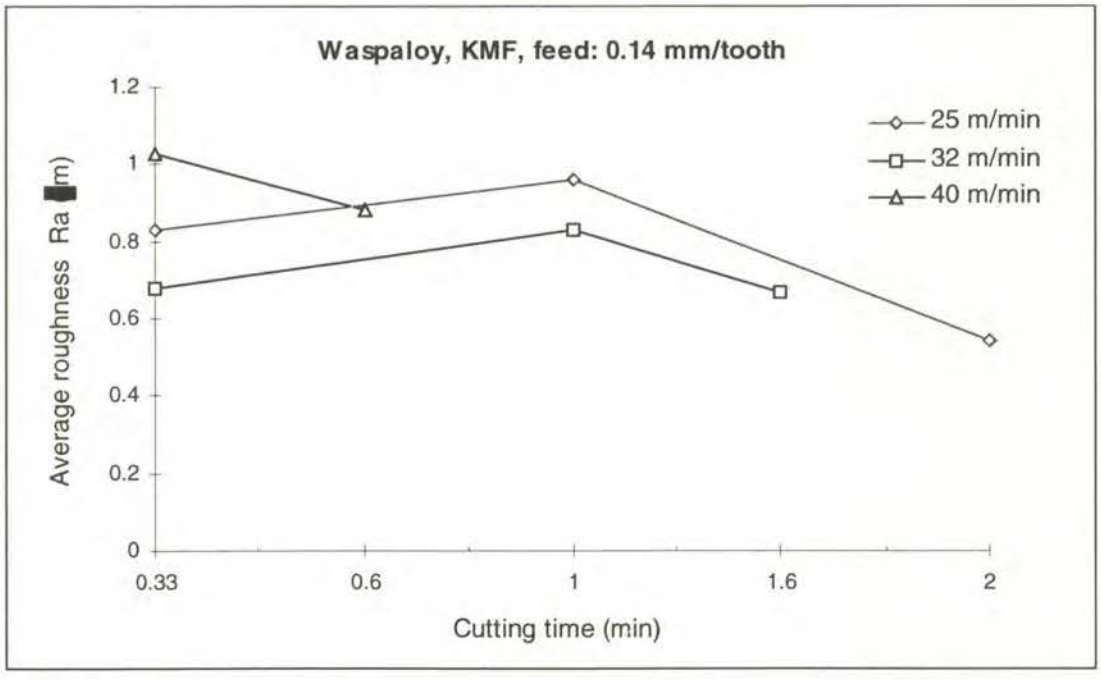

Figure 7. 157 Surface roughness versus cutting time when face milling Waspaloy with KMF tool at various cutting speeds and a feed rate of 0.14 mm/tooth

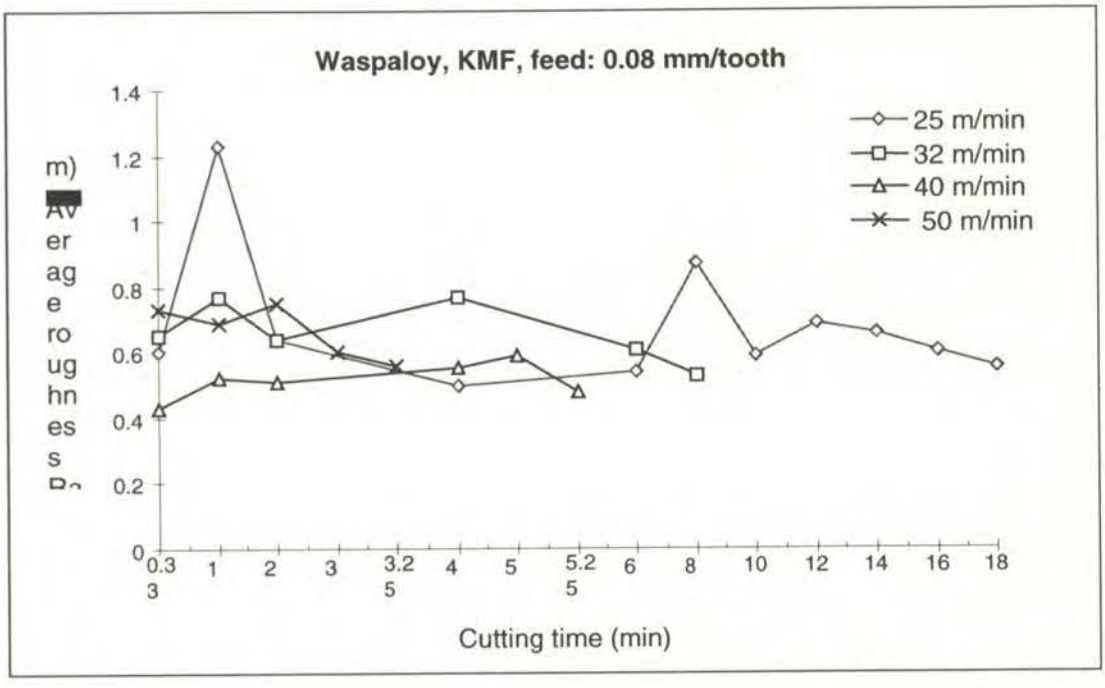

Figure 7. 158 Surface roughness versus cutting time when face milling Waspaloy with KMF tool at various cutting speeds and a feed rate of 0.08 mm/tooth

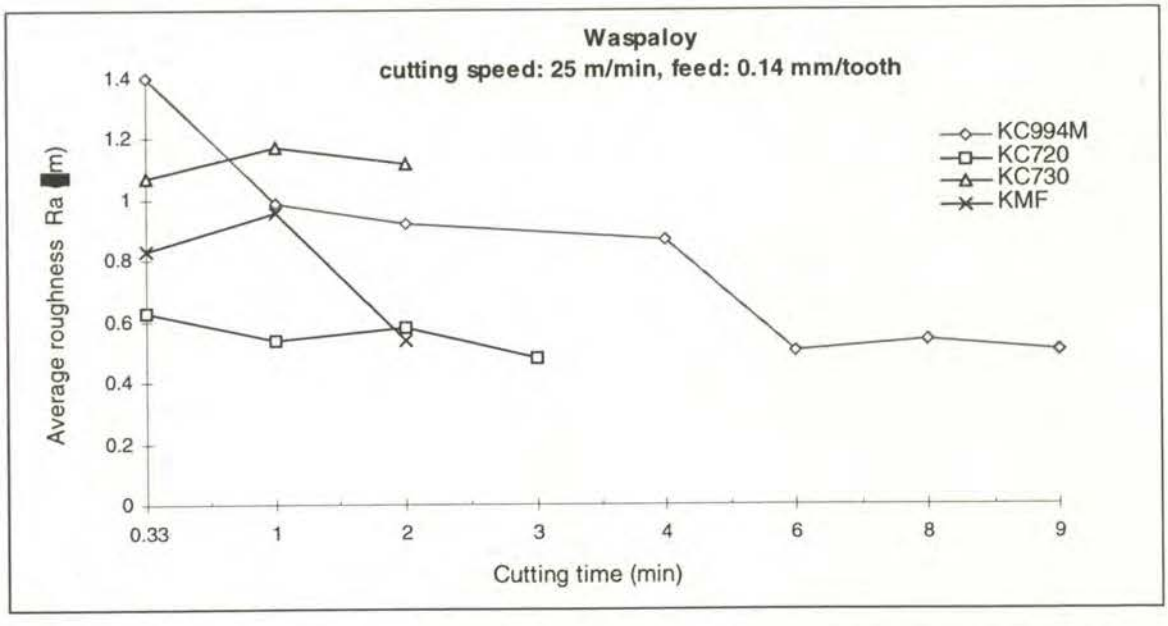

Figure 7. 159 Comparison of surface roughness when face milling Waspaloy with different types cutting tools at a cutting speed of 25 m/min and feed rate of 0.14 mm/tooth

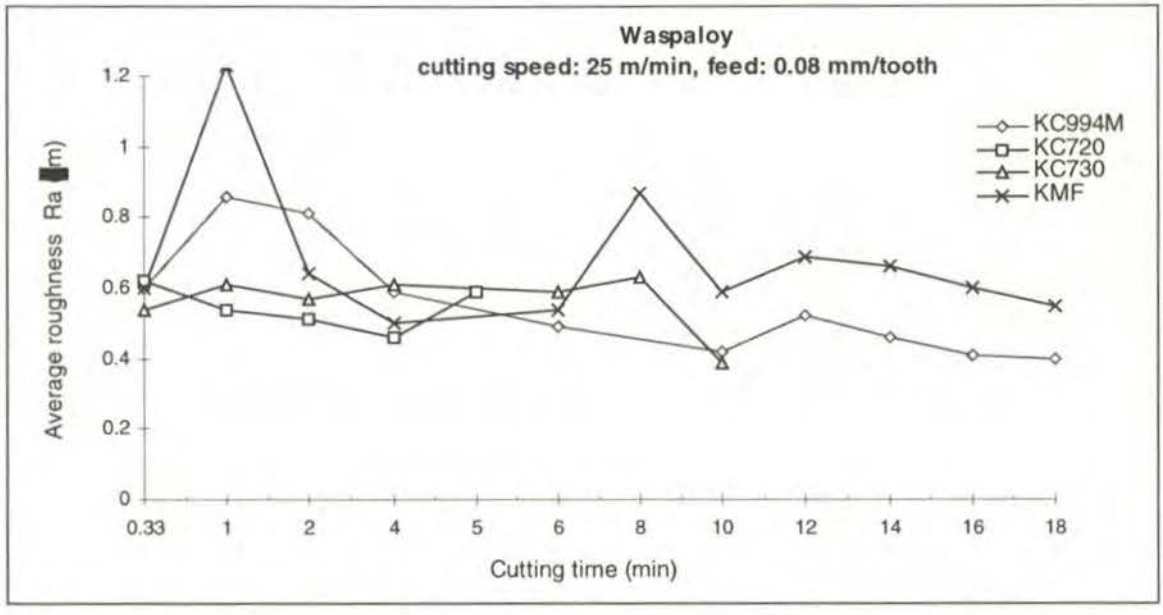

Figure 7. 160 Comparison of surface roughness when face milling Waspaloy with different types cutting tools at a cutting speed of 25 m/min and feed rate of 0.08 mm/tooth

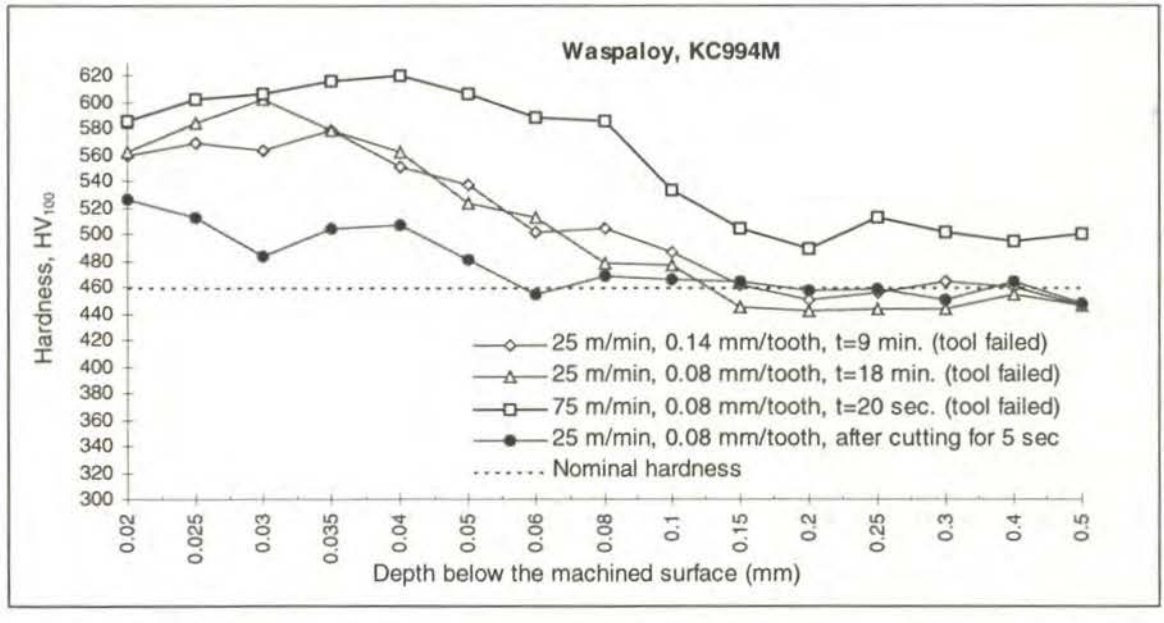

Figure 7. 161 Subsurface microhardness trends of Waspaloy when face milling with KC994M tool at various cutting conditions

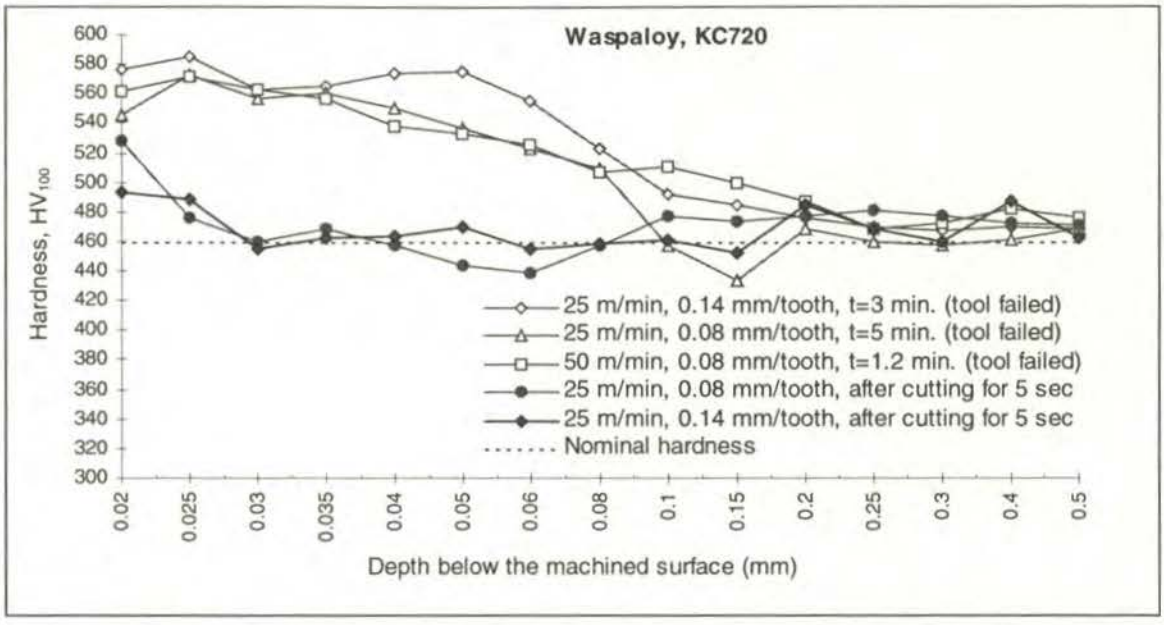

Figure 7. 162 Subsurface microhardness trends of Waspaloy when face milling with KC720 tool at various cutting conditions

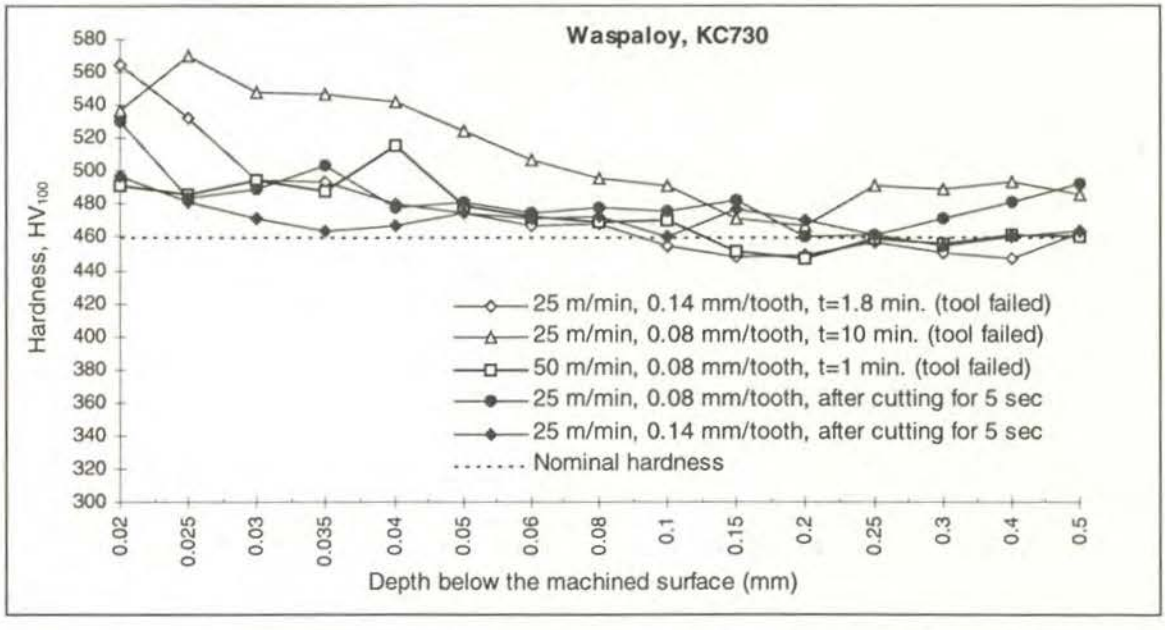

Figure 7. 163 Subsurface microhardness trends of Waspaloy when face milling with KC730 tool at various cutting conditions

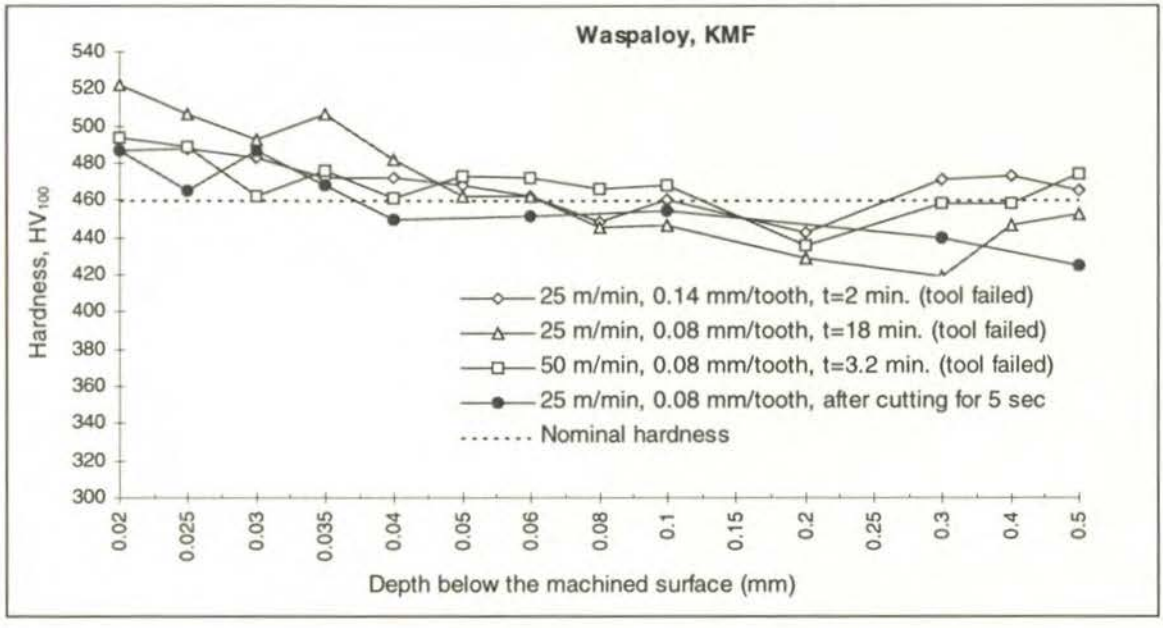

Figure 7. 164 Subsurface microhardness trends of Waspaloy when face milling with KMF tool at various cutting conditions

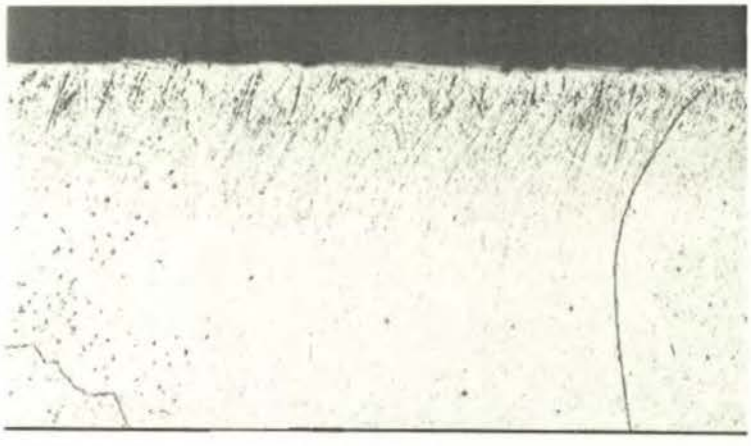

Figure 7. 165 Subsurface plastic flow and slight surface tearing after face milling Waspaloy with KC994M tool for 9 minutes at 25 m/min and 0.14 mm/tooth

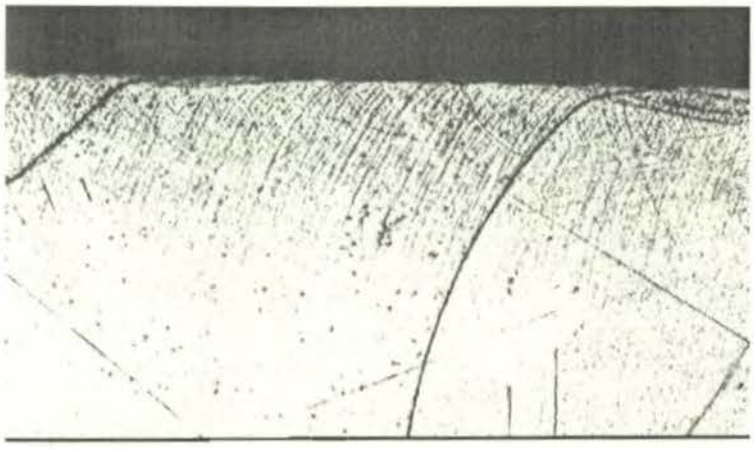

Figure 7. 166 Subsurface plastic flow after face milling Waspaloy with KC994M tool for 18 minutes at 25 m/min and 0.08 mm/tooth

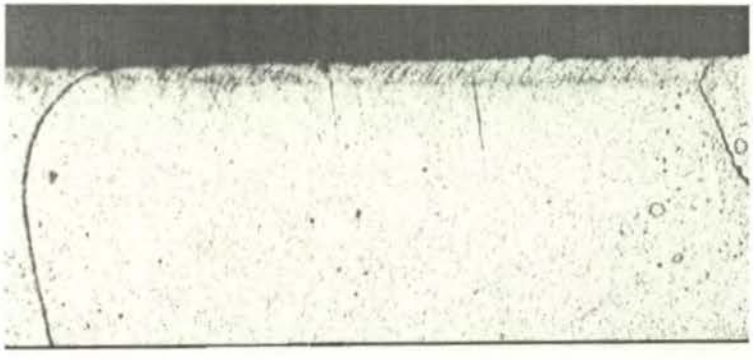

Figure 7. 167 Evidence of slight subsurface plastic flow and surface tearing after 5 seconds of milling Waspaloy with KC994M tool at 25 m/min and 0.08 mm/tooth

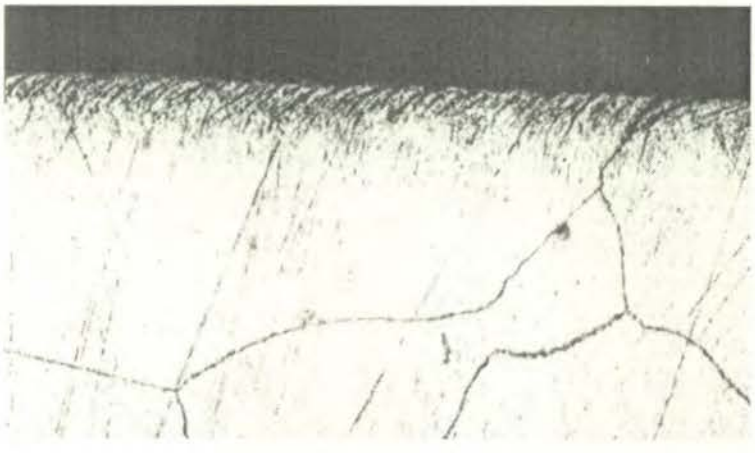

Figure 7. 168 Subsurface plastic flow after face milling Waspaloy with KC994M tool for 5 seconds at 25 m/min and 0.14 mm/tooth

Figure 7. 169 Significant surface tearing after face milling Waspaloy with KC994M tool for 20 seconds at 75 m/min and 0.08 mm/tooth

Figure 7. 170 Subsurface plastic flow after face milling Waspaloy with KC720 tool for 5 minutes at 25 m/min and 0.08 mm/tooth

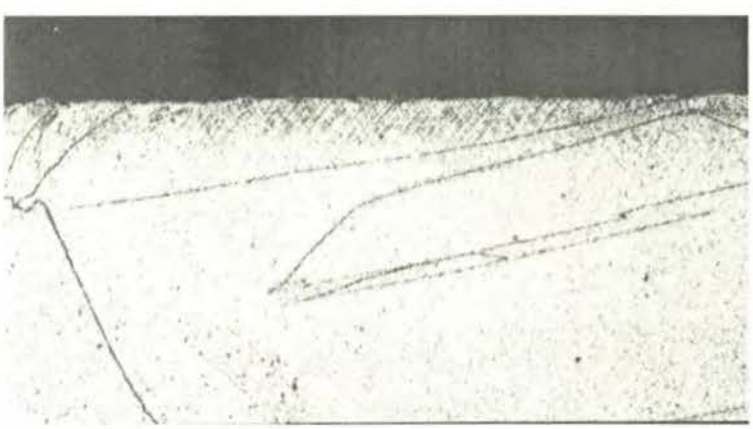

Figure 7. 171 Evidence of subsurface plastic flow and slight surface tearing after face milling Waspaloy with KC720 tool for 5 seconds at 25 m/min and 0.08 mm/tooth

Figure 7. 172 Plastically disturbed surface layer and surface tearing after face milling Waspaloy with KC720 tool for 3 minutes at 25 m/min and 0.14 mm/tooth

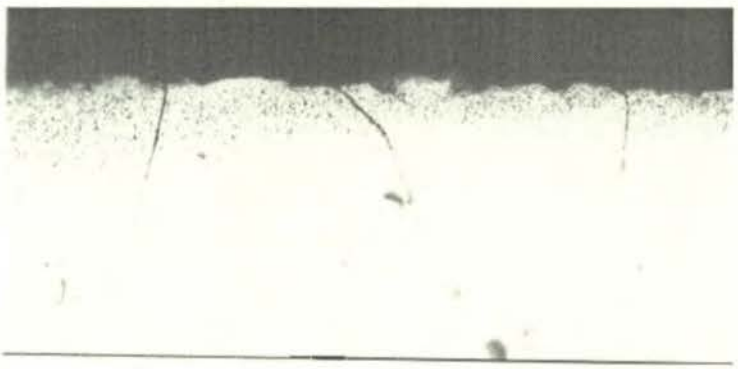

Figure 7. 173 Evidence of initial surface tearing after face milling Waspaloy with KC720 tool for 5 seconds at 25 m/min and 0.14 mm/tooth

Figure 7. 174 Subsurface plastic flow and an embedded external particle into the surface layer after face milling Waspaloy with KC720 tool for 75 seconds at 50 m/min and 0.08 mm/tooth

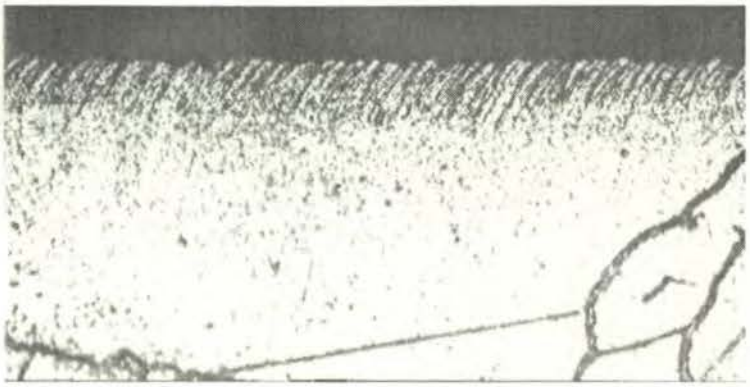

Figure 7. 175 Subsurface plastic flow and slight surface tearing after cutting Waspaloy with KC730 tool for 5 seconds at 25 m/min and 0.14 mm/tooth

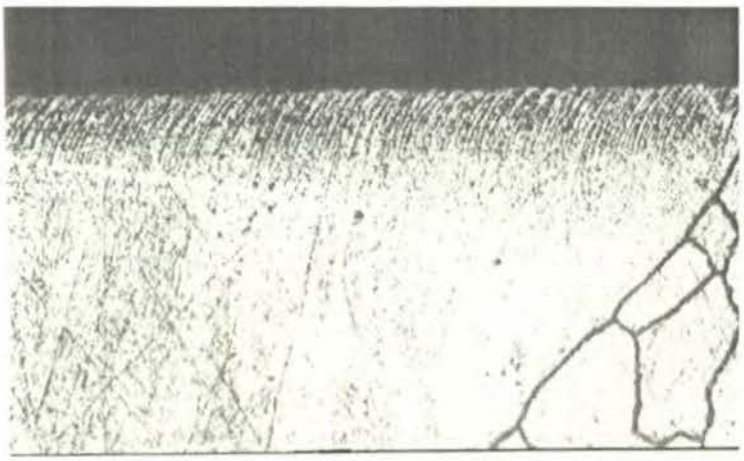

Figure 7. 176 Subsurface plastic flow after cutting Waspaloy with KC730 tool for 5 seconds at 25 m/min and 0.08 mm/tooth

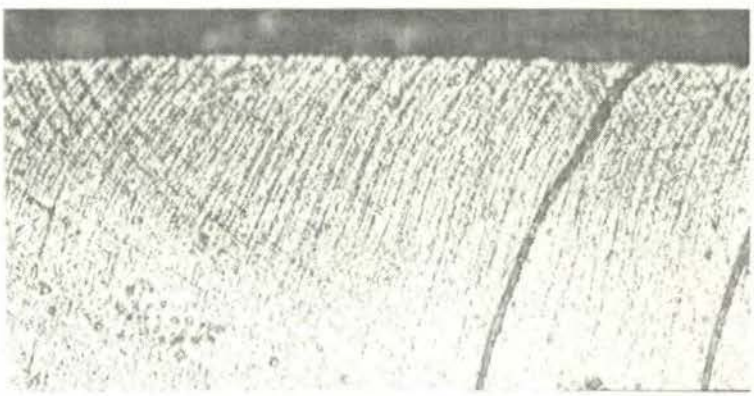

Figure 7. 177 Initial stage subsurface plastic flow after cutting Waspaloy with KC730 tool for 5 seconds at 50 m/min and 0.08 mm/tooth

Figure 7. 178 Subsurface plastic flow after cutting Waspaloy with KC730 tool for 10 minutes at 25 m/min and 0.08 mm/tooth (1200X)

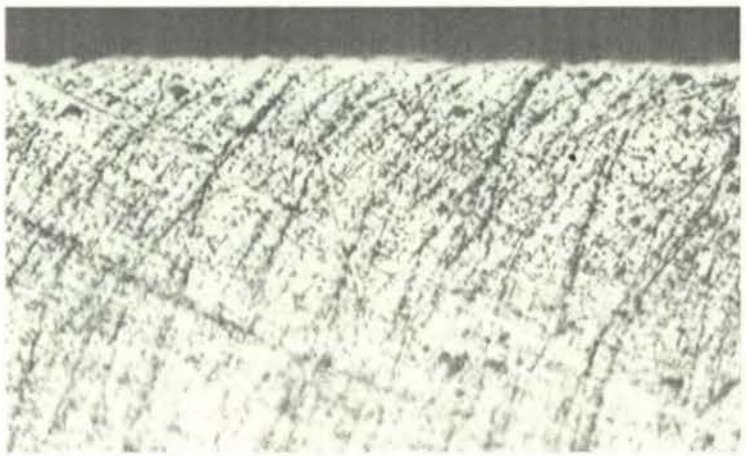

Figure 7. 179 Subsurface plastic flow and slight surface tearing after cutting Waspaloy with KC730 tool for 1 minute at 50 m/min and 0.08 mm/tooth (1200X)

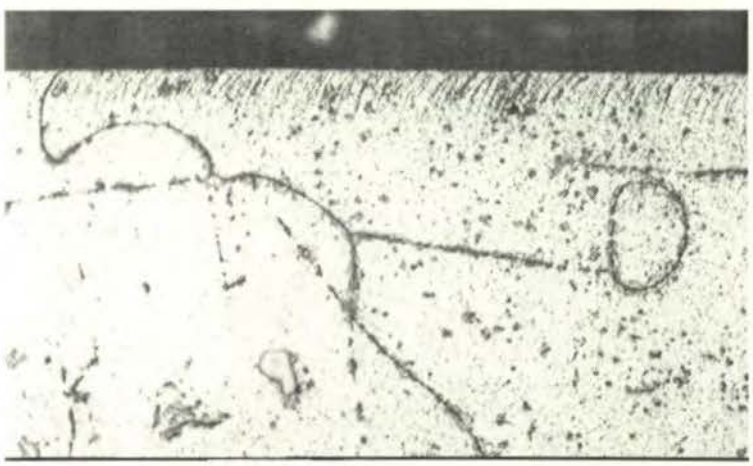

Figure 7. 180 Initial stage subsurface plastic flow after cutting Waspaloy with KMF tool for 5 seconds at 25 m/min and 0.14 mm/tooth

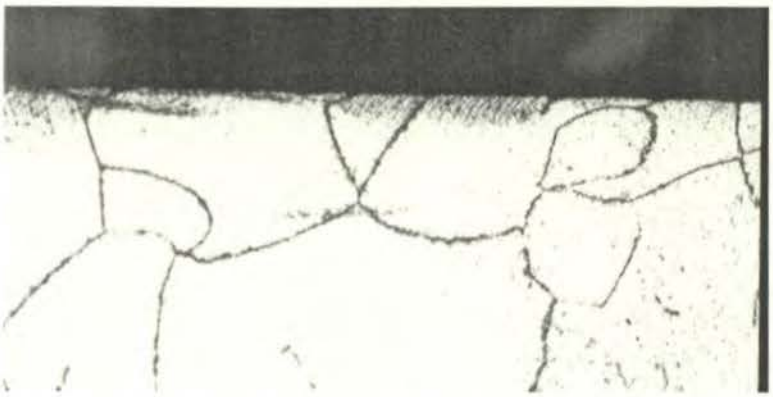

Figure 7. 181 Initial stage subsurface plastic flow after cutting Waspaloy with KMF tool for 5 seconds at 25 m/min and 0.08 mm/tooth

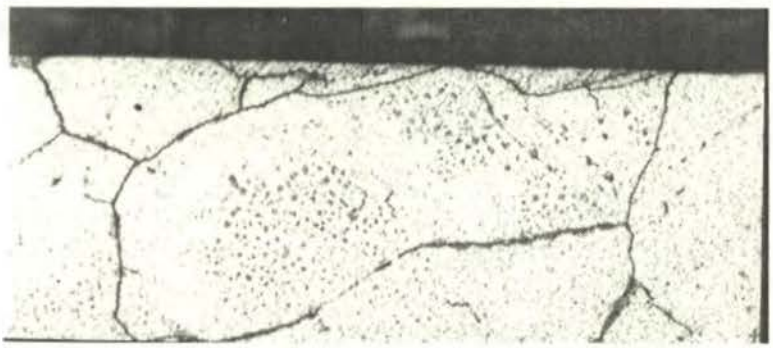

Figure 7. 182 Initial stage subsurface plastic flow after cutting Waspaloy with KMF tool for 5 seconds at 50 m/min and 0.08 mm/tooth

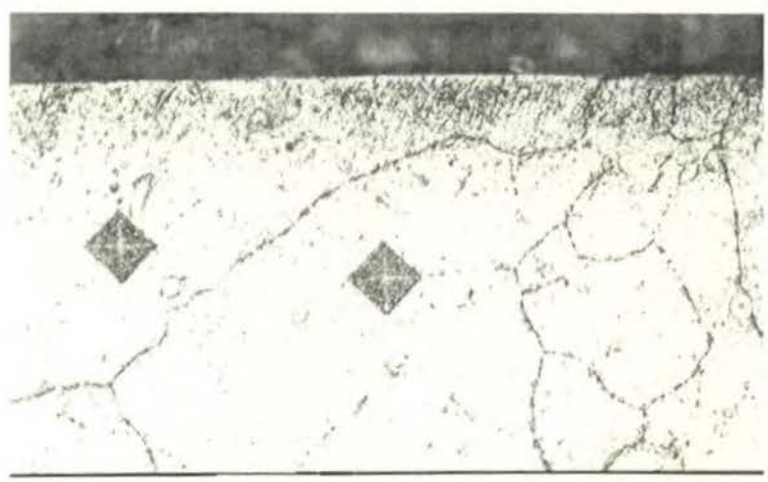

Figure 7.183 Evidence of subsurface plastic flow after cutting Waspaloy with KMF tool for 2 minutes at 25 m/min and 0.14 mm/tooth

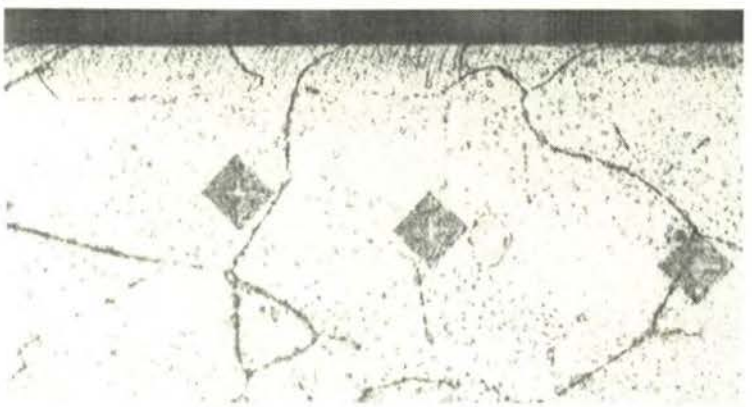

Figure 7.184 Subsurface plastic flow after cutting Waspaloy with KMF tool for 18 minutes at 25 m/min and 0.08 mm/tooth

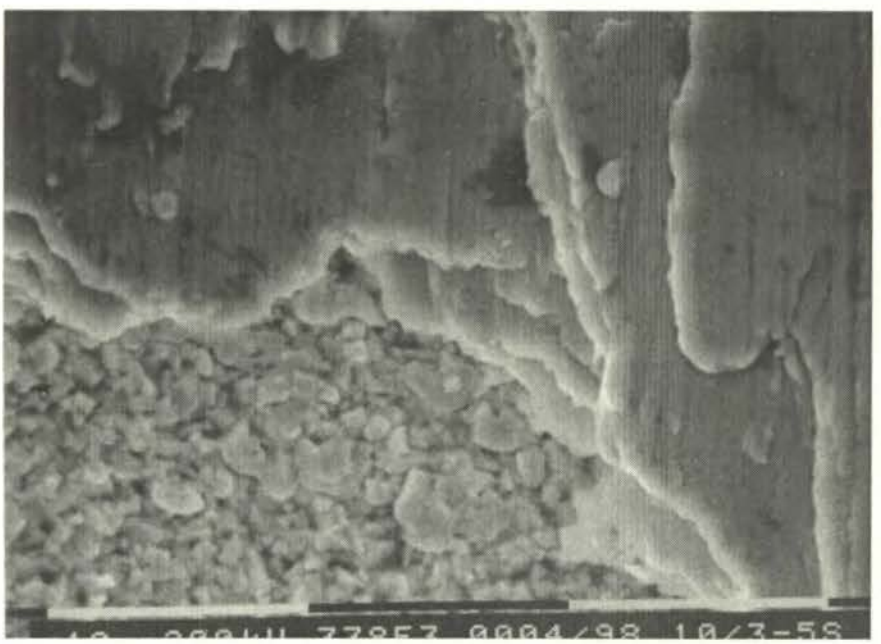

Figure 8. 1 Layers of galled workpiece material on the rake face of a KC730 tool after 5 seconds of cutting, indicating presence of seizure and secondary flow zone when machining Inconel 718 at 75 m/min and 0.14 mm/tooth

Figure 8. 2 Workpiece adhesion in the form of galling and as large lumps on the nose area of a KC720 tool after cutting Inconel 718 for 5 seconds. Coating remained relatively intact on the flank face compared with the rake.

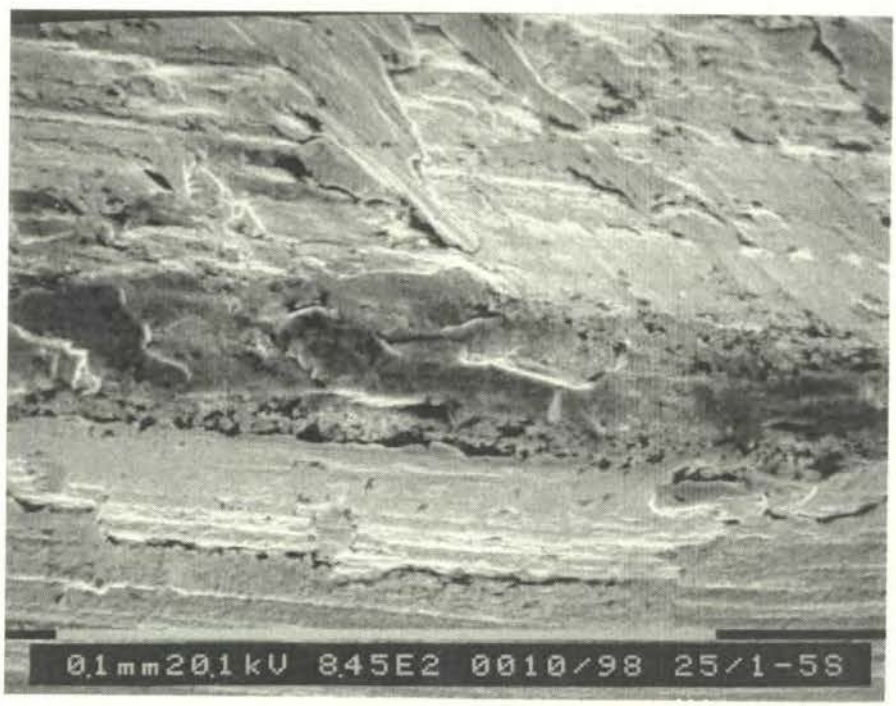

Figure 8. 3 Localised coating delamination on the nose flank of KC730 tool after cutting Waspaloy for 5 seconds at 25 m/min and 0.08 mm/tooth

(a)

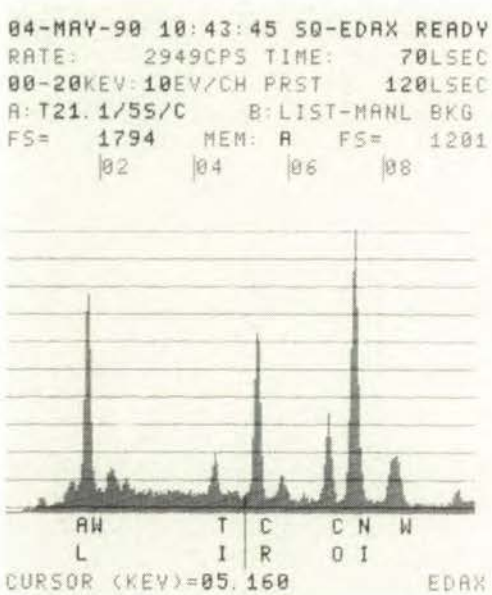

(b)

Figure 8. 4 (a) SEM micrograph showing stuck tool material to the root of a Waspaloy chip produced by KC994M tool after cutting for 5 seconds, (b) Corresponding EDAX analysis proving adherence of tool material

(a)

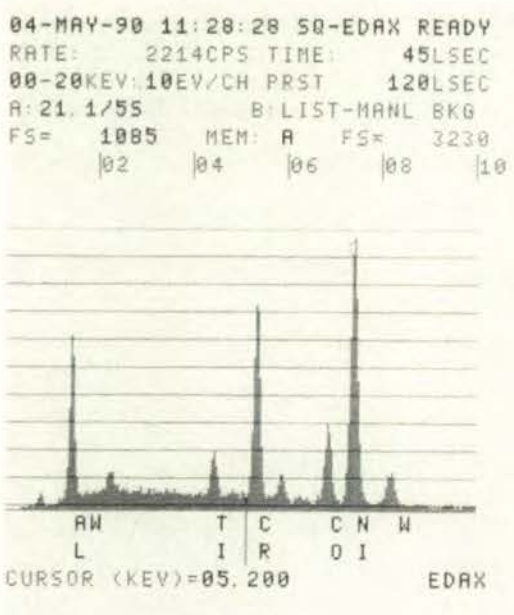

(b)

Figure 8. 5 (a) SEM micrograph showing stuck tool material to the root of a Waspaloy chip produced by KC994M tool after cutting for 5 seconds at 25 m/min and 0.08 mm/tooth. (b) Corresponding EDAX analysis proving the adherence of tool material to the chip

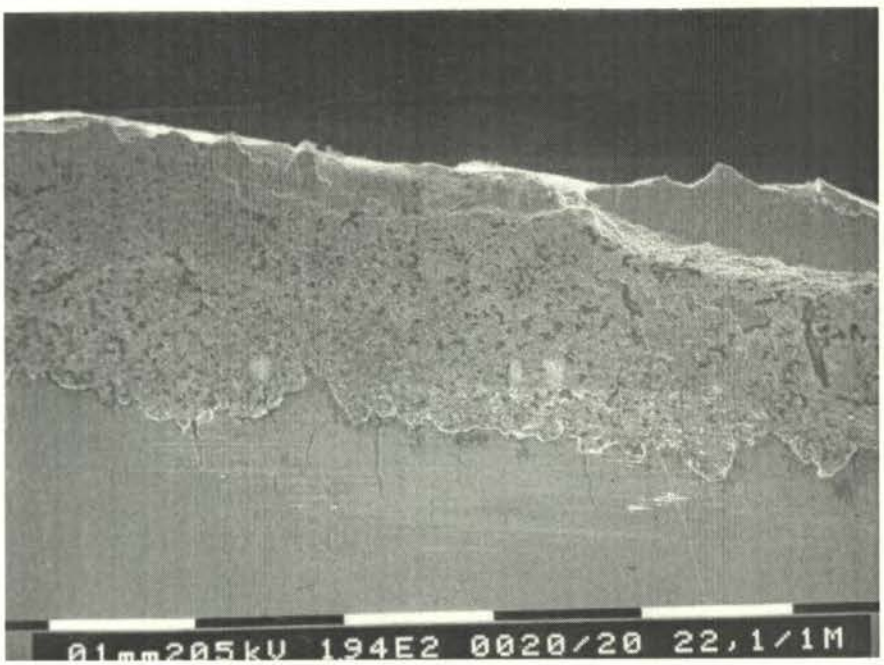

(a)

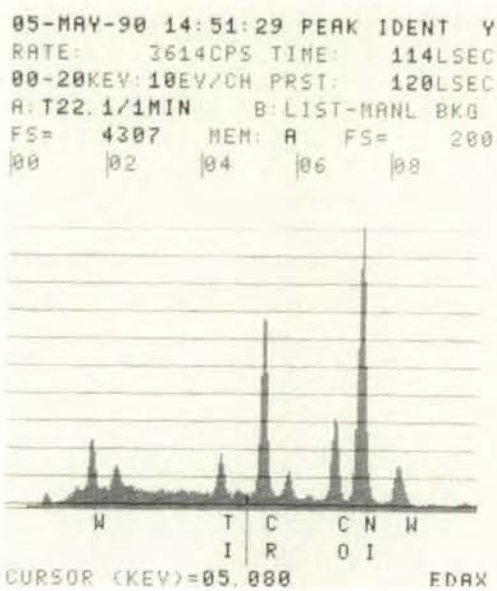

(b)

Figure 8. 6 (a) SEM micrograph showing stuck tool material to the root of a Waspaloy chip produced by KC720 tool after cutting for 1 minute at 25 m/min and 0.14 mm/tooth. (b) Corresponding EDAX analysis proving the presence of tool material on the back side of the chip

(a)

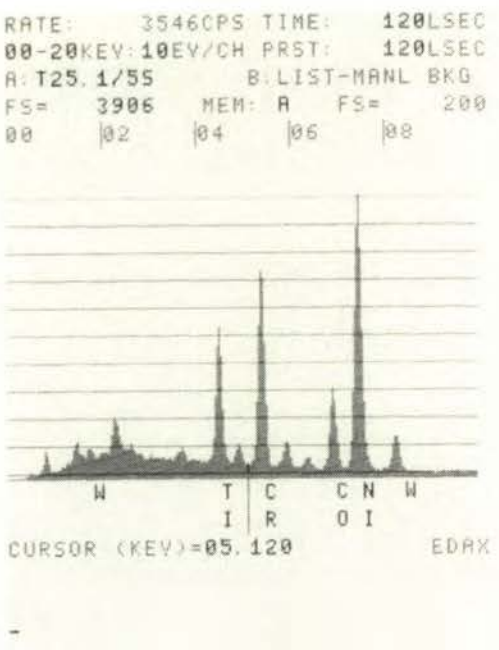

(b)

Figure 8. 7 SEM micrograph showing stuck tool material to the root of a Waspaloy chip produced by KC730 tool after cutting for 5 seconds at 25 m/min and 0.08 mm/tooth. (b) Corresponding EDAX analysis showing the presence of tool material

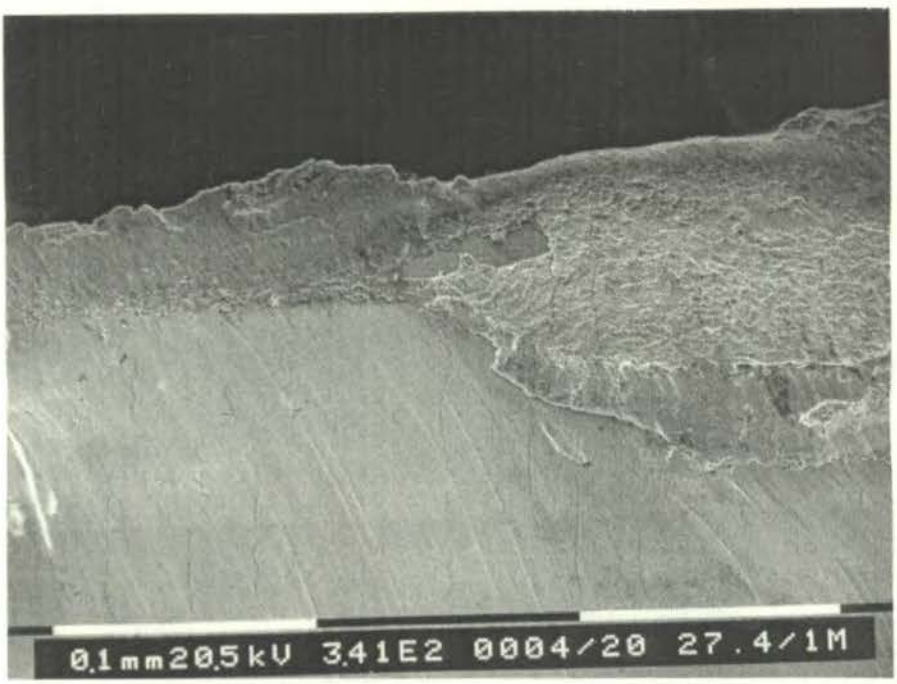

(a)

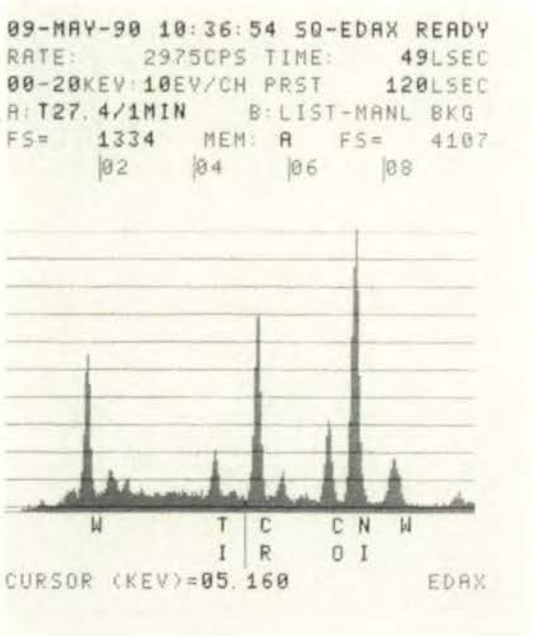

(b)

Figure 8. 8 SEM micrograph showing stuck tool material to the root of a Waspaloy chip produced by KMF tool after cutting for 5 seconds at 50 m/min and 0.08 mm/tooth. (b) Corresponding EDAX analysis showing the presence of tool material

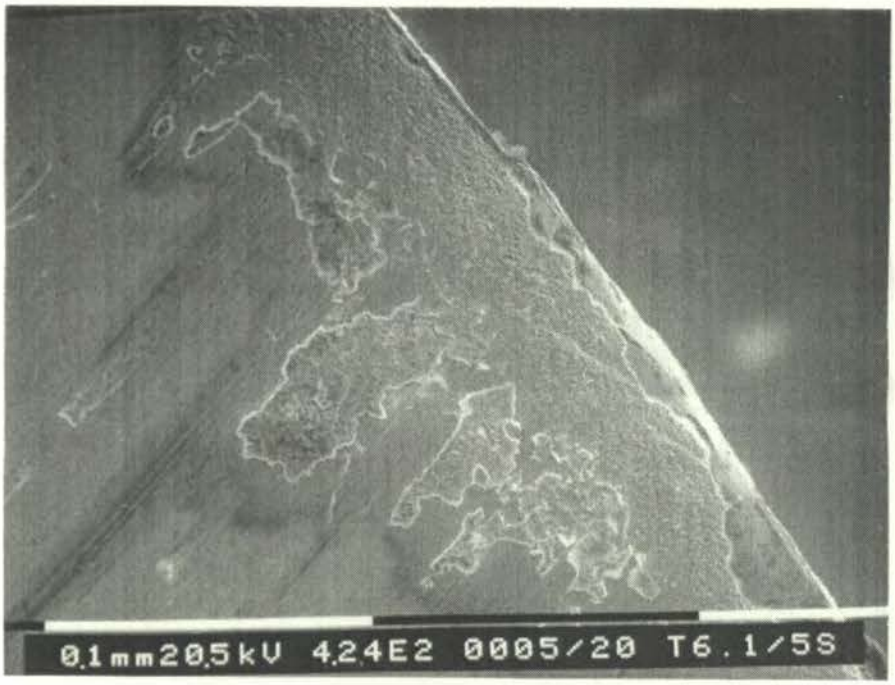

(a)

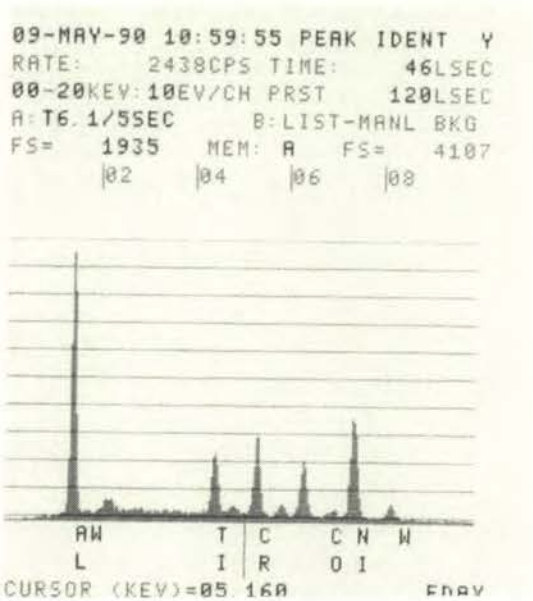

(b)

Figure 8. 9 SEM micrograph showing stuck tool material to the root of an Inconel 718 chip produced by KC994M tool after cutting for 5 seconds at 25 m/min and 0.14 mm/tooth. (b) Corresponding EDAX analysis showing the presence of tool material

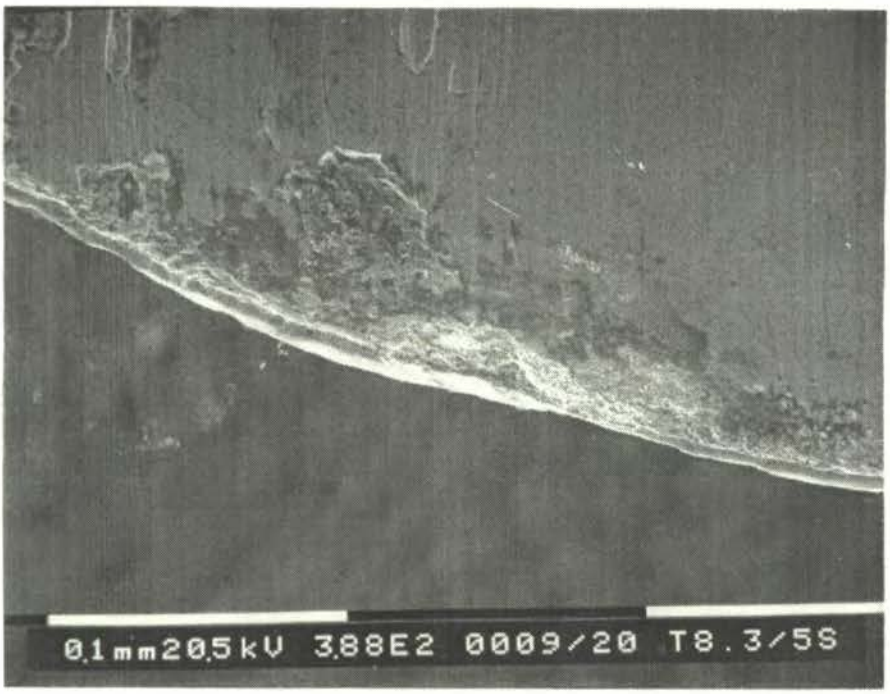

(a)

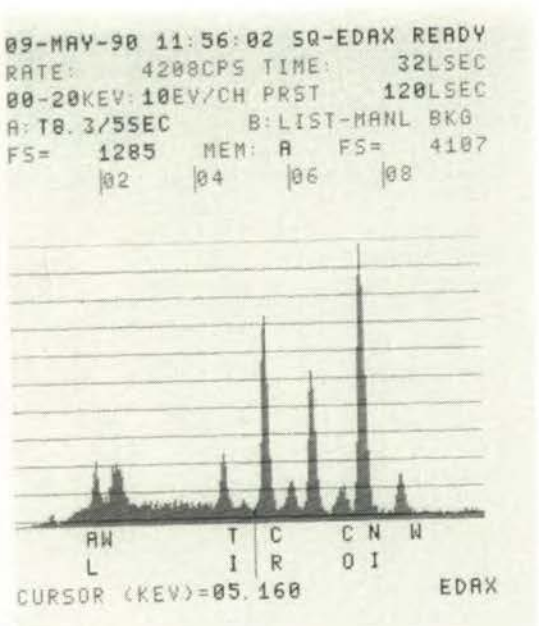

(b)

Figure 8. 10 SEM micrograph showing stuck tool material to the root of an Inconel 718 chip produced by KC720 tool after cutting for 5 seconds at 75 m/min and 0.14 mm/tooth. (b) Corresponding EDAX analysis showing the presence of tool material

(a)

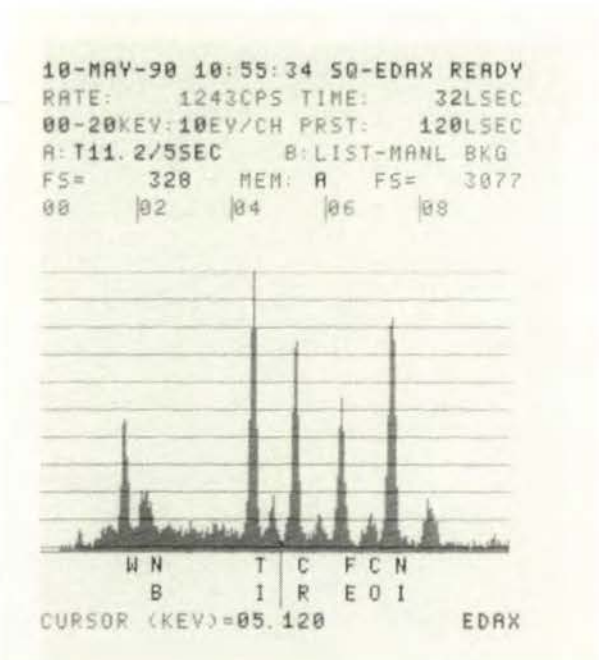

(b)

Figure 8. 11 SEM micrograph showing stuck tool material to the root of an Inconel 718 chip produced by KC730 tool after cutting for 5 seconds at 50 m/min and 0.08 mm/tooth. (b) Corresponding EDAX analysis showing the presence of tool material

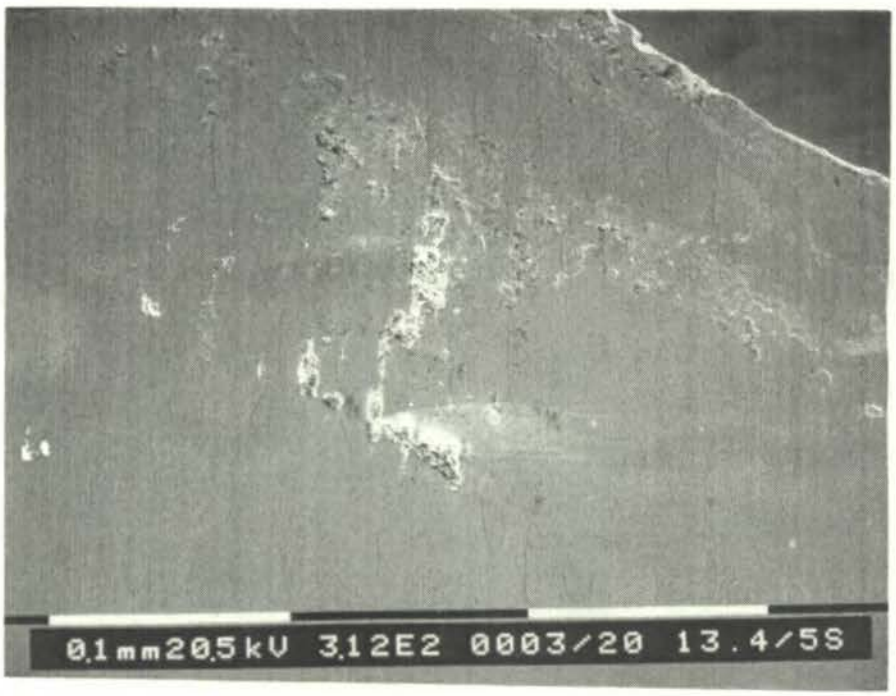

(a)

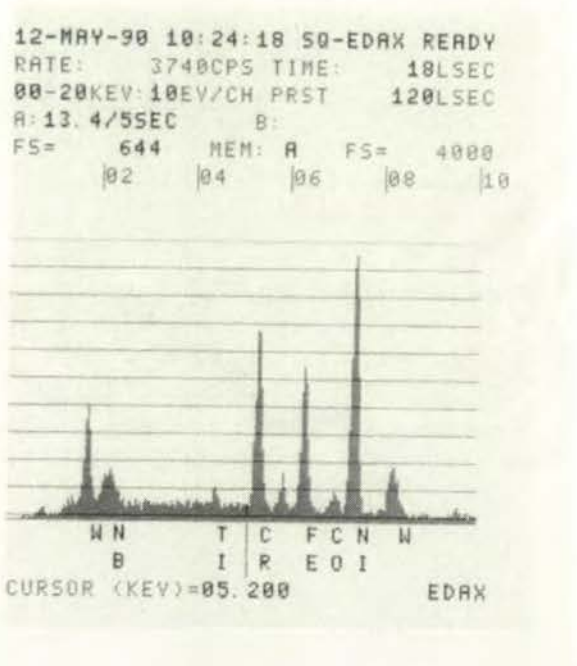

(b)

Figure 8. 12 SEM micrograph showing stuck tool material carried by the chip flow at the root of an Inconel 718 chip produced by KMF tool after cutting for 5 seconds at 50 m/min and 0.08 mm/tooth. (b) Corresponding EDAX analysis showing the presence of tool material

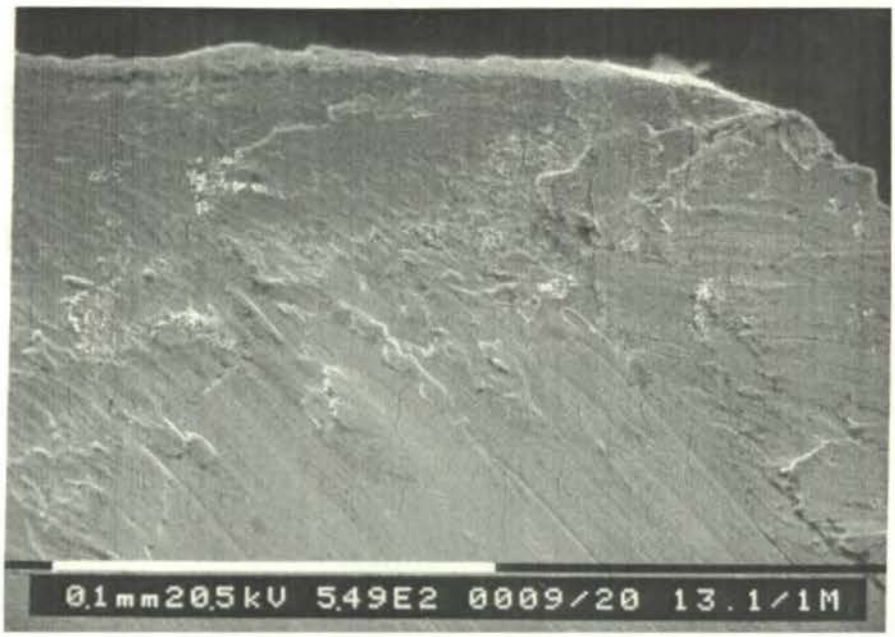

(a)

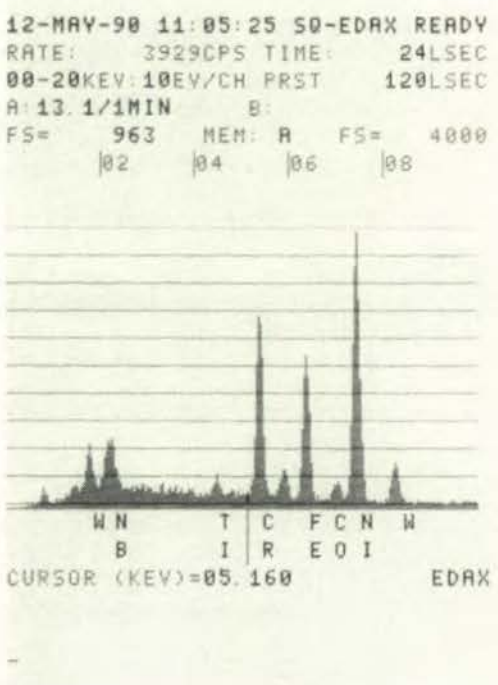

(b)

Figure 8. 13 SEM micrograph showing stuck tool material to the root of an Inconel 718 chip produced by KMF tool after cutting for 1 minute at 25 m/min and 0.08 mm/tooth. (b) Corresponding EDAX analysis showing the presence of tool material

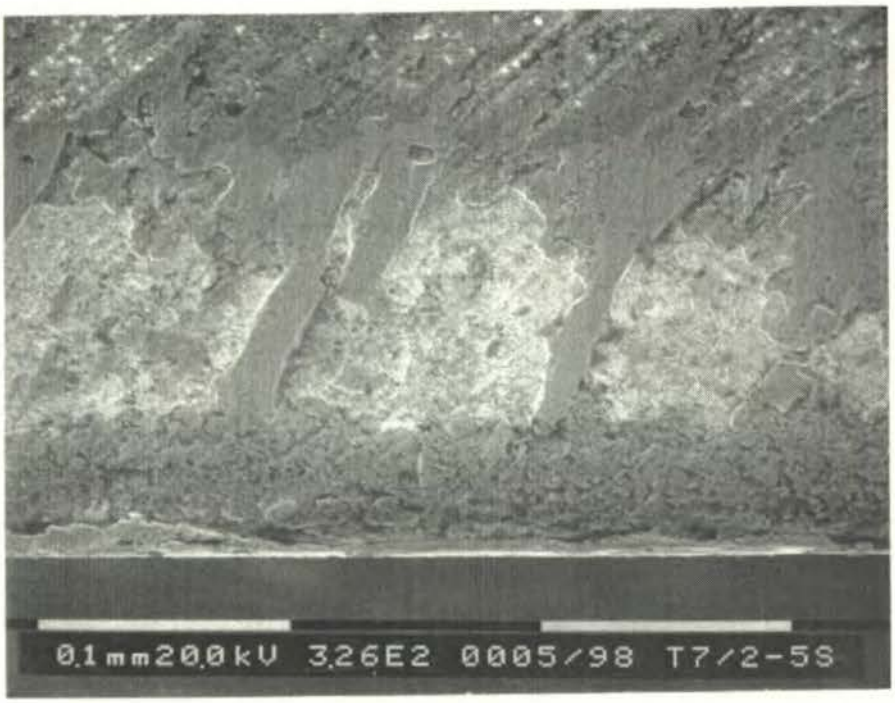

Figure 8. 14 Workpiece galling and associated substrate plucking on the rake face of KC994M tool within first 5 seconds of machining Inconel 718 at 50 m/min and 0.08 mm/tooth.

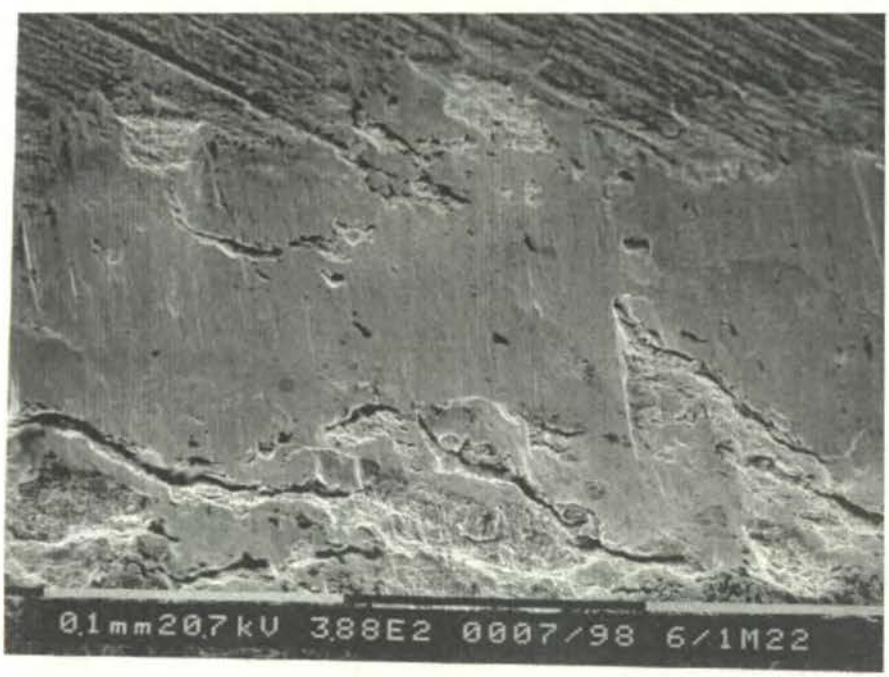

Figure 8. 15 Rake face of a KC994M tool which become highly susceptible to crack initiation, plucking and fracture after cutting Inconel 718 for 22 minutes at 25 m/min and 0.14 mm/tooth.

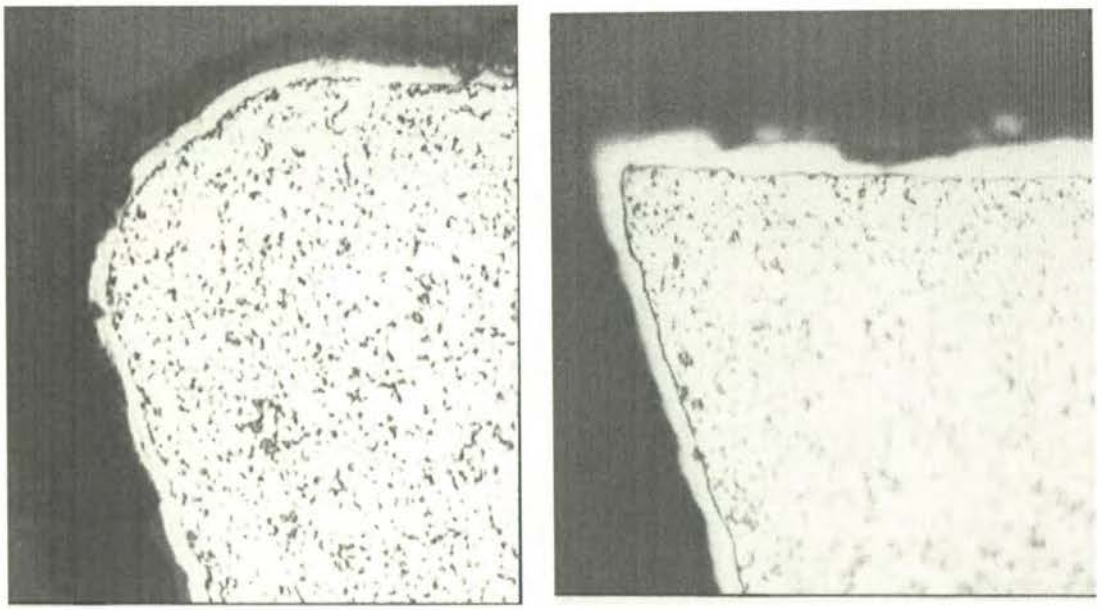

(a) (b)

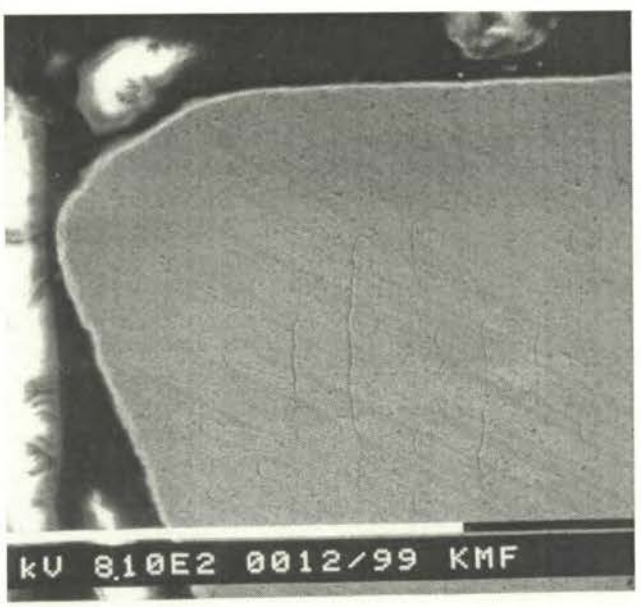

(c)

Figure 8. 16 Sections-through new cutting tools showing difference in cutting edge microgeometry. (a) CVD-coated KC994M, (b) PVD-coated KC730 and KC720, (c) Uncoated KMF tool

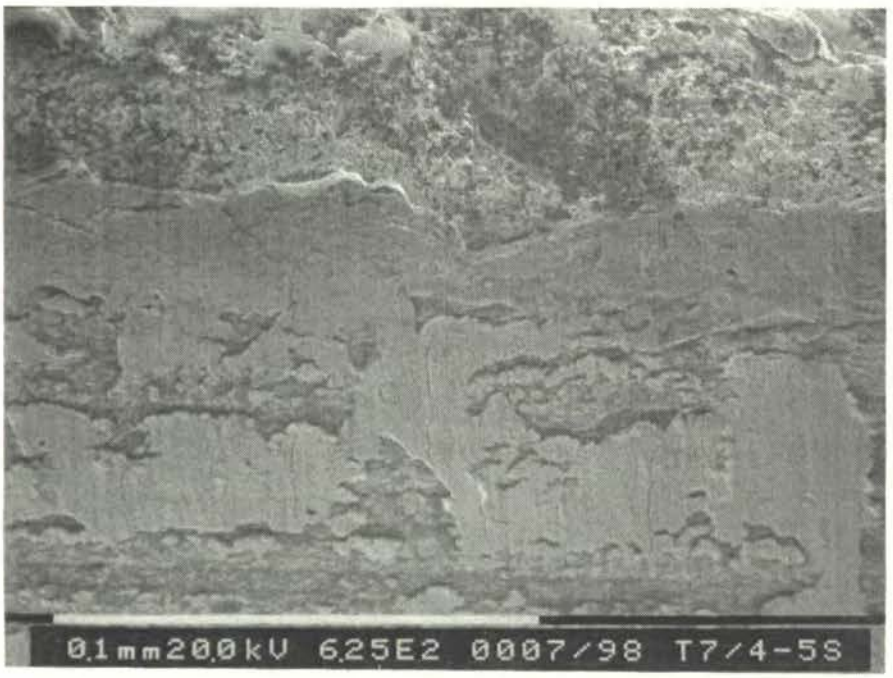

Figure 8. 17 Relatively intact coating on the flank face of a KC994M tool after cutting Inconel 718 for 5 seconds at 100 m/min and 0.08 mm/tooth.

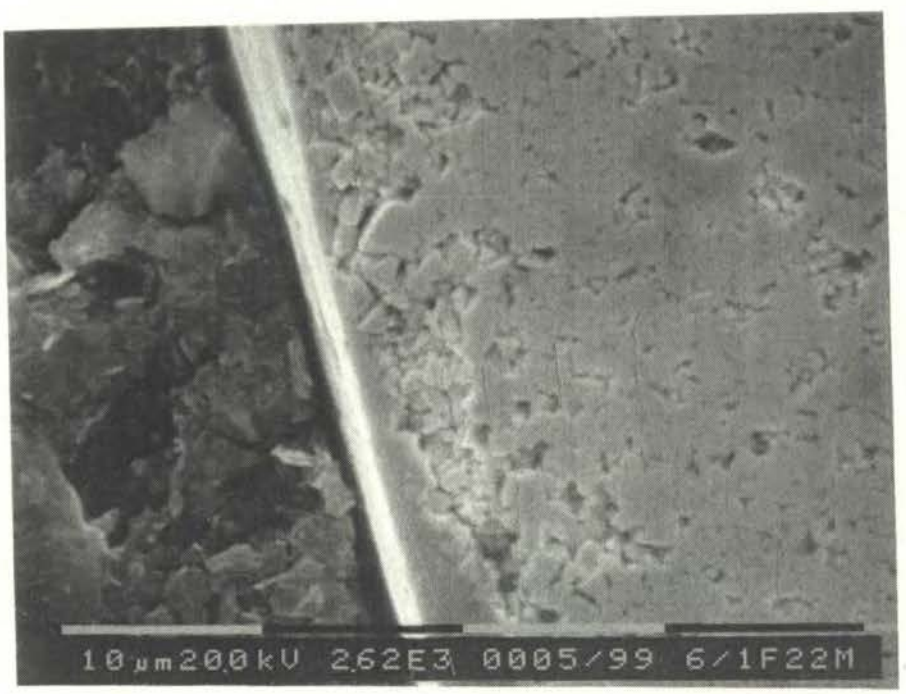

Figure 8. 18 Workpiece material adhesion and associated cracking on the flank face of KC994M tool after cutting Inconel 718 for 22 minutes at 25 m/min and 0.14 mm/tooth.

Figure 8. 19 Sectioned KC720 tool with plucked rake and flank face after cutting Inconel 718 for 16 minutes at 25 m/min and 0.14 mm/tooth.

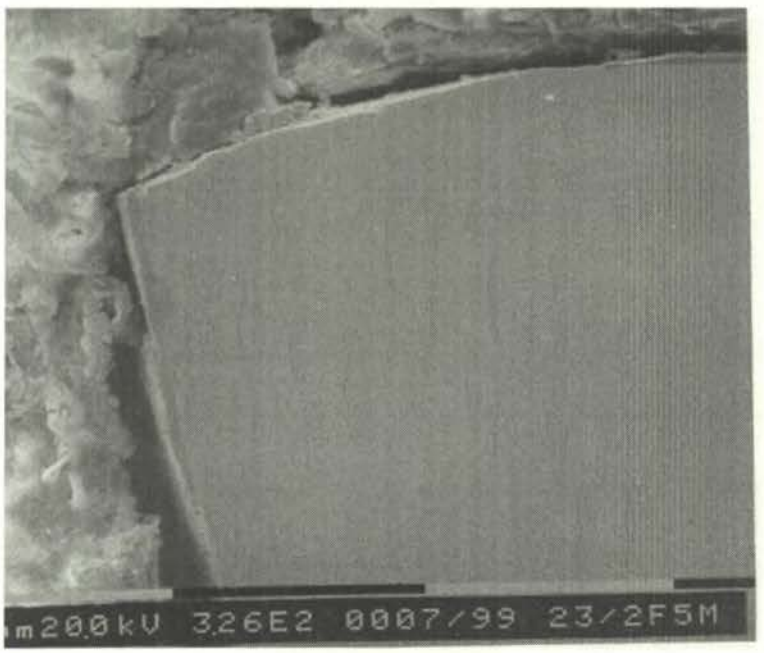

Figure 8. 20 Sectioned KC720 tool showing complete workpiece adhesion on the flank face after cutting Waspaloy for 5 minutes at 25 m/min and 0.08 mm/tooth.

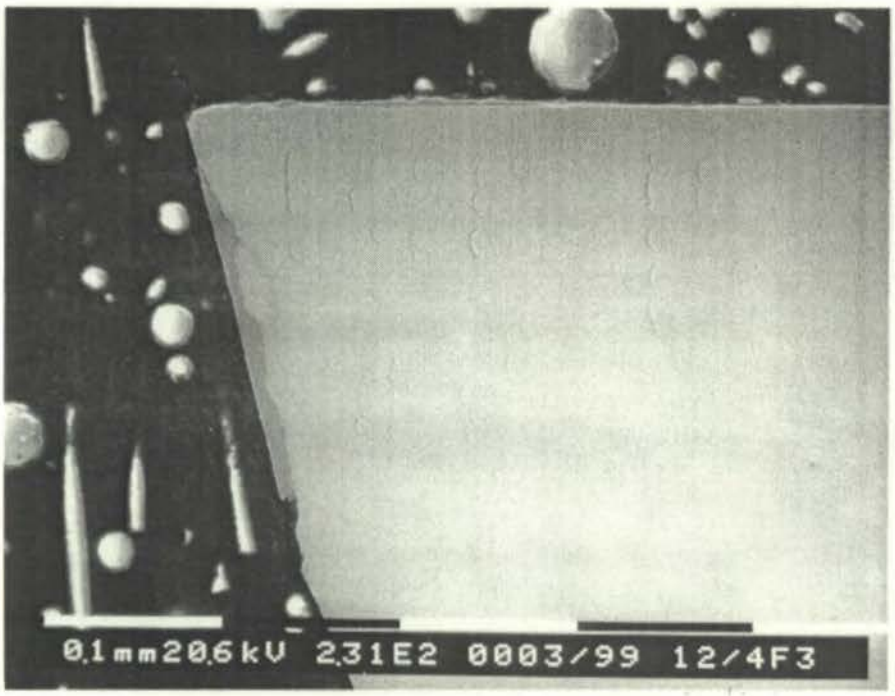

Figure 8. 21 Sectioned KMF tool showing workpiece adhesion over plucked flank and a developed crack after cutting Inconel 718 for 22 minutes at 25 m/min and 0.14 mm/tooth.

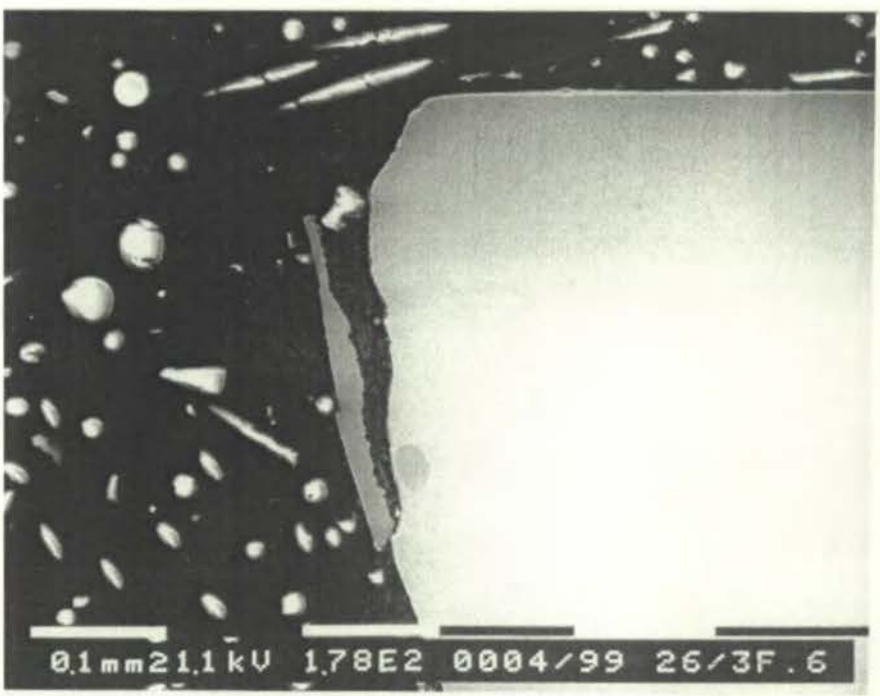

Figure 8. 22 Sectioned KMF tool showing workpiece adhesion over the chipped and plucked flank face after cutting Waspaloy for 2 minutes at 25 m/min and 0.14 mm/tooth.

Figure 8. 23 Magnified view of Figure 8.21 showing evidence of strong adhesion of the workpiece over the fractured areas and detail of propagated crack with initiation point

Figure 8. 24 Magnified view of Figure 8.20 showing strong workpiece adhesion over a fractured region on the flank face

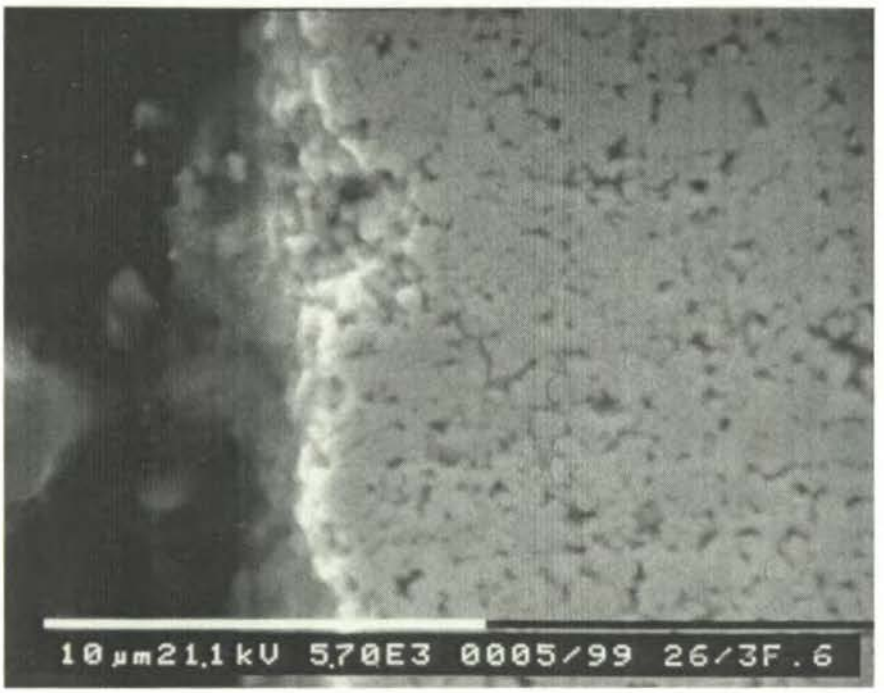

Figure 8. 25 Magnified view of the KMF tool in Figure 8.22 showing initiation of a new crack and its propagation through grain boundaries (cobalt binder)

Figure 8. 26 Magnified view of a KMF tool showing strong workpiece adhesion over smoothly worn flank and suggesting attritional removal of tool grains due detachment of the adhered workpiece after cutting Inconel 718 for 32 minutes at 25 m/min and 0.08 mm/tooth.

Figure 8. 27 Magnified view of a sectioned KC994M tool showing smoothly worn carbide grains on the flank face, suggesting the presence of abrasion/diffusion wear mechanism; after machining Inconel 718 for 22 minutes at 25 m/min and 0.14 mm/tooth.

Figure 8. 28 Magnified view of a sectioned KC720 tool showing smoothly worn carbide grains on the flank face, suggesting the presence of abrasion/diffusion wear mechanism; after machining Inconel 718 for 7 minutes at 50 m/min and 0.08 mm/tooth.

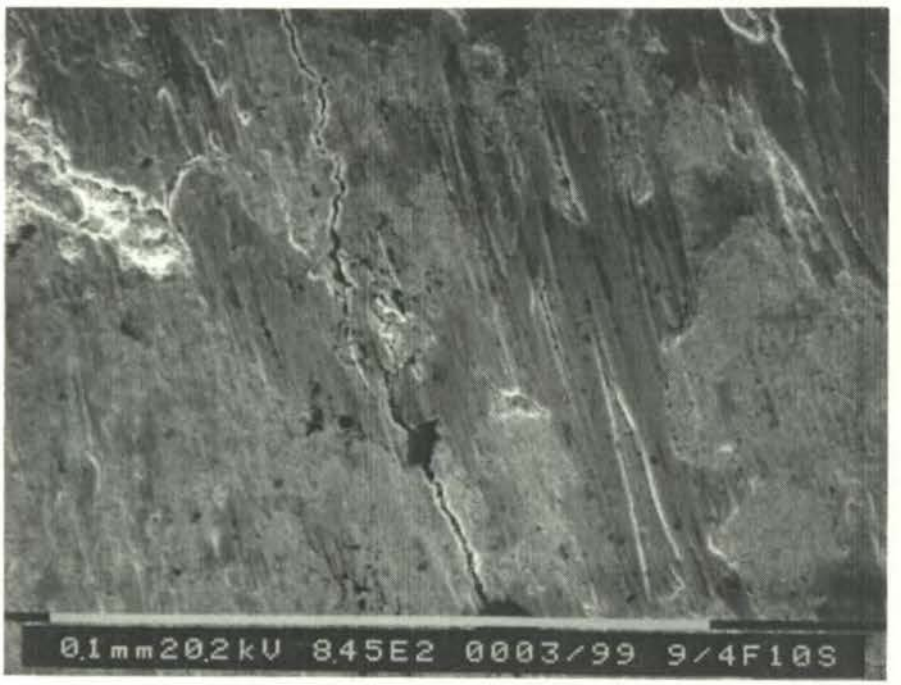

Figure 8. 29 Magnified view of the rake face of a KC720 tool showing crack and a smooth wear pattern indicating the presence of abrasion/diffusion mechanisms; after cutting Inconel 718 for 10 seconds at 100 m/min and 0.08 mm/tooth

Figure 8. 30 Magnified view of the nose flank face of a KMF tool showing smooth wear pattern indicating the presence of abrasion/diffusion mechanisms; after cutting Inconel 718 for 22 minutes at 25 m/min and 0.08 mm/tooth

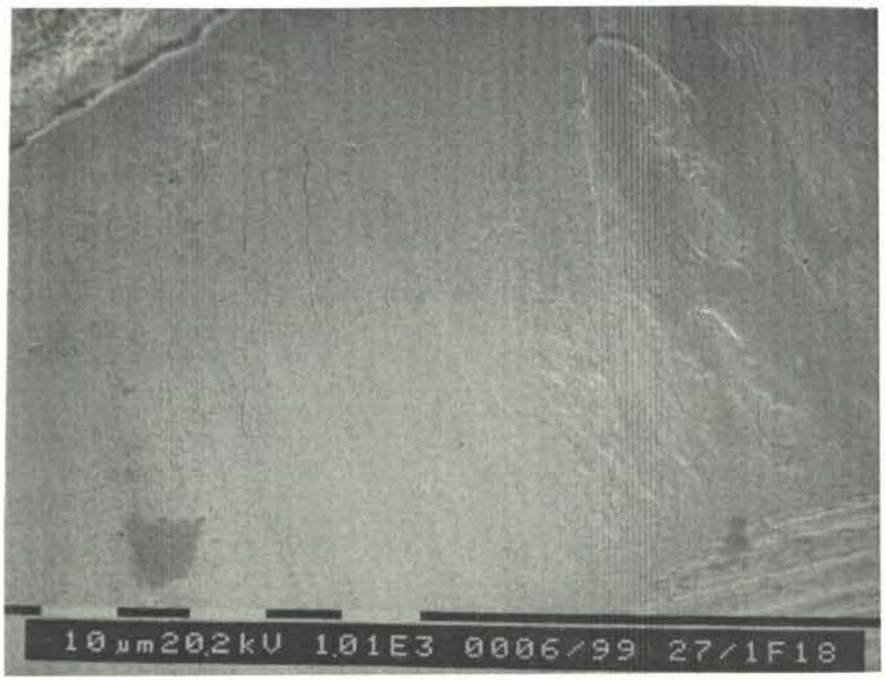

Figure 8. 31 Magnified view of the flank face of a KMF tool showing smooth wear pattern indicating the presence of abrasion/diffusion mechanisms; after cutting Waspaloy for 18 minutes at 25 m/min and 0.08 mm/tooth

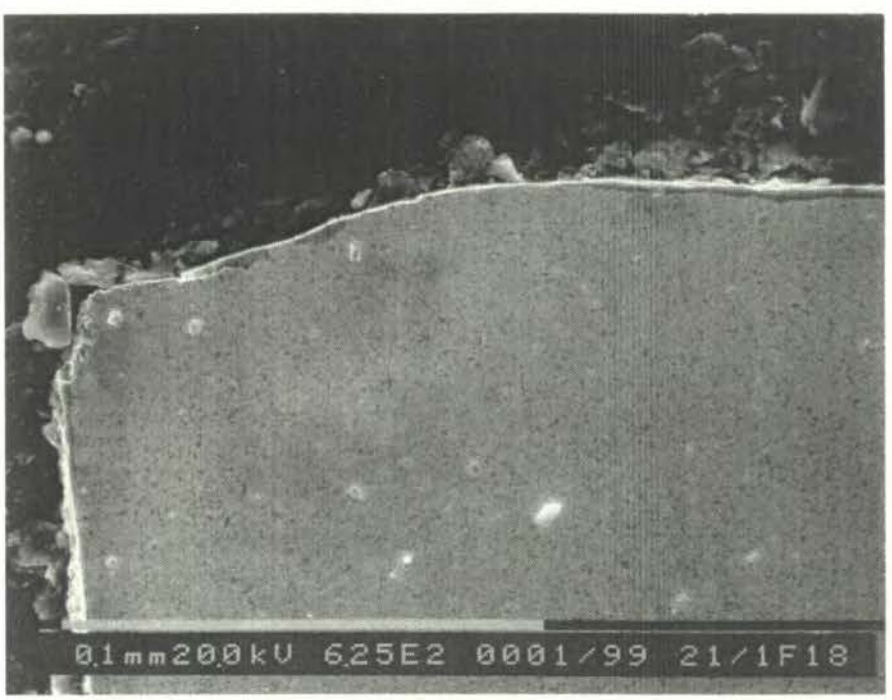

Figure 8. 32 Sectioned KC994M tool showing adhered workpiece on the rake and flank faces, plastic deformation of the rake face and a smoothly worn region on the lower flank after cutting Waspaloy for 18 minutes at 25 m/min and 0.08 mm/tooth

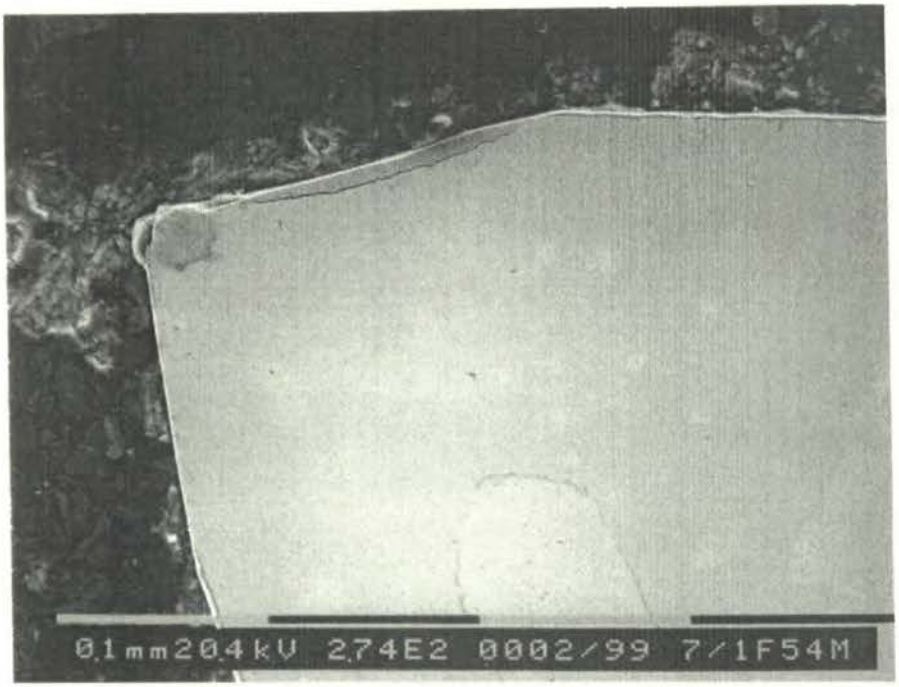

Figure 8. 33 Sectioned KC994M tool showing adhered workpiece on the rake and a smoothly worn region on the flank face; after machining Inconel 718 for 54 minutes at 25 m/min and 0.08 mm/tooth

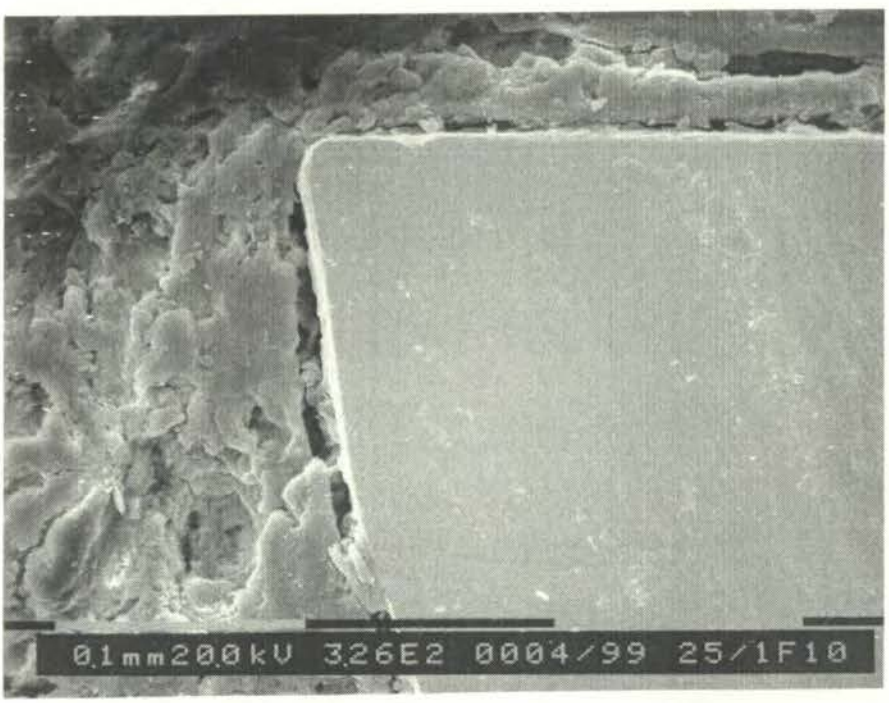

Figure 8. 34 Sectioned KC730 tool showing smooth wear on the flank face, after cutting Waspaloy for 10 minutes at 25 m/min and 0.08 mm/tooth

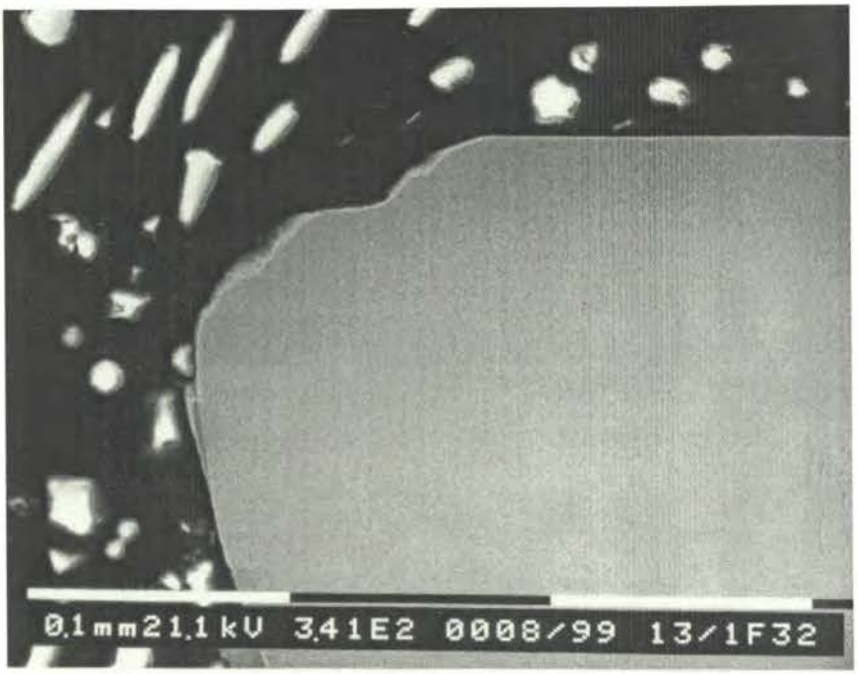

Figure 8. 35 Sectioned KMF tool showing chipped cutting edge and adhered workpiece and smooth wear on the flank face, after cutting Inconel 718 for 32 minutes at 25 m/min and 0.08 mm/tooth

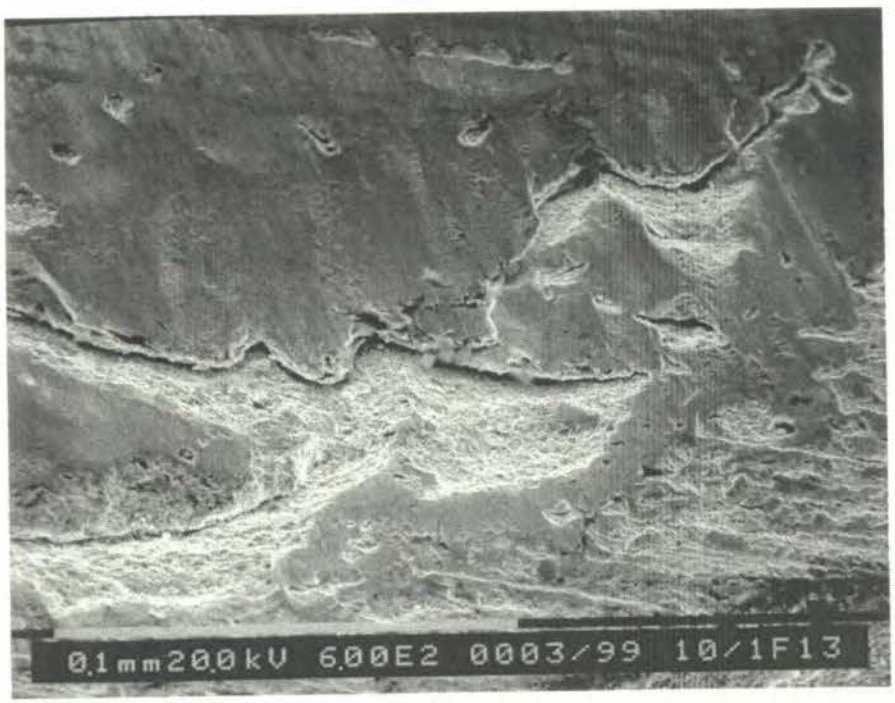

Figure 8. 36 Rake face with multiple cracks and galling of a KC730 tool which become highly susceptible to further plucking/fracture and crack propagation, after cutting Inconel 718 for 13 minutes at 25 m/min and 0.14 mm/tooth

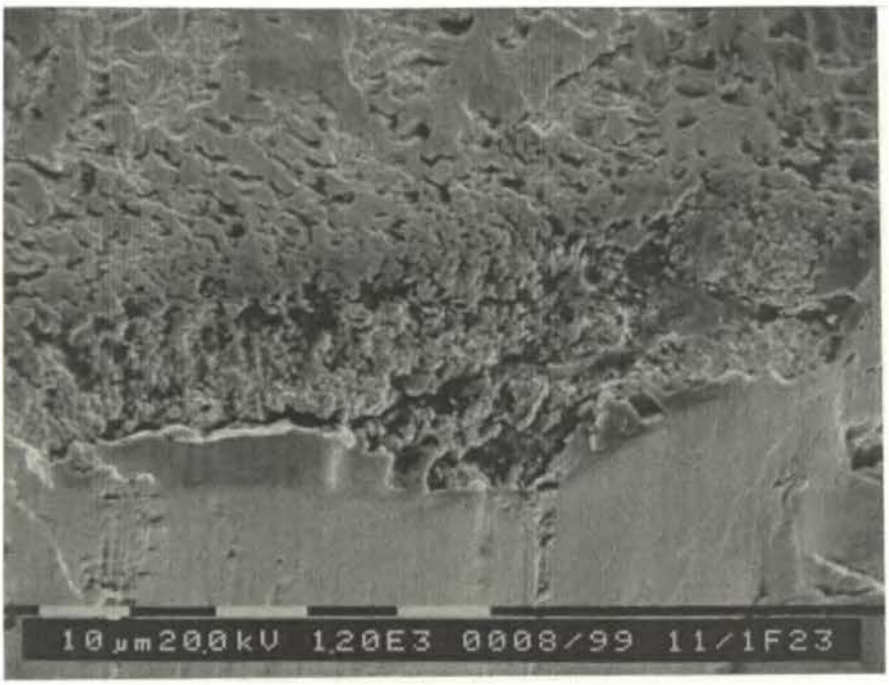

Figure 8. 37 Magnified view of a KC730 tool showing crack at a chipped area of the cutting edge and workpiece galling on the flank, after cutting Inconel 718 for 23 minutes at 25 m/min and 0.08 mm/tooth

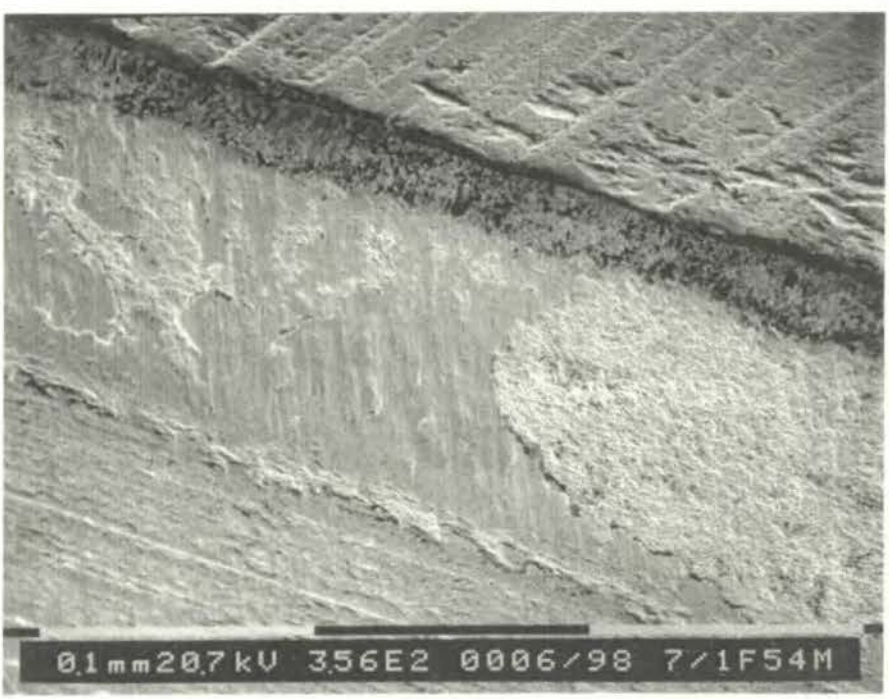

Figure 8. 38 Smeared thin layer of workpiece material on the minor edge of a KC994M tool and substrate pitting due to detachment of adhered material; after cutting Inconel 718 for 54 minutes at 25 m/min and 0.08 mm/tooth

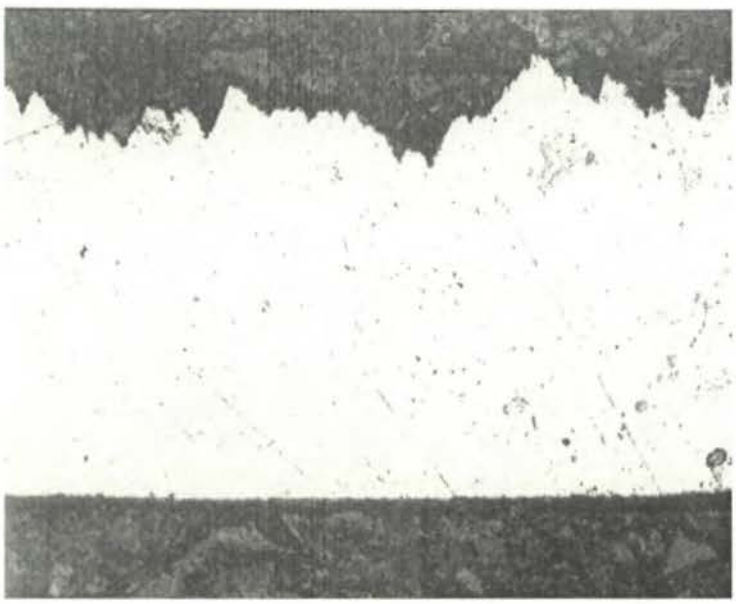

(a)

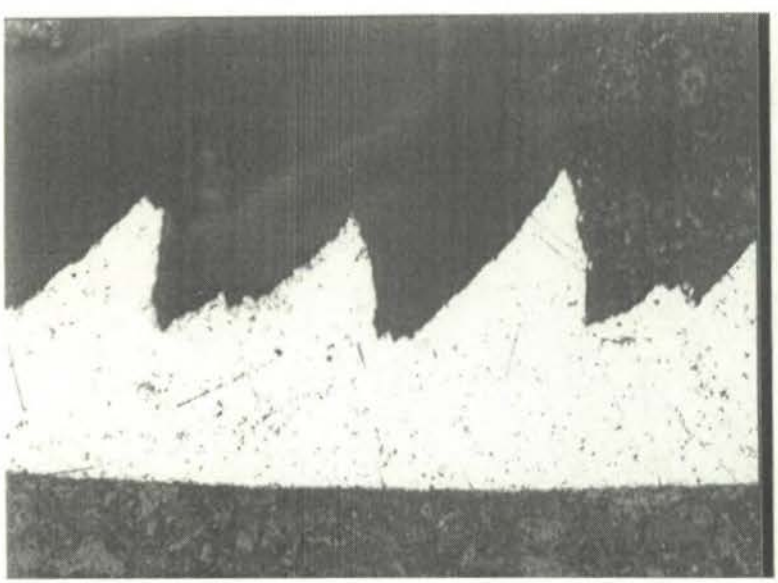

(b)

Figure 8. 39 Longitudinal section of the chips produced at (a) 50 m/min with laminar section and (b) at 100 m/min with serrated (shear localised) section, the latter imposing high frequency fatigue on the cutting edge

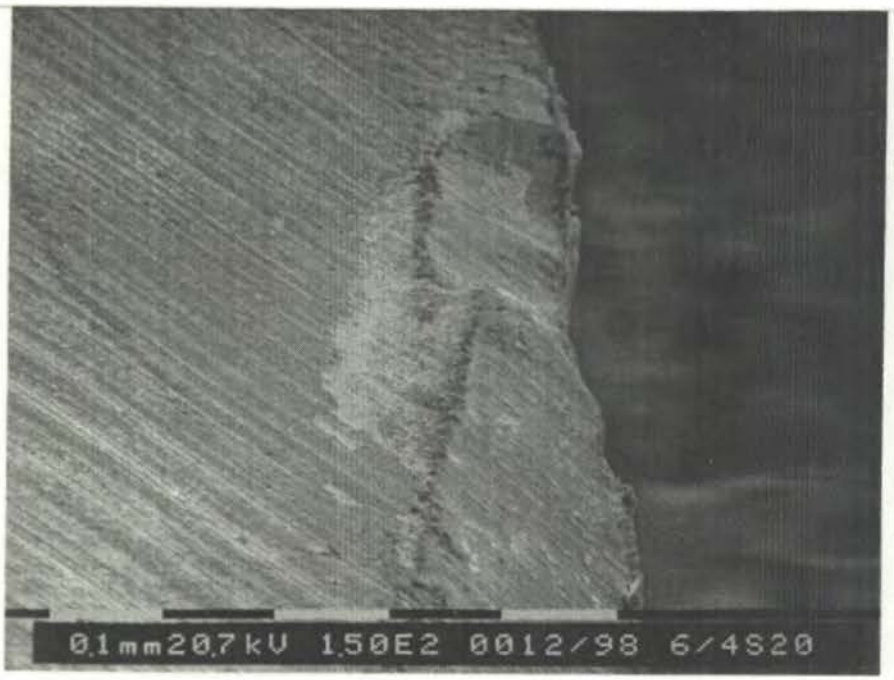

Figure 8. 40 Premature severe chipping of the cutting edge and coating delamination on the rake face due to consequent plastic deformation after cutting Inconel 718 for 20 seconds at 100 m/min and 0.14 mm/tooth

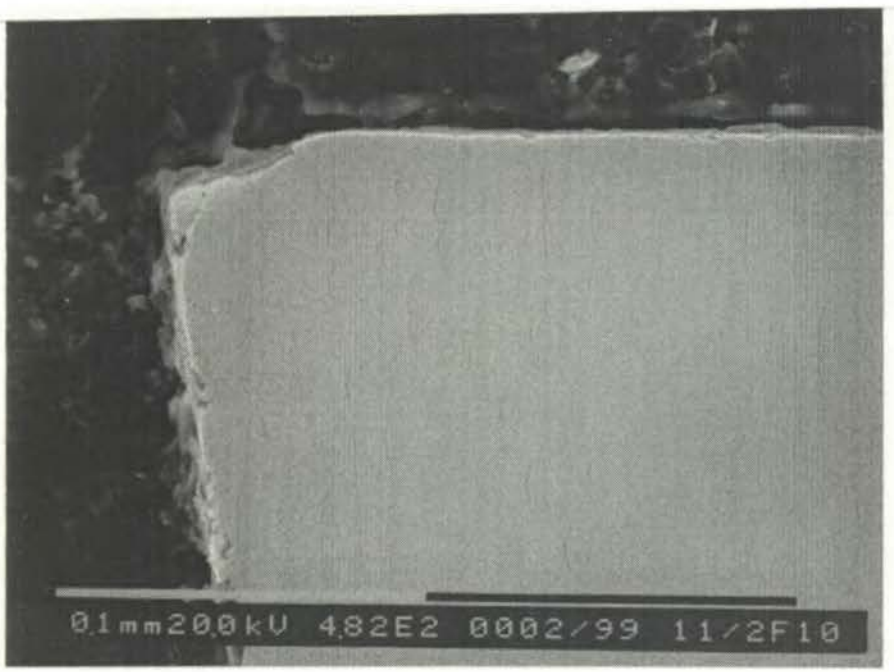

Figure 8. 41 Combination of smoothly worn, chipped and plucked areas on the flank face and plastic deformation and chipping on the rake of a KC730 tool after cutting Inconel 718 for 10 minutes at 50 m/min and 0.08 mm/tooth

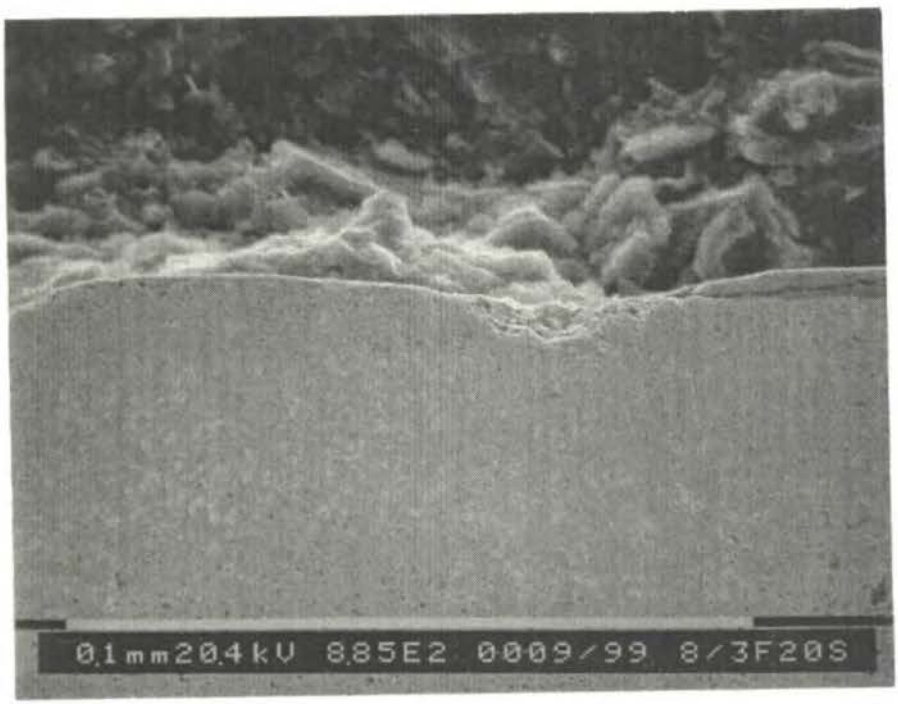

Figure 8. 42 Plastic deformation and associated coating delamination on the rake face of a KC720 tool after cutting Inconel 718 for 20 seconds at 75 m/min and 0.14 mm/tooth